Epidermal Growth Factor Receptor Signalling in the Pulmonary Immune Response - Diverging Roles in Early Life and Adulthood?

Helen Stölting, MSc

Inflammation, Repair and Development Section
National Heart and Lung Institute
Sir Alexander Fleming Building
Imperial College London
London, SW7 2AZ
United Kingdom

A thesis submitted to Imperial College London
for the degree of Doctor of Philosophy

2022

Statement of Originality

I hereby declare that the work described in this thesis was performed by myself, with the following exceptions. Lung function measurements using the FlexiVent system and the related surgical anaesthesia and cannulation of animals was performed by Simone Walker. Paraffin embedding, sectioning and traditional histological staining (H&E, PAS, Sweet's Silver) of specimens was performed by Lorraine Lawrence of the Imperial College London Histology Core Facility. Flow-activated cell sorting was performed by Jane Srivastava and Dr Jessica Rowley of the Imperial College Flow Cytometry Core Facility. Laury Baillon and Rebecca Frise of the Barclay group at the Department of Infectious Disease, Imperial College London, performed the infection of epithelial cells with SARS-CoV-2 and H1N1, collected samples and conducted plaque assays within their Containment Level 3 (CL3) and CL2 laboratories at St. Mary's, Imperial College London. All further downstream analysis was performed by me. The *in vivo* experiments analysed in Figures 3.4F and 3.9D were performed by various lab members as part of a study published as Saglani et al., 2018 (ref. [56]), and Dr Lewis Entwistle performed the *in vivo* experiment analysed in Figure 3.4H. Dr Katie Bonner and Dr Maria Zarcone performed the *in vitro* ALI experiments which were analysed in Figures 3.11A-B and 3.11C-D, respectively. Airway samples were collected by Dr Sejal Saglani, Dr Katie Bonner and other members of the Breathing Together study as well as Dr Richard Hewitt and Dr Philip Molyneaux. RNA sequencing of bronchial epithelial brushings and initial alignment, quality control and read counts were performed by members of the Marsland group at the Department of Immunology and Pathology, Monash University, Australia as part of the Breathing Together research study. I further declare that the intellectual content of this thesis is the product of my own work and that all sources have been appropriately referenced.

Copyright Declaration

The copyright of this thesis rests with the author. Unless otherwise indicated, its contents are licensed under a Creative Commons Attribution-NonCommercial 4.0 International Licence (CC BY-NC). Under this licence, you may copy and redistribute the material in any medium or format. You may also create and distribute modified versions of the work. This is on the condition that: you credit the author and do not use it, or any derivative works, for a commercial purpose. When reusing or sharing this work, ensure you make the licence terms clear to others by naming the licence and linking to the licence text. Where a work has been adapted, you should indicate that the work has been changed and describe those changes. Please seek permission from the copyright holder for uses of this work that are not included in this licence or permitted under UK Copyright Law.

Acknowledgements

Firstly, I would like to thank my supervisors Prof Clare Lloyd and Prof Sejal Saglani, for the opportunity to conduct my PhD within your groups, for your relentless support and mentorship throughout the years, for your trust and for granting me the freedom to grow into the scientist I am today. It has been a great pleasure learning from and with you. A special thank you to my assistant supervisor Franz Puttur, who has not only helped me tremendously in the lab but has supported my scientific journey like no other and has enriched my time in the lab with his positive energy and unparalleled kindness. Franz, you are an amazing and special person.

I would also like to acknowledge Simone Walker, without whom the lab and all its members would likely be in shambles, not only for her technical assistance but for the care, dedication, support and life advice she provides to everyone in our group. I also have to thank (or blame) her and Karim Boustani for sparking my reading addiction. Thank you as well to Will Branchett, Lewis Entwistle and Rob Oliver, for welcoming me into the lab, showing me the ropes and lending me their brains and hands on several occasions. In that vein, I would also like to thank Phebe Ekregbesi, Reuben Day-Weber and Minerva Garcia for their help on harvest days and Ciara Campbell, Laury Baillon and Rebecca Frise for sharing the load of ALI culture experiments. Thank you to Laura Yates and Lisa Gregory, for your kindness, support and positive energy, for holding the lab together and for providing feedback and direction wherever needed. Lorraine Lawrence, thanks not only for doing a stellar job on all my histology but also for the guidance and great conversations you have provided, and Mindy, for helping me navigate Breathing Together and keeping me well-fed with your culinary skills.

Special thanks are due to my twisted sister Gesa Albers, who has not only tolerated having me around nearly 24/7 for the last four years but has been the best friend I could have asked for. Thanks for pretending I can cook, laughing at my jokes, forcing me to work out religiously, indulging my many peculiarities, joining me on surfing holidays, giving me your honest feedback on my colour schemes, baking amazing things despite your reluctance to actually read the recipe you are following, entertaining me with your superior abilities to hurt yourself in silly ways and generally holding me together – both in- and outside the lab. Danai Koftori, thanks for being an amazing housemate and a wonderful friend – I am still not entirely sure how you survived Gesa and me for three years but I am very glad you did. Thank you as well to the rest of my fellow SAFferers™ (Karim, Kornelija Suveizdytė, Lucía Labeur, Nicoletta Bruno and Skye Quinn) for giving me a place to whinge and whine, providing the group therapy we all desperately needed and generally being amazingly supportive and funny people. A shoutout, too, to the members of the Best Row™ (Christina Michalaki, Gesa, Lola Loewenthal and Will Traves), for brightening my day with your banter, making sure we eat well, often and

early, proofreading my emails to make sure they meet British politeness standards and indulging my sausage roll and musical addictions. It has been a great pleasure sharing a row with you! Thank you to James Harker, not only for your dedication to journal club, which has played a vital part in honing my critical thinking skills and making a scientist out of me but also for sharing your boundless wealth of knowledge with the rest of us and importantly, teaching me that walking in the dark for several hours is actually rather enjoyable as long as you are surrounded by your fellow lab members and get Maccies first (Thanks for letting me tag along to the Harker Lab Night Hike!). I would also like to thank all other members of the IRD section, especially those who have fuelled me with their baked goods (Chloe Pyle!), for being such a welcoming bunch and making a cold, dark, dank place like SAF feel like home. At this point, I would like to acknowledge Farmers Market's Brownie Man, the SAF café vegan sausage rolls, my noise-cancelling headphones, my doggo hot water bottle and my snuggie blanket, without which I would not have survived the last four years. Finally, thank you to Simone Wolf, Julia Kugler and Pat Ogger, for always being by my side even when you were physically very far away – your friendship means a lot to me.

Zu guter Letzt möchte ich meiner Familie danken. Riesigen Dank, dass Ihr immer für mich da wart, stets an mich geglaubt habt und mich häufig mit Haribo und Brötchen aus der Heimat versorgt habt. Ohne Eure Unterstützung wäre ich heute nicht hier und ich hoffe, Ihr verzeiht mir, dass Ihr mich so selten zu Gesicht bekommt, und dass ich auch trotz fast 10 Jahren Uni keine Millionen verdienen werde. Ich schulde Euch ein Eis!

I would also like to acknowledge the British Lung Foundation and Breathing Together for funding me throughout my PhD.

Abstract

Asthma is a chronic heterogeneous airway disease characterised by airway inflammation, hyperresponsiveness and remodelling. Onset of asthma primarily takes place in childhood, an aspect that is underrepresented in mouse models of allergic airway disease (AAD), and results in long-lasting deficits in lung function. Epidermal growth factor receptor (EGFR) is ubiquitously expressed, fulfils both protective and pathogenic functions in various disease contexts and was shown to be upregulated in both children and adults with asthma. The aim of this thesis was to define the role of EGFR signalling in early-life AAD and compare it to adulthood.

Analysis of newly generated and published data in Chapter 3 revealed widespread expression of EGFR and its ligands in the lungs of both developing and adult mice and provided evidence for enhanced EGFR signalling upon allergen exposure.

Manipulation of EGFR signalling in various AAD models in Chapter 4 identified a unique role of this pathway in protecting against airway hyperresponsiveness in early life which was not observed in adulthood.

In-depth analysis of EGFR inhibition during early-life AAD conducted in Chapter 5 established a novel role for EGFR signalling in driving sex differences in early-life AAD by augmenting type 2 immune responses of young female animals.

Finally, Chapter 6 investigated EGFR involvement in respiratory infection, comparing SARS-CoV-2 infection between children and adults by studying paediatric and adult airway epithelial cells. This demonstrated SARS-CoV-2 infection to be indistinguishable between paediatric and adult cells but significantly diminished damage and inflammation compared to infection with Influenza H1N1.

Collectively, these findings demonstrate that EGFR signalling is highly active during AAD but fulfils distinct roles depending on age and sex, underscoring the need to use appropriate models of disease. The pathway may constitute therapeutic targets to preserve lung function in early life and may protect young females from developing severe disease.

Contents

Statement of Originality **3**
Copyright Declaration **4**
Acknowledgements **5**
Abstract **7**
Contents **9**
List of Figures **13**
List of Tables **16**
List of Abbreviations **17**
1 Introduction **21**
1.1 Asthma 23
1.1.1 Definition, incidence and aetiology 23
1.1.2 Clinical phenotypes and endotypes 24
1.1.3 Molecular mechanisms of asthma pathology 24
1.1.4 Current treatment strategies 28
1.2 Epidermal growth factor receptor (EGFR) 30
1.2.1 EGFR activation and canonical signalling pathways 30
1.2.2 EGFR ligands 32
1.2.3 Cellular expression patterns of EGFR and its ligands 35
1.2.4 EGFR signalling in health and disease 35
1.2.5 Targeting EGFR signalling clinically 37
1.3 Hypothesis and aims 38
2 Methods **39**
2.1 Human airway and lung samples 41
2.1.1 Paediatric samples 41
2.1.2 Adult samples 41
2.2 Cell Culture 42
2.2.1 General cell culture and cell lines 42
2.2.2 Air-liquid interface (ALI) culture of airway epithelial cells 42
2.2.3 Culture of normal lung fibroblasts 44
2.2.4 Stimulation of murine lymph node cells 44
2.3 Work on live animals 45
2.3.1 Source of animals and general husbandry 45
2.3.2 Models of allergic airway disease (AAD) 45
2.3.3 Assessment of lung function 47
2.3.4 Blood collection 48
2.4 Animal tissue harvest and processing 49
2.4.1 Blood and serum 49
2.4.2 Bronchoalveolar lavage (BAL) 49
2.4.3 Mediastinal lymph nodes (LN) 49
2.4.4 Standard protocol for lung removal and processing 49
2.4.5 *In situ* dispase digest of lungs 50
2.5 Flow cytometry and flow-activated cell sorting 51
2.5.1 Stimulation of cells for intracellular cytokine analysis 51
2.5.2 General staining protocol 51

2.5.3 Acquisition and analysis 54
2.5.4 Flow-activated cell sorting (FACS) 54
2.6 RNA isolation, cDNA synthesis and quantitative PCR 57
2.6.1 RNA isolation 57
2.6.2 cDNA synthesis 57
2.6.3 Quantitative PCR (qPCR) 58
2.6.4 Transcriptomics analysis 58
2.7 Protein analyses 60
2.7.1 Enzyme-linked immunosorbent assay (ELISA) and membrane-based proteome arrays 60
2.7.2 Western blot (WB) 61
2.8 Imaging analysis 62
2.8.1 Agarose-embedding and sectioning of ALI inserts 62
2.8.2 Histological stains 62
2.8.3 Immunofluorescence 63
2.8.4 Image acquisition and analysis 64
2.9 Data analysis, statistics and visualisation 65
2.9.1 Data processing and simple statistical testing 65
2.9.2 Correlations, principal component analysis and network analysis 65
2.9.3 Visualisation 66
3 Results I: Pulmonary levels of EGFR and its ligands – changes during development and with allergen or virus challenge 67
3.1 Introduction 69
3.1.1 Stages of lung development in humans and mice 69
3.1.2 The role of EGFR and its ligands during lung development 70
3.1.3 EGFR signalling during asthma, AAD and respiratory viral infection 71
3.1.4 Hypothesis and aims 72
3.2 Methods 73
3.2.1 Analysis of published data sets 73
3.2.2 Sorting lung cell populations at different stages of development 73
3.2.3 Murine models of allergic airway disease (AAD) 74
3.2.4 Use of primary human samples to investigate effects of allergen on EGFR ligands 74
3.3 Results 76
3.3.1 EGFR and ligand expression throughout pulmonary development 76
3.3.2 Effects of allergen treatment on EGFR gene expression 81
3.3.3 Cell-specific expression of EGFR in the allergic lung 83
3.3.4 Pulmonary levels of EGFR ligands and their release into the airways 87
3.3.5 Measuring EGFR activation in the allergic lung 89
3.3.6 Using primary human airway cells to investigate effects of allergen or viral stimulation on EGFR signalling 91
3.3.7 EGFR and ligand levels in airway samples from children with PSW and severe asthma 94
3.4 Discussion 96
3.5 Concluding remarks and future work 99
4 Results II: Manipulating EGFR signalling during allergic airway disease 101
4.1 Introduction 103
4.1.1 Investigating the role of EGFR signalling in rodent models of AAD 103
4.1.2 Contribution of individual EGFR ligands to AAD 104
4.1.3 Hypothesis and aims 105
4.2 Methods 106
4.2.1 EGFR intervention in murine models of AAD 106
4.2.2 Assessment of key pathological features of AAD 106

4.2.3 Integrative data analysis 106
4.3 Results 107
4.3.1 Exogenous activation of EGFR signalling during acute models of adult AAD 107
4.3.2 Inhibition of EGFR signalling during a chronic model of adult AAD 112
4.3.3 EGFR inhibition during early-life AAD affected monocytic inflammation and lung function 118
4.3.4 EGFR inhibition during early-life AAD had no effect on airway remodelling or sensitisation 123
4.3.5 Integrative data analysis of EGFR inhibition during early-life AAD 127
4.3.6 Exogenous activation of EGFR signalling during early-life AAD 130
4.3.7 Establishing a novel model of early-life AAD using mixed allergens 132
4.3.8 Exogenous EGFR activation in mixed allergen model of early-life AAD 137
4.4 Discussion 140
4.5 Concluding remarks and future work 144
5 Results III: EGFR inhibition abrogates exacerbated type 2 responses to allergen in adolescent female mice 147
5.1 Introduction 149
5.1.1 Sex differences in asthma 149
5.1.2 Use of animal models to study the role of sex hormones in AAD 149
5.1.3 Hypothesis and aims 151
5.2 Methods 151
5.3 Results 152
5.3.1 Augmented type 2 responses in adolescent female animals were dependent on EGFR signalling 152
5.3.2 Comparable responses between sexes in adult AAD 159
5.3.3 EGFR inhibition abrogated HDM-induced type 2 cytokine production *ex vivo* 163
5.4 Discussion 165
5.5 Concluding remarks and future work 171
6 Results IV: Characterising SARS-CoV-2 infection in paediatric and adult airway epithelial cells 173
6.1 Introduction 175
6.1.1 SARS-CoV-2 and COVID-19 in children and adults 175
6.1.2 The role of the airway epithelium and interferons in the defence against SARS-CoV-2 175
6.1.3 Towards understanding differences in COVID-19 severity between children and adults 176
6.1.4 Hypothesis and aims 177
6.2 Methods 178
6.2.1 Collection and culture of primary airway epithelial cells from healthy paediatric and adult donors 178
6.2.2 Infection of airway epithelial cultures with SARS-CoV-2 and H1N1 178
6.2.3 Analysis of the epithelial response to infection 179
6.3 Results 180
6.3.1 Establishing SARS-CoV-2 infection in nasal and bronchial epithelial cell ALI cultures 180
6.3.2 Comparing responses to SARS-CoV-2 infection between bronchial epithelial cells from healthy children and adults 182
6.3.3 Comparing epithelial cell responses to infection with SARS-CoV-2 and H1N1 186
6.3.4 Effects of viral infection on SARS-CoV-2 entry gene expression 192
6.4 Discussion 194
6.5 Concluding remarks and future work 198
7 Discussion 201
7.1 Aim and major findings of this thesis 203
7.1.1 EGFR signalling is induced by allergen exposure 203

7.1.2 Distinct roles for EGFR signalling in early life and adulthood 205
7.2 Overarching themes, limitations and future directions 206
7.2.1 A complex pathway requiring complex tools 206
7.2.2 The advantage of appropriate models 209
7.2.3 Translation and future directions 211
7.3 Concluding remarks 213
References 215
Appendix I: Publications arising from this thesis 245
Appendix II: Conference presentations arising from this thesis 247

List of Figures

Figure 1.1 Type 2 immune responses in (allergic) asthma (simplification). 27

Figure 1.2 Overview of major signalling pathways induced downstream of EGFR. 31

Figure 1.3 Characteristics and signalling modes of EGFR ligands. 33

Figure 2.1 Dead cell exclusion and gating strategy for myeloid cells. 55

Figure 2.2 Gating strategy for structural cells. 56

Figure 2.3 Gating strategy for lymphocytes. 56

Figure 3.1 *Egfr* and ligand expression during pre- and postnatal murine lung development. 77

Figure 3.2 *Egfr* and ligand expression levels in four major lung cell populations at different stages of lung development. 78

Figure 3.3 *EGFR* and ligand expression in the human lung. 80

Figure 3.4 *Egfr* and ligand gene expression in response to allergen or virus challenge. 82

Figure 3.5 Increased EGFR expression on immune and structural cells in the allergic lung. 84

Figure 3.6 Increased EGFR expression on T lymphocytes in the allergic lung. 86

Figure 3.7 EGFR ligand levels increase in lung homogenates but decrease in the airways during adult AAD. 87

Figure 3.8 EGFR ligand levels increase in lung homogenates but decrease in the airways during neonatal AAD. 88

Figure 3.9 Effects of allergen exposure on pulmonary EGFR activation. 90

Figure 3.10 Pulmonary EGFR activation immediately following ligand or allergen exposure. 91

Figure 3.11 HDM induced epithelial EGFR activation without affecting gene expression. 92

Figure 3.12 Epithelial-derived factors can drive fibroblast proliferation, which is partly EGFR-dependent. 93

Figure 3.13 EGFR ligands were present in airway samples from children with PSW or severe asthma. 95

Figure 4.1 Exogenous administration of AREG during acute IL-33-induced airway inflammation did not affect overall inflammation. 107

Figure 4.2 Exogenous administration of AREG during acute IL-33-induced airway inflammation resulted in mild decreases in lung function. 108

Figure 4.3 Exogenous AREG was detectable in bronchoalveolar lavage but did not alter airway or lung ligand levels. 109

Figure 4.4 Exogenous administration of AREG during acute HDM-induced AAD did not affect overall inflammation. 110

Figure 4.5 Exogenous administration of AREG during acute HDM-induced AAD did not affect lung function. 111

Figure 4.6 Exogenous AREG was detectable in bronchoalveolar lavage but did not alter airway or lung ligand levels. 112

Figure 4.7 Gefitinib administration was safe and able to suppress EGFR activation regardless of administration route. 113

Figure 4.8 EGFR inhibition during chronic HDM-induced AAD did not affect overall inflammation. .. 114

Figure 4.9 EGFR inhibition resulted in worsened lung function of PBS- but not HDM-treated animals. 115

Figure 4.10 EGFR inhibition during chronic HDM-induced AAD did not affect lung or airway levels of EGFR ligands. 117

Figure 4.11 EGFR inhibition during chronic HDM-induced AAD does not affect sensitisation or airway remodelling. 118

Figure 4.12 EGFR inhibition during early-life AAD altered lung EGFR and ligand levels. 119

Figure 4.13 EGFR inhibition during early-life AAD restricted monocytic inflammation. 120

Figure 4.14 EGFR inhibition during early-life AAD did not alter T cell responses. 122

Figure 4.15 EGFR inhibition during early-life AAD led to worsened airway hyperresponsiveness. ... 123

Figure 4.16 EGFR inhibition during early-life AAD had no effect on airway remodelling. 124

Figure 4.17 EGFR inhibition during early-life AAD did not alter matrix deposition but may change collagen geometry. 126

Figure 4.18 Type 2 responses were largely unaffected by EGFR inhibition during early-life AAD. ... 127

Figure 4.19 Correlation matrix of various parameters after EGFR inhibition during early-life AAD. .. 128

Figure 4.20 Network analysis of various parameters after EGFR inhibition during early-life AAD. ... 129

Figure 4.21 Exogenous EGFR activation during early-life AAD altered airway monocytic cells. 131

Figure 4.22 Exogenous EGFR activation during early-life AAD did not affect lung function. 132

Figure 4.23 Chronic exposure to mixed allergen during early life drives myeloid inflammation in lungs and airways. 133

Figure 4.24 Early-life mixed allergen exposure evoked extensive pulmonary T cell responses. 134

Figure 4.25 Early-life mixed allergen exposure resulted in airway hyperresponsiveness. 135

Figure 4.26 Early-life mixed allergen exposure elicited mucus hyperplasia and sensitisation. 136

Figure 4.27 Exogenous HB-EGF administration during mixed allergen challenge resulted in exacerbated neutrophilia and Th17 responses. 138

Figure 4.28 Exogenous HB-EGF administration during mixed allergen challenge did not affect airway hyperresponsiveness. 139

Figure 5.1 EGFR inhibition abrogated sex differences in early-life AAD. 152

Figure 5.2 Augmented IL-13 responses of female animals were abrogated by EGFR inhibition. 153

Figure 5.3 Female animals displayed EGFR-dependent increases in type 2 responses. 154

Figure 5.4 Heightened eosinophilia of female mice was dampened by EGFR inhibition. 155

Figure 5.5 EGFR inhibition rescued worsened baseline lung function of female animals. 156

Figure 5.6 Expression of remodelling-associated genes and allergic sensitisation during early-life AAD were sex-dependent. 157

Figure 5.7 Lung and airway levels of EGFR ligands displayed sex-dependent differences. 159

Figure 5.8 Type 2 immune responses of adult animals were comparable between sexes. 160

Figure 5.9 HDM exposure induced comparable airway hyperresponsiveness in adult males and females. 162

Figure 5.10 EGFR inhibition abrogated cytokine production in lymph node cultures from HDM-exposed animals. 164

Figure 5.11 Gonadal hormone concentrations throughout murine development. 166

Figure 5.12 EGFR inhibition abrogates augmented type 2 responses in young females: potential mechanism. 170

Figure 6.1 Fully differentiated nasal and bronchial epithelial cells displayed comparable morphology and SARS-CoV-2 entry factor expression. 180

Figure 6.2 Replication of and interferon responses elicited by SARS-CoV-2 were similar between nasal and bronchial epithelial cells. 181

Figure 6.3 Fully differentiated paediatric and adult bronchial epithelial cells displayed comparable morphology and SARS-CoV-2 entry factor expression. 183

Figure 6.4 SARS-CoV-2 primarily infected ciliated cells in paediatric and adult bronchial epithelial cell cultures. 184

Figure 6.5 Epithelial responses to infection differed between viruses but not between ages. 185

Figure 6.6 Infection with H1N1 but not SARS-CoV-2 resulted in altered epithelial morphology. 186

Figure 6.7 Both SARS-CoV-2 and H1N1 induced EGFR ligand expression in infected cells. 187

Figure 6.8 SARS-CoV-2 and H1N1 induced robust transcriptional interferon responses relative to viral replication. 188

Figure 6.9 SARS-CoV-2 elicited only mild induction of pro-inflammatory genes. 189

Figure 6.10 SARS-CoV-2 infection caused minimal protein release in contrast to H1N1. 190

Figure 6.11 Infection with H1N1 but not SARS-CoV-2 caused release of a range of proteins into the basal media. 191

Figure 6.12 H1N1 infection altered expression of SARS-CoV-2 entry-related genes. 193

Figure 6.13 SARS-CoV-2 infection is comparable between paediatric and adult bronchial epithelial cells but distinct from infection with H1N1. 194

Figure 7.1 Model of EGFR signalling in the allergen-exposed lung. 204

List of Tables

Table 2.1 Coefficient of determination (CoD) cut-offs used in the quality control of lung function data. ... 48

Table 2.2 Antibodies used for staining of extracellular antigens. ... 53

Table 2.3 Antibodies used for staining of intracellular antigens. ... 54

Table 2.4 Flow cytometry panel used to identify airway macrophages, other immune cells, epithelial cells and other structural cells. ... 57

Table 2.5 TaqMan™ assays used for gene expression analysis. ... 59

Table 2.6 List of commercially used ELISA kits used in this thesis. ... 60

Table 2.7 Antibodies and recombinant proteins used for 'homemade' sandwich ELISAs. ... 61

Table 2.8 Antibodies used for WB analysis. ... 62

Table 2.9 Antibodies used for immunofluorescence staining. ... 64

Table 3.1 Gene sets used to validate sorted cell populations. ... 73

Table 3.2 Demographics of donors used for transcriptome analysis of bronchial brushings. ... 75

Table 3.3 Demographics of donors used for gene expression analysis of BAL. ... 75

Table 6.1 Donor demographics. ... 178

List of Abbreviations

Abbreviation	Term
A	
AAD	Allergic airway disease
ACE2	Angiotensin converting enzyme 2
ADAM	A disintegrin and metalloprotease
Akt	Protein kinase B
ALI	Air-liquid interface
ALT	*Alternaria alternata*
AM	Airway macrophage
AR	Androgen receptor
AREG	Amphiregulin
B	
BAL	Bronchoalveolar lavage
BEC	Bronchial epithelial cell
BSA	Bovine serum albumin
BTC	Betacellulin
C	
C	Compliance
CAMK	Ca2+/calmodulin-dependent protein kinase
cDC2	Conventional dendritic cell
CoD	Coefficient of determination
COPD	Chronic obstructive pulmonary disease
COVID-19	Coronavirus disease 19
CPM	Counts per million
C_T	Cycle threshold
D	
DAG	Diacylglycerol
DC	Dendritic cell
DMEM	Dulbecco's Modified Eagle Medium
DMSO	Dimethyl sulfoxide
dpi	Days post-infection
DUOX1	Dual oxidase 1
E	
E	Elastance *or* Embryonic day
E2	β-Oestradiol
EGF	Epidermal growth factor
EGFR	Epidermal growth factor receptor
ELISA	Enzyme-linked immunosorbent assay
EPGN	Epigen
EREG	Epiregulin
ERK	Extracellular signal-related kinase
ERα	Oestrogen receptor alpha
ERβ	Oestrogen receptor beta
exTRAcrine	Exosomal targeted receptor activation

F

FACS	Flow-activated cell sorting
FBS	Foetal bovine serum
FEV_1	Forced exhaled volume in one second

G

G	Tissue damping
GINA	Global Initiative for Asthma
gMFI	Geometric mean fluorescence intensity
GPR30	G protein-coupled receptor 30
GRB2	Growth factor receptor-bound protein 2

H

H	Tissue elastance
H&E	Haematoxylin and eosin
HB-EGF	Heparin-binding EGF-like growth factor
HBSS	Hank's balanced salt solution
HDM	House dust mite
HLCA	Human Lung Cell Atlas
HP-β-CD	Hydroxypropyl-β-cyclodextrin

I

IAV	Influenza A virus
ICS	Inhaled corticosteroids
IFN	Interferon
IL	Interleukin
IL-4Rα	IL-4 receptor alpha chain
ILC2	Type 2 innate lymphoid cells
i.m.	intramuscular
IM/IMMs	Interstitial macrophages/inflammatory monocytes and macrophages
i.n.	Intranasal
i.p.	Intraperitoneal
IP_3	Inositol triphosphate
ISG	Interferon-stimulated gene
ITGB4	Integrin beta-4

L

L_m	Mean linear intercept
LN	Lymph node
LTRA	Leukotriene receptor antagonists

M

MAIT	Mucosal-associated invariant T
MAPK	Mitogen-activated protein kinase
MCh	Methacholine
MDA5	Melanoma differentiation-associated protein 5
moDC	Monocyte-derived DC
MOI	Multiplicity of infection
mTOR	Mammalian target of rapamycin

N

NEC	Nasal epithelial cell
NHLF	Normal human lung fibroblast
NP	Nucleocapsid protein
NRES	National Research Ethics Service
NSCLC	Non-small cell lung cancer

O

OCS	Oral corticosteroids
OD	Optical density
OVA	Ovalbumin

P

P	Postnatal day
PAS	Periodic acid-Schiff
PBS	Phosphate-buffered saline
PCA	Principal component analysis
PFA	Paraformaldehyde
PFU	Plaque-forming units
PI3K	Phosphoinositide 3-kinase
PKC	Protein kinase C
PLCγ	Phospholipase C gamma
PMA	Phorbol 12-myristate 13-acetate
p.o.	Per oral
PRR	Pattern recognition receptor
PSW	Pre-school wheeze

Q

qPCR	Quantitative polymerase chain reaction

R

R	Resistance
RBM	Reticular basement membrane
rho (ρ)	Rank correlation coefficient
RIG-I	Retinoic acid-inducible gene I
RIPA	Radioimmunoprecipitation
Rn	Newtonian resistance
RPMI	Roswell Park Memorial Institute
RSV	Respiratory syncytial virus
RV	Rhinovirus

S

SABA	Short-acting β agonists
SARS	Severe acute respiratory syndrome
SARS-CoV(-2)	Severe acute respiratory syndrome coronavirus (2)
SH2	Scr Homology 2
SHC	SHC adaptor protein
SHG	Second-harmonics generation
SNP	Single-nucleotide polymorphism
SP-C	Surfactant protein C
STAT	Signal transducer and activator of transcription
STRA	Severe therapy-resistant asthma

T

T2	Type 2
TBS	Tris-buffered saline
TG	Timothy grass
TGFA	Transforming growth factor alpha
Th	T helper cell
TKI	Tyrosine kinase inhibitor
TMPRSS2	Transmembrane serine protease 2
Treg	Regulatory T cell
TSLP	Thymic stromal lymphopoietin
TTF-1	Thyroid transcription factor-1

W

WB	Western blot(ting)
WHO	World Health Organisation
WT	Wildtype

1 Introduction

1.1 Asthma

1.1.1 Definition, incidence and aetiology

Asthma is a chronic respiratory disease with an incidence ranging from 2-4% in Asian countries to up to 20% in the UK and other developed countries, amounting to over 250 million cases worldwide[1]. According to the Global Initiative for Asthma (GINA), the condition is defined as variable expiratory airflow limitation in patients with a history of respiratory symptoms such as shortness of breath, chest tightness, wheezing and cough[2]. Although reversibility of airflow obstruction was previously considered a key feature of asthma, irreversible airflow obstruction has been reported in subjects with severe asthma, likely due to the presence of mucus plugs within the airways[3]. Acute exacerbations of asthma (also known as “asthma attacks”) can be triggered by allergen exposure, tobacco smoke, respiratory infections, pollution, chemicals or even exercise or cold air, commonly require the use of medication to achieve relief and can, in serious cases, result in hospitalisation or death.

Asthma is a highly heterogeneous disease and as such encompasses many different aetiologies and clinical phenotypes. Although disease onset can occur at any point in life, with adult-onset often associated with higher severity, faster decline in lung function and absence of atopy[4], asthma develops during early childhood in the vast majority. It is estimated that 80% of cases begin within the first six years of life[5]. Due to the difficulty of definitively diagnosing asthma in very young children, recurrent episodes of wheeze and breathing difficulty seen in children under the age of six are termed pre-school wheeze (PSW)[6]. Although multiple factors can cause wheezing in pre-school children, by far the most common trigger for wheezing is viral respiratory tract infections, which cause episodic wheeze. These episodes are most commonly provoked by infection with respiratory syncytial virus (RSV) or rhinovirus (RV) along with human metapneumovirus and seasonal coronaviruses[7, 8]. Importantly, recurrent viral infections in pre-school children, especially with RSV or RV, are associated with an increased risk of developing asthma[8-11]. Approximately one third of pre-school children wheeze during viral infections, with around 40% of those wheezers going on to develop asthma[12], yet the underlying decisive factors for disease progression remain poorly understood. Of note, children with PSW already display key features of asthma pathology, such as eosinophilic airway inflammation and thickening of the reticular basement membrane (RBM)[13]. These features are further exaggerated in school-aged children with difficult-to-treat or severe therapy-resistant asthma (STRA), whose RBM thickening is comparable to adults with asthma[14, 15]. Importantly, deficits in lung function developed during the first years of life were shown to persist into adulthood[16, 17], conveying urgency to study the mechanisms underlying the development of PSW and asthma in early life.

In addition to early-life respiratory infections, various factors have been implicated in inferring an increased risk of asthma development[18]. Several genetic variants have been associated with asthma risk, including single-nucleotide polymorphisms (SNPs) in the regions of *ORMDL3*/*GSDMB* (specific to childhood-onset asthma), *HLA-DQ*, *IL33*, *IL1RL1*/*IL18R1*, *SMAD3* and *IL2RB*[19]. In addition, both the prevalence and severity of asthma differ between the sexes in an age-dependent manner, wherein males exhibit worse disease during childhood and females display higher incidence and disease severity in adulthood[20, 21]. Further risk factors suggested to affect the development of asthma include atopy, prenatal (maternal) and postnatal tobacco exposure, pollution, antibiotic use, diet, nutrition and obesity[18]. Whereas atopy is less common in adult-onset asthma, exposure to occupational allergens such as cleaning solutions, latex or flour dust can increase the risk of asthma development in adults. Nevertheless, the exact causes of the disease remain elusive and will conceivably differ from patient to patient.

1.1.2 Clinical phenotypes and endotypes

Historically, asthma was thought to be a single disease characterised by atopy, eosinophilia and Th2-driven inflammation. However, it is now well-accepted that the term asthma encompasses various conditions with varying observable features (phenotypes) and underlying biological pathways (endotypes). For example, asthma pheno- and endotypes can be grouped by age of onset (early onset vs. late onset), atopy (atopic vs. non-atopic), the presence of type 2 (T2) inflammation (T2 high vs. T2 low), the kind of inflammation present (eosinophilic, neutrophilic, mixed granulocytic or pauci-inflammatory) or disease triggers (e.g. exercise-induced, obesity-related or aspirin-intolerant)[22-24]. Further distinctions have been identified in patients with severe asthma by unsupervised clustering of clinical parameters, including the response to corticosteroid therapy[25]. Severe asthma is defined as asthma that requires treatment with a second controller or systemic corticosteroids in addition to high-dose inhaled corticosteroids to reach control or asthma which remains uncontrolled despite such therapy[26]. Based on the growing appreciation for the great complexity and heterogeneity of asthma, efforts are being made to define phenotypes that can be linked to the underlying biological mechanisms and thus aid in the development and selection of appropriate therapies.

1.1.3 Molecular mechanisms of asthma pathology

The defining element of asthma is variable airflow obstruction due to a reduction in the diameter of the airways, which is usually reversible with bronchodilators. Other hallmark features with varying presence between asthma phenotypes include chronic inflammation, airway hyperresponsiveness, structural remodelling of the airway wall, such as goblet cell

hyperplasia, increased airway smooth muscle mass and excessive deposition of extracellular matrix, and often also allergic sensitisation. A feature observed across all phenotypes of asthma is epithelial damage, which can be caused by allergens, especially protease-rich ones such as house dust mites or cockroaches, or, in the case of non-allergic asthma, pollutants and microbes[27]. In response to these insults, epithelial cells release a host of mediators, including cytokines and chemokines[28]. The most prominent among these are the so-called 'alarmins' interleukin-33 (IL-33), thymic stromal lymphopoietin (TSLP) and IL-25. IL-33 and TSLP were found to be increased in the bronchoalveolar lavage (BAL) of patients with asthma and both alarmins, but especially IL-33, correlated with the level of lung function decline observed in these patients[29]. In contrast, IL-25 expression was found to be elevated in the bronchial epithelium of a subset of patients with T2-high asthma and good steroid responsiveness[30]. Interestingly, single nucleotide polymorphisms in loci of *IL33* and *IL1RL1* that encode IL-33 and its receptor ST2 are among the genetic variants most strongly associated with asthma risk[19]. In addition, mouse models have shown that intranasal administration of either IL-33 or IL-25 is sufficient to induce key features of asthma pathology, such as airway inflammation, remodelling, airway hyperresponsiveness, neoangiogenesis and expression of type 2 cytokines, although the latter two were only observed after IL-33 treatment[31]. Together these findings suggest that the epithelial release of alarmins, especially IL-33, is likely central to the pathophysiology of various phenotypes of asthma.

Animal models have been a useful tool in the study of the pathophysiology of allergic asthma. A commonly used model involves the peripheral sensitisation of rodents, generally mice, with the model antigen ovalbumin (OVA), followed by an airway challenge, during which OVA is administered intranasally, via the trachea or as an aerosol[32]. Although this approach models key features of asthma biology, such as airway hyperresponsiveness, airway inflammation, especially eosinophilia, the production of type 2 cytokines and allergic sensitisation, it has been criticised not just because peripheral sensitisation is not clinically relevant, but also due to its inability to cause persistent pathology, particularly airway remodelling[33]. These shortcomings were overcome when allergic airway disease (AAD) was instead induced using chronic inhaled exposure to the clinically relevant allergen house dust mite (HDM), which induced severe eosinophilia and type 2 inflammation as well as airway remodelling and airway hyperresponsiveness that persisted even beyond cessation of allergen exposure[34]. Both AAD models, as well as hybrid models combining peripheral sensitisation with chronic allergen challenge, are routinely used within the literature.

These approaches have provided valuable insights into the role of type 2 cytokines such as IL-4, IL-5 and IL-13 in driving pathological features of asthma[28]. These cytokines can be produced by type 2 innate lymphoid cells (ILC2s) or type 2 helper T cells (Th2 cells) directly

in response to IL-33, TSLP or IL-25 within the lung or after activation by conventional type 2 dendritic cells (cDC2s) within the lymph nodes, respectively[35-39]. Activated basophils, mast cells and eosinophils provide an additional source of type 2 cytokines[40]. IL-4 plays a major role in allergic sensitisation by inducing class switching of B cells to IgE and contributes to eosinophil extravasation via the upregulation of adhesion molecules on the vessel wall[41]. Antigen-mediated cross-linking of IgE molecules captured by basophils or mast cells expressing the high-affinity IgE receptor FcεRI triggers their activation and release of mediators, which include histamines, proteases and type 2 cytokines[40]. These molecules can support cell recruitment by increasing vascular permeability and contribute to airway remodelling by inducing mucus production in goblet cells and an increase in smooth muscle mass[40, 42]. In addition, IgE can act directly on smooth muscle cells to induce their proliferation, contraction and secretion of cytokines and chemokines[43]. IL-5 drives the maturation of eosinophils in the bone marrow and also induces their activation within the tissue, triggering the release of various mediators such as the toxic proteins, pro-inflammatory and type 2 cytokines, lipid mediators and fibrinogenic factors, several of which have been implicated in driving airway hyperresponsiveness and remodelling[44]. In addition to its known ability to cause airway hyperresponsiveness and drive mucus hyperplasia[45, 46], IL-13 has recently been suggested to disrupt epithelial barrier function via the breakdown of tight junction molecules[47]. The most important players of the type 2 response in asthma are summarised in **Figure 1.1.**

While the contributions of type 2 cytokines and associated cells to asthma pathophysiology have been well-defined, particularly with the help of mouse models, less is known for example about the role of IL-17 or neutrophils. The fact that many AAD models, especially the OVA sensitisation/challenge approach, primarily or exclusively drive type 2 inflammation has made the study of these pathways *in vivo* challenging with current models. While chronic allergen exposure can drive neutrophilia and Th17 responses[48], these are induced in concert with type 2 inflammation and thus reflect a mixed granulocytic rather than a T2-low phenotype of asthma. The use of existing models has produced conflicting results regarding the role of IL-17 in asthma, with different studies reporting the cytokine to be either protective[49, 50], pathogenic[51] or irrelevant[52] in various models of AAD. Similarly, researchers are unsure whether the presence of neutrophils during asthma is beneficial, detrimental or inconsequential[53]. Nevertheless, the presence of both neutrophils and IL-17 in patients with asthma is associated with more severe disease phenotypes[54, 55], underscoring the urgent need for the development of novel *in vivo* models of neutrophilic asthma that allow the study of the underlying pathophysiology. The same urgency applies to the development of models reflecting other phenotypes of T2-low asthma, such as obesity-associated or smooth-muscle mediated, pauci-granulocytic asthma, as the biological processes driving disease in these patients also remain

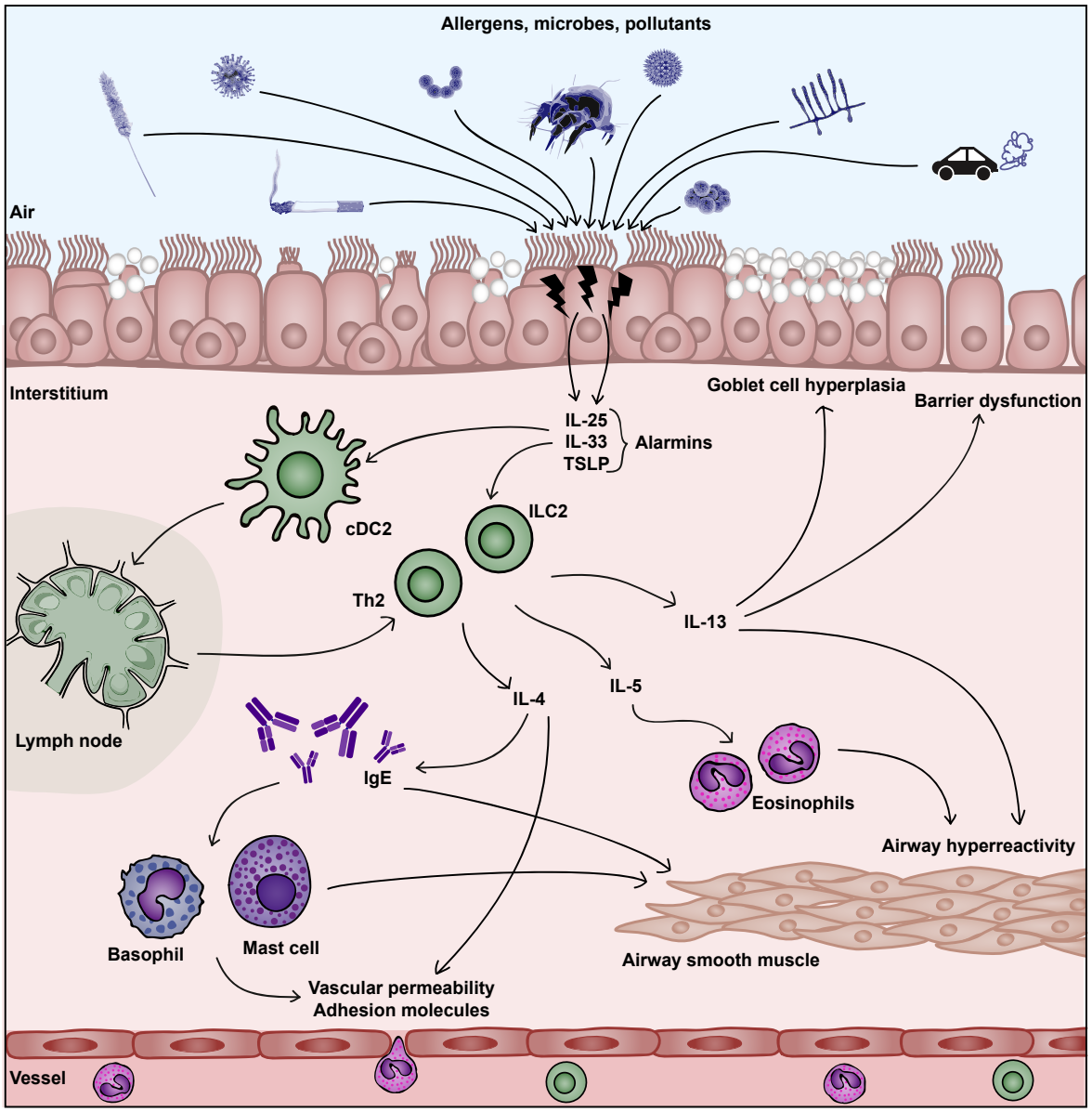


Figure 1.1 Type 2 immune responses in (allergic) asthma (simplification).
Epithelial damage is caused by exposure to allergens, pollutants or microbes and results in the release of alarmins (IL-25, IL-33, TSLP) from airway epithelial cells. These can act on cDC2s, which travel to the lymph node where they activate Th2 cells, or directly activate ILC2s. These type 2 lymphocytes produce the type 2 cytokines IL-4, IL-5 and IL-13. IL-4 can drive IgE production by inducing B cell class switching and contributes to eosinophil extravasation. Antigen-mediated IgE cross-linking activates basophils and mast cells to release a host of mediators, which contribute to vascular permeability and induce an increase in airway smooth muscle mass. IL-5 is crucial for the development and survival of eosinophils, which can drive airway remodelling and hyperreactivity. IL-13 can induce goblet cell hyperplasia, airway hyperreactivity and contributes to barrier dysfunction via the breakdown of epithelial tight junction molecules.

poorly understood. Finally, the majority of *in vivo* studies utilise adult animals and thus fail to reflect a striking feature of the majority of patients with asthma: the onset of the disease during childhood. Work from our group has demonstrated that the inception of early-life AAD in neonatal mice depends on the presence of IL-13^{+} CD4 T cells, whereas IL-13 production from ILC2s was sufficient to induce disease in adult animals[56]. We have also shown that the microbiome plays an important part in educating the immune system and modulating the risk of asthma development: whereas pups exposed to inhaled HDM from day three of life

exhibited exacerbated allergic airway inflammation, mice at two weeks of age showed reduced susceptibility to type 2 inflammation, driven by changes in the abundance and composition in the airway microbiome[57]. In contrast, others have found that, compared to adults, mouse pups of two weeks of age were characterised by an increased production of IL-33 in the lungs which resulted in Th2 cell skewing via the spontaneous activation of type 2 cells by $CD11b^+$ cDCs and was further exacerbated by exposure to HDM[58]. Despite the somewhat conflicting findings regarding the time frame for increased susceptibility to the development of type 2 responses in early life, these studies illustrate that the mechanisms underlying asthma pathology are likely distinct between childhood and adulthood, not least due to changes in the airway microbiome, and highlight the need to study asthma biology in early life by using appropriate models in neonatal mice. Overall, a better understanding of the disease-driving mechanisms will be key to distinguishing different asthma endotypes and refining current treatment strategies, thus improving the quality of life for patients with asthma.

1.1.4 Current treatment strategies

Perhaps not surprisingly given the great heterogeneity in asthma pheno- and endotypes, there is currently no cure for asthma. Nevertheless, several different treatments are available to patients to relieve and control symptoms. Commonly used 'relievers' are short-acting β-agonists (SABA), which act directly on the β2-receptor expressed on smooth muscle cells, causing muscle relaxation and dilation of the airways. Their use for 'as needed' symptom relief was previously recommended for patients across all levels of asthma severity. However, SABA-only treatment of asthma has since been associated with an increased risk of exacerbations and asthma-related death, which prompted GINA to update its guidance on the management of asthma in 2019 to recommend that patients should not be treated with SABA alone[59]. Instead, the use of SABA should be accompanied or replaced by treatment with inhaled corticosteroids (ICS). ICS are another mainstay therapy for asthma and are considered among the most effective controllers of the disease due to their ability to suppress airway inflammation and alleviate airway hyperresponsiveness[60]. GINA recommends their use together with long-acting β-agonists, which have a longer duration of 12 hours compared to the 3-6 hours achieved by SABA, either as needed or daily, depending on the severity of the disease[59]. Another class of drugs available for asthma control are leukotriene receptor antagonists (LTRA), which counteract the ability of cysteinyl leukotrienes to cause bronchoconstriction, airway hyperresponsiveness, eosinophil recruitment, mucus production and vascular permeability[61]. If these treatments are insufficient to provide asthma control, systemic corticosteroids, usually prescribed as oral tablets, can be used for asthma management either long-term or during severe exacerbations[62]. Nevertheless, in nearly a fifth

of adults with asthma, the disease remains uncontrolled despite high doses of ICS in combination with oral corticosteroids (OCS), which is termed difficult-to-treat asthma. While modifiable factors such as poor adherence, incorrect inhaler technique, smoking, comorbidities or persistent allergen exposure can contribute to poor control, around 5-10% of adults suffer from severe asthma, where symptoms are poorly controlled despite maximal therapy and good adherence and inhaler technique[26].

Various biologics have been developed for the treatment of severe asthma, the majority of which target type 2 inflammation[63]. The first biologic to be approved for use in asthma was Omalizumab, which is directed against IgE. Omalizumab was shown to be effective in improving lung function and reducing severe exacerbations and OCS usage in around 70% of patients with moderate-to-severe asthma[64] and is currently used for severe persistent allergic asthma. However, many patients with severe asthma do not qualify for treatment with Omalizumab due to their IgE levels being outside the recommended range, creating the need for alternative therapies. Three monoclonal antibodies targeting IL-5 signalling and thus eosinophilia have been approved for use in severe eosinophilic asthma. While Mepolizumab and Reslizumab target IL-5 directly, Benralizumab induces cytotoxicity in eosinophils and basophils by binding to the IL-5 receptor alpha chain[65]. Dupilumab, a monoclonal antibody against the IL-4 receptor alpha chain (IL-4Rα), which can form a heterodimer with both the common gamma chain to promote IL-4 and the IL-13R to facilitate IL-13 signalling, is currently used for the treatment of severe asthma with type 2 inflammation, as well as moderate-to-severe atopic eczema and severe chronic rhinosinusitis with nasal polyps[66]. Given that Tralokinumab and Lebrikizumab, two biologics targeting IL-13 signalling, failed to show efficacy in phase III trials[67, 68], it is likely that Dupilumab exerts its function by interfering with IL-4 signalling. While these therapies show efficacy in patients with T2-high asthma, approved biologics for the treatment of T2-low asthma are lacking in the UK. Nevertheless, promising results have been achieved in a phase III trial of Tezepelumab[69], a monoclonal antibody targeting TSLP, in adolescents and adults with severe asthma, which has resulted in the approval of this therapy in the US and EU within the last year. Importantly, Tezepelumab reduced asthma exacerbations even in patients with low eosinophil counts[69], making it the first effective biologic treatment for patients with T2-low asthma. In addition to TSLP, therapies targeting other alarmins have also been developed. Itepekimab, an anti-IL-33 antibody, showed some efficacy in patients with moderate-to-severe asthma during phase I and II trials[70, 71], however, phase III trials were aborted[72] and it is no longer pursued for the treatment of asthma. Similarly, Astegolimab, which targets the IL-33 receptor ST2, reduced the rate of asthma exacerbations in adults with severe asthma, including those with low eosinophil counts in a phase IIb trial[73] but further trials are currently only planned to investigate its use in chronic

obstructive pulmonary disease[74]. Together, these findings somewhat surprisingly suggest that targeting IL-33 signalling may not be an effective strategy in the treatment of severe asthma. Overall, there remains a pressing need for the development of novel treatments for patients with T2-low asthma, especially since previous attempts at targeting neutrophilic inflammation by blocking CXCR2, TNFα or IL-17RA have failed to show efficacy[75]. In light of the great heterogeneity of asthma endo- and phenotypes, a better understanding of the underlying pathophysiology will be required to aid the development of novel therapies.

Of the currently licenced biologic therapies, only three are available in the UK for the treatment of asthma in children over six (Mepolizumab, anti-IL-5 and Omalizumab, anti-IgE) or twelve years of age (Dupilumab, anti-IL-4Rα)[76]. Given that asthma develops during early childhood in the vast majority of affected individuals and can result in long-lasting deficits in lung function, greater efforts should be made to better understand the pathophysiology of childhood-onset asthma and develop novel therapies targeted at preventing the progression from childhood to adult asthma and providing long-term improvements in lung function.

1.2 Epidermal growth factor receptor (EGFR)

1.2.1 EGFR activation and canonical signalling pathways

The epidermal growth factor receptor (EGFR), also known as ErbB1 or HER1, is a tyrosine kinase of the ErbB family of growth factor receptors, which also includes ErbB2, ErbB3 and ErbB4. EGFR consists of an extracellular ligand-binding domain, a transmembrane α-helix and an intracellular tyrosine kinase domain. Upon ligand binding, the EGFR molecule forms a dimer either with a second EGFR molecule (homodimerization) or with another member of the ErbB family (heterodimerization)[77] (**Figure 1.2A**). This dimerization is necessary for the allosteric activation of the tyrosine kinase and leads to the cross-phosphorylation of the receptor molecules[78]. The resultant phosphorylated tyrosine residues act as docking sites for various adaptor molecules that induce a myriad of complex signalling cascades downstream of EGFR[79, 80] (**Figure 1.2B**). For example, phospholipase C gamma (PLCγ) can be recruited to tyrosine residues Y992 and Y1173 and activated through phosphorylation, leading to the generation of the secondary messenger molecules inositol triphosphate (IP_3), which triggers the release of Ca^{2+} from the endoplasmic reticulum, and diacylglycerol (DAG), ultimately resulting in the activation of Ca^{2+}/calmodulin-dependent protein kinase (CAMK) and protein kinase C (PKC). The mitogen-activated protein kinase (MAPK)/extracellular signal-regulated kinase (ERK) pathway constitutes what is probably the most important biological response

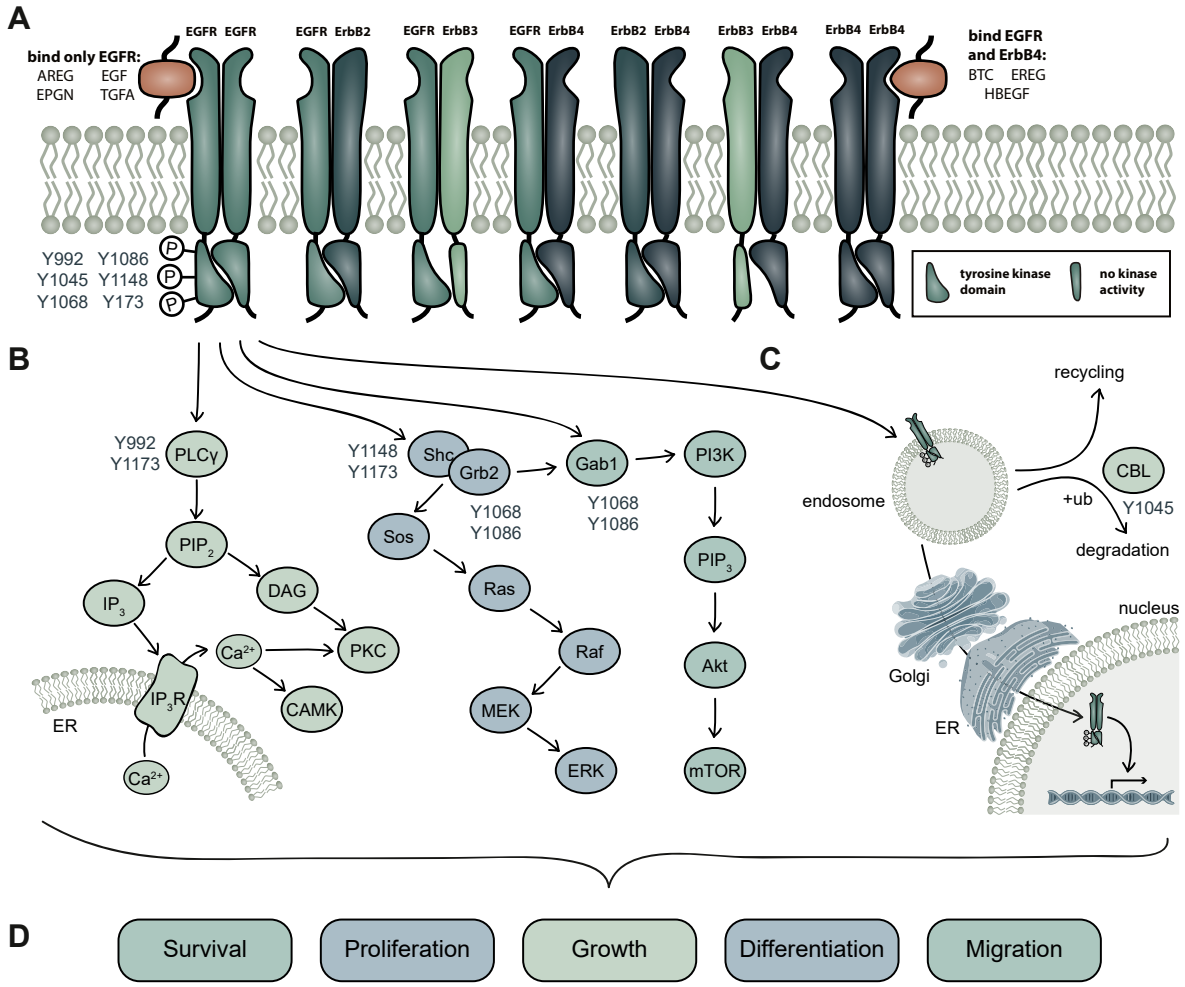


Figure 1.2 Overview of major signalling pathways induced downstream of EGFR.
A Upon ligand binding, EGFR can form homodimers or heterodimers with other members of the ErbB family, which results in the phosphorylation of intracellular tyrosine residues (denoted by "Y"). **B** Simplification of major signalling pathways induced by EGFR. Activated EGFR can amongst others induce the phospholipase pathway, the ERK/MAPK pathway or the PI3K-Akt-mTOR pathway. Phosphorylated tyrosine residues acting as docking sites are denoted next to downstream signalling molecules. **C** Upon activation, EGFR is internalised into endosomes from where it can either be recycled, degraded or trafficked to the nucleus via the golgi apparatus and the endoplasmic reticulum (ER), where it acts as a transcriptional co-activator for several pro-oncogenes. **D** EGFR signalling modulates a myriad of key cellular functions, including survival, proliferation, growth, differentiation and migration. **Abbreviations:** AREG, amphiregulin; BTC, betacellulin; EGF, epidermal growth factor; EGFR, EGF receptor; EPGN, epigen; EREG, epiregulin; HB-EGF, heparin-binding EGF-like growth factor; TGFA, transforming growth factor alpha; Y; tyrosine residue; PLCγ, phospholipase C gamma; PIP_2, phosphatidylinositol biphosphate; IP_3, inositol trisphosphate; IP_3R, IP_3 receptor; DAG, diacyl glycerol; PKC, protein kinase C; CAMK, Ca2+/calmodulin-dependent protein kinase; Shc, SHC adaptor protein; Grb2, growth factor receptor-bound protein 2; Sos, son of sevenless guanine nucleotide exchange factor; Ras, Ras small GTPase; Raf, RAF proto-oncogene serine/threonine-protein kinase; MEK, mitogen-activated protein kinase kinase; ERK, extracellular signal-regulated kinase; Gab1, Grb2-associated protein 1; PI3K, Phosphoinositide 3-kinase; Raf, RAF proto-oncogene serine/threonine-protein kinase; PIP_3, phosphatidyl trisphosphate; Akt, protein kinase B; mTOR, mammalian target of rapamycin; CBL, E3 ubiquitin-protein ligase CBL; ER, endoplasmic reticulum.

induced by EGFR signalling[80] and is induced when phosphorylated tyrosine residues Y1068 and Y1086 or Y1148 and Y1173 in EGFR are bound by growth factor receptor-bound protein 2 (Grb2) or SHC adaptor protein (Shc), respectively, both of which contain a Src Homology 2 (SH2) domain[81]. Y1068 and Y1086 also act as a docking site for Grb2-associated protein 1 (Gab1), which, when phosphorylated, can recruit the p85 subunit of phosphoinositide 3-kinase

(PI3K) and thus initiate the protein kinase B (Akt) pathway that results in mammalian target of rapamycin (mTOR) signalling. Overall, the EGFR signalling pathway is thought to comprise 211 reactions between 322 molecules, including 202 proteins and various ions, oligomers, genes and RNAs[82]. The consequences of such complex signalling are manifold, modulating a number of key biological effects including cell survival, proliferation, growth, differentiation and migration[80] (**Figure 1.2D**).

EGFR activation also results in the rapid internalisation of the receptor via various routes, including clathrin- and caveolae-mediated endocytosis[83] (**Figure 1.2C**). Receptor molecules reach the endosome, where the signalling can continue, and from there they are either recycled to the plasma membrane or, if they have been ubiquitinated by the E3 ubiquitin-protein ligase CBL, targeted to the lysosome for receptor degradation. Interestingly, EGFR can also be translocated from the endosome via the Golgi apparatus and endoplasmic reticulum to the nucleus, where it supports gene expression by acting as a transcriptional co-activator[84] (**Figure 1.2C**). Target genes of nuclear EGFR signalling include *CCND1* and *MYC* (encoding cyclin D1 and c-Myc, respectively), which support cell-cycle progression, as well as several other proto-oncogenes implicated in promoting cancer development[84].

1.2.2 EGFR ligands

There are seven known ligands for EGFR: amphiregulin (AREG), betacellulin (BTC), epidermal growth factor (EGF), epigen (EPGN), epiregulin (EREG), heparin-binding EGF-like growth factor (HB-EGF) and transforming growth factor alpha (TGFα). Of these, BTC, EREG and HB-EGF can also bind to and activate ErbB4[85]. Despite sharing a receptor, the seven ligands were shown to induce disparate biological responses both *in vitro* and *in vivo*[86]. Distinctions between the ligands for example lie in their affinities for EGFR: while BTC, EGF, HB-EGF and TGFA are considered high-affinity ligands, AREG, EREG and EPGN exhibit low affinity for EGFR[87] (**Figure 1.3A-B**). The various ligands further differ in their ability to induce EGFR dimerisation, with low dimerisation capacities exhibited by EREG and particularly EPGN[88]. These discrepancies in the ability to induce dimerisation between the ligands translate to varying lengths of signalling and preferences for inducing receptor internalisation, degradation or recycling, whereby strong inducers of receptor dimerisation tend to favour transient signalling followed by rapid internalisation and degradation of the receptor[88-95] (**Figure 1.3B**). In addition to the strength of dimerisation induced by ligand binding, further factors such as EGFR-ligand saturation (i.e. one or two ligand molecules bound per dimer depending on the concentration of ligand present), local receptor density, spatial organisation and levels of negative feedback regulation through protein tyrosine phosphatases 'fine-tune' the cellular signalling fate following EGFR activation[96]. The ability of cells to integrate these

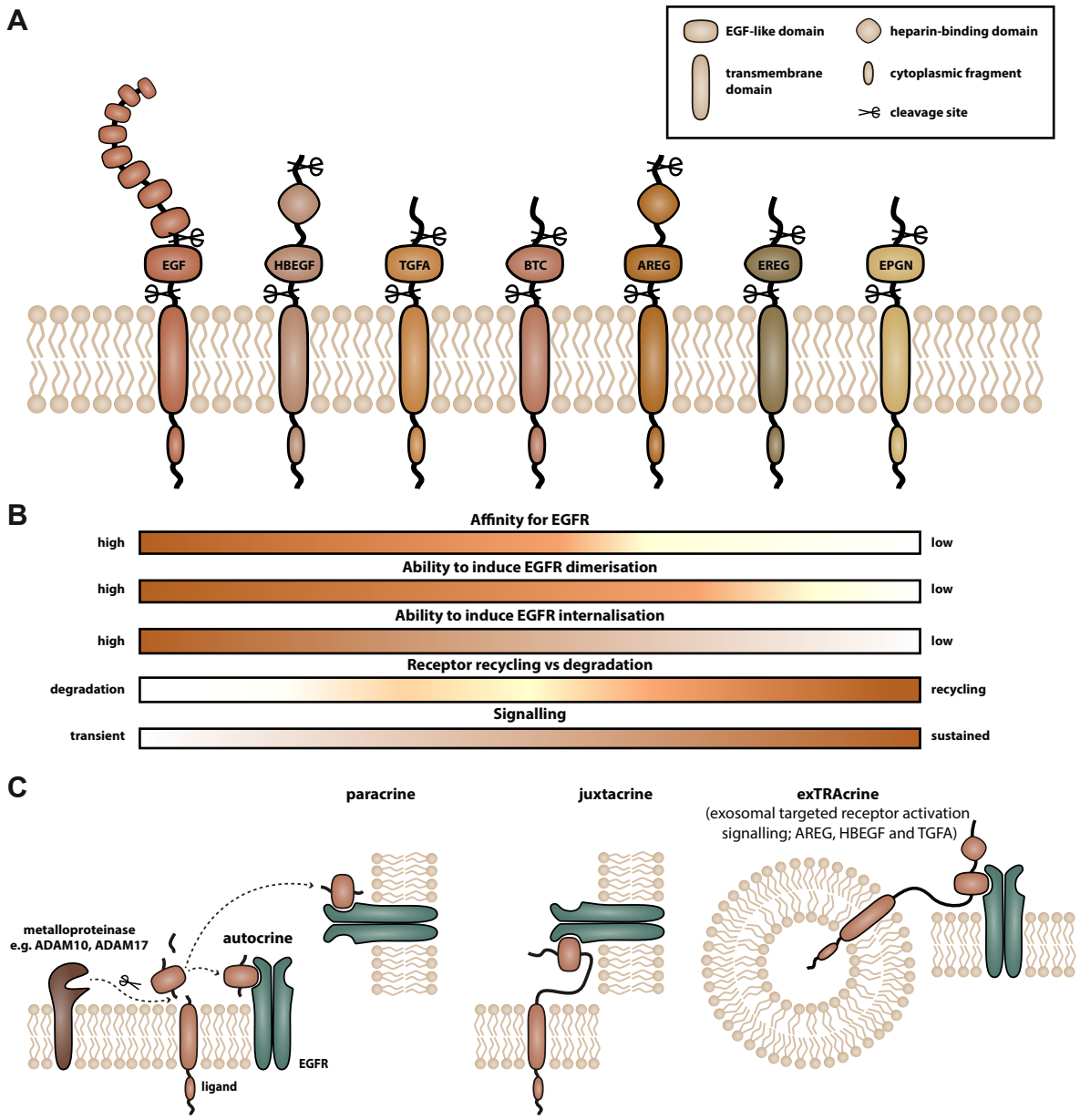


Figure 1.3 Characteristics and signalling modes of EGFR ligands.
A EGFR ligands are produced as type 1 membrane precursors. While all ligands contain an EGF-like domain, only AREG and HB-EGF also contain a heparin-binding domain. **B** EGFR ligands differ in their affinity for the receptor and their ability to induce EGFR dimerisation, which translates into varying induction of receptor internalisation, degradation and signalling durations. **C** EGFR ligands require cleavage by metalloproteinases such as ADAM10 or ADAM17 ('ectodomain shedding') for release from the plasma membrane and auto- or paracrine signalling. BTC, HB-EGF and TGFα can also signal in a juxtacrine manner, which is independent of ectodomain shedding. exTRAcrine signalling occurs when AREG, HB-EGF or TGFα are packaged into exosomes and bind to EGFR on target cells, thereby inducing their internalisation.

various signals explains the divergence in the functional consequences of EGFR engagement, which can induce opposing outcomes such as cell proliferation (transient signalling) or differentiation (sustained signalling) depending on the circumstances[88]. On a molecular level, EGFR ligands also differ in their recruitment of downstream signalling proteins independently of their affinity for the receptor[97] and studies have shown that certain ligands, particularly HB-EGF, displayed a superior ability compared to other ligands to induce activation of Akt and

PLCγ in HeLa cells[98]. In line with this, several reports have described divergent phosphorylation profiles induced by the various ligands, whereby treatment with certain ligands, especially those of low affinity, only resulted in the phosphorylation of a subset of tyrosine residues in the cytoplasmic tail of EGFR[99-103]. Signalling induction was further shown to be dependent on the concentration of ligand present, whereby low concentrations favoured the activation of PLCγ and signal transducers and activators of transcription (STATs) while high concentrations induced most canonical signalling pathways[104].

Adding to the complexity of EGFR signalling, the various ligands differ in their structure, release and the manner in which ligand-receptor interactions occur. While all seven EGFR ligands contain at least one EGF-like domain[90], AREG and HB-EGF also contain a heparin-binding domain, which has been suggested to aid in the localisation of ligands to the point of cell-cell contact and restrict their proteolytic release[105, 106]. EGFR ligands are synthesised as type 1 transmembrane precursors and as such require extracellular domain cleavage for the release of soluble ligands[85] (**Figure 1.3A**). This process, which is commonly referred to as ectodomain shedding, is primarily mediated by members of the a disintegrin and metalloprotease (ADAM) family and can be induced for example by stimulation with phorbol 12-myristate 13-acetate (PMA)[107]. While ADAM17 conveys cleavage of the majority of EGFR ligands, including AREG, EREG, EPGN, HB-EGF and TGFα, ADAM10 was shown to cleave BTC and EGF and ADAM9, -12 or -15 also contributed to ectodomain shedding of EREG[107-109]. Once cleaved, the ligands can induce EGFR activation in an autocrine or paracrine manner (**Figure 1.3C**). Nevertheless, juxtacrine signalling, which does not require ectodomain shedding of the EGFR ligands, has also been reported for BTC, HB-EGF and TGFα[110-113], is thought to depend on the membrane-anchoring domain of these ligands and typically occurs at the site of cell-cell contact[114]. A final mode of signalling termed exosomal targeted receptor activation (exTRAcrine) signalling occurs when AREG, HB-EGF or TGFα are packaged into exosomes in full-length form and induce their internalisation by target cells via interaction with EGFR, a process thought to contribute to the invasiveness of cancer cells[115]. Importantly, exosomal delivery of EGFR ligands was shown to be more effective than soluble ligands regarding the strength and duration of signalling induced, likely because ligands are more highly concentrated and can travel further distances when contained in extravesicular vesicles compared to the limited diffusion of free ligand molecules[96, 116]. While reports of exTRAcrine signalling of EGFR primarily stem from the field of cancer research, it will be interesting to delineate how this signalling mode contributes to the role of EGFR in shaping various immune responses.

1.2.3 Cellular expression patterns of EGFR and its ligands

EGFR was identified in an epidermoid carcinoma cell line[117], hence its designation as *epidermal* growth factor receptor. Its expression however is not restricted to epidermal cells. EGFR is expressed across all tissue types and is most abundant in epithelial and other structural cells[118]. Nevertheless, EGFR expression has also been detected in several different immune cells, such as monocytes[119], macrophages[120-123], neutrophils[124], plasma cells[125] and CD4 T cells[126], particularly Th2 cells[127] and regulatory T cells (Tregs)[128]. Importantly, immune cell expression of EGFR was not only observed in the context of cancer but also atherosclerosis, bacterial or helminth infection and dermatitis as well as during homeostasis[121, 126-128], and EGFR signalling appears to have a unique role in immune cells. Whereas the canonical consequences of EGFR activation, which have primarily been described in parenchymal (cancer) cells, include proliferation, differentiation, growth, migration and survival, a growing number of specialised functions of EGFR signalling in immune cells have been described, such as enhancing the suppressive capacity of Tregs *in vitro* and *in vivo* and conferring activated Th2 cells the ability to produce IL-13 in a TCR-independent manner during helminth infection[127, 128]. These findings illustrate that the relevance of EGFR activation extends beyond the canonical consequences studied *in vitro* and underline the importance of exploring the role of EGFR in various cell types and contexts of health and disease in appropriate *in vivo* models.

In addition to the receptor, immune cells also express a range of EGFR ligands. AREG is the most extensively studied EGFR ligand in the context of immune responses. It is primarily produced by cells of the type 2 immune response, such as ILC2s[129-134], Th2 cells[127, 135, 136], mast cells[128, 137, 138], basophils[139, 140] and eosinophils[141] and is therefore widely considered a type 2 cytokine. However, AREG expression is also found on other subsets of T cells, including Th1 cells[142], CD8 T cells[142, 143] and especially Tregs[132, 144-147] as well as being expressed by macrophages[148-151], dendritic cells[152] and neutrophils[153]. Less is known about the expression of the other EGFR ligands within the immune system. Nevertheless, studies have found that HB-EGF can be produced by synovial macrophages, ILC3s, mucosal-associated invariant T (MAIT) cells and conventional CD4 T cells[154-157], the latter of which also expressed EREG and TGFα[158]. However, more thorough analyses are needed to characterise the expression of all seven EGFR ligands by the various cells of the immune system.

1.2.4 EGFR signalling in health and disease

EGFR is vital for organogenesis and overall survival, exemplified by the fact that global deletion of EGFR in mice results in lethality either during the foetal stage or within the first

three weeks of life[159-161]. Outside of development and homeostasis, EGFR is most studied for its role in tumorigenesis, with EGFR mutations occurring most prominently in lung and breast cancers[162], although its signalling has also been implicated in many other disease contexts. Whether EGFR is protective or detrimental differs from disease to disease: whereas its signalling was generally found to be protective following damage, for example after helminth or viral infection, due to its ability to promote epithelial repair[127, 130-132, 135, 150, 163, 164], EGFR signalling was also implicated in driving aberrant matrix deposition and remodelling in the context of asthma, pulmonary fibrosis or liver fibrosis[136, 157, 165-176].

EGFR ligands fulfil different functions during organogenesis and homeostasis, likely as a result of their diverging cleavage patterns, affinities for the receptor and abilities to induce downstream signalling. While AREG is important for mammary gland development and female reproduction[89], BTC has a role in driving β-cell differentiation and proliferation in the pancreas[91]. EGF is a regulator of stem cells in different tissues, in addition to supporting embryonic growth pre- and post-implantation and trophoblast invasion[90]. Although mice deficient in either EPGN or EREG display no gross morphological defects[177, 178], suggesting that these ligands are not involved in organogenesis, a role for EREG has been identified in female reproduction and angiogenesis[94]. In addition to contributing to heart and lung development, HB-EGF fulfils functions in angiogenesis, adipogenesis and reproduction[92]. Finally, TGFα has important roles in eye and hair development, as demonstrated by the partially opened eyes at birth and wavy coat of TGFα null mice[179, 180]. Despite the various EGFR ligands fulfilling distinct biological roles, the fact that knockout mice for all ligands are viable and fertile suggests a substantial functional overlap that is able to compensate for the loss of individual ligands.

In addition to their functions in organogenesis and homeostasis, many contributions of EGFR ligands to inflammation and repair have been defined. These can be broadly separated into contexts where EGFR signalling is beneficial and those where it is detrimental. As with ligand expression patterns, most is known about the role of AREG. Numerous studies have found AREG to be protective during various diseases, such as after infection with viruses or helminths[127, 130-132, 135, 163, 164], as well as in the context of acute lung injury, neurological recovery after stroke, muscle injury, heart stress and graft-versus-host disease[144, 146-148, 151]. Nevertheless, AREG can also contribute to disease pathology, for example by exacerbating matrix deposition and remodelling during pulmonary fibrosis, lung injury, viral infection and asthma, by establishing a niche for bacterial colonisation and by suppressing anti-tumour responses[128, 136, 173, 174, 181-183]. Similarly, HB-EGF was found to be protective in a model of inflammatory bowel disease[155] but exacerbated airway smooth muscle cell migration and proliferation as well as eosinophilia and mucus production in OVA-driven models of AAD[157,

[171]. In addition, studies described both protective and detrimental roles for HB-EGF in the context of liver fibrosis[172, 184]. Since these studies used genetic deletion or transgenic overexpression of HB-EGF, respectively, both of which resulted in augmented fibrosis, precise regulation of HB-EGF levels may be necessary to prevent exacerbated pathology. Finally, while less is known about the involvement of the other five EGFR ligands in diseases outside of cancer, it has been demonstrated that overexpression of TGFα in murine lungs can drive pulmonary fibrosis[175, 176]. Overall, these findings suggest that EGFR signalling is central to the pathogenesis of many diseases, taking both protective and detrimental roles, and that the careful regulation of EGFR ligand levels may be decisive for the disease outcome in many contexts.

1.2.5 Targeting EGFR signalling clinically

Since 2003, fourteen tyrosine kinase inhibitors (TKIs) targeting EGFR have been approved globally for the treatment of cancer[185]. While the majority of these are indicated in the treatment of non-small cell lung cancer (NSCLC) with or without EGFR mutations, EGFR TKIs are also used in the treatment of squamous cell carcinomas of the lung, pancreatic cancer, medullary thyroid cancer or breast cancers, particularly those inhibitors that also target ErbB2[185]. In addition, four monoclonal antibodies targeting EGFR have been approved for the treatment of metastatic colorectal cancer and squamous cell carcinoma of the head and neck, with many more under development or in clinical trials[186]. Although the vast majority of EGFR-targeting therapies have been developed for the treatment of cancer, the benefits of EGFR inhibition have also been trialled in other conditions. For example, a phase II trial was conducted to test the safety and efficacy of inhalation of the EGFR inhibitor BIBW2948 BS to reduce mucin stores in patients with chronic obstructive pulmonary disease (COPD)[187]. However, this approach showed poor efficacy and caused significant adverse reactions in a subset of subjects. Therefore, the use of EGFR-targeted therapeutics is currently restricted to the treatment of cancers, where the benefits of the therapy outweigh the poor tolerability and risk of adverse effects. Nevertheless, given the importance of EGFR signalling in a host of different contexts, including chronic lung diseases[188], it is likely that efforts will continue to develop safer and highly specific EGFR-targeted therapies in the future. Even so, the currently available strategies for EGFR inhibition have important applications beyond the treatment of diseases, as they constitute useful tools for the study of EGFR signalling *in vivo* and *in vitro*.

1.3 Hypothesis and aims

While mouse models of AAD have been a valuable tool for the investigation of the mechanisms underlying asthma pathophysiology, the vast majority of *in vivo* models were performed in adult mice. However, asthma onset primarily takes place during childhood and results in permanent deficits in lung function, underpinned by airway remodelling. A greater understanding of the mechanisms contributing to remodelling and pathology during childhood is key in developing therapeutics to prevent the transition to adult asthma and preserving lung function and may even pave the way towards a cure for asthma. Therefore, there is a pressing need to study the pathophysiologic mechanisms of AAD in early-life models, which encompass allergen exposure and disease onset during childhood.

Overall hypothesis

EGFR signalling is induced by allergen exposure, contributes to the pathology of asthma and AAD and fulfils distinct functions between early-life and adult onset of AAD.

Overall aims

1. To characterise the expression of EGFR and its ligands during postnatal development compared to adulthood.
2. To define the effects of allergen or viral exposure on EGFR signalling during early life and adulthood.
3. To investigate the contributions of EGFR signalling to the pathology of AAD using various manipulation strategies in models of early-life or adult allergen exposure.

2 Methods

2.1 Human airway and lung samples

2.1.1 Paediatric samples

All paediatric samples included in this thesis were recruited as part of the Breathing Together[189] or Patterns of airway infection and inflammation in children studies under appropriate ethics approval (NRES 16/LO/1518, 17/LO/0013 and 15/LO/1885). Five- to ten-day-old infants born at term (37 to 42 weeks) were recruited for the collection of nasal brushings for airway epithelial culture. Children between one and five years old with a history of recurrent episodes of wheeze and difficulty in breathing who were due to undergo a clinically indicated bronchoscopy were recruited in the PSW group ("pre-school wheezers"). Children between six and sixteen years of age with a diagnosis of severe asthma made by a specialist paediatrician, healthcare professional-documented wheeze and evidence of reversible airway hyperresponsiveness (>12% change from baseline FEV_1) were recruited in the severe asthma group ("school-aged severe asthma"). Children under the age of five with mild or moderate wheezing or no history of wheezing were recruited as controls ("pre-school controls"). Children between two and fourteen years of age who were undergoing a clinically indicated bronchoscopy as part of investigation for recurrent chest infections or chronic cough were recruited as controls ("disease controls"). Inclusion and exclusion criteria for all groups have been described in detail previously[189, 190].

Nasal brushings were collected from all four groups using a Dent-O-Care interdental brush 620 (2.7 mm brush) (Dent-O-Care, London, UK). Bronchial brushings were collected from groups two to four using sheathed 10-mm disposable cytology brushes (Olympus, Hamburg, Germany). For group 2, blind bronchial brushings were performed during elective surgical procedures. For groups three and four, bronchial brushings were obtained under direct vision during clinically indicated bronchoscopies. All brushes were placed in Dulbecco's Modified Eagle Medium (DMEM; Gibco, Waltham, USA) containing 100 U/ml penicillin and 100 µg/ml streptomycin (P/S; Gibco) immediately upon collection for transport to the laboratory, where they were processed.

BAL was collected at bronchoscopy for those that underwent clinically indicated bronchoscopy. Three 1 ml/kg (to a maximum of 40 ml) aliquots of normal saline were instilled into and aspirated back from the airways.

2.1.2 Adult samples

Healthy adult volunteers were recruited at the Royal Brompton Hospital, London, UK, under National Research Ethics Service (NRES) ethics 15/LO/1399. All subjects had normal spirometry and exclusion criteria included self-reported history of lung disease and infection

within six months before sample collection. Bronchial brushings for epithelial cell culture were taking from the right middle lobe during bronchoscopy using single use 3 mm cytology brushes (Olympus) and placed directly into DMEM media containing P/S for transport to the laboratory.

For the outgrowth of normal lung fibroblasts, lung resections were collected under NRES 15/SC/0101 from patients undergoing lung cancer surgery or lung transplantation at Royal Brompton Hospital.

2.2 Cell Culture

2.2.1 General cell culture and cell lines

All cells were cultured under sterile conditions and incubated at 37° C and 5% CO_2 in a humidified incubator. MFB-F11 cells were maintained in DMEM containing 10% foetal bovine serum (FBS), For stimulation, 1.2×10^6 cells were plated in 6-well plates in serum-free DMEM containing P/S and rested overnight. Cells were incubated with 10 μM Gefitinib (Abcam, Cambridge, UK) or vehicle (dimethyl sulfoxide, DMSO; Sigma-Aldrich, Burlington, USA) for 2 hours before addition of 100 ng/ml recombinant mouse amphiregulin (AREG; R&D Systems, Minneapolis, USA) for 15 mins. Cells were then washed once in ice-cold tris-buffered saline (TBS) before lysis in Radioimmunoprecipitation (RIPA) buffer (Abcam) containing 2 mM sodium orthovanadate (Na_3VO_4; Sigma) and cOmplete™ protease inhibitor cocktail (Roche, Basel, Switzerland). Cells were scraped off, collected into tubes and incubated on ice with agitation for one hour. Lysates were then spun at full speed (> 12,000 rcf) and supernatants were stored for western blot analysis.

2.2.2 Air-liquid interface (ALI) culture of airway epithelial cells

Expansion and cryopreservation of basal cells

Cells were detached from nasal or bronchial brushes by vigorous agitation and basal cells were expanded in fully supplemented Airway Epithelial Growth Medium (Promocell, Heidelberg, Germany) containing 100 μg/ml Primocin (InvivoGen, San Diego, USA) in flasks coated with 100 μg/ml (nasal) or 30 μg/ml (bronchial epithelial cells) PureCol® bovine Type I Collagen Solution (Advanced BioMatrix, Carlsbad, USA) for two passages, at which point they were cryopreserved in freezing medium (10% DMSO, 10% FBS, 80% Airway Epithelial Growth Medium containing P/S).

Differentiation of epithelial layers at ALI

For the establishment of ALI cultures, cryopreserved basal cells were expanded on collagen-coated flasks in fully supplemented Airway Epithelial Growth Medium containing P/S for one passage before 3×10^4 cells were seeded per 6.5 mm Transwell insert with polyethylene terephthalate membrane and 0.4 µm pores (Corning, Somerville, USA) coated with 30 µg/ml collagen. During seeding and the submerged phase of the culture, a 1:1 mixture of Airway Epithelial Growth Medium and DMEM constituted with P/S, 25 mM HEPES (Gibco), 1.5 µg/ml bovine serum albumin (Sigma) and all supplements provided with the Airway Epithelial Growth Medium except for Triiodo-L-thyronine was used as growth medium and supplied to the apical (200 µl) and basal (500 µl) compartment. Medium was refreshed every 2-4 days until cells reached confluency, at which point the apical medium was removed and the basal medium was replaced with PneumaCult™-ALI Medium containing 0.0004% Heparin, 0.48 µg/ml hydrocortisone (all Stemcell, Vancouver, Canada) and P/S, thereby air-exposing the cultures. Basal medium was refreshed every 2-4 days for 4-9 weeks until cells were fully differentiated as indicated by the movement of cilia and production of mucus. Where necessary, mucus was removed by performing apical washes (see below). At least 48 hours prior to experiments, hydrocortisone was excluded from the media.

Allergen treatment and viral infection

All treatments were prepared in serum-free DMEM and added to the apical compartment. For stimulation with HDM, 25 µg or 50 µg of *Dermatophagoides pteronyssinus* extract (Citeq, batch 15J02, Groningen, Netherlands) in 50 µl was added and incubated for 24 hours (cf. Figure 3.11A-B) or 4 hours (cf. Figure 3.11C-D). For viral infections, a cell density of 2.5×10^5 cells per insert was assumed. The viral strains used in this thesis were RSV BT2a (clinical isolate[191]), SARS-CoV-2/England/IC19/2020 (early clinical isolate) and Influenza H1N1 A/England/195/ 2009 (2009 pandemic strain). Apical compartments were washed once with PBS before infection. For infection with RSV 6.25×10^4 plaque-forming units (PFU) of RSV (MOI 0.25) in 50 µl DMEM were added and incubated for two hours, after which two apical washes were performed. For infection with SARS-CoV-2 or H1N1, 2.5×10^3 PFU (MOI 0.01) or 2.5×10^2 PFU (MOI 0.001), respectively, in 100 µl DMEM were added and cells were incubated for one hour, after which the apical liquid was removed and cells were returned to the incubator.

Sample collection

Basal media and apical washes were collected every 1-2 days during experiments, as indicated in the relevant figure legends. Apical washes were performed by the addition of 100-

200 µl of PBS to the apical compartment followed by incubation at room temperature for 10 minutes. Presence of SARS-CoV-2 or H1N1 infectious particles in apical washes was determined by members of the Barclay Group (Department of Infectious Disease, Imperial College London, London, UK) using plaque assays as described in Stölting et al. 2022 (ref. [192]). For mediator analysis after SARS-CoV-2 and H1N1 infection, apical washes and basal media were UV-inactivated prior to storage at -80° C. For RNA analysis, cell layers were lysed in 350 µl RLT buffer (QiAGEN, Hilden, Germany) or 200 µl Maxwell® homogenisation buffer containing 1-Thioglycerol (Promega, Madison, USA). For imaging, cell layers were fixed in 4% paraformaldehyde (PFA) in PBS for 20 minutes, followed by one wash in PBS and storage in PBS at 4° C. For western blot analysis, cells were washed once in ice-cold TBS prior to lysis in RIPA buffer containing 2 mM sodium Na_3VO_4 and cOmplete™ protease inhibitor cocktail and cell debris was removed as described above for fibroblasts (see 2.2.1).

Basal media from untreated epithelial cells were collected for use in fibroblast proliferation experiments.

2.2.3 Culture of normal lung fibroblasts

Outgrowth culture and maintenance

Normal lung fibroblasts were derived from 1 mm pieces of non-cancerous lung tissue obtained from lung resections by outgrowth culture in DMEM containing 10% FBS and P/S as previously described[193] and maintained in the same medium for up to eight passages.

Proliferation assays

For real-time proliferation assays, 1-2.5 × 10^3 cells per well were seeded in serum-free DMEM in 96-well plates and rested overnight. At the start of the experiment, the medium was replaced with epithelial cell-conditioned media (neat or diluted in serum-free DMEM) in the presence or absence of 1-10 µM Gefitinib. Serum-free DMEM or DMEM containing 10% FBS were used as negative and positive controls for proliferation, respectively.

For live imaging, cells were placed within the JuLI™ Stage Real-Time Cell History Recorder (NanoEnTek, Seoul, Korea) within a humidified incubator and images were recorded using a 4x objected at 30-minute to 2-hour intervals for 72-96 hours. Cell confluence was calculated using the PHANTAST plugin[194] for Fiji[195] and normalised to starting confluence.

2.2.4 Stimulation of murine lymph node cells

Single-cell suspension of mediastinal lymph node cells were prepared as described below (see 2.4.3). For *ex vivo* stimulation, cells were harvested, processed and cultured in DMEM

without phenol red containing 4.5 g/l glucose, L-glutamine, 25 mM HEPES, 10% dialysed, heat-inactivated FBS (Sigma), P/S and 50 µM β-mercaptoethanol (Gibco). Cells were seeded at 4 × 10^5 cells per well in round-bottom 96-well plates and stimulated with 10 µg HDM (Greer lot 360923; resuspended in PBS) or 20 ng/ml PMA and 1.5 µg/ml ionomycin in the presence or absence of 10 nM β-oestradiol (E2; Sigma; resuspended in ethanol) and/or 10 µM Gefitinib (resuspended in DMSO). Supernatants were collected four days post stimulation and analysed by ELISA (see 2.7.1 below).

2.3 Work on live animals

2.3.1 Source of animals and general husbandry

All animal experiments were conducted in accordance with the Animals (Scientific Procedures) Act 1986 under project licence P996A24E1. Adult wildtype (WT) BALB/c and C57BL/6J mice were purchased from Charles River Laboratories (Margate, UK). Mice were housed at Imperial College Central Biomedical Services (CBS) under specific pathogen-free conditions and with free access to food and water. Experimental animals and studs used for breeding were fed a general maintenance diet ("RM1"), whereas female breeders received a highly nutritious diet specifically used for breeding, lactation and growth of young animals ("RM3").

For experiments in adult animals, female mice were used unless indicated otherwise and animals were between 7-9 weeks old when experiments commenced. For neonatal experiments, mice were bred in-house and both sexes were used. Mice were time-mated as duos or trios to synchronise due dates of dams. Pregnant females were singly housed approximately two weeks into gestation. Pups were housed with their dams until weaning at 20-21 days of life.

Unless stated otherwise, mice were sacrificed by intraperitoneal injection with pentobarbital and death was confirmed by intersection of the femoral artery, in accordance with Schedule 1 of the Animals (Scientific Procedures) Act 1986.

2.3.2 Models of allergic airway disease (AAD)

Preparation of allergens, recombinant cytokines and inhibitors

Lyophilised extracts of *Alternaria alternata* (ALT) (lot 322776), house dust mite (HDM; *Dermatophagoides pteronyssinus*) (lot 360923) and timothy grass (TG; *Phleum pratense*)

(lot XP28-D12-21.43) were purchased from Greer Laboratories, Lenoir, USA and reconstituted in sterile PBS to a protein concentration of 0.4 mg/ml for ALT, 1 mg/ml for HDM and 0.808 mg/ml for TG.

Carrier-free recombinant mouse IL-33 was purchased from BioLegend (San Diego, California), diluted to 1 mg/ml using sterile PBS and bovine serum albumin (BSA) was added to a final concentration of 0.1 % (w/v). Carrier-free recombinant mouse AREG was purchased from R&D Systems (Minneapolis, USA) and resuspended in sterile PBS at a concentration of 100 µg/ml. Recombinant mouse HB-EGF (Novus Biologicals, Centennial, USA) was reconstituted in PBS containing 0.1 % (w/v) BSA at a concentration of 100 µg/ml.

Suspensions of EGFR tyrosine kinase inhibitor Gefitinib were prepared in 6% hydroxypropyl-β-cyclodextrin (HP-β-CD; Thermo Fisher Scientific) or 1% Tween® 80 (Merck) at a concentration of 10 mg/ml.

Neonatal models of AAD

To establish AAD, pups were intranasally administered with allergen three times per week from day 6-8 of life. During the first two weeks of life, mice were administered 5 µg ALT, 10 µg HDM or 4.5 µg TG in a volume of 10 µl PBS and dosing was performed without anaesthesia. From the third week of life, or fourth dose, mice were dosed intranasally under light isoflurane anaesthesia using 10 µg ALT, 15 µg HDM or 9 µg TG in a total volume of 15 µl PBS.

For the mixed allergen challenge, a third of a ‘dose equivalent’ of ALT, HDM and TG were administered combinedly, corresponding to 1.67 µg ALT, 3.33 µg HDM and 1.5 µg TG during the first week of dosing and 3.33 µg ALT, 5 µg HDM and 3 µg TG thereafter.

Adult models of AAD

Mice were dosed intranasally three times per week with either 25 µg HDM or 1 µg IL-33 in a total volume of 25 µl PBS. All dosing was performed under light isoflurane anaesthesia.

Interventions

Unless otherwise stated, Gefitinib was administered by oral gavage three times a week, approximately 4-6 hours prior to allergen dosing. Neonatal mice received 1 mg Gefitinib in 100 µl vehicle per dose, whereas adult mice were given 1.5 mg Gefitinib in 150 µl vehicle per dose. In 4.3.2, where the optimal route for Gefitinib administration was established, 7-day old mice received three doses of Gefitinib in 6% HP-β-CD over the course of one week either via

the intranasal (0.1 mg Gefitinib in 10 µl 6% HP-β-CD), intraperitoneal (0.4 mg Gefitinib in 40 µl 6% HP-β-CD) or oral (0.4 mg Gefitinib in 40 µl 6% HP-β-CD) route.

AREG was administered intranasally three times per week either in combination with recombinant IL-33, or 4-6 hours after allergen challenge. Neonatal mice received 0.4 µg AREG in 10 µl PBS during the second week of life, 0.6 µg AREG in 15 µl PBS during the third week of life and 0.75 µg AREG in 15 µl PBS from the fourth week of life, whereas the dose for adult mice was 1 µg AREG in 25 µl PBS. HB-EGF was administered intranasally 4-6 hours before allergen challenge three times per week at a dose of 0.5 µg in 10 µl PBS in the second week of life or 0.75 µg in 15 µl PBS thereafter.

2.3.3 Assessment of lung function

Lung function was assessed using the FlexiVent system (Scireq, Montreal, Canada) and unless otherwise stated, measurements were performed one day post last allergen challenge. Surgical anaesthesia was induced by administration of 50 mg/kg pentobarbital (Sigma-Aldrich) intraperitoneally and 100 mg/kg ketamine (Zoetis, Parsippany-Troy Hills, USA) intramuscularly. Mice were tracheotomised and connected to the ventilator using a 19-gauge blunt-ended cannula, from whence they were ventilated at 150 breaths per minute, using a tidal volume of 7 ml/kg body weight and a positive end-expiratory pressure of approximately 2cm H_2O.

Perturbations and measurements

A user-written script was used for the measurement of different lung function parameters. Firstly, three deep inflations were performed to bring lungs to total lung capacity and normalise lung volume. Next, mice were subjected to a brief, single-frequency 2.5 Hz forced perturbation (‘Snapshot-150’), followed by two sets of broadband forced oscillations lasting 3 seconds each (‘Quick Prime-3’) with intermittent periods of normal ventilation. Snapshot and Quick Prime perturbations were repeated five times for a total of six and twelve readings, respectively.

Calculation of parameters

Measures of upper airway resistance, Resistance (R, expressed as cmH_2O×s/ml), Elastance (E, expressed as cmH_2O/ml) and Compliance (C, expressed as ml/cmH_2O) were calculated by the FlexiVent software from Snapshot readings using multiple linear regression fitting to a single compartment model. Newtonian Resistance (Rn, expressed as cm H_2O×s/ml), Tissue Damping (G, expressed as cmH_2O/ml) and Tissue Elastance (H, expressed as cmH_2O/ml) were calculated by the FlexiVent software from Quick Prime readings in a number of steps

including Fourier transformation of frequency superposition, calculation of input impedance at every oscillating frequency and finally, the application of a Constant Phase Model fit.

Methacholine challenge

Measurements were acquired at baseline, as well as in response to increasing concentrations of methacholine (MCh) (Sigma-Aldrich), which was administered via the nebuliser prior to Snapshot and Quick Prime measurements. MCh solutions were prepared in PBS and used at concentrations between 1 to 100 mg/ml.

Quality control of data

Computed measurements were inspected for the quality of the model fit using the coefficient of determination (CoD) values determined by FlexiVent software. Different cut-offs were applied based on the AAD model and the age of mice (listed in **Table 2.1**). Where different allergens were given within the same experiment, the lowest CoD cut-off was used. Where fewer than 50% of measurements from a single animal at a specific dose met quality requirements, this dose was excluded for the animal in question.

Table 2.1 Coefficient of determination (CoD) cut-offs used in the quality control of lung function data.

Age of mice	Model	CoD Cut-off
Neonates	HDM, TG	0.85
Neonates	ALT, Mixed allergen	0.80
Adults	HDM	0.90
Adults	IL-33	0.85

2.3.4 Blood collection

Where indicated, blood from live animals was collected using tail vein puncture. To this end, mice were warmed in a heating chamber set to 37° C for at least 10 minutes. A small incision to the tail vein was made using a No.11 surgical scalpel (Swann-Morton, Sheffield, UK) and blood was collected using heparinised capillary tubes (Hirschmann Laborgeräte, Eberstadt, Germany). No more than 10% of the total blood volume was withdrawn on any one occasion and no more than 15% of the total blood volume in any 28 days.

2.4 Animal tissue harvest and processing

2.4.1 Blood and serum

Blood was collected from mice either via tail vein puncture (see 2.3.4 above), by blind cardiac puncture under terminal anaesthesia or by intersection of and collection from the jugular vein. For tail vein punctures, where heparinised capillaries were used for collection, blood was transferred to Eppendorf tubes and centrifuged for 10 minutes at 20,000 rcf at 4° C to separate layers. The serum layer was collected and stored at -80° C. Otherwise, blood was collected directly into Microtainer serum separating tubes (BD, Franklin Lakes, USA) and centrifuged for 5 minutes at a minimum speed of 10,000 rcf prior to storage at -80° C.

2.4.2 Bronchoalveolar lavage (BAL)

The trachea was exposed and cannulated using a blunt-ended needle secured by surgical sutures. A syringe was attached to the needle, lungs were carefully flushed with PBS and lavage was recovered in the syringe. Unless stated otherwise, a total of three washes was performed. A volume of 0.4 ml per wash was used in animals from four weeks of age, whereas a reduced volume of 0.3 ml per wash was used in animals between two and three weeks of age. Recovered BAL fluid was centrifuged at ≥ 300 rcf and supernatant was stored at -80° C for subsequent analysis. Cells were resuspended 0.5 ml complete RPMI (cRPMI; Roswell Park Memorial Institute 1640 medium + 10% FBS + P/S; all Gibco), counted and analysed by flow cytometry (see 2.5 below).

2.4.3 Mediastinal lymph nodes (LN)

Mediastinal lymph nodes were collected prior to the removal of lungs. To obtain a single-cell suspension for flow cytometry analysis or *ex vivo* cultures, lymph nodes were passed through 70 µm cell strainers, centrifuged and resuspended in 0.5 ml cRPMI.

2.4.4 Standard protocol for lung removal and processing

Unless stated otherwise, lungs were removed as a whole and lobes were separated according to downstream applications.

Left lobe (flow cytometry)

In the standard protocol, the left lung lobe was used for flow cytometry analysis of lung immune cells. The lobe was minced using scissors and digested for 45-60 minutes at 37° C in a solution containing 150 µg/ml collagenase D and 25 µg/ml DNase I (both Roche) in cRPMI.

Following digest, the tissue was passed through 70 µm cell strainers and erythrocytes were lysed by incubation in red blood cell lysis buffer (155 mM NH_4Cl, 13 mM $KHCO_3$, 100 µM EDTA, pH 7.4) for five minutes at room temperature. Lung cells were resuspended in 1 ml cRPMI, counted and used for analysis.

Right superior lobe (histology)

The right superior lobe was inflated with PBS, enclosed in a histology cassette and fixed in 10% neutral buffered formalin for 24 hrs before transfer to 70% ethanol. All further processing, such as paraffin embedding, slicing and standard histology stains were performed by Lorraine Lawrence of the Histology Facility at Imperial College London.

Right middle and inferior lobes (protein)

The right middle and inferior lobes were collected for protein analyses by enzyme-linked immunosorbent assay (ELISA) and western blot (WB), respectively. Lobes were snap-frozen in liquid nitrogen and stored at -80° C until further processing.

Right post-caval lobe (RNA)

Post-caval lobes were incubated in RNAlater® (Sigma-Aldrich) for 24 hours at 4° C prior to storage at -80° C.

Lung homogenates

Lung homogenates used for RNA and protein assays were prepared by mechanical disruption of tissue using Lysing Matrix D beads and a FastPrep®-24 homogeniser instrument (both MP Biomedicals, Santa Ana, USA). Different buffers were used for homogenisation: for RNA extraction, RLT buffer (QiAGEN) containing 1% (v/v) 2-mercaptoethanol was used; when prepared for ELISA, Hank's Balanced Salt Solution (HBSS) without Mg^{2+} or Ca^{2+} (Thermo Fisher Scientific) supplemented with cOmplete™ Protease Inhibitor (Roche) was used and when prepared for WB, RIPA buffer supplemented with cOmplete™ Protease inhibitor and 2 mM sodium orthovanadate was used. A fixed volume of 500 µl buffer was used for RNA extraction, whereas buffer volumes were normalised to lung weights for protein assays, using 1 ml of buffer per 50 mg or 100 mg of lung tissue for ELISA and WB, respectively.

2.4.5 *In situ* dispase digest of lungs

A different digest method was used for the recovery of both immune ($CD45^+$) and structural ($CD45^-$) cells from lungs. Perfusion of the lungs was achieved by intersection of the abdominal aorta and subsequent injection of 5 ml of ice-cold PBS into the right ventricle of the heart. The

trachea was cannulated and lungs were inflated with an age-appropriate volume (between 0.15 ml for 3-day-old mice and 1.5 ml for adult animals) of 5 mg/ml dispase II (grade II; Sigma-Aldrich) in PBS. Digest solution was trapped in the lungs by injection of 0.1-0.5 ml 1% (w/v) low melting point agarose (Thermo Fisher Scientific) in PBS, warmed to 37-40° C. Once the agarose was solidified, lungs were removed *en bloc* and incubated in dispase II solution for 40 minutes at room temperature and then transferred into a petri dish containing DMEM supplemented with 25 mM HEPES and 50 µg/ml DNase I. Lung lobes were gently teased apart using forceps and incubation for 10 minutes at room temperature with gentle agitation. Tissue was then forced through a 70 µm cell strainer and red blood cell lysis was performed as described above (see 2.4.4). Cells were resuspended in DMEM containing 25 mM HEPES for counting and subsequent analysis.

In some cases, only the left lung lobe was digested with dispase. To this end, all right lung lobes were tied off using suture thread before inflation. Volumes were decreased appropriately and all other processing steps were performed as described above.

2.5 Flow cytometry and flow-activated cell sorting

2.5.1 Stimulation of cells for intracellular cytokine analysis

To assess the potential of lymphocytes to produce cytokines, cells were seeded in 96-well round- or V-bottom plates and stimulated with 20 ng/ml PMA and 1.5 µg/ml ionomycin in the presence of 5 µg/ml Brefeldin A (all Sigma-Aldrich) in cRPMI for 4 hours at 37° C in a humidified incubator containing 5% CO_2.

2.5.2 General staining protocol

Unless stated otherwise, staining of cells for flow cytometry was carried out in 96-well V- or round-bottom plates with a maximum of 5×10^6 cells per well. Cells were washed at least once between individual staining steps in the buffer last used for staining.

For discrimination of cells based on viability, cells were incubated for 15-20 minutes at room temperature, in the dark, in 40 µl of LIVE/DEAD™ Fixable Blue Dead Cell Stain (Thermo Fisher Scientific) diluted to working concentration in PBS.

For staining of extracellular antigens, antibodies (see **Table 2.2**) were diluted in FACS buffer (PBS containing 1% BSA and 0.05% sodium azide) and cells were incubated with 30 µl antibody mixture for 20-30 minutes at 4° C, in the dark. Purified Anti-Mouse CD16 / CD32 (Fc

block) (Tonbo Biosciences, San Diego, USA) was included in all extracellular antigen stains to block non-specific binding.

Cells were then fixed either in IC Fixation Buffer or, where fixation was followed by transcription factor staining, Foxp3 / Transcription Factor Fixation/Permeabilization working solution (both Thermo Fisher Scientific) for 10-15 minutes at room temperature. In some cases, cells were stored in FACS buffer overnight at 4° C at this point.

Where intracellular staining was performed, cells were resuspended in 100 µl Permeabilization buffer (Thermo Fisher Scientific) for 5 minutes at room temperature followed by a 20–30-minute incubation at 4° C, in the dark, with 30 µl antibody mix also prepared in permeabilization buffer (see **Table 2.3** for antibodies). Where indicated, staining for EGFR was performed before intracellular staining with directly conjugated antibodies. Cells were stained with 30 µl of rabbit anti-EGFR antibody (clone D1P9C; Cell Signaling Technology, Danvers, USA) diluted 1:100 in Permeabilization buffer for 20-30 minutes at 4° C. Following a wash step, staining for intracellular antigens was continued as described above, with inclusion of Alexa Fluor™ 594-conjugated donkey anti-rabbit IgG (H+L) highly cross-absorbed secondary antibody (Thermo Fisher Scientific) at a dilution of 1:100. Finally, cells were resuspended in FACS buffer and acquired on the same day.

Single stains for compensation were prepared using Anti-Rat and Anti-Hamster Ig κ /Negative Control Compensation Particles (BD), except for the single stain of the viability dye, for which a mixture of live and dead cells was used.

Table 2.2 Antibodies used for staining of extracellular antigens.
† denotes markers included in the lineage cocktail for the ILC panel.

Antigen	Clone	Conjugates	Supplier	Dilution
CD103	2E7	FITC	BioLegend	1:100
CD11b†	M1/70	APC	BioLegend	1:200
CD11c†	N418	APC, APC-Cy7	BioLegend	1:100
CD127 (IL-7Rα)	A7R34	BV711	BioLegend	1:100
CD146	ME-9F1	APC	BioLegend	1:100
CD19†	6D5	BV605, APC	BioLegend	1:200
CD25	PC61	BV510	BioLegend	1:100
CD31	390	BV421, FITC	BioLegend	1:100
CD326 (EpCAM)	9C4	PE-Cy7	BioLegend	1:100
CD335 (NKp46)	29A1.4	BV510, BV605	BioLegend	1:100
CD3ϵ	145-2C11	PE-Cy7	BioLegend	1:100
CD4	RM4-5	BV421, BV510	BioLegend	1:100-1:200
CD44	IM7	PerCP-Cy5.5	BioLegend	1:200
CD45	30-F11	BV711, AF700	BioLegend	1:100-1:200
CD49b	DX5	PE-Dazzle	BioLegend	1:100
CD49e	5H10-27	PE	BioLegend	1:200
CD5†	53-7.3	APC	BioLegend	1:100
CD62L	MEL-14	BV605	BioLegend	1:200
CD64 (FcγRI)	X54-5/7.1	BV421	BioLegend	1:50
CD69	H1.2F3	APC	BioLegend	1:200
CD86	GL-1	PE-Dazzle	BioLegend	1:100
CD8a	53-6.7	PE-Cy7	BioLegend	1:100
CD90.2 (Thy-1.2)	53-2.1	BV605	BioLegend	1:100
F4/80†	BM8	PE-Cy7, APC	BioLegend	1:50-1:100
FcϵRIα†	MAR-1	APC	BioLegend	1:100
I-A/I-E (MHC-II)	M5/114.15.2	PerCP-Cy5.5	BioLegend	1:100
Ly-6A/E (Sca-1)	D7	BV785	BioLegend	1:100
Ly-6C	HK1.4	BV510, AF700	BioLegend	1:100
Ly-6G	1A8	BV510, BV605, AF700	BioLegend	1:100
Ly-6G/Ly-6C (Gr1)†	RB6-8C5	APC	BioLegend	1:100
LYVE-1	223322	APC	R&D Systems	1:100
Siglec F	E50-2440	PE	BD	1:100
TCR β chain†	H57-597	PE-Cy7, APC	BioLegend	1:100-1:200
TCR γ/δ†	GL3	APC, APC-Fire 750	BioLegend	1:100
TER-119†	TER-119	APC	BioLegend	1:100

Table 2.3 Antibodies used for staining of intracellular antigens.

Antigen	Clone	Conjugates	Supplier	Dilution
FOXP3	FJK-16s	PE	BioLegend	1:100
Gata-3	TWAJ	PerCP-eFluor 710	Thermo Fisher	1:25
IFN-γ	XMG1.2	FITC	BioLegend	1:100
IL-10	JES5-16E3	APC	BioLegend	1:100
IL-13	eBio13A	PE	Thermo Fisher	1:100
IL-17A	TC11-18H10.1	PerCP-Cy5.5, AF700	BioLegend	1:100
IL-5	TRFK5	BV421	BioLegend	1:100
RORγT	Q31-378	BV786	BD	1:25
T-bet	4B10	BV711	BioLegend	1:25
Vimentin	O91D3	Vimentin	BioLegend	1:100

2.5.3 Acquisition and analysis

Samples were acquired on LSRFortessa™ machines with either four or five lasers running FACSDiva™ software (both BD). Data analysis was performed in FlowJo software (BD). All analyses were restricted to non-debris, live, single cells (**Figure 2.1A**). Representative gating strategies for the identification of myeloid cells (**Figure 2.1B-C**), T lymphocytes (**Figure 2.3A-B**), innate lymphoid cells (**Figure 2.3C**) and structural cells (**Figure 2.2**) are shown below. NK cells were gated from live, single, $CD45^+$ lymphocytes based on their expression of NKp46.

2.5.4 Flow-activated cell sorting (FACS)

Lung cells were stained and sorted following dispase digest (see 2.4.5 above). Antibodies (see **Table 2.4** for panel) were diluted in a low-protein FACS buffer (PBS containing 0.1% BSA, 1 mM EDTA and 25 mM HEPES) in the presence of Fc block and cells were stained in a volume of 200 µl for 30 minutes at 4° C, in the dark. Cells were washed once in low-protein FACS buffer after staining and filtered into tubes with 35 µm filter caps (Corning, Corning, USA) prior to acquisition. TO-PRO™-3 Iodide viability dye (Thermo Fisher Scientific) was added to a final concentration of 50 nM immediately before acquisition.

Cells were sorted by staff of the Imperial College Flow Cytometry Core Facility using a FACSAria III machine (BD) with a 100 µm nozzle. Purity setting were applied and cells were collected into PBS containing 10% FBS and 25 mM HEPES. A gating strategy for the

identification of airway macrophages, other immune cells, epithelial cells and other structural cells is shown in Chapter 3 (**Figure 3.2B**).

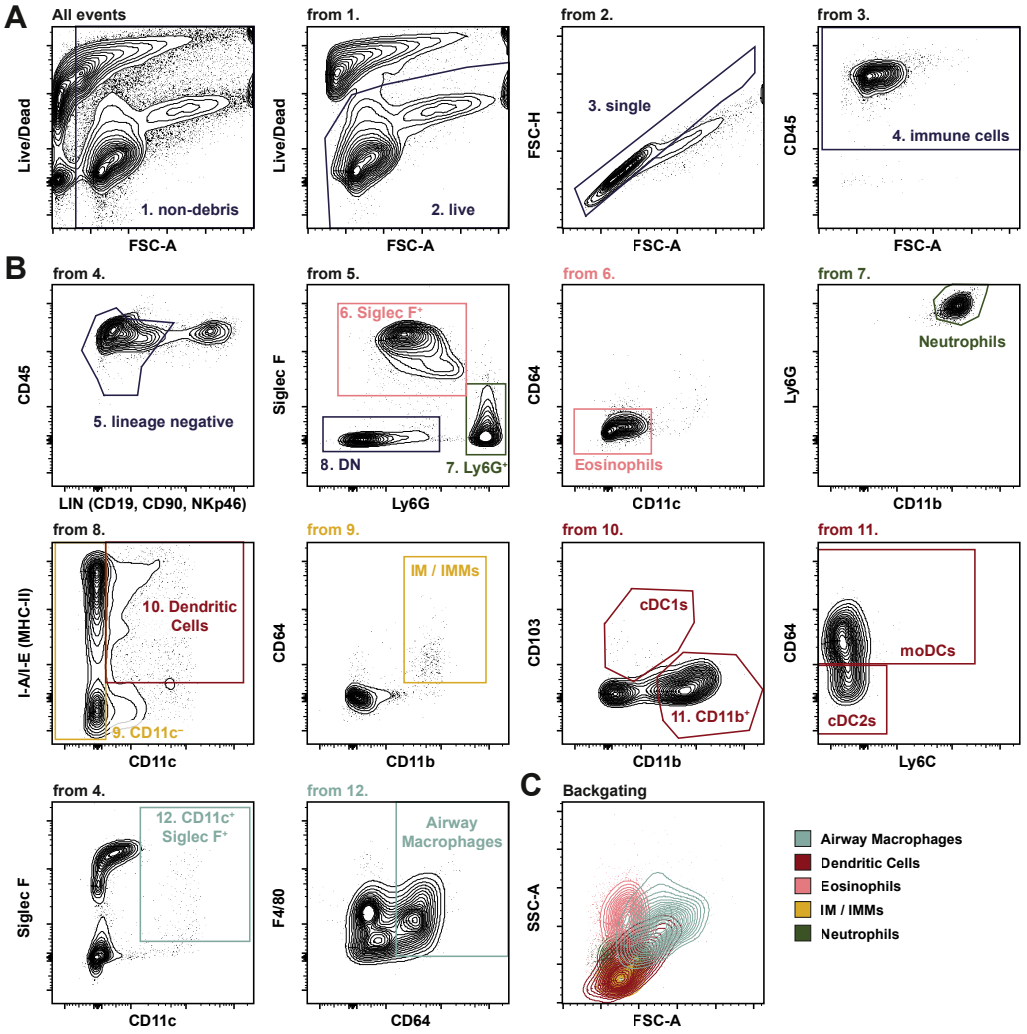


Figure 2.1 Dead cell exclusion and gating strategy for myeloid cells.
A Gating steps for exclusion of debris, dead cells and doublets. Analysis was restricted to CD45⁺ cells for immune cells. **B** Gating strategy for myeloid cells. **C** Backgating analysis of myeloid cell populations showing their size (FSC-A) and granularity (SSC-A).

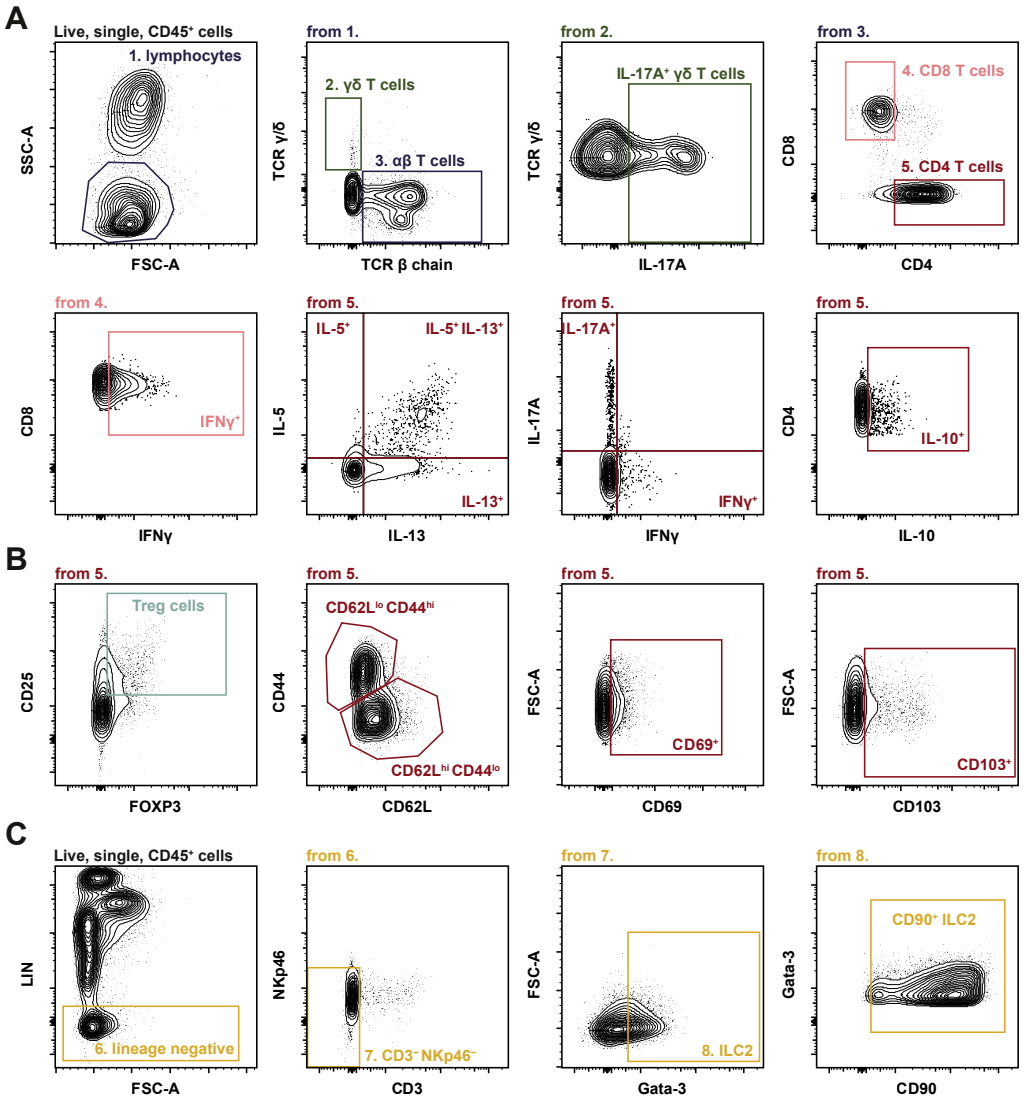


Figure 2.3 Gating strategy for lymphocytes.
A Gating strategy for cytokine-producing T lymphocytes after stimulation with PMA and ionomycin in the presence of Brefeldin A. **B** Gating strategy for Treg cells and phenotyping of CD4 T cells. **C** Gating strategy for ILC2s. Markers included in the lineage mix are indicated in Table 2.2.

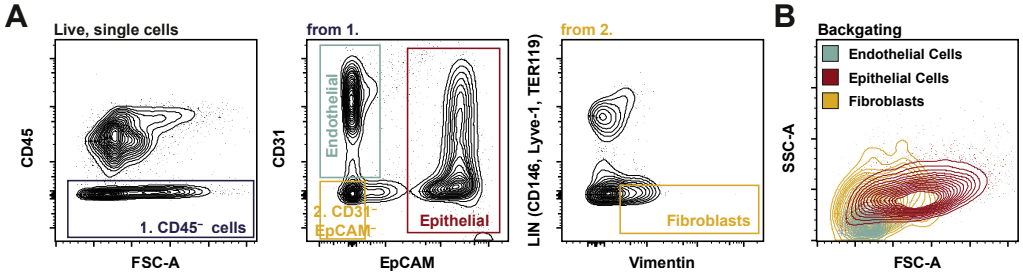


Figure 2.2 Gating strategy for structural cells.
A Gating strategy for structural cells in dispase-digested lungs. **B** Backgating analysis of structural cell populations showing their size (FSC-A) and granularity (SSC-A).

Table 2.4 Flow cytometry panel used to identify airway macrophages, other immune cells, epithelial cells and other structural cells.

Antigen	Fluorochrome	Use
CD64	BV421	Identification of airway macrophages
CD19	BV605	Exclusion of B cells (CD19), T cells and innate lymphoid cells (CD90.2) and NK cells (NKp46)
CD90.2	BV605	
NKp46	BV605	
CD45	BV711	Identification of immune cells
CD31	FITC	Exclusion of endothelial cells
Siglec F	PE	Identification of airway macrophages
EpCAM	PE-Cy7	Identification of epithelial cells
TO-PRO™-3	n/a	Exclusion of dead cells
CD11c	APC-Cy7	Identification of airway macrophages

2.6 RNA isolation, cDNA synthesis and quantitative PCR

2.6.1 RNA isolation

Commercially available kits were used for the isolation of RNA from tissues and cell lysates. The RNeasy Mini Plus kit (QiAGEN) was used for the extraction of RNA from lung homogenates. Flow-sorted cells and cell monolayers were lysed in RLT Plus buffer containing 1% (v/v) 2-mercaptoethanol and RNA were isolated using the RNeasy Micro Plus kit (QiAGEN). RNA from epithelial cells grown at ALI was extracted using either the RNeasy Mini Plus kit or the Maxwell® RSC automated RNA isolation platform with the simplyRNA Blood, Tissue or Cells Kit (all Promega). RNA quantity and quality were measured using either the NanoDrop™ 1000 spectrophotometer (Thermo Fisher Scientific) or the 2200 TapeStation instrument and reagents (Agilent, Santa Clara, USA).

2.6.2 cDNA synthesis

Equal amounts of RNA were transcribed into cDNA using the High Capacity cDNA Reverse Transcription Kit (Thermo Fisher Scientific) for inputs between 200 ng to 1 µg of RNA or the GoScript™ Reverse Transcriptase kit with random primers (Promega) for lower inputs. Where possible, controls lacking either RNA template or reverse transcriptase were prepared alongside sample preparation.

2.6.3 Quantitative PCR (qPCR)

qPCR reaction mixes were prepared from TaqMan™ FAM probes and Fast Advanced Master Mix (both Thermo Fisher Scientific). A list of all TaqMan™ probes used in this thesis can be found in **Table 2.5**. Per reaction, 3.6 µl of reaction mix was added to 2.4 µl of diluted cDNA per well. All conditions were run in duplicates in 384-well plates on a ViiA 7 Real-Time PCR system (Thermo Fisher Scientific) using manufacturer-recommended settings. QuantStudio Real-Time PCR software (Thermo Fisher Scientific) was used to determine cycle threshold (C_T) values and consistent thresholds for the calculation of C_T values were assigned for each target to allow for comparison between individual experiments. Relative expression of genes was calculated using the following formula:

$$Relative\ Expression = 2^{\Delta C_T},$$

$$where\ \Delta C_T = C_T(housekeeping\ gene) - C_T(gene\ of\ interest)$$

Actb and *Gapdh* or *ATP5B* and *YWHAZ* were used as housekeeping genes for mouse or human samples, respectively and C_T values were averaged before calculation of relative expression.

2.6.4 Transcriptomics analysis

Bulk RNA sequencing of bronchial brushes from children with PSW, severe asthma or controls was performed by members of the Marsland lab (Department of Immunology and Pathology, Monash University, Melbourne, Australia) as previously described[196]. Sequence alignment, processing and quality control were also performed by the Marsland group. Gene counts were then normalised as counts per million (CPM) using the *edgeR* package in RStudio and genes were filtered to include only those that were expressed (CPM > 0.5) in at least *n* = 13 samples (smallest group size). Genes of interest where then plotted on a logarithmic scale using the *ggplot2* package in RStudio.

Table 2.5 TaqMan™ assays used for gene expression analysis.
* indicates housekeeping genes.

Gene	Species	Assay ID	Gene (cont.)	Species (cont.)	Assay ID (cont.)
AREG	Human	Hs00950669_m1	***Ccl5***	Mouse	Mm01302427_m1
ACE2	Human	Hs00222343_m1	***Ccl7***	Mouse	Mm00443113_m1
ATP5B*	Human	Hs00969569_m1	***Ccl11***	Mouse	Mm00441238_m1
BTC	Human	Hs01101204_m1	***Ccl12***	Mouse	Mm01617100_m1
CTSL	Human	Hs00964650_m1	***Ccl17***	Mouse	Mm01244826_g1
CXCL8	Human	Hs00174103_m1	***Ccl24***	Mouse	Mm00444701_m1
CXCL10	Human	Hs01124252_g1	***Chil3***	Mouse	Mm00657889_mH
DDX58	Human	Hs01061436_m1	***Col1a1***	Mouse	Mm00801666_g1
EGF	Human	Hs01099990_m1	***Col3a1***	Mouse	Mm01254476_m1
EGFR	Human	Hs01076090_m1	***Col4a1***	Mouse	Mm01210125_m1
EPGN	Human	Hs02385424_m1	***Dcn***	Mouse	Mm00514535_m1
EREG	Human	Hs00914313_m1	***Egf***	Mouse	Mm00438696_m1
FOXJ1	Human	Hs00230964_m1	***Egfr***	Mouse	Mm01187858_m1
FURIN	Human	Hs00965485_g1	***Epgn***	Mouse	Mm00504344_m1
HBEGF	Human	Hs00181813_m1	***Ereg***	Mouse	Mm00514794_m1
IFIH1	Human	Hs00223420_m1	***Fn1***	Mouse	Mm01256744_m1
IFIT1	Human	Hs00356631_g1	***Gapdh****	Mouse	Mm99999915_g1
IFNB1	Human	Hs01077958_s1	***Hbegf***	Mouse	Mm00439306_m1
IFNL1	Human	Hs00601677_g1	***Ifng***	Mouse	Mm01168134_m1
IL6	Human	Hs00174131_m1	***Il4***	Mouse	Mm00445259_m1
ISG15	Human	Hs01921425_s1	***Il5***	Mouse	Mm00439646_m1
KRT5	Human	Hs00361185_m1	***Il10***	Mouse	Mm01288386_m1
MUC5AC	Human	Hs01365616_m1	***Il13***	Mouse	Mm00434204_m1
MUC5B	Human	Hs00861595_m1	***Il17a***	Mouse	Mm00439618_m1
NRP1	Human	Hs00826128_m1	***Il25***	Mouse	Mm00499822_m1
NRP2	Human	Hs00187290_m1	***Il33***	Mouse	Mm00505403_m1
TGFA	Human	Hs00608187_m1	***Mmp2***	Mouse	Mm00439498_m1
TJP1	Human	Hs01551861_m1	***Mmp9***	Mouse	Mm00442991_m1
TMPRSS2	Human	Hs01122322_m1	***Mmp12***	Mouse	Mm00500554_m1
TNF	Human	Hs00174128_m1	***Mmp13***	Mouse	Mm00439491_m1
YWHAZ*	Human	Hs01122445_g1	***Mmp14***	Mouse	Mm00485054_m1
Acta2	Mouse	Mm00725412_s1	***Muc5ac***	Mouse	Mm01276705_g1
Actb*	Mouse	Mm00607939_s1	***Muc5b***	Mouse	Mm00466391_m1
Adam8	Mouse	Mm01163449_g1	***Piezo1***	Mouse	Mm01241549_m1
Areg	Mouse	Mm00437583_m1	***Retnla***	Mouse	Mm00445109_m1
Arg1	Mouse	Mm00475988_m1	***Tgfa***	Mouse	Mm00446232_m1
Btc	Mouse	Mm00432137_m1	***Tnc***	Mouse	Mm00495662_m1
Ccl2	Mouse	Mm00441242_m1	***Tslp***	Mouse	Mm01157588_m1
Ccl3	Mouse	Mm00441259_g1			

2.7 Protein analyses

2.7.1 Enzyme-linked immunosorbent assay (ELISA) and membrane-based proteome arrays

Protein concentrations in bronchoalveolar lavage fluid, lung homogenates and cell supernatants were measured using commercially available sandwich ELISA kits (**Table 2.6**) or matched antibody pairs. Unless stated otherwise, assays were performed in 96 well half-area microplates (Corning) following manufacturer's recommendations but reducing all volumes by 60%. The matched antibody pairs and recombinant proteins used for 'homemade' sandwich ELISAs are listed in **Table 2.7**. For matched antibody pairs, plates were coated with capture antibody diluted in 0.1 M $NaHCO_3$ pH 8.6 overnight at room temperature, washed three times and blocked in 3% BSA in PBS for one hour, also at room temperature. Samples and standards (7-point standard curve using two-fold dilutions) were diluted in sample diluent (PBS containing 1% BSA with or without 0.05% Tween® 20) and incubated overnight at 4° C. Plates were then subsequently incubated with detection antibody for two hours and streptavidin-HRP (R&D Systems) for 30 minutes, both prepared in sample diluent, at room temperature. Following each step, plates were washed thrice with PBS containing 0.05% Tween® 20 (PBS-T). Assays were developed by addition of Enhanced K-Blue® TMB substrate (Neogen, Lansing, USA) and enzymatic reactions were stopped by the addition of 2N H_2SO_4. Optimal density (OD) was measured using a SpectraMax® i3x plate reader (Molecular Devices, San Jose, USA) and protein concentrations were interpolated from standard values using 4-parameter nonlinear regression.

Table 2.6 List of commercially used ELISA kits used in this thesis.

Analyte	Species	Detection Range	Supplier
IFN-beta	Human	7.8-500 pg/ml	R&D Systems
IL-8/CXCL8	Human	31.2-2000 pg/ml	R&D Systems
IL-6	Human	9.4-600 pg/ml	R&D Systems
IL-29/IL-28B (IFN-lambda 1/3)	Human	62.5-4000 pg/ml	R&D Systems
Amphiregulin	Mouse	15.6-1000 pg/ml	R&D Systems
Betacellulin	Mouse	7.8-500 pg/ml	R&D Systems
Epiregulin	Mouse	125-8000 pg/ml	R&D Systems
HB-EGF	Mouse	31.2-2000 pg/ml	R&D Systems
IFN gamma	Mouse	31.2-2000 pg/ml	Thermo Fisher Scientific
IL-13	Mouse	7.8-500 pg/ml	Thermo Fisher Scientific
IL-17A (homodimer)	Mouse	7.8-500 pg/ml	Thermo Fisher Scientific
IL-33	Mouse	15.6-1000 pg/ml	R&D Systems

Table 2.7 Antibodies and recombinant proteins used for 'homemade' sandwich ELISAs.

Capture antibodies	Clone	Concentration	Supplier
Purified Rat Anti-Mouse IgE	R35-72	2 µg/ml	BD Biosciences
Purified Rat Anti-Mouse IgG1	A85-3	2 µg/ml	BD Biosciences
Purified Rat Anti-Mouse IgG2a	R11-89	2 µg/ml	BD Biosciences
Purified Rat Anti-Mouse IL-4	11B11	2 µg/ml	BD Biosciences
Purified Rat Anti-Mouse IL-5	TRFK5	2 µg/ml	BD Biosciences
Standard	**Clone/Cat.**	**Concentration**	**Supplier**
Purified Mouse IgE, κ Isotype Control	C38-2	6.25-400 ng/ml	BD Biosciences
Purified Mouse IgG1, κ Isotype Control	MOPC-21	0.156-10 ng/ml	BD Biosciences
Purified Mouse IgG2a, κ Isotype Control	G155-178	7.81-500 ng/ml	BD Biosciences
Recombinant Mouse IL-4	550067	15.6-1000 pg/ml	BD Biosciences
Recombinant Mouse IL-5	554581	31.2-2000 pg/ml	BD Biosciences
Detection antibodies	**Clone**	**Concentration**	**Supplier**
Biotin Rat Anti-Mouse IgE	R35-118	2 µg/ml	BD Biosciences
Biotin Rat Anti-Mouse IgG1	A85-1	2 µg/ml	BD Biosciences
Biotin Rat Anti-Mouse IgG2a	R19-15	0.5 µg/ml	BD Biosciences
Biotin Rat Anti-Mouse IL-4	BVD6-24G2	0.5 µg/ml	BD Biosciences
Biotin Rat Anti-Mouse IL-5	TRFK4	2 µg/ml	BD Biosciences

The Proteome Profiler Human XL Cytokine Array Kit (R&D Systems) was used to detect 105 different cytokines and chemokines in pooled basal media from infected ALI cultures. The assay was performed according to the manufacturer's recommendations and membranes were images using the myECL™ Imager (Thermo Fisher Scientific). Mean grey values of duplicate spots was determined using Fiji software (National Institutes of Health, Bethesda, USA) and abundance of proteins relative to reference spots was calculated after background subtraction.

2.7.2 Western blot (WB)

Prior to western blot analysis, protein content in clarified cell lysates and lung homogenates was determined using Pierce™ BCA protein assay (Thermo Fisher Scientific). Samples were diluted in RIPA buffer to yield equal concentrations, NuPAGE™ LDS Sample Buffer (4X) (Thermo Fisher Scientific) was added and samples were incubated at 90° C for 5 minutes. Up to 30 µg of protein or 3 µl of Precision Plus Protein™ Kaleidoscope™ Prestained Protein Standards were then loaded into 4-12% Criterion™ XT Bis-Tris Protein gels (both Bio-Rad, Hercules, USA) and run in electrophoresis chambers filled with 1X Bolt™ MES SDS Running

buffer (Thermo Fisher Scientific) at a constant voltage of 110 V until the lowest protein standard reached the end of the gel. Proteins were then transferred from gels onto PVDF transfer membranes (Thermo Fisher Scientific) by wet transfer for 30 minutes at 110 V in cassettes submerged in WB transfer buffer (25 mM Tris-base, 192 mM glycine, 20% (v/v) methanol). Immediately after transfer, the position of the visible protein standards was indicated using Western Blot Marker Pen (Abcam) to allow visualisation of protein standards with chemiluminescence. Membranes were then blocked in 5% BSA in TBS containing 0.1% Tween® 20 (TBS-T), followed by incubation in primary antibodies in 5% BSA/TBS-T overnight. Membranes were washed thrice for five minutes in TBS-T and then incubated with secondary antibody diluted in 5% BSA/TBS-T for one hour. All antibodies are listed in **Table 2.8**. Following three more washes in TBS-T, membranes were developed using Pierce™ ECL PLUS Western Blotting Substrate and chemiluminescence was captured using a myECL™ Imager (both Thermo Fisher Scientific). Image processing and quantification of bands was performed in Image Studio™ Lite software (LI-COR Biosciences, Lincoln, USA).

Table 2.8 Antibodies used for WB analysis.

Antibody	Clone/Cat.	Dilution	Supplier
EGF Receptor (Mouse Preferred)	D1P9C	1:1000	Cell Signaling Technology
Phospho-EGF Receptor (Tyr1068)	D7A5	1:1000	Cell Signaling Technology
Anti-alpha Tubulin	EPR13478(B)	1:2000	Abcam
Anti-rabbit IgG, HRP-linked	7074	1:2000	Cell Signaling Technology

2.8 Imaging analysis

2.8.1 Agarose-embedding and sectioning of ALI inserts

Cross-sections of ALI inserts were prepared for imaging analysis. Membranes were excised from the inserts and embedded in 4% low-melting point agarose, followed by paraffin-embedding and sectioning at 4 µm thickness at the Histology Facility at Imperial College London.

2.8.2 Histological stains

Wax embedding, sectioning as well as haematoxylin and eosin (H&E) staining, periodic acid-Schiff (PAS) and Gordon & Sweet's silver staining were performed by Lorraine Lawrence of the Imperial College Histology Facility. The mean linear intercept (L_m) of the lung parenchyma

was calculated by overlaying 8 parallel lines on images of H&E-stained lungs and counting the number of airspaces intercepted by the lines. L_m values were averaged from four fields of view per mouse and expressed as distance between intercepts in µm. Mucus staining was assessed by scoring all airways within an entire lung section, from an individual mouse, based on the degree of PAS^+ cells in the epithelium using the following scoring system: 0 = <5% PAS^+ cells; 1 = 5-25% PAS^+ cells; 2 = 25-50% PAS^+ cells; 3 = 50-75% PAS^+ cells; 4 = > 75% PAS^+ cells. Scores across all airways were averaged. Reticulin thickness was measured using Fiji software at ten points per airway in sections stained with Gordon & Sweet's silver stain and averaged across all airways per lung section for each mouse. Epithelial height was measured in H&E-stained cross-sections of epithelial cells at ten points across the epithelial layer using ImageScope Software (Leica, Wetzlar, Germany)

2.8.3 Immunofluorescence

Immunofluorescence staining was performed on lung section or cross-sections of epithelial layers from ALI cultures. Paraffin-embedded section were passed through two changes of D-Limonene (GENTACLEAR; Genta Medical, York, United Kingdom) and rehydrated using decreasing concentration of ethanol (100%, 90%, 70% for 1 minute each followed by PBS). Slides were placed in 90° C EDTA buffer (1 mM EDTA, pH 8) or Tris-EDTA buffer (10 mM Tris-base, 1 mM EDTA, pH 9) and incubated covered for 30 minutes for heat-induced antigen retrieval. Samples were blocked and permeabilised in PBS containing 10% donkey serum and 0.5% Tween® 20 for one hour at room temperature followed by two five-minute washes in PBS. Slides were then incubated with primary antibodies diluted in 1% BSA in PBS overnight at 4° C. After two further washes in PBS, samples were incubated with secondary antibodies diluted in 1% BSA in PBS for at least one hour at room temperature. Where staining panels contained conjugated and unconjugated antibodies raised in the same species, the staining with the unconjugated primary and conjugated secondary antibody was followed by an additional blocking step in serum of the species that the primary antibody was raised in prior to staining with the conjugated primary antibody. Following secondary antibody staining, slides were washed twice in PBS. In some instances, 0.1 µg/ml DAPI (Sigma) was included in the last wash step as a counterstain for nuclei. Samples were mounted using ProLong™ Diamond Antifade Mountant and allowed to cure at room temperature for 24 hrs before imaging or storage at 4° C. A list of all antibodies used for immunofluorescence imaging within this thesis can be found in **Table 2.9**.

Table 2.9 Antibodies used for immunofluorescence staining.

Primary antibodies			
Antibody (Host/clone)	**Conjugate**	**Conc.**	**Supplier**
ACE2 (Goat polyclonal)	-	4 µg/ml	R&D Systems
Alpha-smooth muscle actin (Mouse 1A4)	AF488	2.5 µg/ml	Thermo Fisher Scientific
Alpha-tubulin (Mouse 6-11B-1)	-	10 µg/ml	Abcam
Cytokeratin 5 (Rabbit EP1601Y)	AF647	2.5 µg/ml	Abcam
Goat IgG, polyclonal isotype control	-	2-4 µg/ml	Abcam
Mucin 5AC (Rabbit EPR16904)	AF555	5 µg/ml	Abcam
PIEZO1 (Rabbit polyclonal)	-	10 µg/ml	Novus Biologicals
Rabbit IgG, polyclonal isotype control	-	10 µg/ml	Vector Labs
SARS NP (Rabbit polyclonal)	-	10 µg/ml	Novus Biologicals
Type I Collagen (Goat polyclonal)	-	2 µg/ml	Southern Biotech
Secondary antibodies			
Antibody	**Conjugate**	**Conc.**	**Supplier**
Donkey anti-goat IgG	AF488	10 µg/ml	Thermo Fisher Scientific
Donkey anti-goat IgG	AF647	10 µg/ml	Thermo Fisher Scientific
Donkey anti-mouse IgG	AF488	10 µg/ml	Thermo Fisher Scientific
Donkey anti-rabbit IgG	AF546	10 µg/ml	Thermo Fisher Scientific
Donkey anti-rabbit IgG	AF594	10 µg/ml	Thermo Fisher Scientific

2.8.4 Image acquisition and analysis

Fluorescence imaging

Fluorescence images were acquired on a Leica DM 2500 microscope with a Leica DFC300 FX camera or using the Aperio VERSA slide scanner (all Leica) with a maximum magnification of 400x. Images were cropped, rotated and adjusted for brightness and contrast using Fiji software, which was also used to assign pseudocolours and add scale bars. For quantification of α-smooth muscle actin staining, regions of interest were drawn around the large airways and underlying smooth muscle and the amount of α-smooth muscle actin staining within these areas was calculated using Fiji software.

Second-harmonic generation

Second-harmonic generation images of fibrillar collagens were generated by two-photon imaging of dewaxed, dehydrated and mounted lung sections using a Leica SP5 inverted confocal multi-photon fluorescence lifetime measures microscope. Tissue autofluorescence

was recorded in an additional channel to allow orientation within sections. Z-stacks were generated with a constant number of steps and Z-step size (around 1 µm) and maximum projections were generated using Fiji software. Collagen organisation was analysed within collagen regions across four angles (0°, 45°, 90°, 135°) using the GLCM-TextureToo plugin for Fiji and yielded values for contrast (measure of local variations in the image), angular second moment (represent the uniformity of the image), entropy (statistical measure of randomness) and inverse difference moment (measure of similarity).

2.9 Data analysis, statistics and visualisation

2.9.1 Data processing and simple statistical testing

All data processing, calculations and analyses were conducted within RStudio to allow for reproducibility and automation. The R *stats* package was used for statistical analyses. Since normality of data could not be assumed, non-parametric analyses were conducted. Unless stated otherwise, two groups were compared by calculating exact *p* values using a two-sided Mann-Whitney test, with *p* values < 0.05 being considered statistically significant. Where matched data existed, groups were compared using a paired Wilcoxon test. Where three or more groups were compared, the R *rstatix* packages was used to perform a Kruskal-Wallis test followed by a Dunn's post-hoc test between individual groups. *P* values were corrected for multiple comparisons using the Bonferroni.

2.9.2 Correlations, principal component analysis and network analysis

The R *stats* package was used to perform principal component analyses and compute correlations. For principal component analysis of complete records of continuous variables, data were scaled and centred and the first two principal components were plotted. The Spearman method was used for correlation analysis, yielding exact *p* values and rank correlation coefficients (ρ). Venn diagrams of overlapping significant correlations (*p* value < 0.05 and a |ρ| > 0.5) between assigned clusters were created using the *ggvenn2* package. Network analysis was conducted on correlation data, whereby correlations with a *p* value < 0.05 and a |ρ| > 0.75 were considered as interactions (edges) between variables (nodes). A node-edge diagram of correlations with 'fr' layout was created using *tidygraph* and *ggraph* packages. Interesting valuables (nodes) were labelled in the network map.

2.9.3 Visualisation

Graphs were created using the *ggplot2* package. Unless stated otherwise, data are shown as box-and-whisker plots with the whiskers ranging from minimum to maximum, the box indicating the interquartile range and the line denoting the median. Where possible, individual data points are shown.

3 Results I:

Pulmonary levels of EGFR and its ligands – changes during development and with allergen or virus challenge

3.1 Introduction

3.1.1 Stages of lung development in humans and mice

The key physiological role of the lungs is the successful gas exchange between the external environment and the blood in order to support the supply of oxygen to all tissues. During embryonic development, oxygen is supplied from the mother via the umbilical cord, which allows the development of the lungs during this period. However, even though human lung development is sufficiently advanced even at around 36 weeks of gestation to support gas exchange in infants born at term or slightly pre-term[197], classical alveolarization continues until around 3 years of age and the lungs undergo further maturation processes up until young adulthood[198]. Lung development of both humans and mice can be divided into five main histological stages[198-201] (**Figure 3.1A**, page 77).

During the *embryonic stage*, which spans gestational week 4-7 in humans and embryonic days (E)9.5-12 in mice, the lung buds emerge from the ventral foregut endoderm and separate from the oesophagus, resulting in the formation of the lung primordium, a primitive larynx and trachea, the latter of which bifurcates shortly after. During this stage, the primordial tubes complete their branching to give rise to the five main lobes of the lungs.

The subsequent *pseudoglandular phase* (week 5-17 in humans; E12-16.5 in mice) is named for the resemblance the branching epithelial tubes bear to exocrine glands. As a result of this branching process, a primitive respiratory tree is formed, which is fluid-filled at this stage and thus unable to support gas exchange.

The *canalicular stage* (week 16-26 in humans; E16.5-17.5) is a short stage characterised by significant changes in morphology. This phase sees the first immergence of immature terminal sacs, formed when terminal bronchioles are divided into the proximal respiratory bronchioles and the distal alveolar ducts, as well as increases in vascularisation and angiogenesis as the respiratory tree expands.

These immature terminal sacs develop further to form primitive respiratory sites during the *saccular stage* (week 24-38 in humans; E17.5 to postnatal day (P)4 in mice). In this phase, the alveolar epithelial cells differentiate into alveolar type I and type II cells, the latter of which produce surfactants which prevent the lungs from collapsing. At the same time, the interstitium of the lungs thins, accompanied by further increases in capillaries, innervation and lymphatics in the lungs. At the end of this stage, the primitive respiratory sites are sufficiently developed to support gas exchange, which is particularly crucial in prematurely born infants.

During the final phase of lung development, the *alveolar stage* (from week 36 of gestation in humans; P4-P21 in mice), the terminal sacs formed during the previous stages of lung organogenesis develop into mature alveolar ducts and alveoli, resulting in the formation of the majority of the gas exchange surface. While classical alveolarization, during which alveoli are formed by the development of secondary septa, is concluded by around 3 years of age in humans or P21 in mice, septation and maturation of the microvasculature continue into young adulthood.

3.1.2 The role of EGFR and its ligands during lung development

EGFR signalling plays a crucial role during lung development. Studies analysing EGFR-deficient mice have reported immature lungs and a lack of proper alveolarization in those animals that survived past gestation[160, 161]. It was later shown that EGFR is crucial for successful branching and that EGFR-deficient mice showed defects as early as E12, resulting in an overall 50% reduction in alveolar volume and thus severely impaired gas exchange[202]. The same study also found that EGFR contributed to the maturation of alveolar type II cells, particularly the formation of multilamellar bodies, and that treatment of healthy lung organ cultures with EGF was sufficient to induce expression of surfactant protein C (SP-C) and thyroid transcription factor-1 (TTF-1), both of which are markers of alveolar type II cell maturation. EGFR signalling is further necessary for expression of SP-A in the lungs[203], and Wang and colleagues (ref. [204]) have reported that mechanical stretch of embryonic type II alveolar cells can result in shedding of HB-EGF and TGFα, which induced SP-B and SP-C by signalling via EGFR, thus driving type II cell differentiation. Finally, mice deficient for ADAM17, the enzyme responsible for membrane shedding of AREG, EREG, HB-EGF and TGFα, showed visible respiratory distress and failed to form normal saccular structures, characterised by impaired branching morphogenesis, a thick-walled mesenchyme and deficient septation[205], providing further evidence for a central role for EGFR signalling during lung development.

Despite the clear importance of EGFR in pulmonary development, the individual contributions of each of the seven ligands is less clear. Although a role for AREG in lung branching has been predicted using *ex vivo* and *in vitro* approaches[206], AREG null mice displayed no gross or histological abnormalities of the lungs[207]. Similarly, studies characterising mice deficient for BTC, EGF, EPGN, EREG or TGFα, or triple-deficient mice for AREG/EGF/TGFα or EGF/EREG/TGFα, did not report any gross defects in the lungs of these animals[177-180, 207, 208], indicating that these ligands are dispensable or only contribute minorly to lung development. It is also possible that the loss of one or a few ligands can be compensated for by the remaining ligands. In contrast, roughly half of HB-EGF null mice displayed lung defects, including thickened mesenchymal tissue between alveoli as well as an overall reduction in the number

of alveoli and defects in the differentiation of alveolar type II cells[208], suggesting that HB-EGF plays a major, non-redundant role in lung development. However, further studies dissecting the exact contribution of each individual ligand are currently lacking. In addition, although some efforts have been made to analyse the presence and expression patterns of EGFR and some of its ligands within the lungs[209-211], cell-type specific pulmonary expression of the receptor and all of its seven ligands has not yet been described.

3.1.3 EGFR signalling during asthma, AAD and respiratory viral infection

There is overwhelming evidence to suggest that EGFR signalling is altered during asthma and AAD, as well as in response to viral infection. EGFR and its ligands AREG, HB-EGF and EGF were increased in the bronchial epithelium of adult and paediatric patients with asthma compared to controls[212-218] and elevated levels of AREG or EGF were found in the sputum of children with asthma[219, 220]. Additional studies have reported elevated nasal EGF levels in children and adults with wheeze[221] as well as increased numbers of AREG-expressing cells[138] or subepithelial expression of ADAM17[222] in bronchial biopsies from patients with asthma. Augmented expression of EGFR ligands and receptor activation compared to controls was present in nasal and bronchial cells from patients with asthma[218, 223, 224]. Importantly, EGFR or ligand expression correlated with several key disease parameters, such as sputum eosinophilia, airway hyperresponsiveness, forced expiratory volume, mucus production or reticular basement membrane thickness[138, 214, 215, 220, 223], indicating that EGFR signalling may actively contribute to disease pathogenesis.

Further insight can be gained from evaluating *in vivo* and *in vitro* studies. For example, it has been shown that the fungal allergen *Alternaria alternata* (ALT) can induce phosphorylation of EGFR in human bronchial epithelial cells[225]. Similarly, the aeroallergen house dust mite (HDM) acted cooperatively with IL-4 and IL-13 to induce the expression of TGFα along with IL-8 and GM-CSF in bronchial epithelial cells from healthy controls or patients with asthma[224]. The ability of allergens to induce EGFR signalling has also been demonstrated *in vivo* in various rodent models. Using traditional sensitisation-challenge models of AAD, several groups have shown increases in EGFR phosphorylation and expression of HB-EGF in the lungs upon challenge with OVA or HDM[157, 168, 169, 226, 227]. These findings are complemented by studies employing more physiologically relevant models of chronic inhaled allergen exposure, which describe increases in EGFR ligand levels or augmented activation of EGFR in the airway epithelium of mice upon repeated exposure to HDM or ALT[134, 136, 166, 223]. These results clearly highlight that EGFR signalling is active during AAD, although there is little data available to show how the levels of the individual ligands change with allergen exposure or suggest which ligand(s) may be involved in driving EGFR activation in this context.

However, increased EGFR activation is not unique to inhaled allergen exposure. Of particular relevance to PSW and asthma are respiratory viral infections, as these are common triggers of exacerbations and may also predispose to disease development. Various common respiratory viruses, such as RSV, RV or influenza A virus (IAV) can induce EGFR phosphorylation in primary epithelial cells or cell lines[228-237]. Importantly, the induction of mucins such as MUC5AC by these viruses was shown to depend on EGFR signalling[231, 235, 238]. These findings are especially interesting as mucus hypersecretion is also a key pathological feature of asthma, and similar EGFR-dependent mechanisms may be driving pathology in this context.

Overall, despite overwhelming evidence for the importance of EGFR signalling both during lung development and during asthma and viral infection, comprehensive approaches to study the individual roles of all seven ligands in these contexts are lacking. In addition, little is known about EGFR signalling during early-life AAD. This chapter aimed to address both of these questions.

3.1.4 Hypothesis and aims

Hypothesis

EGFR is central to lung development as well as the pulmonary response to allergens and viruses both in early life and adulthood, with unique roles for the individual ligands.

Aims

1. To analyse how EGFR ligand levels change during pulmonary development.
2. To investigate which cells are the primary sources of EGFR and ligands in the naïve lung at different stages of life.
3. To measure how EGFR signalling, including expression of the various ligands, is affected by allergen or viral challenge in early life and compare it to adulthood.

3.2 Methods

3.2.1 Analysis of published data sets

The whole genome expression data set prepared by Beauchemin et al. 2016 (ref. [239]) was used to analyse *Egfr* and ligand gene expression in the developing murine lung. Expression data were downloaded directly from http://lungdevelopment.jax.org/ and plotted without further transformation.

Expression patterns of *EGFR* and ligand genes in the human lung were analysed in the single-cell RNA sequencing data set prepared by Travaglini et al. 2020 (ref. [240]). Data from the 10X genomics sequencing approach were explored using the Chan Zuckerberg CELLxGENE Discover cellular visualisation tool, restricting the analysis to lung tissue (https://cellxgene.cziscience.com/d/krasnow_lab_human_lung_cell_atlas_10x-1.cxg/).
Genes or gene sets were visualised directly within the tool and resultant graphs were exported for use in this thesis. Cell population identity was confirmed by plotting population-specific gene sets (**Table 3.1**).

Table 3.1 Gene sets used to validate sorted cell populations.

Population	Gene set
Immune	*PTPRC*
Stromal	*VIM*, *DCN*, *COL1A2*, *ACTA2*
Endothelial	*PECAM1*, *CDH5*, *TIE1*
Epithelial	*EPCAM*, *KRT19*, *AQP3*, *SFTPC*, *FOXJ1*, *KRT5*, *MUC1*

3.2.2 Sorting lung cell populations at different stages of development

Naïve C57BL/6J mice were culled at different postnatal timepoints and lungs were dissociated into single-cell suspensions using dispase and DNase digestion. Four major lung cell populations, airway macrophages (AMs), other immune cells, epithelial cells and other structural cells, were isolated using fluorescence-activated cell sorting. Gene expression of *Egfr* and ligands was measured using qPCR.

3.2.3 Murine models of allergic airway disease (AAD)

AAD was induced in neonatal or adult BALB/c mice by repeated intranasal dosing with recombinant mouse IL-33, HDM or ALT. In some cases, mice were also infected with RSV or treated with AREG. Organs were harvested 24 hours after the final challenge. Details of which models were used are given in the relevant figure legends.

3.2.4 Use of primary human samples to investigate effects of allergen on EGFR ligands

Primary airway epithelial cells were collected from 5-8-day-old infants, a 3-year-old child with lower respiratory tract infection and non-asthmatic pre-school children or adults by nasal or bronchial brushing. Cells were grown at air-liquid-interface (ALI) for at least three weeks until fully differentiated and then challenged with HDM and/or RSV. Gene expression and protein levels were analysed in cell lysates using qPCR and western blot, respectively.

Normal human lung fibroblasts (NHLFs) were isolated from human lung resections using outgrowth cultures. Fibroblasts were treated with basal media from naïve differentiated nasal epithelial cells in the presence or absence of EGFR inhibitor Gefitinib and cell proliferation was determined using live imaging and subsequent image analysis.

Children of pre-school or school-age with or without wheeze or severe asthma were recruited for sampling by bronchoscopy as previously described[189, 190]. Brushings of the large airways and BAL were collected for gene expression analysis by bulk RNA sequencing or qPCR, respectively. Donor demographics of samples used for analysis of bronchial brushes and BAL cells can be found in **Table 3.2** and **Table 3.3**, respectively. Atopy was defined specific IgE > 0.35 kUA/l against common allergens (grass pollen, tree pollen, cat, dog, HDM, moulds).

Table 3.2 Demographics of donors used for transcriptome analysis of bronchial brushings.

	Pre-school controls (*n* = 28)	Pre-school wheeze (*n* = 13)	School-aged severe asthma (*n* = 14)
Female sex (%)	11 (39%)	4 (31%)	10 (71%)
Median age (range) in months	48.5 (18-67)	46 (31-70)	161 (80-205)
Ethnicity (%)			
Asian	5 (18%)	2 (15%)	1 (7%)
Black	-	3 (23%)	-
White	4 (14%)	7 (54%)	8 (57%)
Mixed	18 (64%)	1 (8%)	3 (21%)
Any other	1 (4%)	-	1 (7%)
Unknown	-	-	1 (7%)
Atopy status (%)			
Atopic	7 (25%)	5 (38%)	8 (57%)
Non-atopic	11 (39%)	8 (62%)	6 (43%)
Unknown	10 (36%)	-	-
Viral PCR			
Positive	-	7 (54%)	7 (50%)
Negative	-	4 (31%)	6 (43%)
Unknown	28 (100%)	2 (15%)	1 (7%)

Table 3.3 Demographics of donors used for gene expression analysis of BAL.

	Disease controls (*n* = 8)	Pre-school wheeze (*n* = 9)	School-aged severe asthma (*n* = 6)
Female sex (%)	5 (63%)	2 (22%)	4 (67%)
Median age (range) in months	49.5 (25-159)	33 (27-49)	140 (74-205)
Ethnicity (%)			
Asian	-	1 (11%)	1 (17%)
Black	-	1 (11%)	-
White	-	7 (78%)	1 (17%)
Mixed	-	-	4 (67%)
Any other	-	-	-
Unknown	8 (100%)	-	-
Atopy status (%)			
Atopic	1 (13%)	4 (44%)	3 (50%)
Non-atopic	7 (87%)	4 (44%)	3 (50%)
Unknown	-	1 (11%)	-
Viral PCR			
Positive	5 (63%)	3 (33%)	2 (33%)
Negative	3 (37%)	3 (33%)	3 (50%)
Unknown	-	3 (33%)	1 (17%)

3.3 Results

3.3.1 EGFR and ligand expression throughout pulmonary development

While the requirement for EGFR signalling for successful pulmonary development has been described previously, the contribution of the individual ligands has not been studied in detail, nor how their expression might change during the different stages of pre- or postnatal lung development (**Figure 3.1A**). Even though the individual contribution of each ligand to successful lung development is difficult to assess without the detailed study of knockout animals, a publicly available data set was used to delineate pulmonary gene expression of EGFR and its ligands during lung development. Beauchemin and colleagues (ref. [239]) collected whole lungs from male mice of three different inbred stains (A/J, C3H/HeJ and C57BL/6J) at several embryonic (E11.5 to E19.5) and postnatal stages (P0 to P56), as well as whole embryos at E9.5, and performed whole genome gene expression analysis on RNA extracted from these tissues. From this data set, expression levels of *Egfr* and its ligands throughout lung development were extracted (**Figure 3.1B**). *Egfr* exhibited strong expression in both developing and mature lungs, and levels were elevated compared to those measured in whole embryos at E9.5, underlining the prominence of EGFR in the lungs. While all ligands were detected in the data set, expression levels of *Areg*, *Hbegf* and *Tgfa* were higher compared to the other ligands, potentially pointing towards a greater role for these molecules in lung development. Interestingly, transcript levels of both *Egfr* and its ligands remained largely stable during both embryonic and postnatal stages, with the exception of *Hbegf*, whose expression increased steadily throughout development. *Hbegf* was also the only gene that showed differential expression between the different mouse strains, with elevated levels measured in C3H/HeJ mice. Together, these observations may suggest particular importance of *Hbegf* compared to its fellow EGFR ligands in the murine lung. However, it was not possible to infer distinct roles for either of the ligands in pulmonary development from these data.

A limitation of the approach used by Beauchemin et al. (ref. [239]) is its inability to measure cell-specific changes in gene expression. In order to address which cells displayed the highest expression of *Egfr* and its ligands in the murine lung, as well as how cell-specific expression levels might change during postnatal development, FACS was used to divide lung cell suspensions collected at different postnatal timepoints into four main populations: airway macrophages (AMs; $CD45^+$ Siglec F^+ $CD11c^+$ $CD64^+$), other immune cells ($CD45^+$), epithelial cells ($CD45^-$ $EpCAM^+$ $CD31^-$) and other structural cells ($CD45^-$) (**Figure 3.2A-B**). While *Epgn* transcripts were not reliably detected throughout the time course in any population and *Egf* mRNA was only present in other structural cells at all timepoints, robust expression of *Egfr* and the remaining ligands was observed, especially in the structural compartment (epithelial

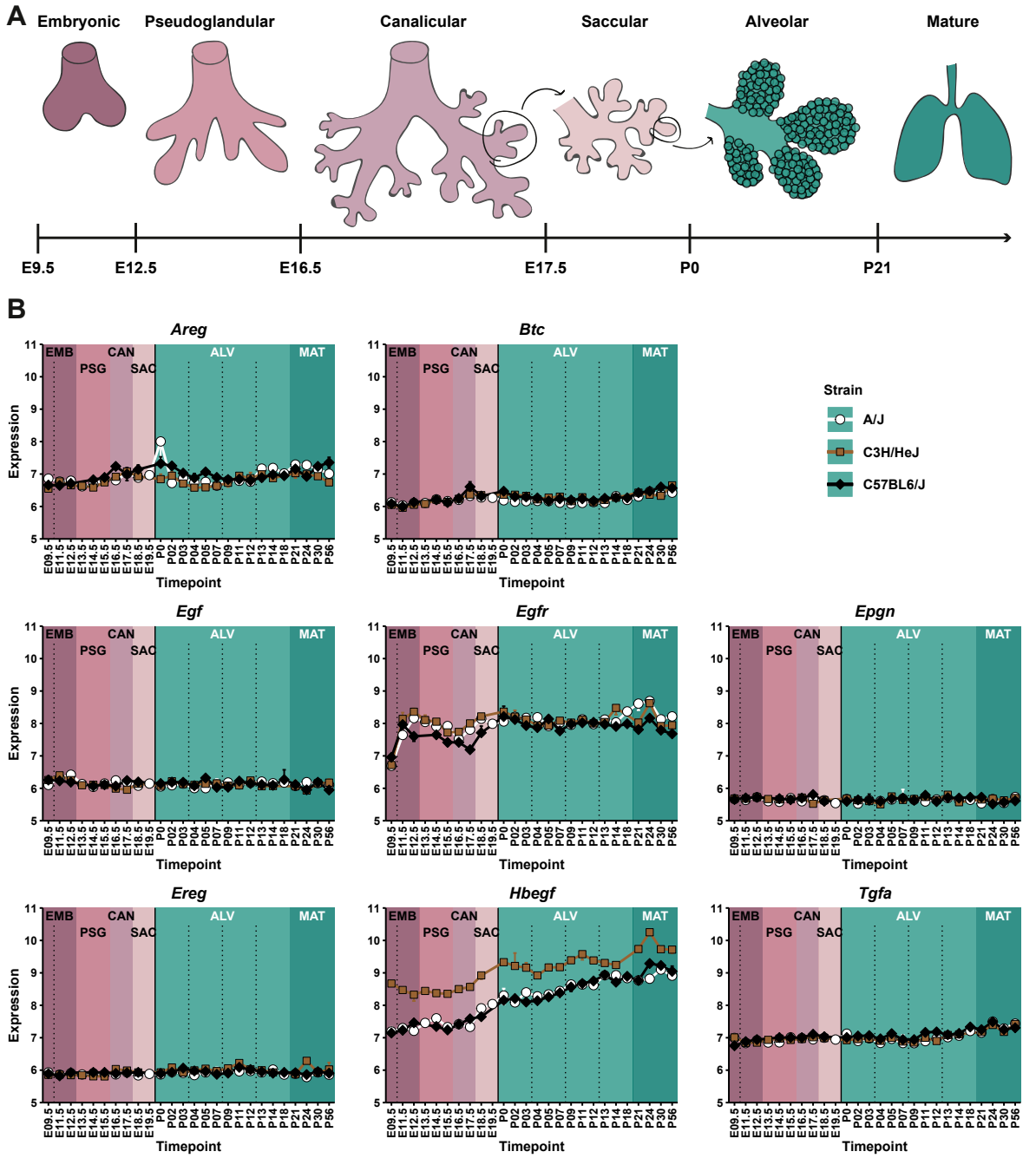


Figure 3.1 *Egfr* and ligand expression during pre- and postnatal murine lung development.
A Schematic illustrating pre-natal (embryonic, EMB; pseudoglandular, PSG; canicular, CAN; saccular, SAC) and post-natal (alveolar, ALV; mature, MAT) stages of lung development. **B** Gene expression (log_2 probe intensity) of indicated genes in whole embryos (E09.5) or lungs of male A/J, C3H/HeJ or C57BL6/J during different stages of development, as reported by Beauchemin et al., 2016 (ref. [239]). Data are shown as median (interquartile range) of *n* = 2-3 per strain and timepoint.

cells and other CD45$^-$) (**Figure 3.2C**). In comparison, *Egfr* and ligand expression levels were lower in immune cells, particularly in AMs. In line with whole lung expression (cf. Figure 3.1), mRNA levels were largely stable throughout development in all populations except AMs, which displayed timepoint-dependent differences in expression of *Egfr* and its ligands, potentially

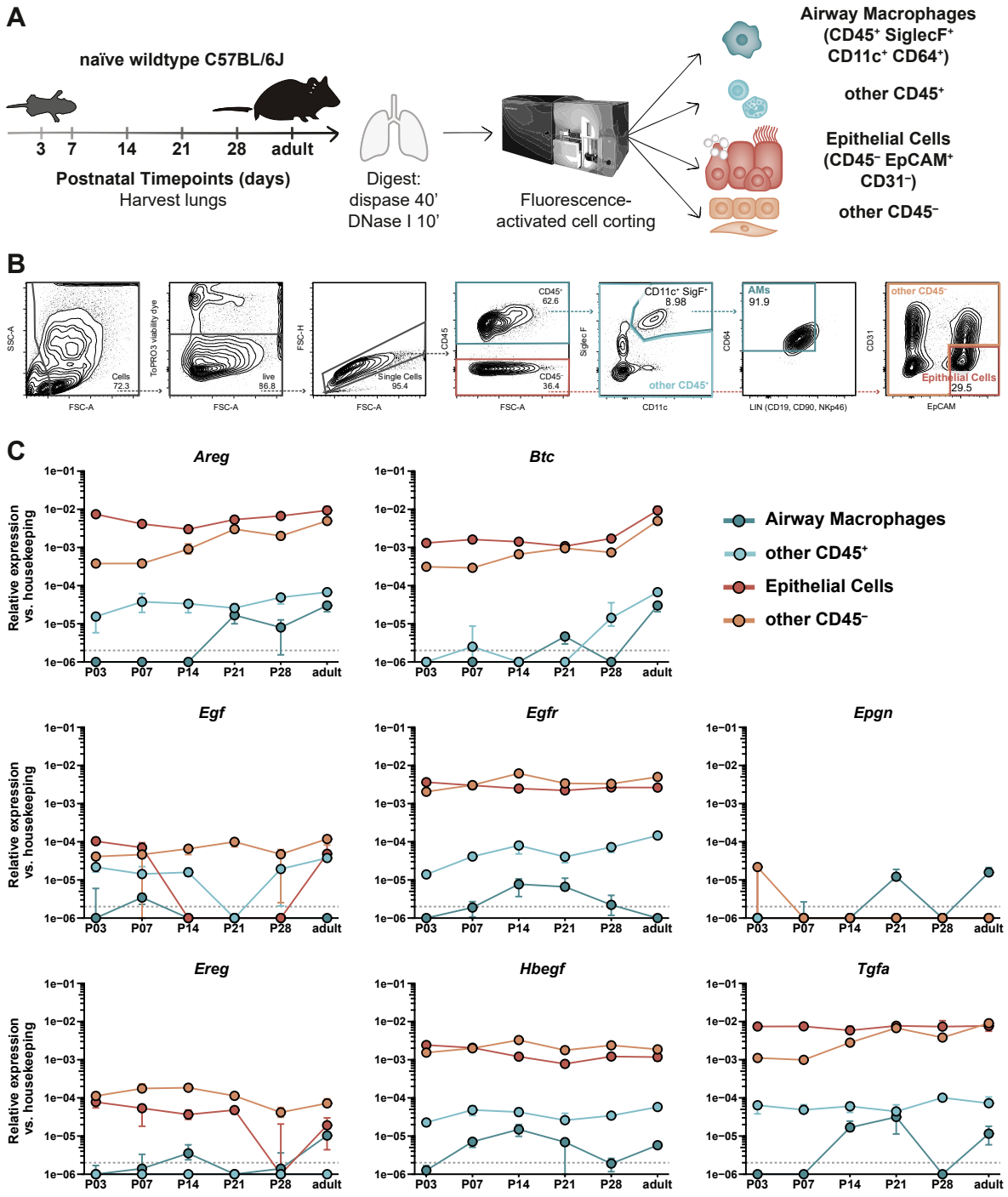


Figure 3.2 *Egfr* and ligand expression levels in four major lung cell populations at different stages of lung development.
A Schematic overview of experimental approach. WT C57BL/6J mice were culled at various postnatal timepoints and four major cell populations were isolated from lungs using fluorescence-activated cell sorting. **B** Gating strategy for the isolation of airway macrophages (AMs), other CD45$^+$ cells, epithelial cells and other CD45$^-$ cells. **C** Gene expression by qPCR of indicated genes in four major lung cell populations across various postnatal timepoints. Data are shown as median (interquartile range) of n = 3-8 mice per timepoint. Dotted line denotes limit of detection.

pointing towards a role for these cells in alveolarization. Overall, these data show that *Egfr* and most of its ligands were widely expressed in the murine lung and that the CD45$^-$ compartment was the dominant source of transcript.

In order to address whether cell-specific expression patterns of *EGFR* and its ligands were comparable in the human lung, publicly available single-cell sequencing data from normal lung resections of patients undergoing lobectomy for focal lung tumours, collected by Travaglini and colleagues[240] as part of the Human Lung Cell Atlas (HLCA), were explored (**Figure 3.3A**). Tissue from three donors was collected from three different regions of the lung (proximal, medial and distal) and dissociated into cell suspensions, which were enriched for epithelial ($EPCAM^+$), endothelial/immune ($CD31^+$ $CD45^+$) or stromal ($EPCAM^-$ $CD31^-$ $CD45^-$) cells prior to single-cell sequencing using the 10x genomics platform (**Figure 3.3A**). While distal lung tissue was available for all donors, medial and proximal were only collected from one donor, respectively (**Figure 3.3B**). Sequencing data were visualised using the Chan Zuckerberg CELLxGENE Discover cellular visualisation tool, which generated a tSNE plot for each cellular compartment (n = 4, across) and donor (n = 3, down). To confirm the appropriate assignment of the cellular compartments, expression of cell type-specific gene sets was visualised on the tSNE plots (**Figure 3.3C**, cf. Table 3.1). As expected, expression of *PTPRC*, the gene encoding CD45, was restricted to the immune compartment, while stromal cells could be identified by their high expression of *VIM*, *DCN*, *COL1A2* and *ACTA2*. Similarly, the expression of endothelial (*PECAM1*, *CDH5* and *TIE1*) and epithelial cell gene sets (*EPCAM*, *KRT19*, *AQP3*, *SFTPC*, *FOXJ1*, *KRT5* and *MUC1*) was restricted to their respective cellular compartments, thus validating the assignment of each of the populations. The expression of *EGFR* and each of its seven ligands within these data was then plotted to investigate their cell type-specific expression within the human lung (**Figure 3.3D**). As observed in the murine lung, *EGFR* expression was highest in structural (stromal, endothelial and epithelial) populations. Ligand expression was varied, with *AREG* and *HBEGF* displaying high expression across all compartments, whereas other ligands, such as *BTC*, *EPGN*, *EREG* and *TGFA,* were restricted to one or two compartments. *EGF* expression was rare in any compartment. Overall, these data suggest that similar to the findings in the murine lung, *EGFR* and some of its ligands, particularly *AREG* and *HBEGF*, are widely expressed in the adult human lung.

While the HLCA provides detailed information on cell type-specific gene expression patterns, it only reflects gene expression of adult (46- to 75-year-old) individuals. In order to assess the influence of age, as well as anatomical location, on the gene expression of *EGFR* and its ligands in human epithelial cells, primary nasal (NEC) or bronchial (BEC) epithelial cells were collected from non-asthmatic infants, pre-school children or adults and grown into well-differentiated pseudostratified epithelial layers in air-liquid interface (ALI) cultures (**Figure 3.3E**). Gene expression analysis of these cultures revealed comparable expression of *EGFR* and its ligands across ages and locations, with only minor differences detected in *EGFR* expression between infants and pre-school children and *TGFA* between NECs and

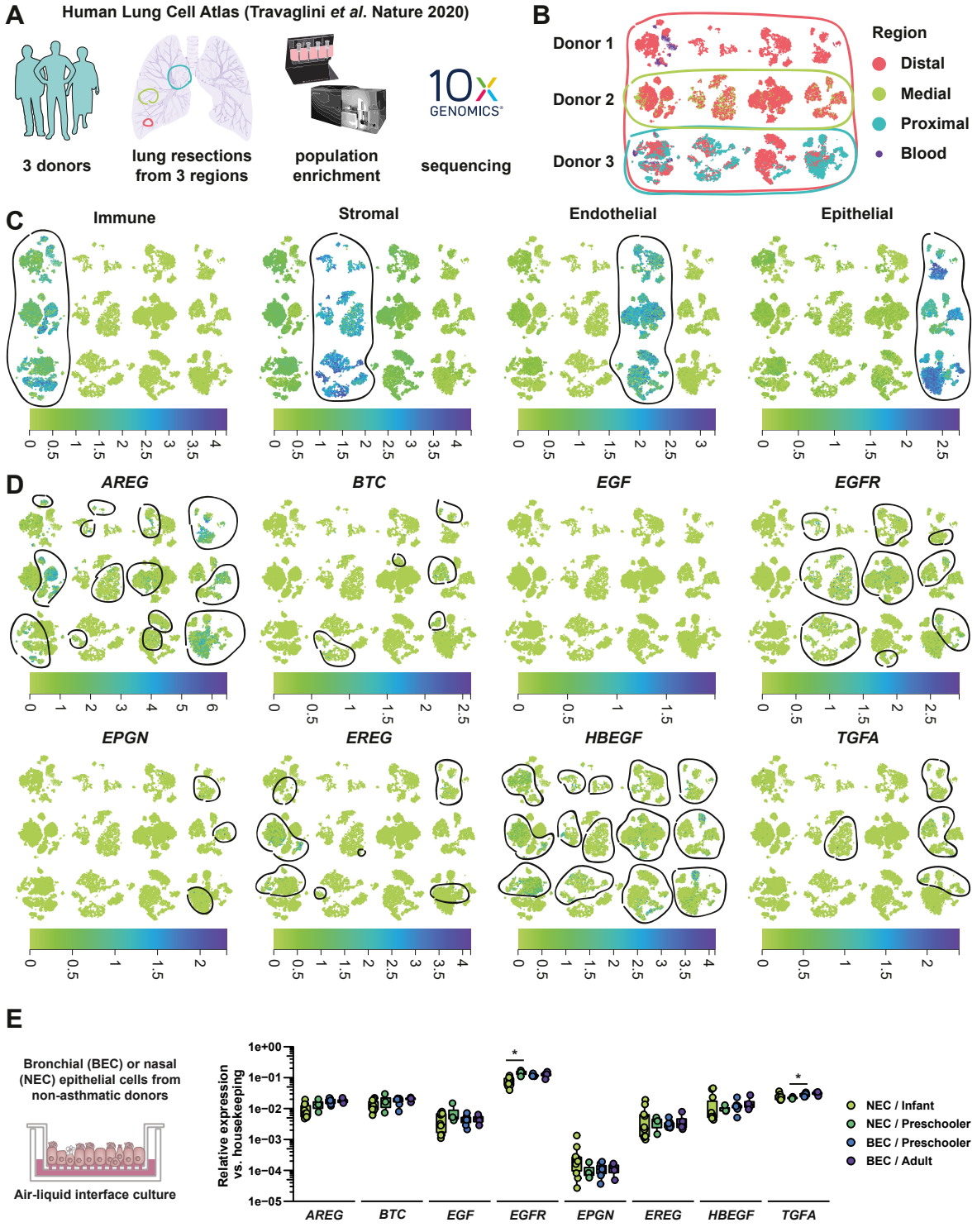


Figure 3.3 *EGFR* and ligand expression in the human lung.
A Travaglini et al. (ref. [240]) performed single-cell RNA sequencing (scRNA-seq) on immune, stromal, endothelial and epithelial cells enriched from lung resection from three adult donors. **B** tSNE plot of scRNA-seq data showing tissue location for all donors. **C** tSNE plots showing expression of key subset defining genes: Immune: *PTPRC*; Stromal: *VIM*, *DCN*, *COL1A2* and *ACTA2*; Endothelial: *PECAM1*, *CDH5* and *TIE1*; Epithelial: *EPCAM*, *KRT19*, *AQP3*, *SFTPC*, *FOXJ1*, *KRT5* and *MUC1*. **D** tSNE plots showing expression of *EGFR* and ligand genes. **E** Gene expression of *EGFR* and ligand genes by qPCR in differentiated nasal (NEC) or bronchial (BEC) epithelial from infants, pre-school children or adults without respiratory pathology. n = 3-10. Statistics: Mann-Whitney test between indicated groups. *, $p < 0.05$.

BECs of pre-school children, respectively. Of note, the level of gene expression in these epithelial cell cultures resembled those previously observed in both human and murine lungs, with high expression of the receptor as well as the ligands *AREG*, *BTC*, *HBEGF* and TGFA and lower expression of ligands such as *EGF* or *EPGN*, suggesting that both ALI cultures of epithelial cells and murine models are suitable approaches to study EGFR in the lung.

3.3.2 Effects of allergen treatment on EGFR gene expression

The role of EGFR in wound healing, remodelling and repair and its wide expression within the lungs prompted the question of how the EGFR pathway would respond to allergen or virus challenge. To this end, whole lung gene expression analysis (**Figure 3.4A**) was performed in various models of neonatal and adult AAD routinely used in our group (**Figure 3.4B-E**). First, three well-established[56] short neonatal AAD models where 3-day-old neonatal mice were intranasally administered a total of six doses of ALT, HDM or the epithelial alarmin IL-33 over the course of two weeks were compared (**Figure 3.4B**). Interestingly, both allergen and cytokine exposure resulted in the downregulation of various ligands, while pulmonary mRNA of *Egfr* remained unaffected (**Figure 3.4F**). A possible explanation for this pattern would be that the reduction in whole lung transcript results from an influx of immune cells into the lungs, as previous data (cf. Figure 3.2, Figure 3.3) would suggest that these exhibit lower expression of EGFR ligands compared to the structural compartment. Thus, pulmonary gene expression was also measured in a chronic neonatal allergen exposure model (**Figure 3.4C**), where remodelling and repair pathways would be more prominent. However, the pulmonary gene expression after five weeks of HDM exposure mirrored that of the two-week model, with significant decreases in the whole lung expression of *Btc*, *Egf*, *Epgn* and *Tgfa* (**Figure 3.4G**), suggesting that allergen exposure resulted in the downregulation of EGFR pathway members in the lung. In order to investigate whether these transcriptional changes were maintained even after cessation of allergen challenge, gene expression was measured in the lungs of neonatal mice which were allowed to resolve for four weeks following three weeks of allergen exposure (**Figure 3.4D**). A subset of mice was additionally infected with RSV, a virus which has been implicated in disease development and exacerbation in children with wheeze and asthma[8-11] and previously shown to induce EGFR signalling[229, 232], 24 hours prior to tissue harvest. With the exception of *Epgn* and *Hbegf*, which were slightly up- and downregulated, respectively, there were no long-lasting effects of HDM exposure on pulmonary expression of EGFR pathway genes (**Figure 3.4H**). Interestingly, viral infection had diverging effects, resulting in the downregulation of some ligands, such as *Egf*, *Epgn* and *Tgfa* while simultaneously inducing the expression of *Btc*, *Ereg* and *Hbegf*. These effects were independent of whether the animals had previously been exposed to HDM. Overall, these

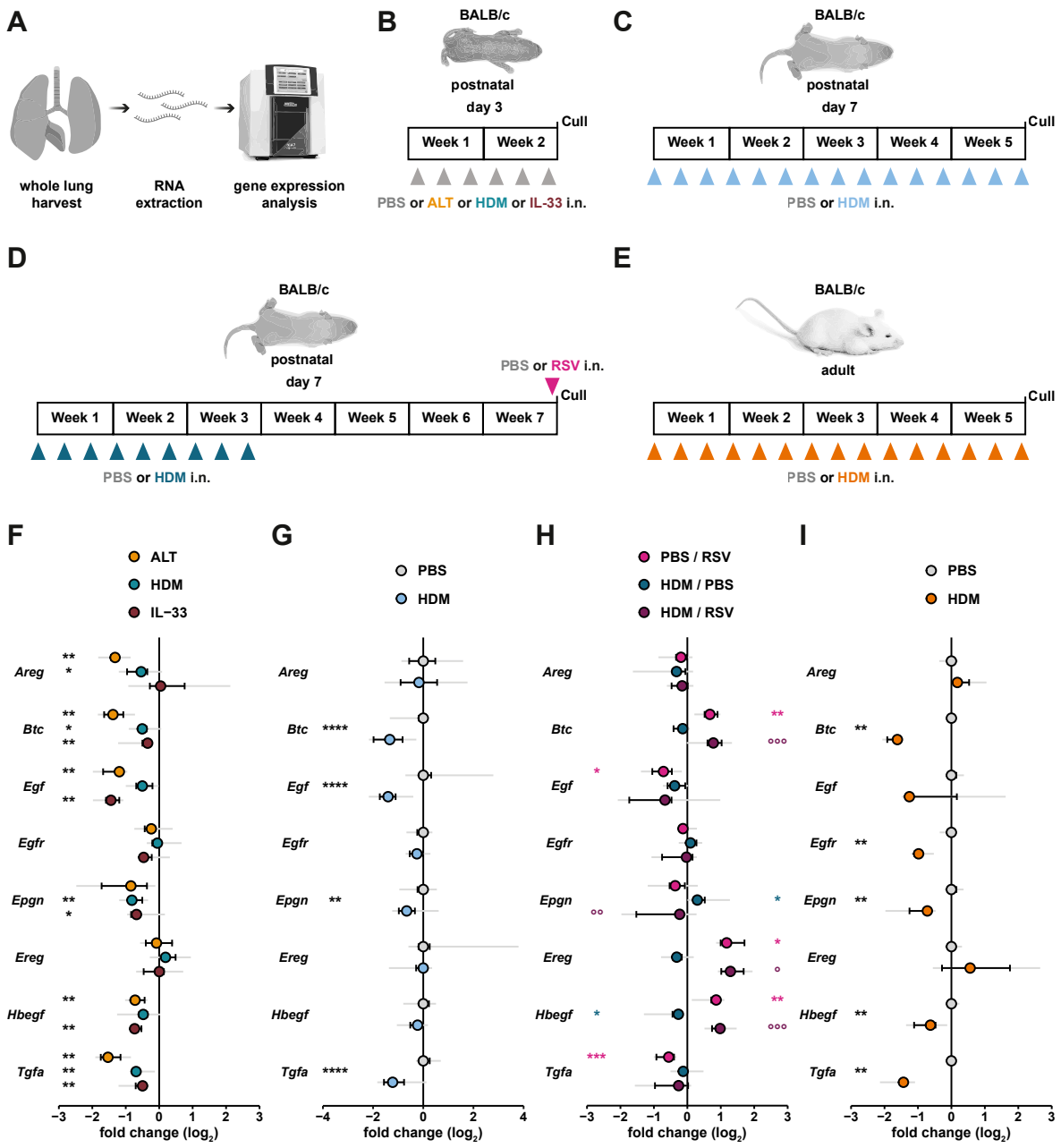


Figure 3.4 *Egfr* and ligand gene expression in response to allergen or virus challenge.
A RNA was extracted from lung lobes and gene expression measured using qPCR. **(B-E)** Schematics depicting experimental approaches. All animals were dosed intranasally and lungs were harvested 24 hours after the final dose. **B** 3-day-old BALB/c mice were treated with 50 µg/kg IL-33, 20 µg HDM or 5 µg *A. alternata* extract three times a week for two weeks. *n* = 3-9. **C** 7-day-old BALB/c mice were dosed with HDM (10 µg in week 1, 15 µg thereafter) three times a week for five weeks. *n* = 12-16. **D** 7-day-old BALB/c mice were treated with HDM (10 µg in week 1, 15 µg thereafter) three times per week for three weeks, rested for four weeks and then infected with a single dose of 1×10^6 PFU RSV. *n* = 7-8. **E** Adult female BALB/c mice were treated with 25 µg HDM five times per week for five weeks. *n* = 4-6. **F-I** Whole lung gene expression of indicated genes in previously described models (F→B, G→C, H→D, I→E), shown as fold-change from PBS-treated controls. Black error bars depict interquartile range, grey bars depict range. Statistics: Mann-Whitney test between indicated group and PBS control (*, **, ***) or HDM/PBS group (º, ºº, ººº; H only). */º, $p < 0.05$; **/ºº, $p < 0.01$; ***/ººº, $p < 0.001$.

results suggest that the transcriptional regulation of EGFR pathway members is highly complex and differs between the various ligands. Finally, in order to address whether the observed effects of allergen treatment on gene expression were specific to neonatal animals, mRNA levels were also measured in lungs from female adult mice exposed to HDM for five

weeks (**Figure 3.4E**). This analysis revealed patterns of ligand and receptor downregulation upon allergen treatment which were comparable to the neonatal model (**Figure 3.4I**), indicating that the ability of HDM to suppress the expression of EGFR pathway genes was not age specific.

3.3.3 Cell-specific expression of EGFR in the allergic lung

While the analysis of whole lung mRNA allowed the study of the effects of allergen exposure on EGFR pathway gene expression in a variety of models, a limitation of this method is the inability to capture cell-specific expression. To address this issue, flow cytometry was used to measure EGFR expression on lung cells of neonatal mice following two weeks of allergen challenge (**Figure 3.5A**). Hierarchical gating strategies for various cell populations are shown in Figure 2.1, Figure 2.2 and Figure 2.3 of the methods chapter (cf. 2.5.3). As expected, HDM challenge resulted in significant increases in the total numbers of lung cells (**Figure 3.5B**), driven primarily by recruitment of immune cells such as eosinophils, neutrophils and dendritic cells, although slight increases in epithelial cell numbers were also observed (**Figure 3.5C**). In naïve animals, EGFR expression was primarily detected on epithelial cells and fibroblasts (**Figure 3.5D-E**), while HDM exposure led to receptor expression on greater proportions of dendritic cells and eosinophils as well as epithelial cells (**Figure 3.5F**). In addition, increased geometric mean fluorescence intensity (gMFI) of EGFR was observed on dendritic and epithelial cells upon allergen exposure, suggesting an upregulation of the receptor on a per-cell basis (**Figure 3.5G**). In contrast, AMs from HDM-challenged mice displayed reduced per-cell expression of EGFR compared to controls. Overall, these data indicate that while EGFR is primarily restricted to structural cells in the naïve lung, immune cells can upregulate EGFR expression in the context of allergen challenge.

In addition to measuring EGFR expression on myeloid and structural lung cells in two independent experiments (cf. Figure 3.5), T cells and BAL were also analysed in one of the two repeats and an additional treatment with recombinant EGFR ligand amphiregulin (AREG) was included to investigate whether exogenous activation of EGFR would affect its expression (**Figure 3.6A**). Similar to the lungs, HDM exposure also led to significant influx of cells into the airways (**Figure 3.6B**), primarily driven by eosinophil and neutrophil recruitment (**Figure 3.6C**). In addition, there were increased numbers of $CD4^+$ T cells in the lungs (**Figure 3.6D**), the majority of which could be identified as $GATA3^+$ Th2 or $Foxp3^+$ regulatory T (Treg) cells (**Figure 3.6E**).

AREG treatment had no effects on either airway or lung cellularity, suggesting that EGFR activation alone did not induce cell recruitment. Similarly, EGFR expression levels were also unaffected by AREG treatment.

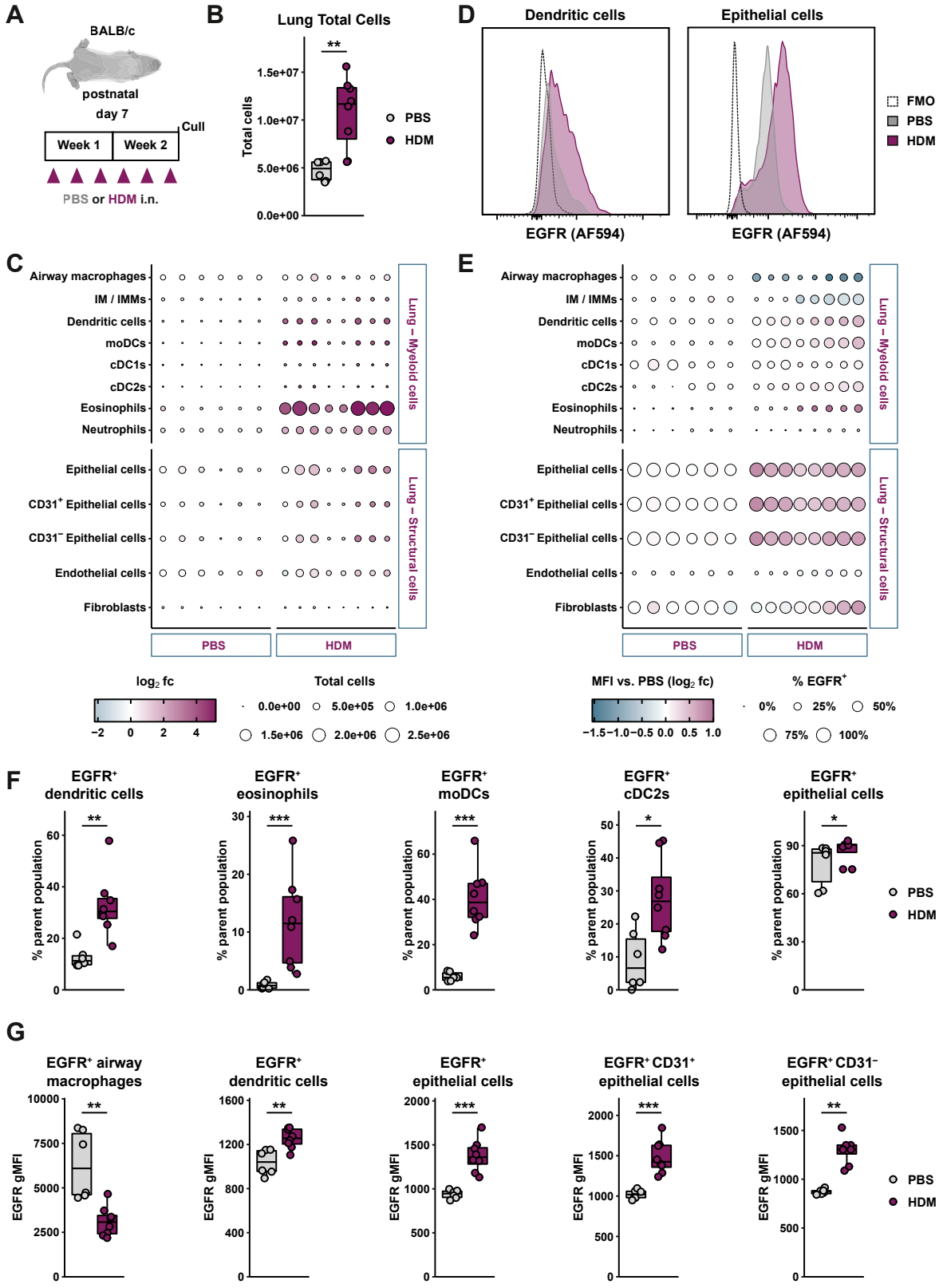


Figure 3.5 Increased EGFR expression on immune and structural cells in the allergic lung.
A 7-day-old BALB/c mice were treated with HDM (10 µg in week 1, 15 µg in week 2) three times per week for two weeks and culled 24 hours after the last dose. **B** Total cell counts per left lung lobe. **C** Myeloid and structural cell numbers in the lung. One circle per mouse and population, where the size of the circle depicts total cell numbers per left lung lobe and the colour represents change from the PBS control. **D** Representative histograms showing EGFR staining on dendritic or epithelial cells. *(legend continued on next page)*

(legend continued from previous page)
E EGFR staining on lung myeloid and structural cells. One circle per mouse and population, where the size of the circle depicts fraction of cells expression EGFR and the colour represents change in EGFR geometric mean fluorescence intensity (gMFI) from PBS control. **F** Frequency of EGFR expression on indicated lung cell populations. **G** gMFI of EGFR on indicated lung cell populations expressing the receptor. n = 6-7. Data pooled from two independent experiments. Statistics: Mann-Whitney test between indicated groups. *, $p < 0.05$; **, $p < 0.01$; ***, $p < 0.001$.

In line with its effect in the lung, HDM exposure induced upregulation of EGFR on myeloid cells in the airways, although the analysis of its effects was somewhat confounded by the low frequencies of these cells in naïve animals (**Figure 3.6F**). EGFR expression was detected on T lymphocytes (**Figure 3.6G-H**) and its expression was significantly increased on $CD4^+$ T cells upon HDM exposure, particularly on Th2 and Treg cells, both on population (**Figure 3.6I**) and cellular level **(Figure 3.6J**). In summary, HDM had profound effects on EGFR expression of eosinophils, dendritic cells, Th2 and Treg cells, all of which are central to the immune response during AAD, providing further incentive to study the role of EGFR signalling in this context.

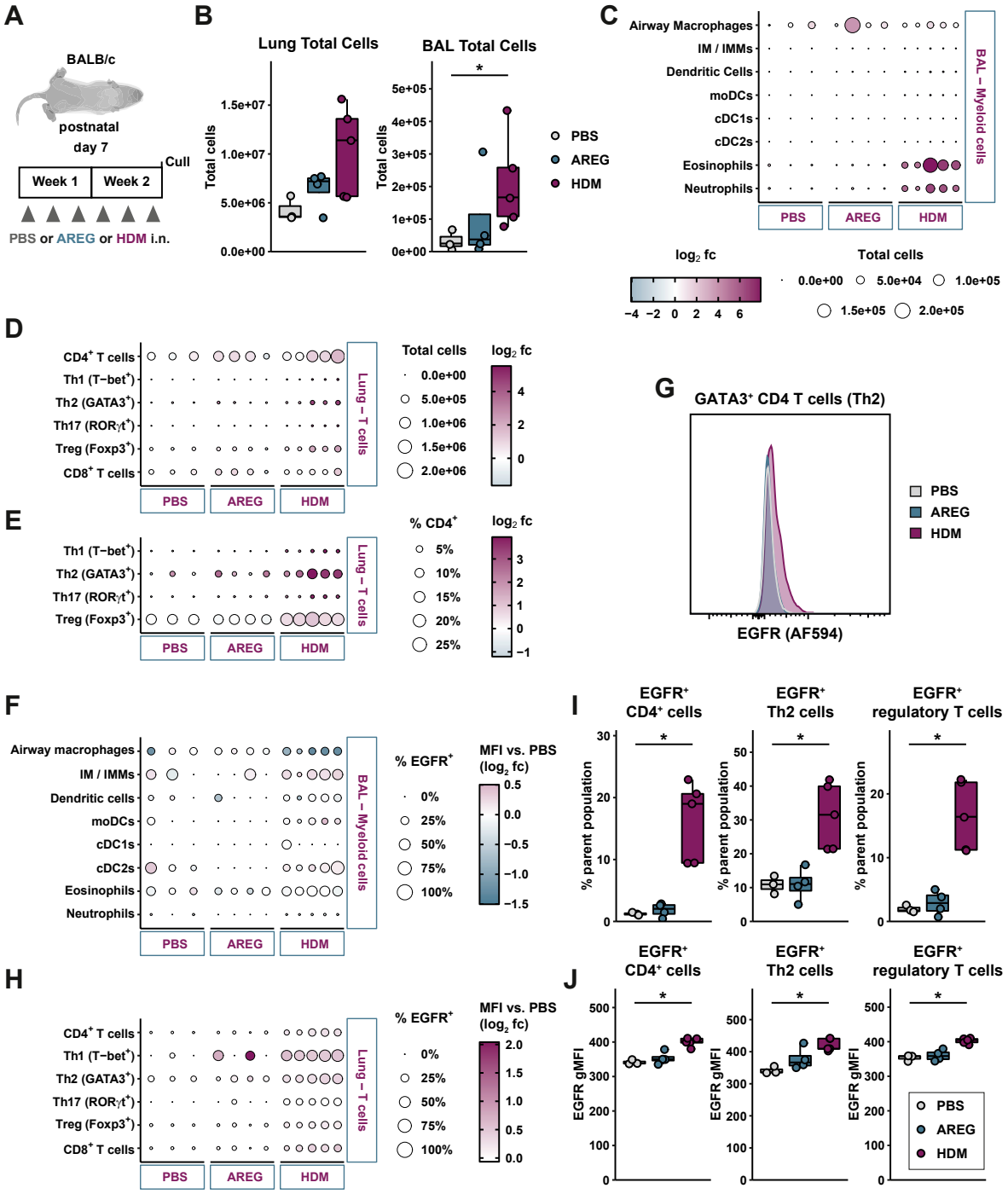


Figure 3.6 Increased EGFR expression on T lymphocytes in the allergic lung.
A 7-day-old BALB/c mice were treated with HDM (10 µg in week 1, 15 µg in week 2) or amphiregulin (AREG 0.4 µg in week1, 0.6 µg in week 2) three times per week for two weeks and culled 24 hours after the last dose. **B** Total cell counts in left lung lobe or bronchoalveolar lavage (BAL). **C** Myeloid cell numbers in BAL. One circle per mouse and population, where the size of the circle depicts total cell numbers per ml BAL and the colour represents change from the PBS control. **D** T cell numbers in the lung. One circle per mouse and population, where the size of the circle depicts total cell numbers per left lung lobe and the colour represents change from the PBS control. **E** T cell frequencies in the lung. One circle per mouse and population, where the size of the circle depicts the frequencies of CD4⁺ T cells and the colour represents the change from PBS control. **F** EGFR staining on BAL myeloid cells. One circle per mouse and population, where the size of the circle depicts fraction of cells expression EGFR and the colour represents change in EGFR geometric mean fluorescence intensity (gMFI) from PBS control. **G** Representative histogram showing EGFR staining on GATA3⁺ CD4 T cells. **H** EGFR staining on lung T cells, represented as in (F). **I** Frequency of EGFR expression on indicated lung cell populations. **J** gMFI of EGFR on indicated lung cell populations expressing the receptor. *n* = 3-5. Statistics: Mann-Whitney test between indicated groups. *, $p < 0.05$.

3.3.4 Pulmonary levels of EGFR ligands and their release into the airways

The use of flow cytometry has provided valuable insights into the cell-specific expression patterns of EGFR and how receptor levels were affected by allergen treatment. However, canonical induction of EGFR signalling requires the receptor to be bound by one of its ligands. Therefore, the levels of four EGFR ligands, AREG, BTC, EREG and HB-EGF, were measured by ELISA in both acute (**Figure 3.7A-B**) and chronic (**Figure 3.7C**) models of AAD.

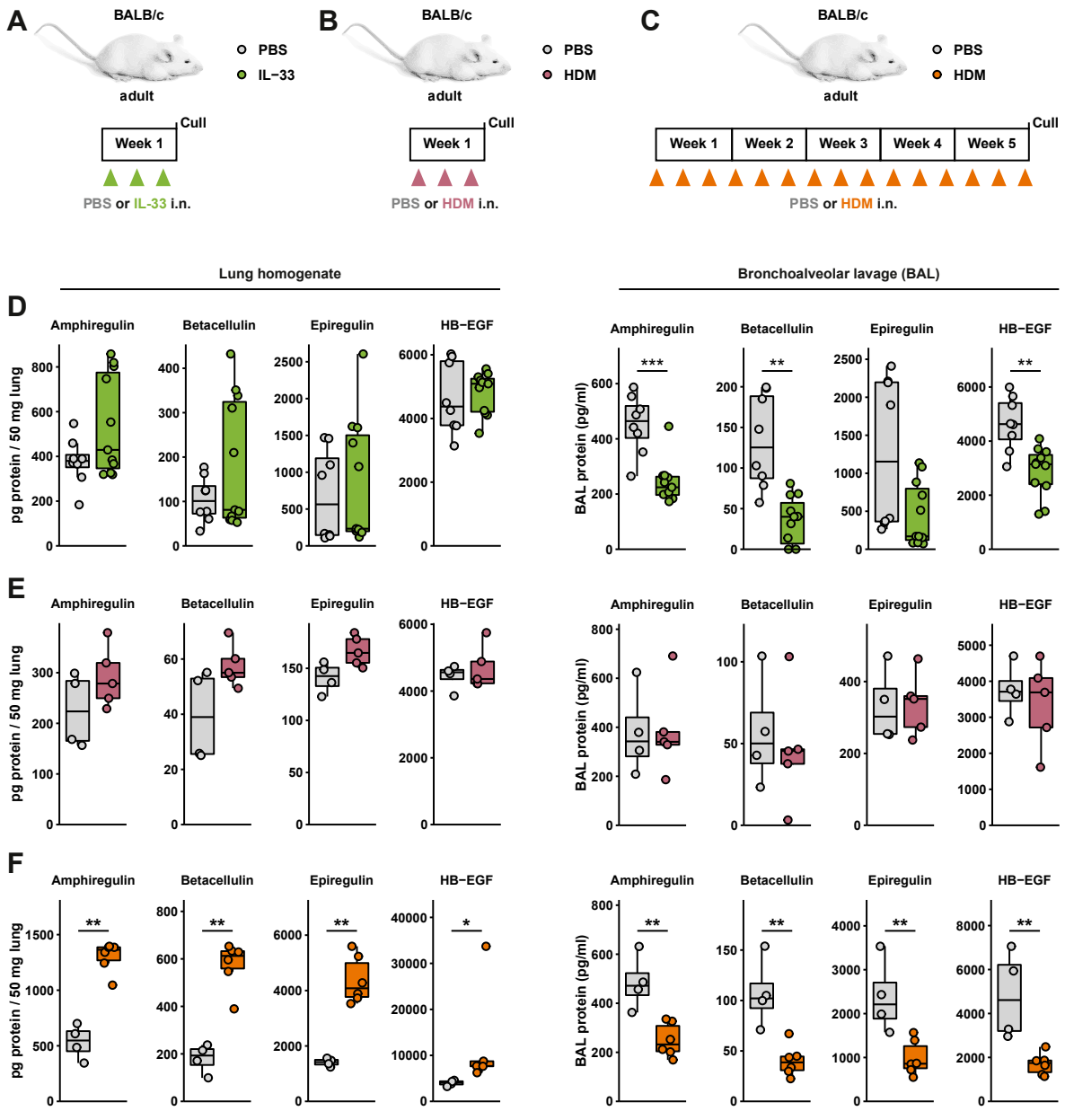


Figure 3.7 EGFR ligand levels increase in lung homogenates but decrease in the airways during adult AAD.
A-C Schematics depicting experimental approaches. Adult female BALB/c mice were dosed intranasally with 1 µg IL-33 (A) or 25 µg HDM (B-C) for one (A-B) or five (C) weeks and culled 24 hours after the final dose. **D-F** Levels of EGFR ligands in lung homogenates (left) or bronchoalveolar lavage (BAL; right) from mice treated as previously depicted (D→A; E→B, F→C). *n* = 4-6. Statistics: Mann-Whitney test between indicated groups. *, $p < 0.05$; **, $p < 0.01$.

Interestingly, the effects of alarmin or allergen exposure were divergent between levels measured in the lung homogenates and BAL, with increases in ligand levels in the lungs but decreases in the airways (**Figure 3.7D-F**). The greatest changes in ligand levels were found in the chronic HDM exposure model (**Figure 3.7F**), although similar trends were observed after one week of treatment with either IL-33 or HDM, suggesting that both alarmins and allergens can alter EGFR ligand availability in the lungs and airways. Analysis of EGFR ligand levels in two chronic neonatal AAD models produced comparable results to the chronic adult AAD model (**Figure 3.8**), suggesting that these allergen-induced effects were not age specific. Since EGFR ligands are produced in a membrane-bound form prior to release by enzymes such as metalloproteases, these results could suggest that, while more ligand is being produced within the lungs, less is being released into the airways. However, another potential explanation is that BAL ligand levels were decreased as a consequence of more uptake of

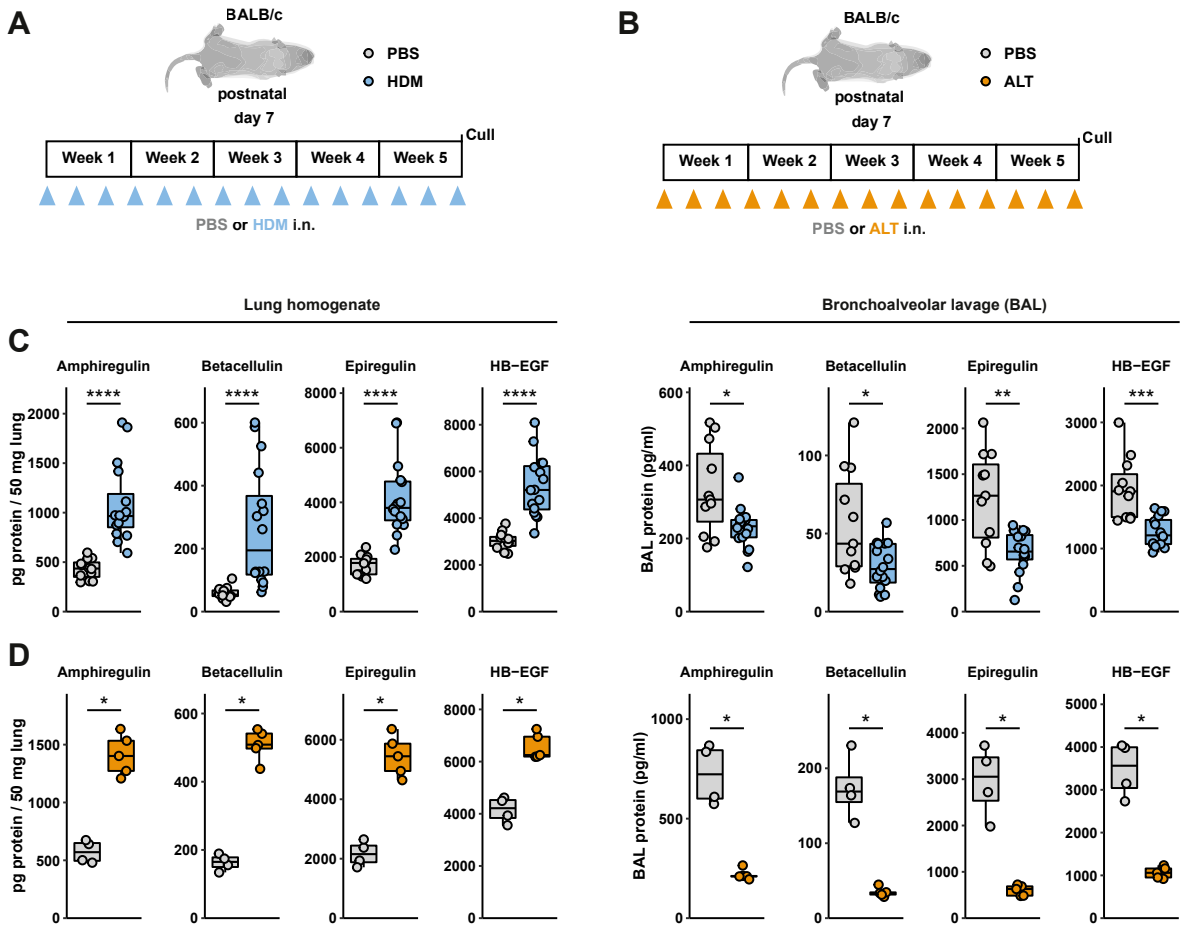


Figure 3.8 EGFR ligand levels increase in lung homogenates but decrease in the airways during neonatal AAD.
A-B Schematics depicting experimental approaches. 7-day-old BALB/c mice were dosed intranasally with HDM (10 µg in week 1, 15 µg thereafter; A) or ALT (5 µg in week1, 10 µg thereafter; B) for five weeks and culled 24 hours after the final dose. **C-D** Levels of EGFR ligands in lung homogenates (left) or bronchoalveolar lavage (BAL; right) from mice treated as previously depicted (C→A; D→B). (C) n = 12-16, pooled from two independent experiments (D) n = 4-5. Statistics: Mann-Whitney test between indicated groups. *, $p < 0.05$; **, $p < 0.01$; ***, $p < 0.001$; ****, $p < 0.0001$.

ligand by receptor-expressing cells, which would indicate an overall increase in EGFR signalling.

3.3.5 Measuring EGFR activation in the allergic lung

Western blot analysis of phosphorylated tyrosine residue Y1068 of EGFR was performed as a measure of EGFR autophosphorylation, indicative of receptor activation. To validate this method, murine fibroblasts were treated with the EGFR ligand AREG in the presence or absence of the pharmacological EGFR inhibitor Gefitinib (**Figure 3.9A**). As expected, an increase in Y1068 phosphorylation was observed upon treatment with AREG and abrogated in the presence of Gefitinib (**Figure 3.9B**), suggesting that the western blot method is a valid approach to study EGFR activation. To investigate how allergen exposure would affect pulmonary EGFR activation, Y1068 phosphorylation was measured in lung homogenates from neonatal mice that were treated with HDM for one, two or five weeks (**Figure 3.9C**). While total levels of the receptor seemed to be unaffected by allergen treatment, slight reductions in Y1086 phosphorylation were observed after one and two weeks of allergen exposure, suggesting less overall EGFR activation. Results after five weeks of HDM treatment were more variable and no clear trends were obvious. Similarly, there were no clear patterns when lung homogenates from neonatal mice treated with ALT for two weeks were analysed (**Figure 3.9D**). Although these findings may suggest that a reduction of EGFR signalling is specific to short-term treatment with the allergen HDM, a concern was that the chosen timepoint for the analysis, 24 hours after the last allergen challenge, may contribute to the variability of the results. Receptor phosphorylation is a transient event which often occurs within minutes following a stimulus[97], and although this approach shed light on the overall EGFR activation state of the allergic lung, it did not inform of whether allergen exposure could directly result in receptor phosphorylation. To address this question, a timepoint directly following allergen exposure was analysed. To this end, three-week-old mice were intranasally administered a single dose of either IL-33, HDM or ALT and lungs were harvested 15 minutes later (**Figure 3.10A**). Treatment with AREG was included as a positive control and administered both intranasally and intraperitoneally, to study the effect of both local and systemic ligand exposure on pulmonary EGFR activation. However, this approach produced no clear results and levels of Y1068 phosphorylation were highly variable even within the control groups (**Figure 3.10B**), indicating that caution should be exerted when interpreting whole lung EGFR activation data. Unfortunately, it was therefore not possible to confirm whether allergen exposure could directly result in EGFR activation or suppression in this model.

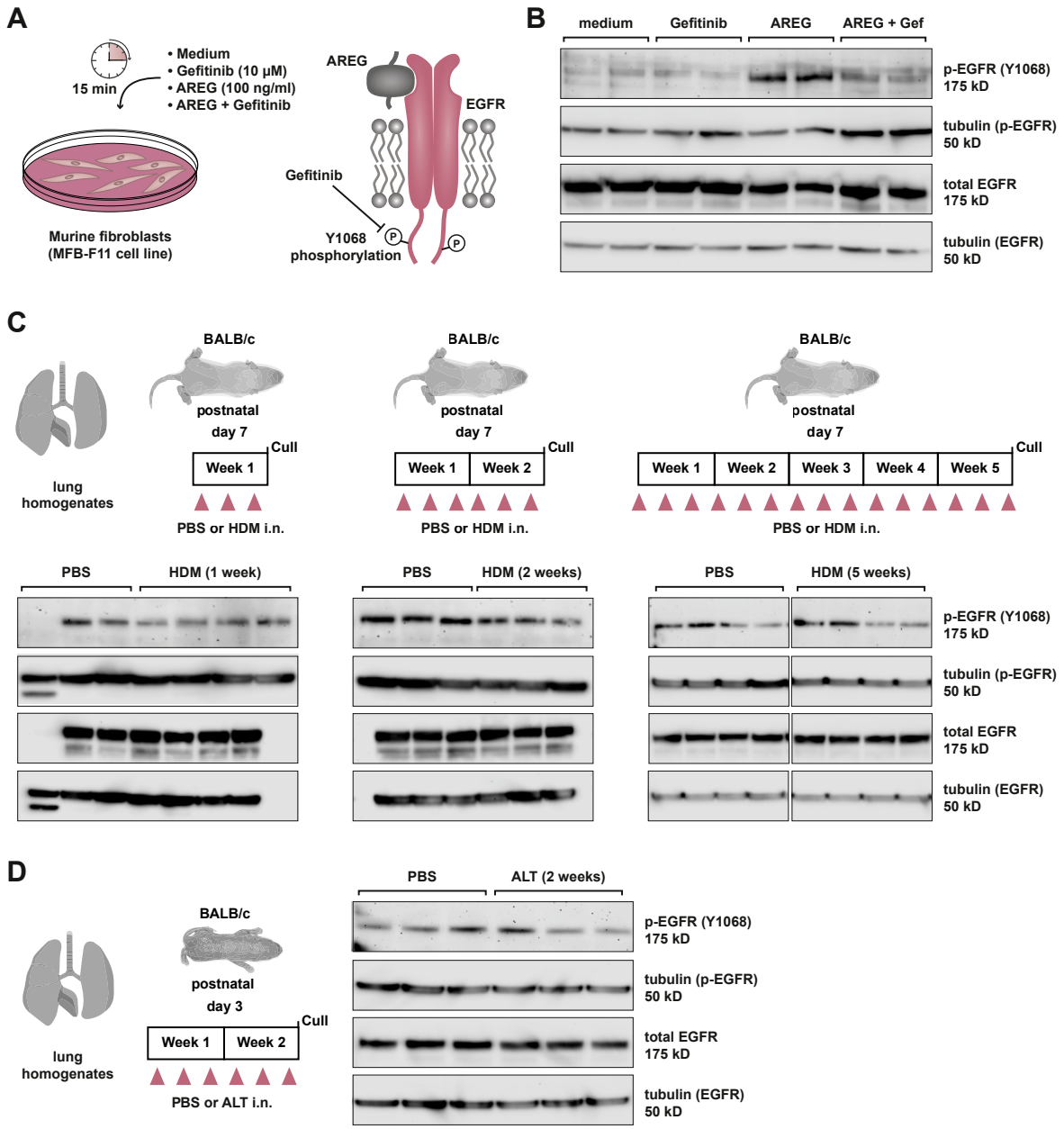


Figure 3.9 Effects of allergen exposure on pulmonary EGFR activation.
A MFB-F11 cells were treated with 100 ng/ml AREG in the presence or absence of 10 μM Gefitinib for 15 min prior to lysis for western blot analysis. **B** Western blot of MFB-F11 lysates treated as in (A), using indicated antibodies. **C** 7-day-old BALB/c mice were intranasally treated with HDM (10 μg in week 1, 15 μg thereafter) three times per week for one, two or five weeks and culled 24 hours after the last dose. Lung homogenates were analysed by western blot using the indicated antibodies. **D** 3-day-old mice were intranasally treated with 10 μg ALT three times a week for two weeks and lung homogenates were analysed by western blot using the indicated antibodies. *n* = 3-4 per treatment.

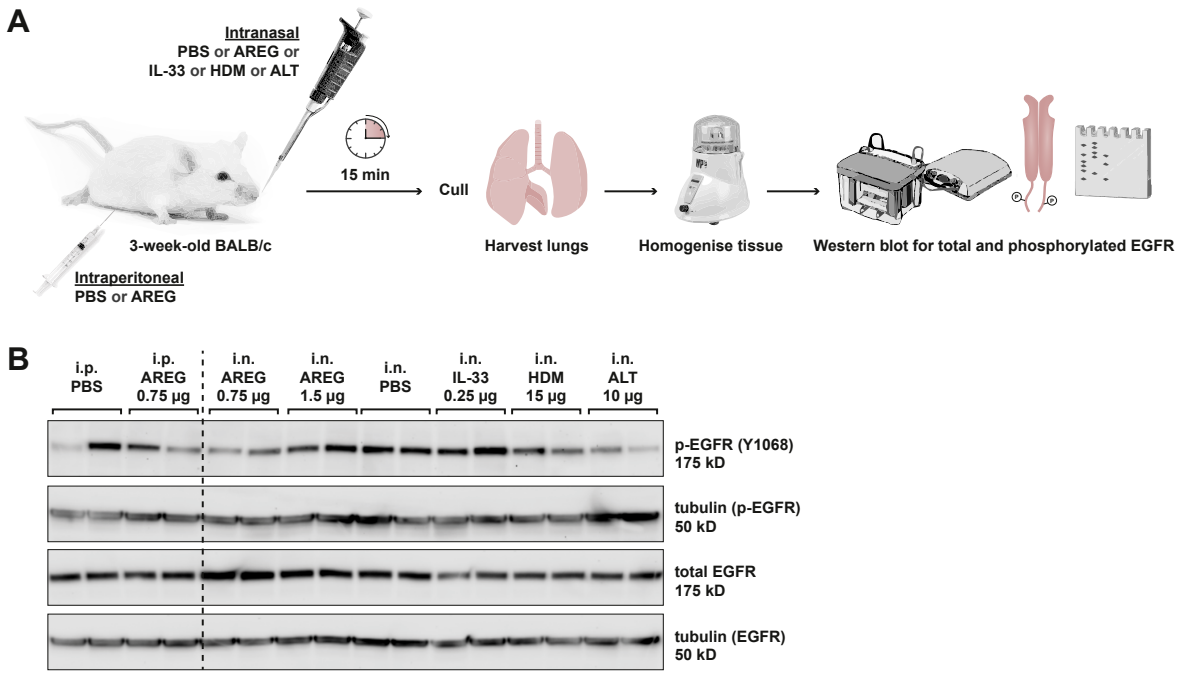


Figure 3.10 Pulmonary EGFR activation immediately following ligand or allergen exposure.
A 3-week-old mice were given a single dose of AREG (0.75 µg or 1.5 µg), IL-33 (0.25 µg), HDM (15 µg) or ALT intranasally or intraperitoneally. Lungs were harvested 15 min later and homogenised for western blot analysis. **B** Western blot analysis of lung homogenates using indicated antibodies. *n* = 2 per treatment.

3.3.6 Using primary human airway cells to investigate effects of allergen or viral stimulation on EGFR signalling

To overcome the issues posed by analysing whole lung homogenates, ALI cultures of primary airway epithelial cells were used to study the effects of allergen or viral infection on EGFR signalling. Airway epithelial cells are among the first cells to encounter and defend against invading particles, such as allergens and viruses, and together with the strong expression of EGFR pathway members by epithelial cells, as well as the great degree of epithelial differentiation and polarisation achieved during air exposure, this makes ALI cultures a highly relevant model to study EGFR signalling in the airways. Well-differentiated nasal epithelial cells from 5- to 8-day-old infants were infected with RSV 24 hours after exposure to HDM and gene expression was analysed 4 days post-infection (**Figure 3.11A**). While there were no effects of a single HDM challenge on EGFR pathway gene expression, RSV infection significantly induced the expression of several EGFR ligands, regardless of whether the cells had previously been exposed to allergen (**Figure 3.11B**). This may suggest that EGFR signalling is part of the repair response induced by viral infection. However, since allergen exposure, especially with HDM, is rarely a single event, the effects of daily HDM treatment in conjunction with viral infection were also tested in bronchial epithelial cells from a non-asthmatic pre-school-aged disease control donor (**Figure 3.11C**). As with the single HDM

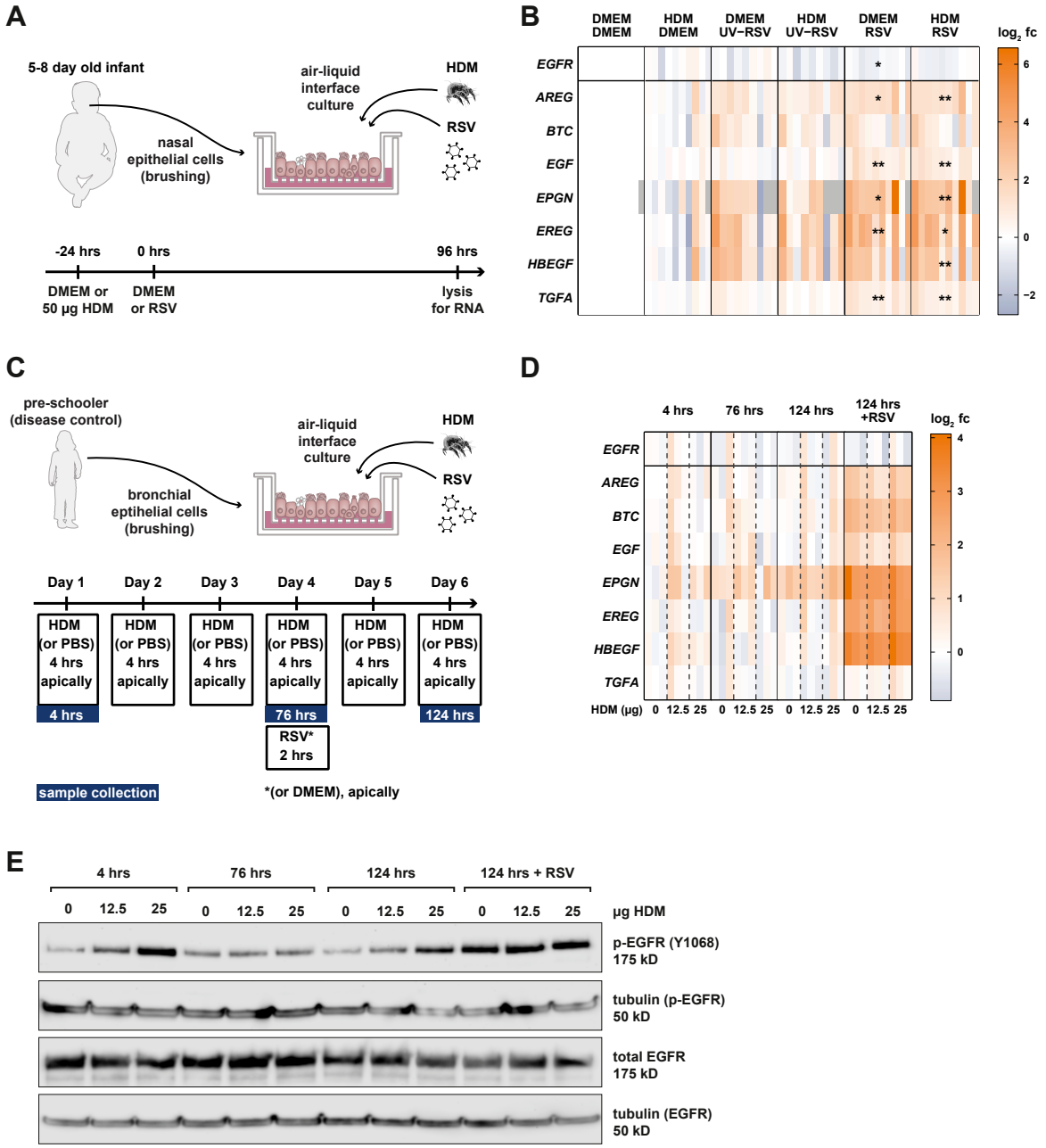


Figure 3.11 HDM induced epithelial EGFR activation without affecting gene expression.
A Nasal differentiated epithelial cells from 5-8-day-old infants were differentiated at air-liquid interface (ALI). Cells were infected with 5×10^4 $TCID_{50}$ RSV 24 hours after stimulation with 50 µg HDM and lysed 96 hrs post-infection. **B** Gene expression by qPCR of *EGFR* and ligands in cell lysates from (A), shown as change from DMEM control group. Asterisks indicate statistically significant change from relevant uninfected group. Statistics: paired Wilcoxon test with Bonferroni correction for multiple ($n = 5$) comparisons. *, $p < 0.05$; **, $p < 0.01$. **C** Bronchial epithelial cells from a single 3-year-old donor were differentiated at ALI and treated with HDM (12.5 or 25 µg) daily. Cells were infected with 5×10^4 $TCID_{50}$ RSV on day four as indicated and lysed on day 4, 76 or 124 hours after the first HDM challenge as indicated. **D** Gene expression by qPCR of *EGFR* and ligands in cell lysates from (C), shown as change from DMEM control at 4hrs. **E** Western blot analysis of cell lysates from (C) using the indicated antibodies.

treatment, there were no effects of allergen exposure on gene expression but viral infection resulted in upregulation of EGFR ligands (**Figure 3.11D**). Nonetheless, dose-dependent increases in Y1068 phosphorylation of EGFR could be observed as early as four hours post HDM treatment, suggesting that exposure to the allergen was able to induce EGFR signalling

directly without affecting gene expression (**Figure 3.11E**). In line with its effects on gene expression, receptor activation was also strongly induced by infection with RSV. Overall, these findings suggest that EGFR signalling was active in airway epithelial cells upon challenge with allergens or viruses, and it will be interesting to dissect if and how this pathway may contribute to repair and remodelling during AAD.

In a first attempt to study remodelling pathways in the lungs and how they are shaped by the interactions between cell types, the effects of epithelial cell-derived factors on fibroblast proliferation were analysed. To this end, normal human lung fibroblasts were treated with basal media from well-differentiated cultures of nasal epithelial cells collected from pre-school children and fibroblast proliferation was measured using live cell imaging (**Figure 3.12A**). Treatment with normal fibroblast medium (DMEM) with or without addition of serum served as

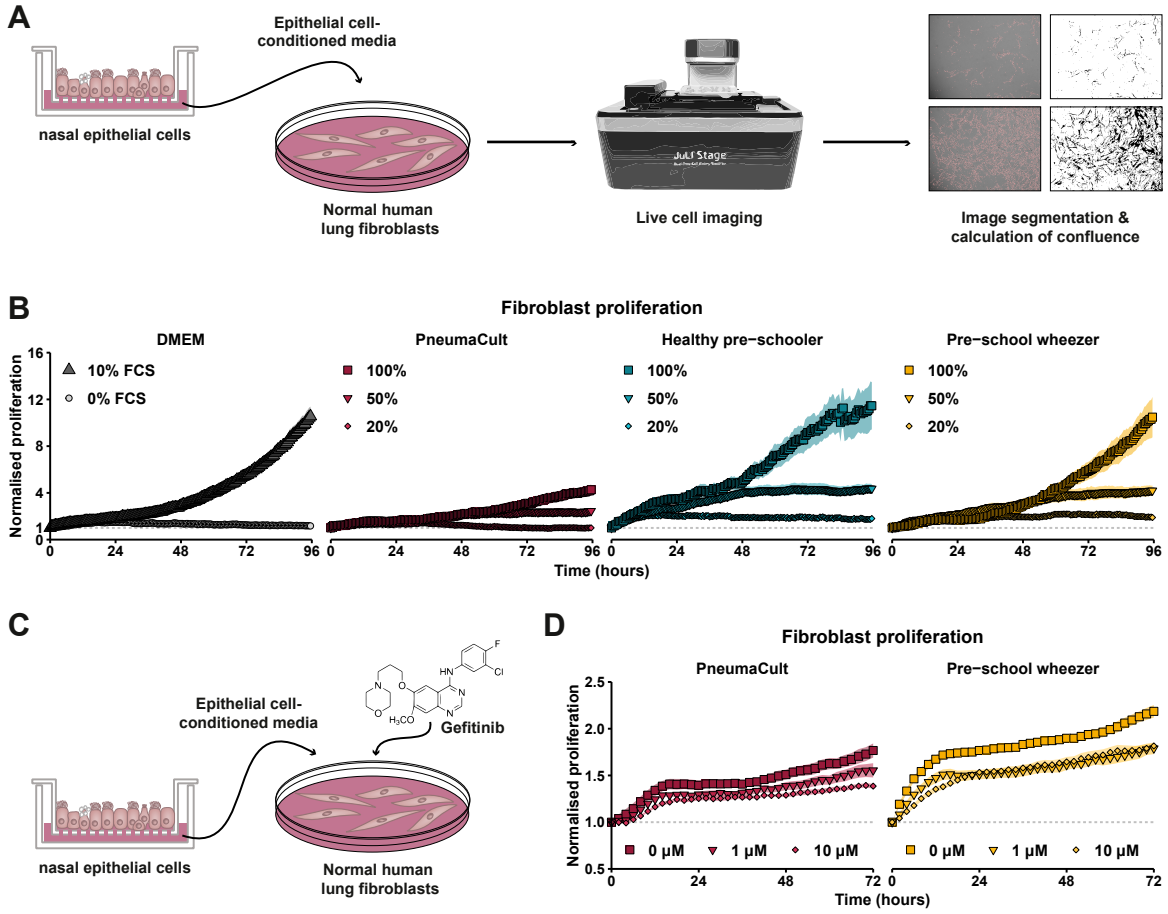


Figure 3.12 Epithelial-derived factors can drive fibroblast proliferation, which is partly EGFR-dependent. **A** Normal human lung fibroblasts (NHLF) were treated with basal media from differentiated nasal epithelial cells (NECs) and their proliferation was measured using live cell imaging. **B** Fibroblast proliferation after treatment with DMEM containing either no or 10% FCS (panel 1), fresh epithelial cell media (PneumaCult), either neat or diluted in serum-free DMEM (panel 2) or epithelial-cell conditioned media from NECs isolated from a healthy (panel 3) or wheezing (panel 4) child of pre-school age, either neat or diluted in serum-free DMEM. **C** NHLF were treated with basal media from differentiated NECs in the presence or absence of EGFR inhibitor Gefitinib. **D** Fibroblast proliferation after treatment with fresh (panel 1) or conditioned (panel 2) epithelial cell media in the presence of varying doses of Gefitinib. Data are shown as mean +/- standard error of *n* = 3-6 technical replicates.

positive or negative control for proliferation, respectively, and fresh epithelial cell medium (PneumaCult) was included as an additional control (**Figure 3.12B**). While fibroblasts displayed dose-dependent proliferation in both fresh and epithelial cell-conditioned PneumaCult, the cells replicated more rapidly when treated with epithelial cell-conditioned media, suggesting that epithelial cells release factors that can drive fibroblast expansion. In order to test the role of EGFR signalling in this context, these experiments were repeated in the presence of Gefitinib (**Figure 3.12C**). EGFR inhibition slowed down proliferation of fibroblasts treated with either fresh or epithelial cell-conditioned PneumaCult (**Figure 3.12D**), indicating that fibroblast replication was at least in part EGFR-dependent. These findings provide further weight to the question of how the EGFR pathway may contribute to airway remodelling during AAD.

3.3.7 EGFR and ligand levels in airway samples from children with PSW and severe asthma

A major aim of this chapter was to address whether EGFR signalling is augmented during PSW or asthma. To this end, gene expression analyses were performed in brush and BAL samples from children with PSW or severe asthma and their expression of EGFR pathway members was compared to non-asthmatic children (**Figure 3.13A**). Although EGFR expression levels obtained from bulk RNA sequencing of brushes were largely comparable between groups, samples from children with PSW or severe asthma exhibited modest but significant increases in *AREG* and *HBEGF* compared to controls, suggesting that these ligands may be involved in airway inflammation or remodelling (**Figure 3.13B**). Of note, brushes contained high levels of *EGFR* and its ligands *BTC*, *HBEGF* and *TGFA*, whereas *EPGN* was not detectable, which corresponds to previous findings in both murine and human lungs (cf. Figure 3.2, Figure 3.3). Similarly, when gene expression was analysed in cell pellets derived from BAL, robust expression of *EGFR* and its ligands *AREG*, *BTC*, *EREG*, *HBEGF* and *TGFA* was observed, whereas mRNA levels of *EGF* and *EPGN* were low or undetectable (**Figure 3.13C**). In contrast to bronchial brushings, there were no differences in ligand or receptor expression levels between disease groups in BAL samples. Overall, these results suggest that children with PSW or severe asthma exhibit a modestly augmented EGFR gene signature, which is most likely driven by epithelial cells and may contribute to disease.

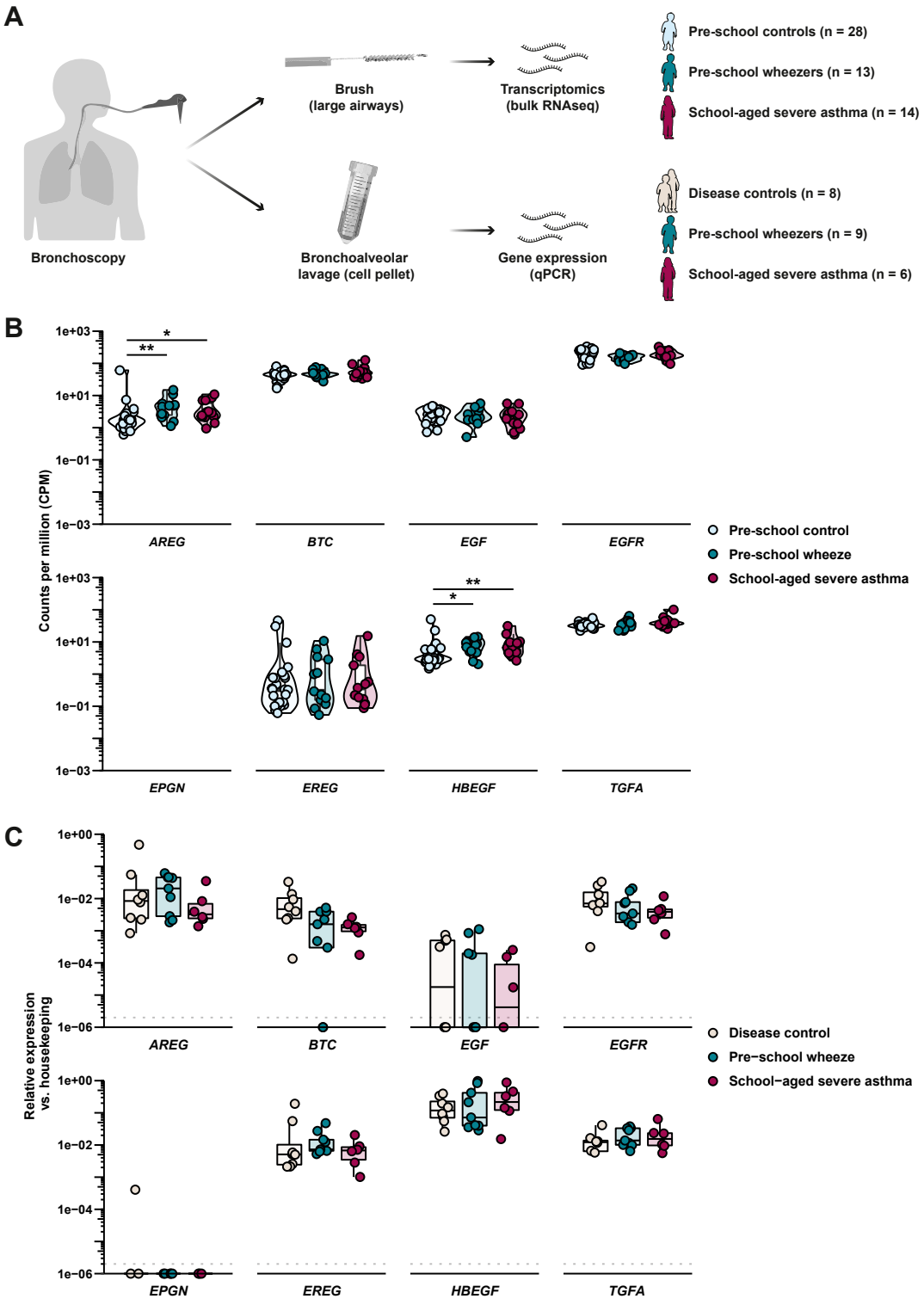


Figure 3.13 EGFR ligands were present in airway samples from children with PSW or severe asthma. **A** Children of pre-school or school-age with or without wheeze, asthma or lower respiratory tract infections (disease controls) were recruited for bronchoscopy. Gene expression in bronchial brushes or bronchoalveolar lavage (BAL) was analysed by bulk RNA sequencing (RNAseq) and qPCR, respectively. **B** Gene expression in bronchial brushes of indicated patient groups by RNAseq. **C** Gene expression in BAL cell pellets from indicated patient groups by qPCR. Statistics: Kruskal Wallis test followed by Dunn's post-hoc test using Bonferroni correction for multiple comparisons. *, $p < 0.05$; **, $p < 0.01$.

3.4 Discussion

This chapter investigated the expression patterns of EGFR and each of its seven ligands within diverse cell types and at various stages of life, with a particular focus on lung development and early life. A variety of different methods were used to study how EGFR and ligand levels are affected by allergen exposure or viral infection and presence of EGFR ligands in primary airway samples of children with PSW or severe asthma was confirmed. Finally, the role of EGFR signalling in fibroblast proliferation was examined as a first step of the investigation of the potential role of EGFR in driving asthma pathology.

Multiple techniques were employed, namely gene expression analysis by qPCR, flow cytometry, ELISA and western blotting, to study expression patterns of EGFR and its seven ligands during development and in different disease contexts. Each of these approaches comprised unique advantages and disadvantages. For example, while gene expression analysis is a highly sensitive high-throughput technique, cell-type specific analysis can only be achieved by prior sorting of cells, followed by either traditional qPCR analysis or single-cell sequencing. In addition, measuring gene expression of EGFR and its ligands provides no insight into whether the signalling pathway is active, as the ligands must undergo several post-transcriptional processes such as translation, transport to and shedding from the cell membrane before signalling can be initiated.

Some of these shortcomings can be overcome by the use of ELISA to measure ligand levels, for example in lung homogenates or BAL. While this technique is able to capture actual protein levels and, in the case of analysis of BAL analysis, also provides insights into protein shedding from cells, it requires relative high amounts of sample and is not cell-type specific. Analysis by flow cytometry is a sample-efficient approach to determine cell-specific protein expression in a high-throughput manner. However, although this method has been successfully applied to measure expression of EGFR within this thesis, the analysis of ligand expression provided challenges. While it is possible to detect ligand expression in *in vivo* samples by flow cytometry, for example in BAL airway macrophages of mice infected with *Nippostrongylus brasiliensis*[150], analysis of lung homogenates using this method did not yield any results, likely due to cleavage of ligands during the digestion process. To overcome this issue, researchers have either employed intracellular transgenic reporters[155] or administered the protein transport inhibitor Brefeldin A either directly *in vivo*[150] or during *ex vivo* restimulation of cells[131, 136] to allow measurement of intracellular EGFR ligands by flow cytometry.

Nevertheless, none of the approaches discussed thus far directly capture EGFR signalling. Here, western blot analysis of tyrosine phosphorylation (Y1068) was used as a measure of receptor activation. Although western blot bands were not quantified, which would have

allowed a more detailed analysis of the obtained results and should be considered in the future, these analyses provided some insights into the feasibility of using western blotting as a way to determine EGFR activation. While this method produced robust results in human epithelial cells and in a murine fibroblast cell line, Y1068 phosphorylation levels in murine lung homogenates were highly variable even within the same experimental group. Since receptor phosphorylation is a transient modification, it seems likely that extensive processing, such as is needed to derive homogenates of whole lung lobes, may alter the signal. As such, the use of western blotting to measure Y1068 phosphorylation may be restricted to the analysis of cell lysates of *in vitro* cultures. An additional caveat of the western blotting approach as performed in this thesis is that it was restricted to phosphorylation at a single tyrosine residue, namely Y1068. However, different ligands exhibit varying preferences of phosphorylation sites and future analyses should also probe for other phosphorylated tyrosine residues, such as Y992, which is the primary phosphorylation site induced by AREG[99, 100]. A final approach to study EGFR signalling would be the use of immunofluorescence imaging, for example of lung sections. Although only semiquantitative and labour-extensive, this technique provides the opportunity to combine the staining for EGFR (total or phosphorylated) and its ligands with other cell-specific markers or morphological features to allow the analysis of EGFR signalling in different tissue regions.

Overall, despite the unique advantages of each of the techniques discuss above, the study of EGFR signalling in complex systems such as the allergic lung remains challenging. Nevertheless, some interesting observations were made within this chapter. Overall, there were no gross differences in EGFR expression or activation between early life and adulthood, suggesting that EGFR signalling is governed by similar processes during both stages of life. However, the expression levels and patterns differed between the various ligands of EGFR, as well as in their responses to stimulation with allergen or virus. This highlights that despite sharing a receptor, the various ligands are likely to fulfil unique roles in the lungs, in line with their varying affinities for EGFR[87] and outcomes of receptor activation[97, 98].

Out of the seven ligands, HB-EGF was the only one to display increases in gene expression during lung development. It was also among the most highly expressed EGFR ligands in both human and murine lungs at various stages of life. Together, these findings suggest that HB-EGF may play a crucial, non-redundant role during lung development and homeostasis. This hypothesis is supported by the finding that mice deficient for EGFR and HB-EGF, but not any of the other ligands, display defective lung development[160, 161, 177-180, 207, 208], as do mice lacking the enzyme responsible for shedding of HB-EGF from the cell surface[205]. HB-EGF levels were increased in the lungs after chronic allergen exposure, in line with previous reports of induction of HB-EGF using the traditional OVA sensitisation/challenge model[157, 168]. *HBEGF*

gene expression was also elevated in bronchial epithelial cells from children with PSW and severe asthma compared to controls, similar as previously described in the airway epithelium of adults with asthma[218]. This suggests that, in addition to its pivotal role during lung development, HB-EGF may contribute to asthma pathology. Indeed, Wang and colleagues (ref. [168]) showed that administration of anti-HB-EGF blocking antibodies in OVA-sensitised mice resulted in ameliorated mucus hyperplasia and reduced airway smooth muscle thickness upon aerosol challenge. The same group later found that administration of HB-EGF in a similar model led to exacerbated airway smooth muscle thickening and promoted migration of airway smooth muscle cells[171]. Farahnak et al. (ref. [157]), who identified CD4 T cells as a source of HB-EGF, further demonstrated that CD4-specific deletion of HB-EGF was sufficient to reduce mucus, inflammation, eosinophilia, airway hyperresponsiveness and IL-5 production after OVA-challenge of sensitised mice. Overall, these studies illustrate that HB-EGF can drive key pathological features of AAD in the OVA sensitisation/challenge model and that its function in this context cannot be compensated for by either of the other six EGFR ligands. It will be important to investigate whether HB-EGF is of similar relevance in more physiological models of AAD, such as chronic exposure to inhaled HDM.

Interestingly, measurement of EGFR ligand levels after chronic allergen exposure detected increases in the lungs concurrent with significant decreases in the BAL. In the polarised airway epithelium, EGFR expression is largely restricted to the basal cells, whereas ligands such as EGF are primarily released at the apical surface[241], providing a natural sequestration between receptor and ligand. Upon disruption of the epithelial layer, EGFR becomes exposed and signalling can be initiated. Since many allergens such as HDM and ALT contain proteases that can directly damage the epithelium, it is likely that the reduction in airway levels of free EGFR ligands in our model of chronic allergen exposure is caused by increased receptor engagement following epithelial damage and thus reflects a net increase in EGFR signalling. In support of this, we found that HDM could directly induce EGFR activation in polarised cultures of primary bronchial epithelial cells. These findings suggest that the increased EGFR signalling previously described in lung samples derived from both patients with asthma[223] and mouse models of AAD[134, 166, 222, 223] may at least in part be the direct result of allergen exposure. However, EGFR signalling is not restricted to epithelial cells in the lungs and receptor expression was detected on fibroblasts as well as several key immune cells of the allergic type 2 response, such as eosinophils, monocyte-derived dendritic cells and Th2 lymphocytes within this thesis. While epithelial damage may also increase availability of epithelial-derived ligands to structural and immune cells in the underlying tissues, EGFR activation in these cells is likely governed by complex autocrine and paracrine signalling processes during allergic inflammation and will need to be elucidated in more detail. In particular, it would be interesting

to explore whether ligands found in the lungs and airways exist in the cleaved, soluble form or whether they are contained in exosomes. As EGFR ligands in extracellular vesicles have been shown to induce stronger signals, attributed to their increased concentration of ligand molecules and ability to travel further distances than achieved by diffusion of soluble ligands[96, 116], the presence of exosome-contained EGFR ligands in the lungs and airways may be a further indicator of active and directional EGFR signalling between the various cells present in this environment.

Finally, the investigation of the potential consequences of increased EGFR signalling revealed that increased fibroblast proliferation in response to epithelial cell-derived mediators was at least in part EGFR-dependent, suggesting that EGFR activation of fibroblasts may potentially contribute to asthma pathology *in vivo*. In line with this, studies have shown that AREG can drive proliferation of primary human lung fibroblasts[137]. Future studies will aim to characterise the effects of epithelial-derived mediators on fibroblast phenotype and production of extracellular matrix components, as well as the EGFR-dependence of these processes. In addition, it will be interesting to investigate whether media derived from allergen-exposed or virus-infected epithelial cells would elicit augmented fibroblast proliferation or matrix deposition, thus providing some mechanistic insights into disease pathogenesis of asthma. Efforts will be made to develop co-culture models of primary, polarised epithelial cells and lung fibroblasts as a tool to dissect the contribution of EGFR signalling to airway remodelling.

3.5 Concluding remarks and future work

Overall, despite considerable challenges in the analysis of EGFR signalling in the asthmatic or allergic lungs, the work described in this chapter has demonstrated widespread expression of the receptor and its ligands in various key cell populations, as well as described how ligand levels and receptor activation are affected by allergen exposure and viral infection. Furthermore, this chapter has provided evidence that the expression of two EGFR ligands, *AREG* and *HBEGF*, is upregulated in bronchial epithelial cells from children with PSW or severe asthma and that EGFR signalling may contribute to fibroblast proliferation induced by epithelial-derived mediators. Future experiments will aim to define which EGFR ligands are released by bronchial epithelial cells in response to allergens or viruses, test whether these are contained in exosomes and explore their effect on fibroblast phenotype and function, particularly with respect to extracellular matrix production. In addition, the following chapter (see Chapter 4), describes how various interventions and models of AAD were used to study the contribution of EGFR signalling to disease pathology.

4 Results II:

Manipulating EGFR signalling during allergic airway disease

4.1 Introduction

4.1.1 Investigating the role of EGFR signalling in rodent models of AAD

The previous chapter (see Chapter 3) characterised how expression and activation of EGFR and its ligands are altered during asthma or AAD. This chapter will focus on the functional contribution of EGFR signalling to AAD pathology. Various studies have employed pharmacological inhibition to study the role of EGFR in mouse models of AAD. In the traditional OVA sensitisation/challenge model, treatment with EGFR inhibitors resulted in reductions in airway eosinophilia and levels of type 2 cytokines such as IL-4 and IL-13[165, 170]. Importantly, the intervention also resulted in ameliorated airway hyperresponsiveness and remodelling, as shown by decreased staining for mucus, airway smooth muscle and, in a subset of studies, also collagens[136, 165, 168, 170]. Improvements in hallmark features of AAD upon EGFR inhibition were also observed in studies using inhaled HDM models of AAD, which described reductions in airway type 2 inflammation, goblet cell hyperplasia, airway smooth muscle thickening, collagen deposition and expression of remodelling-associated genes[136, 166, 167, 169, 242]. Collectively, these reports provide compelling evidence for a detrimental role of EGFR signalling in driving AAD pathology. Inhibition of EGFR signalling in rat OVA sensitisation/challenge models of AAD also led to ameliorated lung function, airway inflammation and abundance of mucus and airway smooth muscle[227, 243], illustrating that the pathogenic contributions of EGFR signalling to disease extend beyond the mouse model. Interestingly, amelioration of lung function and type 2 inflammation was only achieved when an EGFR inhibitor was administered during the allergen challenge, but not during the sensitisation phase of the rat OVA model[243, 244]. Nevertheless, EGFR inhibition during sensitisation resulted in reduced airway inflammation[244], suggesting distinct contributions of EGFR signalling during different stages of disease.

Further, albeit circumstantial, evidence for the contribution of EGFR to AAD pathogenesis can be gleaned from studies employing interventions that result in changes in EGFR signalling. For example, activation of EGFR was reduced upon genetic deletion of dual oxidase 1 (DUOX1) during HDM-induced AAD, as were airway hyperresponsiveness, neutrophils, mucus hyperplasia, collagen deposition and airway smooth muscle thickening[223]. Similarly, animals deficient for ADAM17, the enzyme responsible for membrane shedding of several EGFR ligands, displayed reduced EGFR activation along with ameliorated lung function and airway remodelling upon sensitisation and challenge with OVA[222]. In contrast, conditional deletion of integrin beta-4 (ITGB4) from airway epithelial cells of HDM-exposed animals resulted in augmented EGFR signalling accompanied by exacerbated airway hyperresponsiveness and inflammation[242]. Given the great similarity in phenotypes between

EGFR inhibition and the genetic interventions described above, it seems conceivable that the pathology of the latter was, at least in part, driven by EGFR-related mechanisms. Interestingly, airway epithelial-specific deletion of ITGB4 was also described in neonatal mice, where it resulted in exacerbated inflammation and airway hyperresponsiveness both at baseline and after inhaled HDM exposure[245]. To our knowledge, this is the only study characterising the role of EGFR signalling during early-life AAD, albeit only indirectly, and the contribution of EGFR to AAD pathology in early life and how it may differ from adults is unknown.

4.1.2 Contribution of individual EGFR ligands to AAD

In addition to defining the role of EGFR in driving AAD pathology, efforts have been made to characterise the contribution of individual ligands. Several studies have focused on the role of HB-EGF, a high-affinity EGFR ligand ubiquitously expressed in the lungs. Blockade of HB-EGF using neutralising antibodies in a mouse OVA sensitisation/challenge model resulted in reduced airway smooth muscle and mucus[168], whereas genetic deletion of HB-EGF from CD4 T cells in a similar AAD model led to diminished airway inflammation, eosinophilia and IL-5, along with ameliorated lung function and decreased mucus hyperplasia[157]. Conversely, intratracheal installation of HB-EGF caused exacerbated airway smooth muscle thickening in OVA-sensitised and -challenged mice[171]. These findings suggest that HB-EGF may be the primary EGFR ligand involved in driving key features of AAD pathology in the OVA model. In line with this, a study comparing parameters of allergic inflammation between WT and AREG-deficient animals after sensitisation and challenge with OVA did not observe any differences between phenotypes[246], indicating that the low-affinity ligand AREG is dispensable in this context. In contrast, Morimoto et al. 2018 (ref.[136]) found reduced collagen deposition and expression of remodelling-associated genes in AREG-deficient mice compared to WT animals using an inhaled HDM model of AAD, illustrating that the individual contribution of each of the EGFR ligands is likely highly context-dependent.

Overall, the literature provides overwhelming evidence for a pathogenic role of EGFR in driving pathology of AAD. This chapter will build on these findings by characterising the role of EGFR signalling in different models, for example during acute AAD or after exposure to the alarmin IL-33, using both EGFR inhibition and ligand administration. Importantly, this work will define the contribution of EGFR signalling to key features of disease pathology in early life by employing various intervention strategies in neonatal models of AAD.

4.1.3 Hypothesis and aims

Hypothesis

EGFR signalling is important in the development of AAD and its absence will result in less severe pathology in adult animals but has a different impact on disease in early life.

Aims

1. To study the role of EGFR signalling in acute and chronic models of AAD by receptor activation or inhibition.
2. To compare the contribution of EGFR signalling to hallmark features of AAD between early life and adulthood.
3. To establish a mixed allergen challenge model of AAD as a novel approach to studying the role of EGFR signalling.

4.2 Methods

4.2.1 EGFR intervention in murine models of AAD

Full details of dosing regimens are given in the relevant figures and legends. Briefly, AAD was induced in female adult BALB/c mice or neonatal BALB/c mice of both sexes by repeated intranasal exposure to recombinant IL-33 or HDM. A novel model of early-life AAD was established in 7-day-old animals by administration of an allergen mix made up of ALT, HDM and timothy grass (TG) and compared to administration of each of the allergens alone.

To activate EGFR signalling, recombinant ligands AREG or HB-EGF were given intranasally either together with or 4-6 hours after alarmin or allergen treatment. EGFR inhibitor Gefitinib was administered orally 4-6 hours prior to allergen exposure to block EGFR signalling.

4.2.2 Assessment of key pathological features of AAD

Animals were culled one day after the last alarmin or allergen dose. Inflammation of airways and lungs was assessed by flow cytometry analysis of BAL and lung homogenates using markers to identify myeloid cells, innate lymphoid cells and T lymphocytes as well as cytokine production potential and activation state of these cells. Baseline lung function and airway hyperresponsiveness to the inhaled bronchoconstrictor methacholine (MCh) were measured in anaesthetised and tracheotomised animals using the Scireq FlexiVent system. EGFR activation levels and ligand, cytokine or antibody levels were analysed in lung homogenates and/or BAL or serum by western blot and ELISA, respectively. Pulmonary gene expression changes were measured using qPCR. Traditional Periodic Acid-Schiff or Gordon & Sweet's silver staining as well as immunofluorescence and second-harmonic generation imaging of collagen fibres were used to study airway remodelling.

4.2.3 Integrative data analysis

To allow more in-depth analysis of EGFR inhibition during neonatal AAD, complete quantitative data sets from ELISA, flow cytometry, lung function and qPCR analyses were analysed combined. Correlations between individual parameters were calculated using the Spearman rank method and correlation coefficients and *p*-values were plotted as a correlation matrix. In an attempt to identify shared drivers, four clusters of parameters with significant differences between inhibitor- and vehicle-treated HDM-exposed animals were defined and a Venn diagram was created to visualise shared correlations between clusters. Finally, relationships between individual parameters were interrogated using network analysis, where significant correlations were represented as edges between parameters (nodes).

4.3 Results

4.3.1 Exogenous activation of EGFR signalling during acute models of adult AAD

A major aim of this chapter was to use EGFR ligands or inhibitor to activate or block EGFR signalling, respectively, as a way to establish the contribution of EGFR signalling to the pathology of AAD. To start off, effects of exogenous AREG administration on disease were analysed in an acute model of IL-33-induced airway inflammation (**Figure 4.1A**). There were

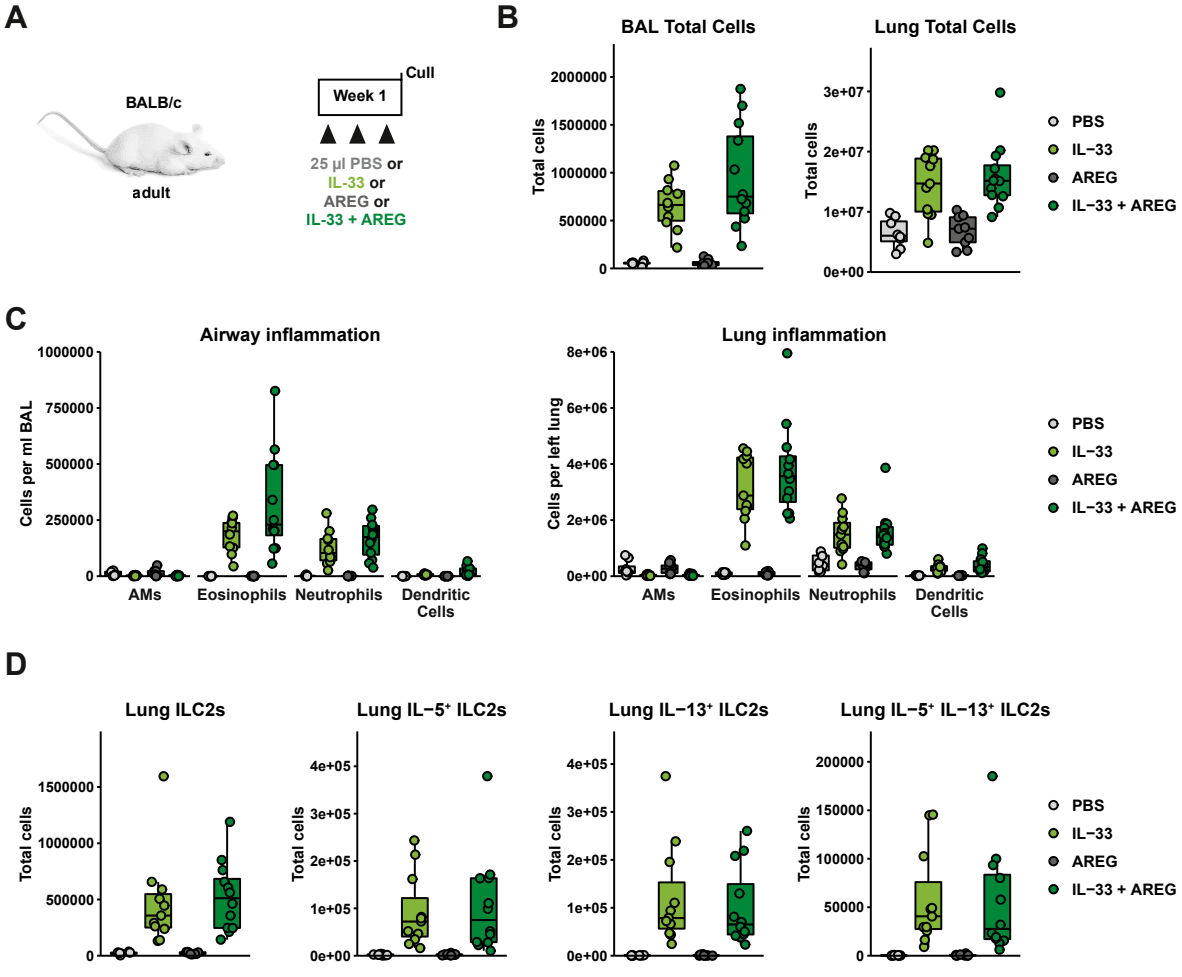


Figure 4.1 Exogenous administration of AREG during acute IL-33-induced airway inflammation did not affect overall inflammation.
A Schematic depicting experimental approach. Adult female BALB/c mice were given three intranasal doses of 1 µg recombinant IL-33 and/or 1 µg recombinant AREG in 25 µl PBS in the span of one week and animals were sacrificed on the day following the last dose. **B** Total cells in bronchoalveolar lavage or the left lung lobe. **C** Numbers of airway macrophages (AMs), eosinophils, neutrophils and dendritic cells in bronchoalveolar lavage or the left lung lobe, as measured by flow cytometry. **D** Numbers of lung type 2 innate lymphoid cells (ILC2s) and their potential to produce cytokines after stimulation with PMA and ionomycin in the presence of Brefeldin A, as measured by flow cytometry. (B-D) *n* = 8-12, pooled from two independent experiments.

no effects of AREG treatment on overall inflammation in the airways or lungs (**Figure 4.1B-C**), nor on the numbers or cytokine production potential of ILC2s (**Figure 4.1D**).

Baseline lung function and airway hyperresponsiveness were also largely unaffected by AREG administration (**Figure 4.2A**), with the exception of mildly exacerbated compliance and tissue elastance in response to 100 mg/ml MCh (**Figure 4.2B**). However, the lung function measurements at the highest dose of MCh were highly variable and up to half the animals in

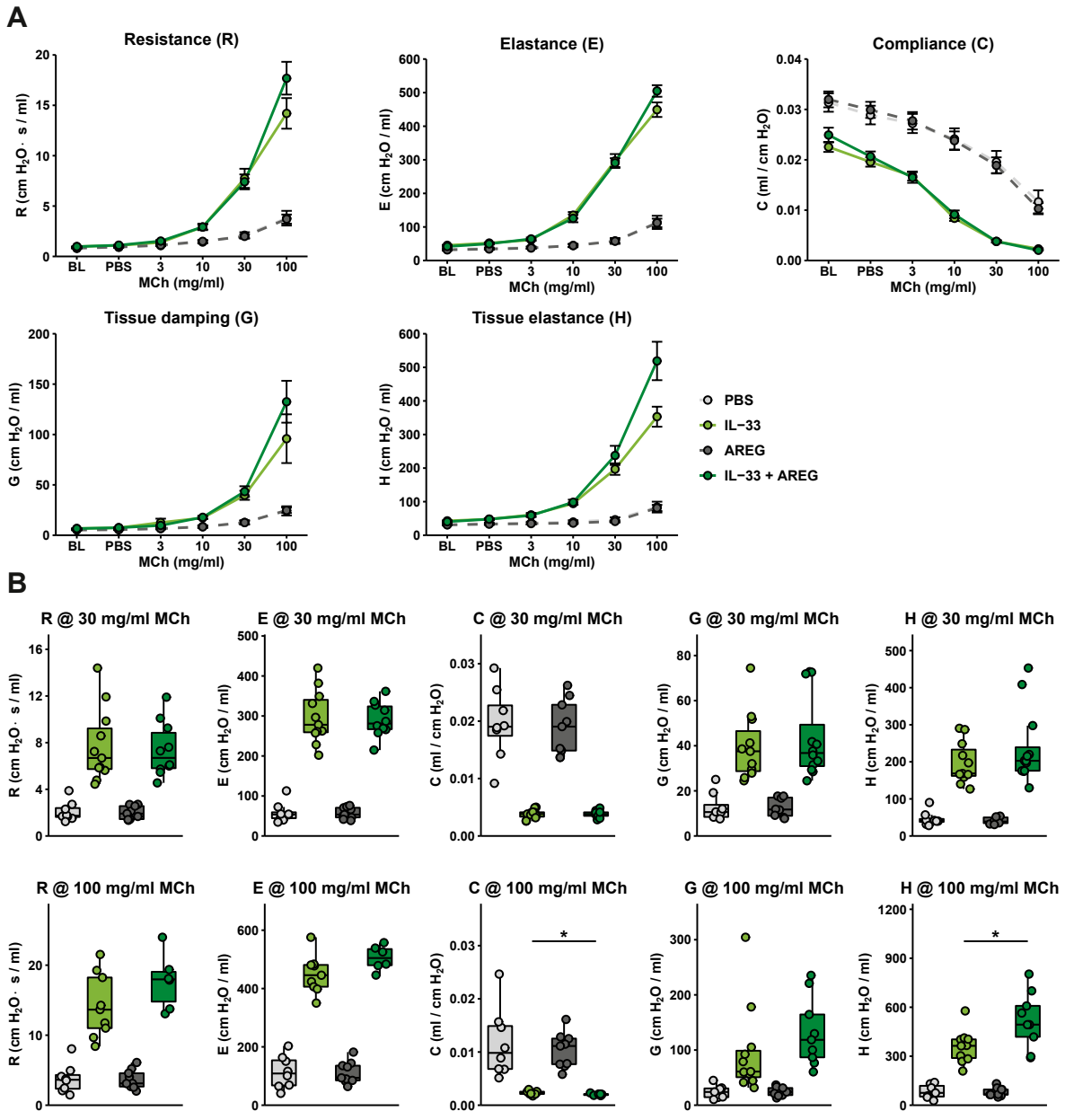


Figure 4.2 Exogenous administration of AREG during acute IL-33-induced airway inflammation resulted in mild decreases in lung function.
Animals were treated as described in Figure 4.1A. **A** Various lung function parameters in response to increasing doses of bronchoconstrictor methacholine (MCh). Data are shown as mean +/- standard error. **B** Lung function parameters at indicated doses of MCh. (A-B) *n* = 6-12; measurements for some animals had to be excluded for not meeting quality control standards. Data are pooled from two independent experiments. Statistics: Mann-Whitney test between indicated groups. *, $p < 0.05$.

the IL-33-treated groups had to be excluded during quality control, indicating that these results should be interpreted with caution.

Given the lack of effect of AREG administration in this model, western blot analysis of Y1068 phosphorylation was performed to validate receptor activation (**Figure 4.3A**). While not statistically significant, there was a trend towards increased EGFR phosphorylation in AREG-treated animals (**Figure 4.3B**), suggesting that the administration of AREG was likely sufficient to induce EGFR signalling. The absence of a strong Y1068 signal in response to recombinant AREG administration may be attributed to the fact that AREG preferentially induces phosphorylation of Y992[99, 100]. In addition, there were significantly increased levels of AREG, but not any of the other ligands, in the BAL of animals treated with both IL-33 and AREG compared to IL-33 alone (**Figure 4.3C**), providing further evidence for the successful delivery of recombinant AREG to the airways. Interestingly, AREG treatment had no effect on lung

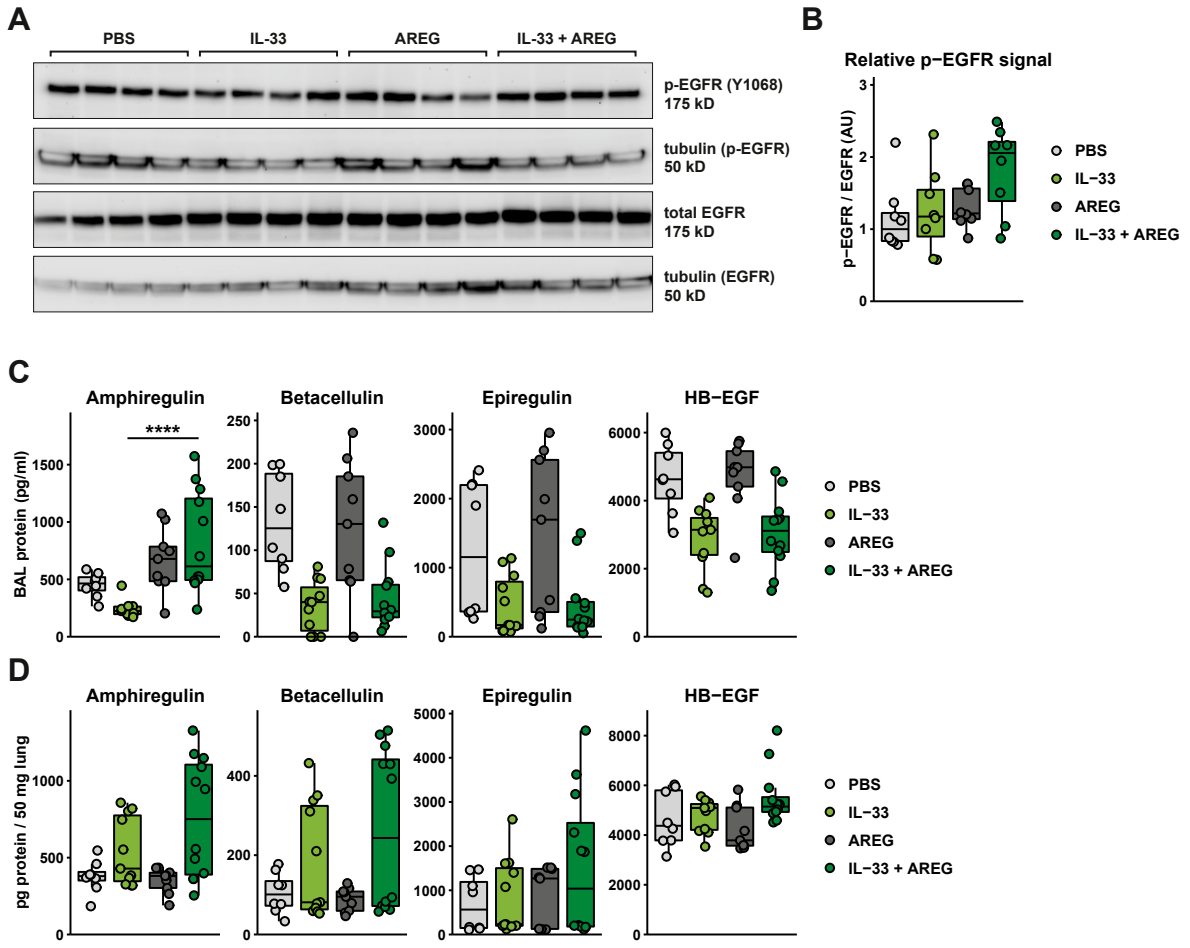


Figure 4.3 Exogenous AREG was detectable in bronchoalveolar lavage but did not alter airway or lung ligand levels.
Animals were treated as described in Figure 4.1A. **A** Representative western blot of lung homogenates using indicated antibodies. **B** Quantification of p-EGFR signal relative to EGFR signal in western blots from two independent experiments. **C-D** EGFR ligand levels in bronchoalveolar lavage (C) and lung homogenates (D). (A) $n = 4$. (B) $n = 8$. (C-D) $n = 6$-12. Data shown are pooled from two independent experiments. Statistics: Mann-Whitney test between indicated groups. ****, $p < 0.0001$.

ligand levels (**Figure 4.3D**), which may indicate that exogenous AREG was unable to traverse the epithelial barrier. Overall, exogenous administration of AREG had little effect on inflammation and lung function during acute IL-33-induced airway inflammation.

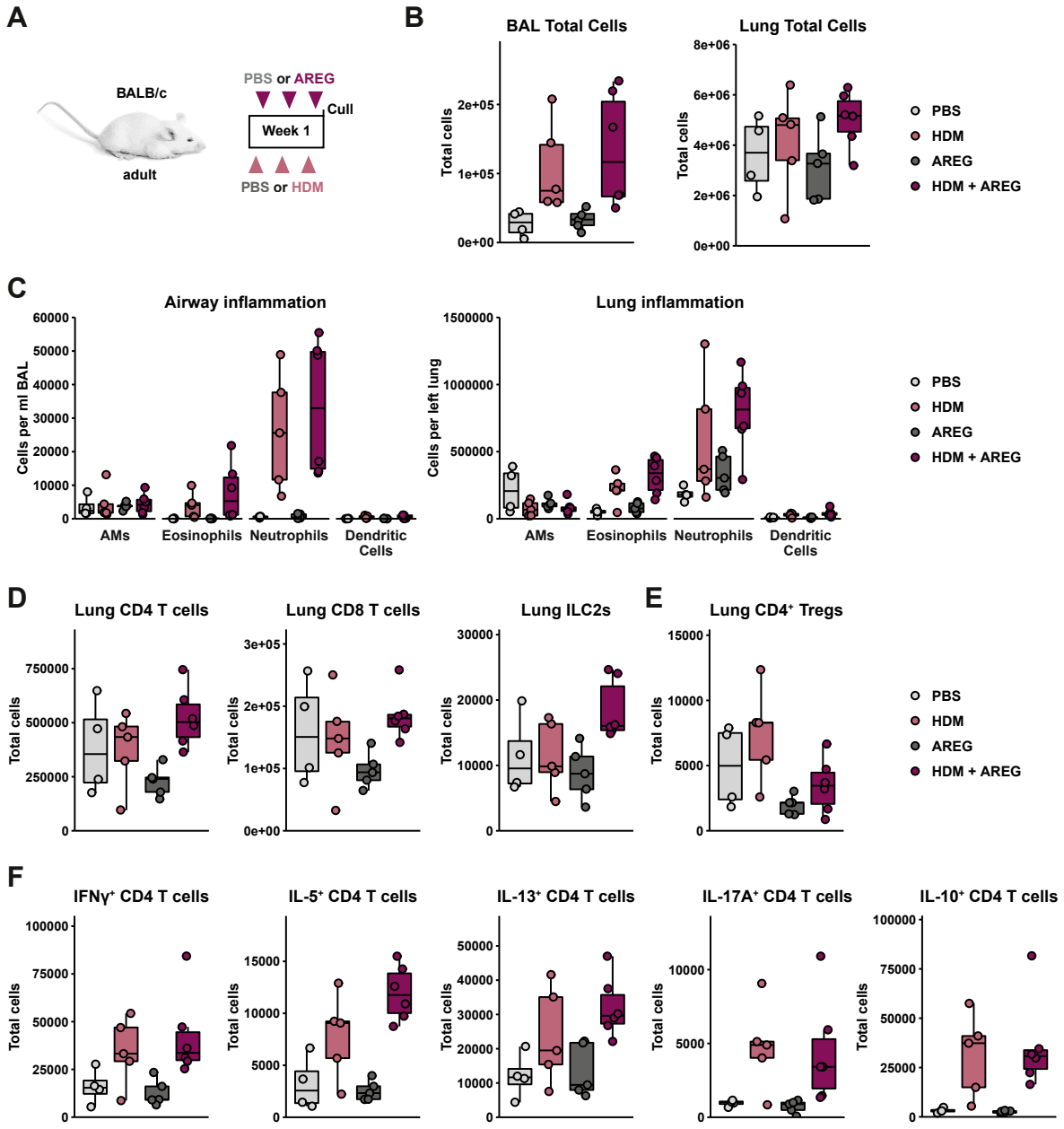


Figure 4.4 Exogenous administration of AREG during acute HDM-induced AAD did not affect overall inflammation.
A Schematic depicting experimental approach. Adult female BALB/c mice were given three intranasal doses of HDM (25 µg) in the span of one week. Recombinant AREG (1 µg) was given intranasally 4-6 hrs after allergen challenge and animals were sacrificed on the day following the last dose. **B** Total cells in bronchoalveolar lavage or the left lung lobe. **C** Numbers of airway macrophages (AMs), eosinophils, neutrophils and dendritic cells in bronchoalveolar lavage or the left lung lobe, as measured by flow cytometry. **D-F** Numbers of different lymphocyte populations (D, E) and their potential to produce cytokines after stimulation with PMA and ionomycin in the presence of Brefeldin A (F), as measured in left lung lobes by flow cytometry. (B-D) *n* = 4-6, data from one experiment.

To test whether these findings were model-specific, the consequences of AREG administration were also assessed in an acute model of HDM-induced AAD (**Figure 4.4A**). Similar to the observations during IL-33-induced airway inflammation, there were no effects of exogenous AREG treatment on overall inflammation in airways and lungs (**Figure 4.4B-C**), the numbers of lymphocytes in the lungs (**Figure 4.4D-E**) or their potential to produce cytokines (**Figure 4.4F**). In line with this, there were also no changes in lung function upon AREG administration, even at high doses of MCh (**Figure 4.5**). Nevertheless, AREG was present at elevated levels in the airways of animals treated with the recombinant cytokine (**Figure 4.6A**), while the levels of other ligands remained unaffected (**Figure 4.6A-B**).

Taken together, exogenous EGFR activation with the low-affinity ligand AREG during two acute models of airway inflammation did not result in any overt changes in disease pathology.

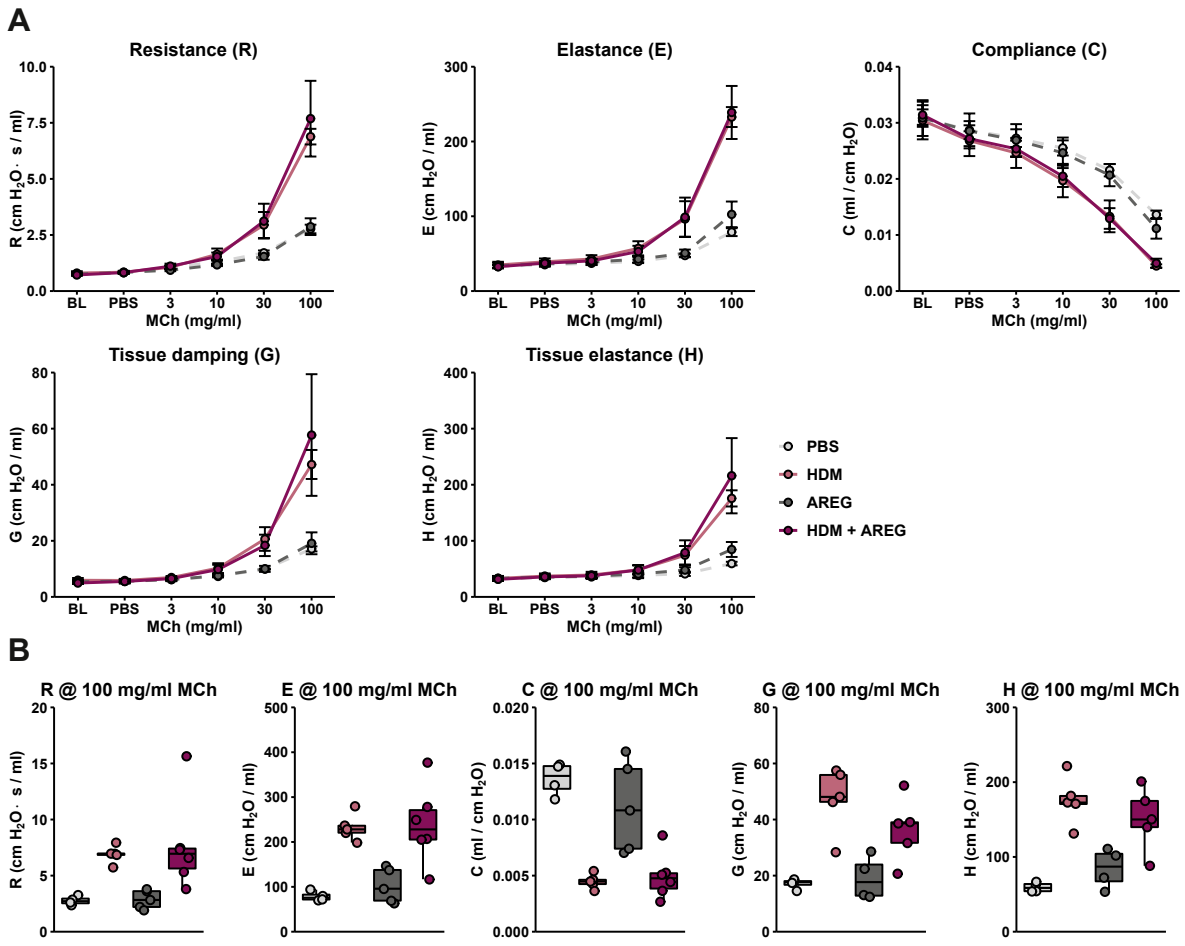


Figure 4.5 Exogenous administration of AREG during acute HDM-induced AAD did not affect lung function.
Animals were treated as described in Figure 4.4A. **A** Various lung function parameters in response to increasing doses of bronchoconstrictor methacholine (MCh). Data are shown as mean +/- standard error. **B** Lung function parameters at 100 mg/ml MCh. (A-B) *n* = 2-6; measurements for some animals had to be excluded for not meeting quality control standards.

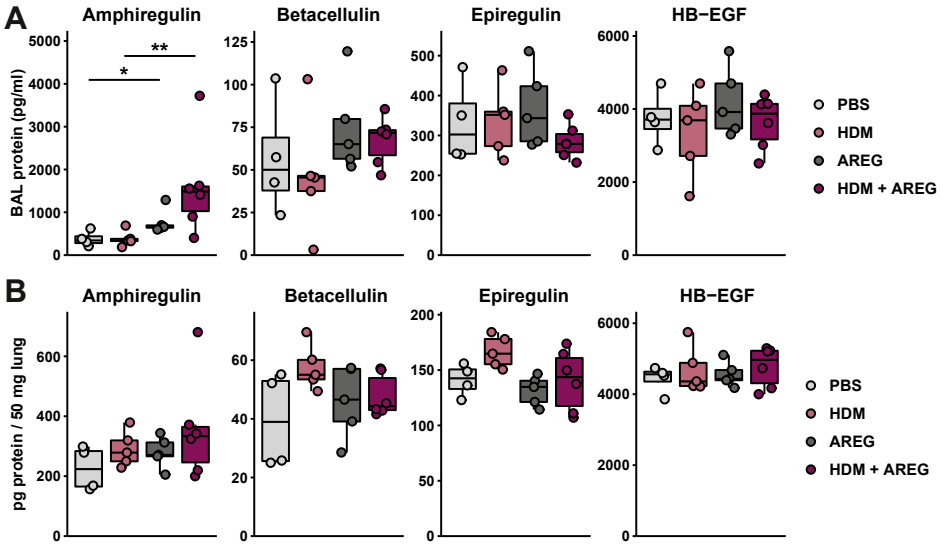


Figure 4.6 Exogenous AREG was detectable in bronchoalveolar lavage but did not alter airway or lung ligand levels.
Animals were treated as described in Figure 4.4. **A-B** EGFR ligand levels in bronchoalveolar lavage (A) and lung homogenates (B). n = 4-6, data from one experiment. Statistics: Mann-Whitney test between indicated groups. *, $p < 0.05$; **, $p < 0.01$.

4.3.2 Inhibition of EGFR signalling during a chronic model of adult AAD

The next aim was to investigate the effects of EGFR inhibition rather than activation on pathology of AAD. While receptor inhibition can be achieved through various means, for example with blocking antibodies, the majority of *in vivo* studies have used EGFR TKIs due to their ease-of-use, commercial availability and cost effectiveness. Gefitinib is a first-generation EGFR TKI clinically approved for the treatment of non-small cell lung cancer[185] and was chosen in this thesis for its extensive tissue distribution, especially to the lungs[247], its potential to suppress pathology in an adult AAD *in vivo* model[165] as well as its increased solubility and relative low cost compared to other available EGFR TKIs. To start off, the ideal route of administration for the EGFR inhibitor Gefitinib, as well as its safety for use *in vivo*, was investigated first. Neonatal BALB/c mice were given three doses of Gefitinib within one week, either via the intranasal, intraperitoneal or oral route. One day after the final Gefitinib dose, mice were administered recombinant AREG intranasally to activate EGFR signalling and tissues were collected two hours later (**Figure 4.7A**). Inhibitor treatment did not affect weight gain of the pups (**Figure 4.7B**) and had no effects on overall cellularity of the lungs (**Figure 4.7C**). Western blot analysis of Y1068 phosphorylation was used as a measure of EGFR activation and showed that Gefitinib suppressed pulmonary EGFR signalling regardless of administration route (**Figure 4.7D**). However, as white deposits were found on the lungs of animals treated with Gefitinib intranasally or intraperitoneally, likely caused by drug precipitation, oral gavage was used as route of administration in future experiments.

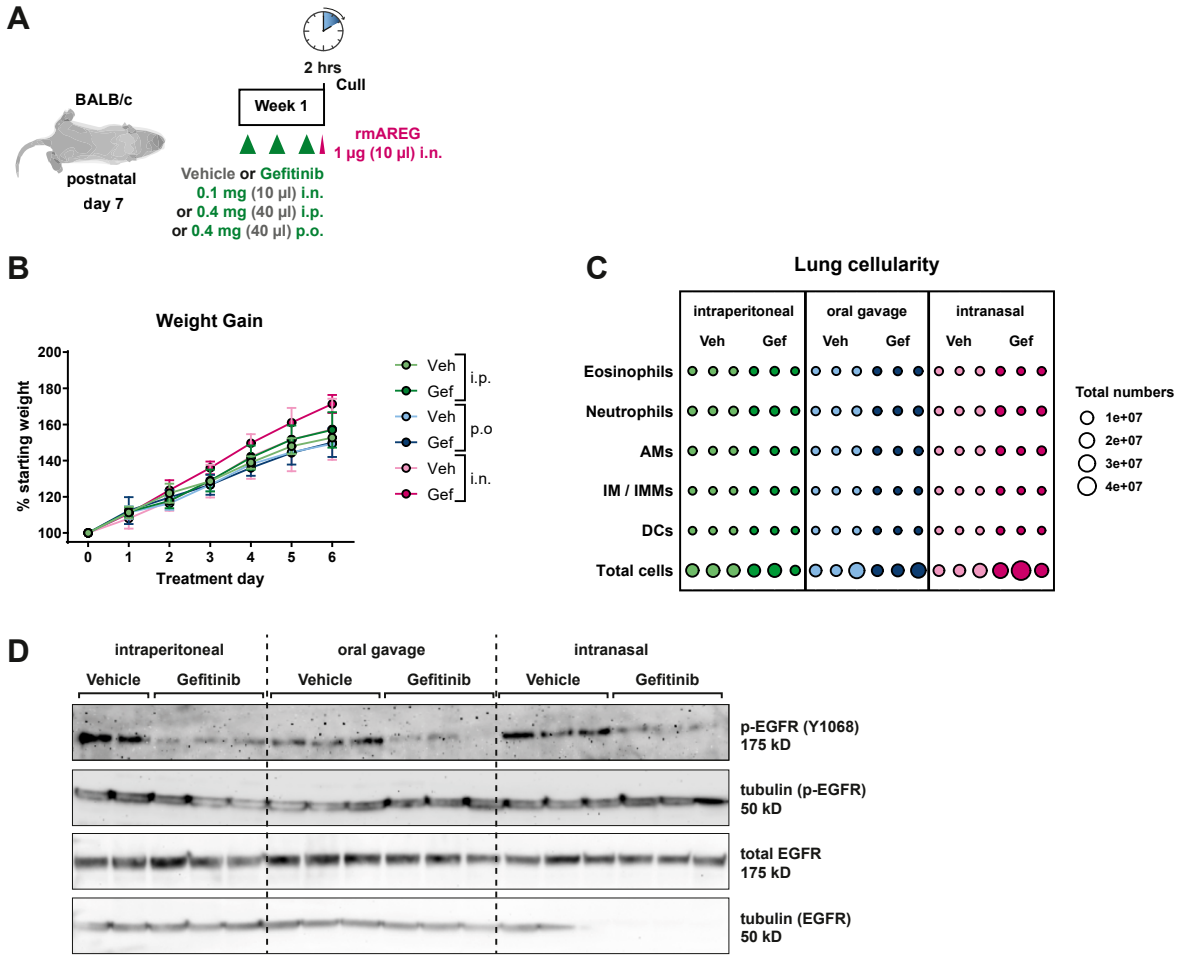


Figure 4.7 Gefitinib administration was safe and able to suppress EGFR activation regardless of administration route.
A Schematic depicting experimental approach. 7-day-old mice were treated with three doses of Gefitinib (Gef) or vehicle (Veh) intranasally (0.1 mg / 10 µl), intraperitoneally (0.4 mg / 40 µl) or orally 0.4 mg / 40 µl) on days 0, 3 and 5. All mice were given 1 µg AREG intranasally on day 6 and culled 2 hours later. **B** Weight gain of pups relative to starting weight. **C** Total numbers (indicated by circle size) of different myeloid lung cell populations as measured by flow cytometry. **D** Western blot analysis of lung homogenates using indicated antibodies. *n* = 2-3, data from one experiment.

To investigate the role of EGFR signalling in established AAD, female adult BALB/c mice were intermittently exposed to inhaled HDM for five weeks and Gefitinib was administered at a dose roughly equivalent to 75 mg/kg 4-6 hours prior to HDM dosing during weeks three to five of allergen exposure (**Figure 4.8A**). This dosing regimen was chosen to test the therapeutic potential of Gefitinib in modifying AAD pathology while minimising the risk of drug-related adverse effects such as the development of interstitial lung disease or inflammation[203, 248, 249] by administering the drug less frequently than the widely reported six to seven weekly doses of EGFR TKIs[165-167, 169]. Overall inflammation, as well as recruitment of myeloid cells to the lungs and airways, were unaffected by EGFR inhibition (**Figure 4.8B-C**). Similarly, there were no effects of Gefitinib treatment on pulmonary lymphocyte populations (**Figure 4.8D-E**), nor

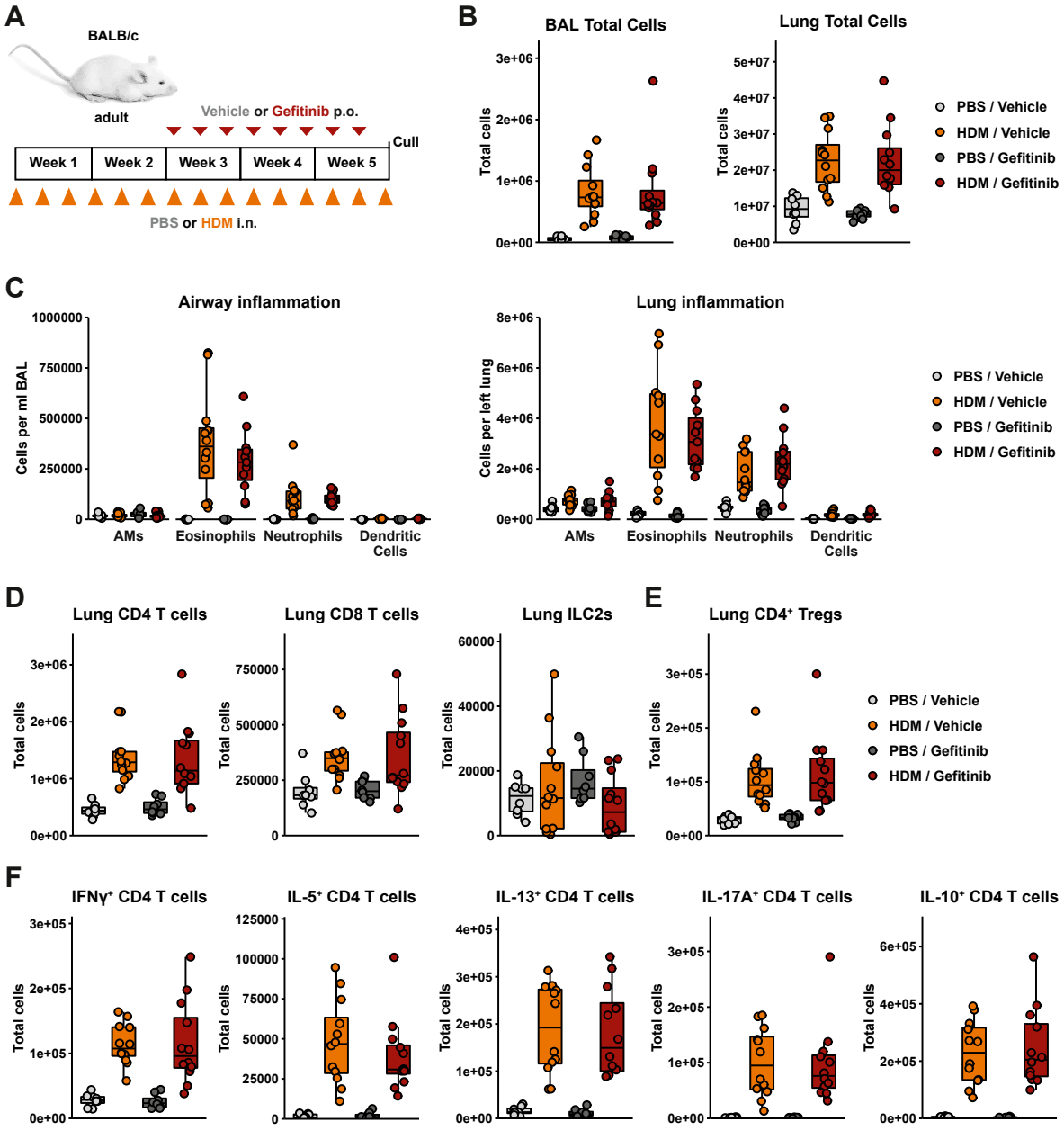


Figure 4.8 EGFR inhibition during chronic HDM-induced AAD did not affect overall inflammation.
A Schematic depicting experimental approach. Adult female BALB/c mice were given inhaled HDM (25 µg) three times per week for five weeks. During weeks three to five, mice were orally administered Gefitinib (1.5 mg) approx. 4-6 hours prior to allergen challenge and animals were sacrificed on the day following the last dose. **B** Total cells in bronchoalveolar lavage or the left lung lobe. **C** Numbers of airway macrophages (AMs), eosinophils, neutrophils and dendritic cells in bronchoalveolar lavage or the left lung lobe, as measured by flow cytometry. **D-F** Numbers of different lymphocyte populations (D, E) and their potential to produce cytokines after stimulation with PMA and ionomycin in the presence of Brefeldin A (F), as measured in left lung lobes by flow cytometry. (B-D) *n* = 8-12. Data are pooled from two independent experiments.

on the ability of CD4 T cells to produce cytokines in response to *ex vivo* stimulation with PMA and ionomycin (**Figure 4.8F**).

Interestingly, measurement of airway hyperresponsiveness in response to increasing doses of MCh in these animals revealed significantly reduced lung function in control but not HDM-treated animals upon EGFR inhibition (**Figure 4.9**). Specifically, Gefitinib treatment resulted

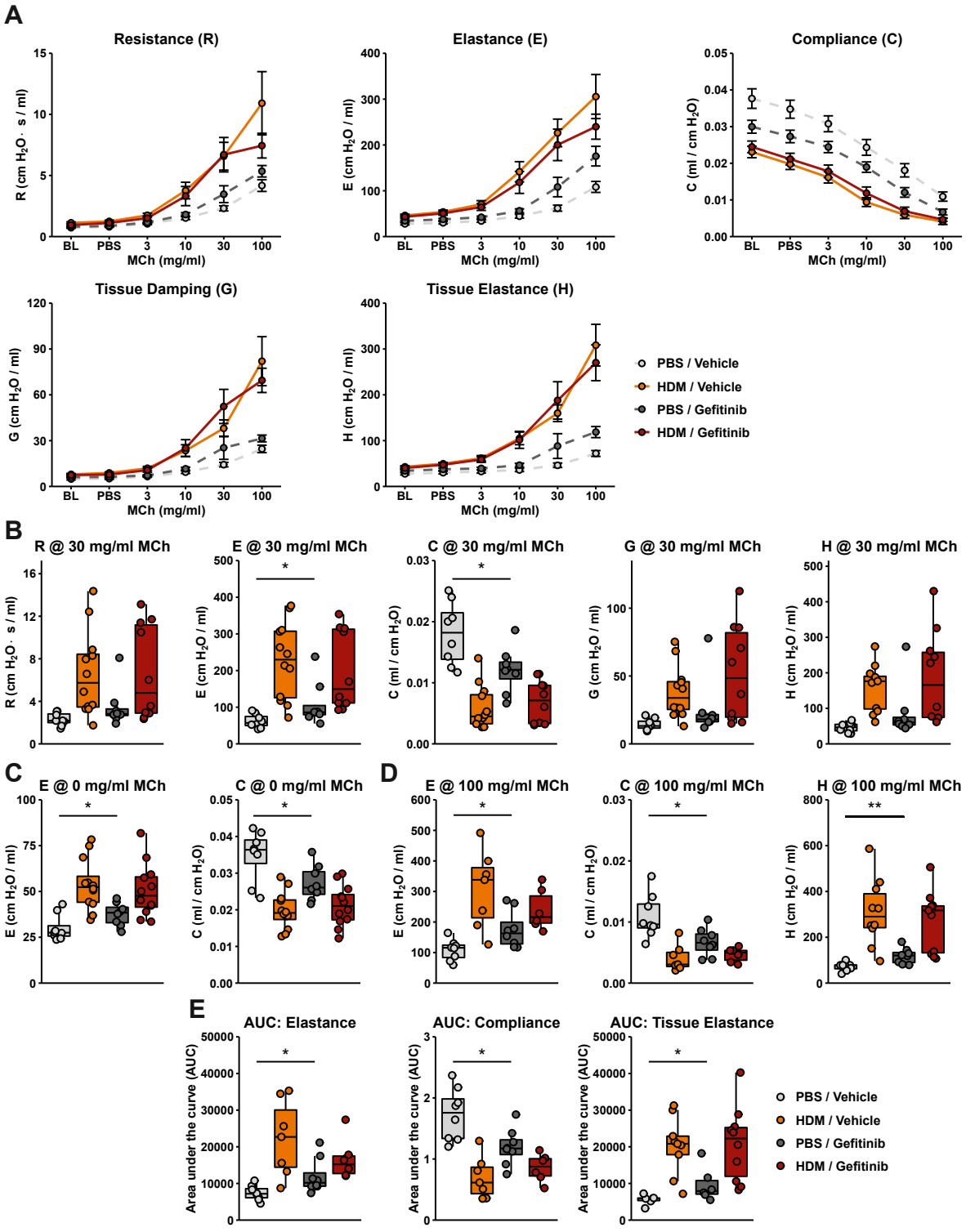


Figure 4.9 EGFR inhibition resulted in worsened lung function of PBS- but not HDM-treated animals. Animals were treated as described in Figure 4.8A. **A** Various lung function parameters in response to increasing doses of bronchoconstrictor methacholine (MCh). Data are shown as mean +/- standard error. **B-D** Lung function parameters at indicated doses of MCh. **E** Area under the curve of lung function in response to increasing doses of MCh. (A-E) n = 6-12; measurements for some animals had to be excluded for not meeting quality control standards. Data are pooled from two independent experiments. Statistics: Mann-Whitney test between indicated groups. *, $p < 0.05$; **, $p < 0.01$.

in worse elastance and compliance, both in response to the lowest and highest concentrations of MCh (**Figure 4.9B-D**). In addition, there was significantly worsened tissue elastance of

PBS-exposed mice treated with Gefitinib compared to untreated controls (**Figure 4.9D**), and these animals displayed increased area under the curve for all three lung function parameters (**Figure 4.9E**). These results suggest that some EGFR signalling is necessary to maintain lung function in naïve animals.

As previously shown for AREG administration, western blot analysis of Y1068 phosphorylation in lung homogenates was performed to validate the ability of Gefitinib to inhibit EGFR signalling. However, this approach failed to reliably detect p-EGFR in these samples (**Figure 4.10A**) and it was thus not possible to draw conclusions regarding the activity of Gefitinib in this model. In addition, there were no differences in EGFR ligand levels between inhibitor- and vehicle-treated animals (**Figure 4.10B**), suggesting that Gefitinib treatment did not alter ligand availability in the lungs or airways. Since it was not possible to confirm the activity of Gefitinib *in vivo*, an *in vitro* approach was used to validate its ability to suppress EGFR activation. To this end, fully differentiated bronchial epithelial cells from a healthy pre-school child were treated with 10 µm Gefitinib or vehicle for one hour prior to lysis. Western blot analysis revealed robust Y1068 phosphorylation in the absence of intervention, which was reduced by administration of Gefitinib dissolved in either 6% hydroxypropyl-β-cyclodextrin (HP-β-CD; *in vivo* vehicle) or dimethyl sulfoxide (DMSO; *in vitro* vehicle) (**Figure 4.10C**). Although it was possible to confirm that Gefitinib dissolved in the vehicle HP-β-CD was able to suppress EGFR activation, inhibition appeared weaker than when dissolved in DMSO. Gefitinib is insoluble in water and reconstituting the drug in HP-β-CD proved difficult, as the resulting suspension was unstable and the drug precipitated within minutes. Therefore, sonication was used to aid the even reconstitution of Gefitinib in the vehicle, which may have resulted in some loss of activity, as suggested by our *in vitro* findings. Nevertheless, other solvents such as DMSO and ethanol would cause adverse effects at the concentrations needed to deliver doses of up to 1.5 mg Gefitinib to mice. For that reason, a second *in vivo* vehicle, 1% (w/w) Tween® 80, was tested, which resulted in slightly better reconstitution results (data not shown) and produced comparable results *in vivo* (cf. Figure 4.8**-**Figure 4.10, where data are pooled from two experiments).

Thus far, there were no effects of EGFR inhibition during chronic AAD on inflammation or lung function, two key features of disease pathology. However, other hallmark characteristics of AAD, such as sensitisation and airway remodelling were also measured. Total serum IgE, IgG1 and IgG2a antibody levels were unaffected by EGFR inhibition (**Figure 4.11A**). There were also no effects of Gefitinib treatment on HDM-induced expression of genes encoding extracellular matrix components (**Figure 4.11B**). Interestingly, however, there was significantly lower expression of *Col1a1*, as well as slightly reduced levels of *Col4a1*, after Gefitinib treatment of PBS-challenged animals, which may potentially be linked to the worse

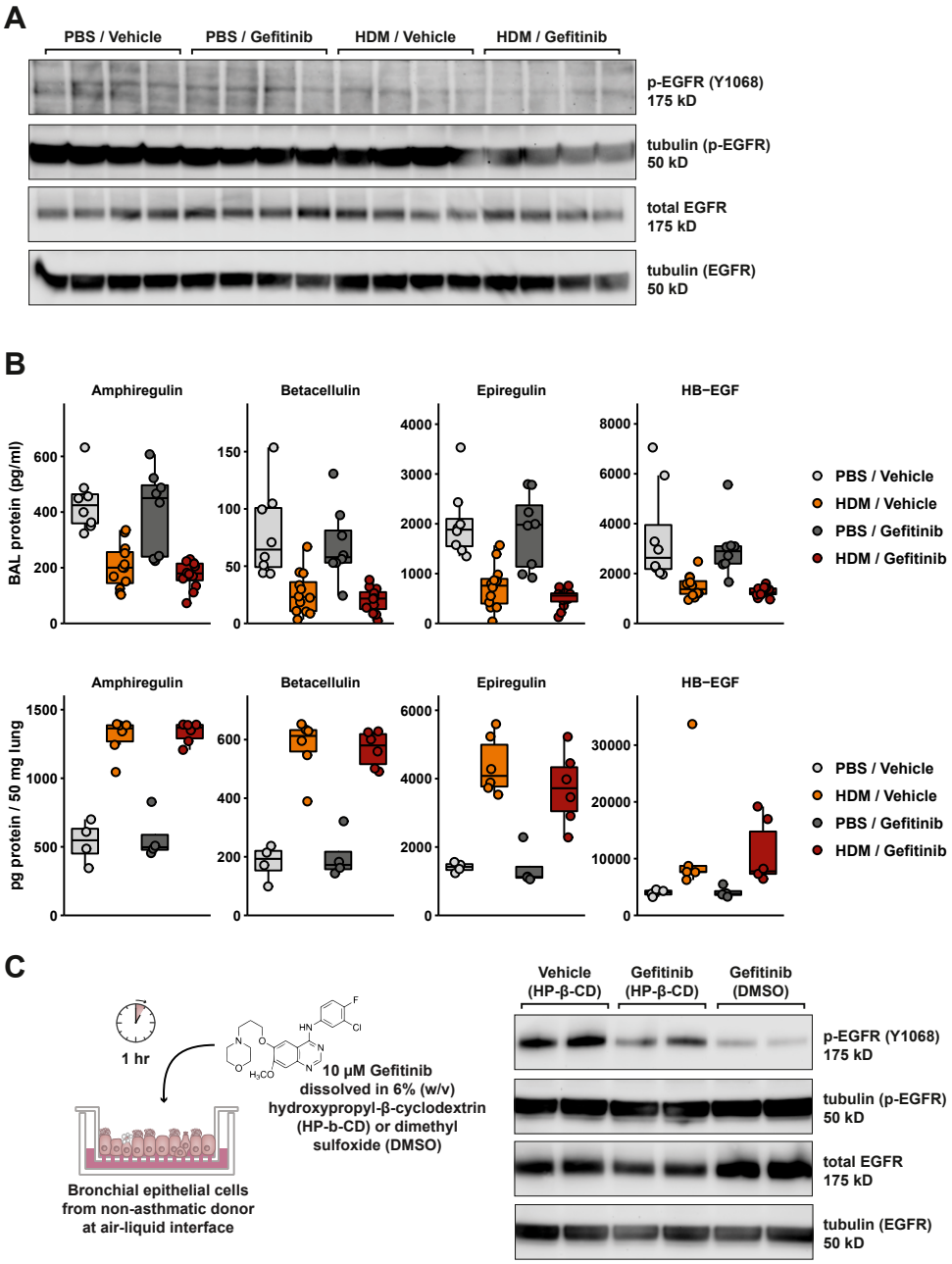


Figure 4.10 EGFR inhibition during chronic HDM-induced AAD did not affect lung or airway levels of EGFR ligands.
Animals were treated as described in Figure 4.8A. **A** Western blot of lung homogenates using indicated antibodies. **B** EGFR ligand levels in bronchoalveolar lavage (top) and lung homogenates (bottom). *n* = 4-12, data from one experiment (A, B bottom) or pooled from two independent experiments (B top). **C** Bronchial epithelial cells from a non-asthmatic donor were cultured at air-liquid interface until fully differentiated. Cells were treated with 6% hydroxypropyl-β-cyclodextrin (HP-β-CD; vehicle) or 10 µM Gefitinib dissolved in either 6% HP-β-CD or dimethyl sulfoxide (DMSO for 1 hour. Cells were lysed and analysed by western blot using indicated antibodies. n=2 technical replicates per group; data from one experiment.

lung function observed in these animals. Finally, histological analyses were used to characterise mucus production and airway smooth muscle deposition in our model, which did not reveal any effects of Gefitinib treatment in either PBS- or HDM-exposed mice

(**Figure 4.11C**). Taken together, these results suggest that this EGFR inhibition approach did not modify hallmark pathologic features of established AAD in adult animals.

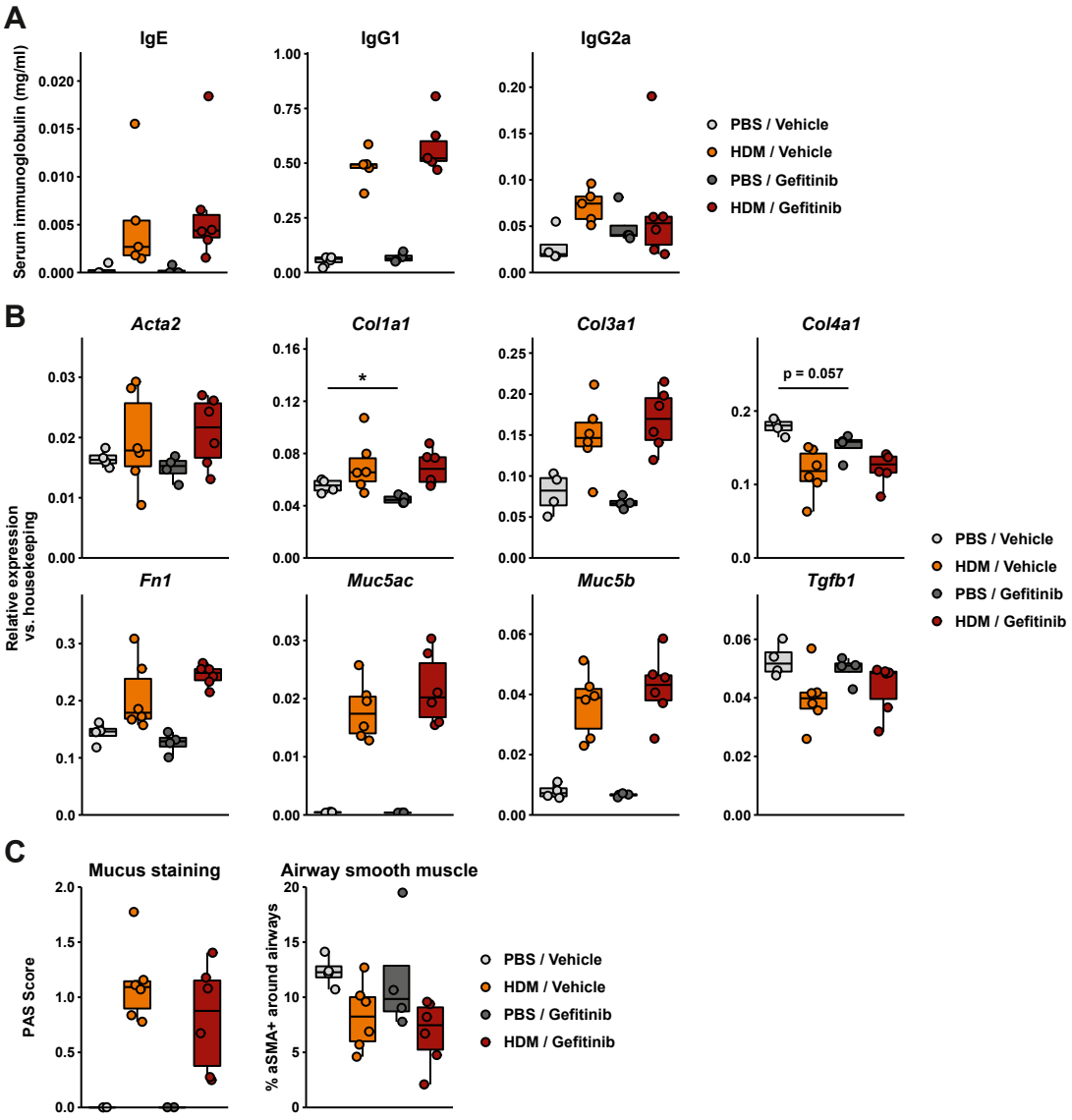


Figure 4.11 EGFR inhibition during chronic HDM-induced AAD does not affect sensitisation or airway remodelling.
Animals were treated as described in Figure 4.8A. **A** Total antibody levels in serum as determined by ELISA. **B** Whole lung gene expression of indicated genes by qPCR. **C** Quantification of Periodic-Acid Schiff (PAS) staining or immunofluorescence staining for α-smooth muscle actin (αSMA) in 4 µm lung sections. (A-C) n = 4-6; data from one experiment. Statistics: Mann-Whitney test between indicated groups. *, $p < 0.05$.

4.3.3 EGFR inhibition during early-life AAD affected monocytic inflammation and lung function

The data previously discussed showed no effects of EGFR inhibition during adult AAD. However, the hypothesis of this chapter was that the mechanisms underlying disease pathology would be distinct in early life. The consequences of EGFR inhibition were therefore

also investigated in a neonatal model of AAD. In line with the adult model, neonatal mice were exposed to inhaled HDM three times a week for five weeks, and Gefitinib was administered orally during the last three weeks of allergen exposure (**Figure 4.12A**). While EGFR inhibition did not affect pulmonary gene expression of *Egfr* or its ligands (**Figure 4.12B**), there were decreased ligand levels, particularly in the lungs, of Gefitinib-treated HDM-exposed animals when compared to vehicle controls (**Figure 4.12C**). In addition, there was a reduction of total

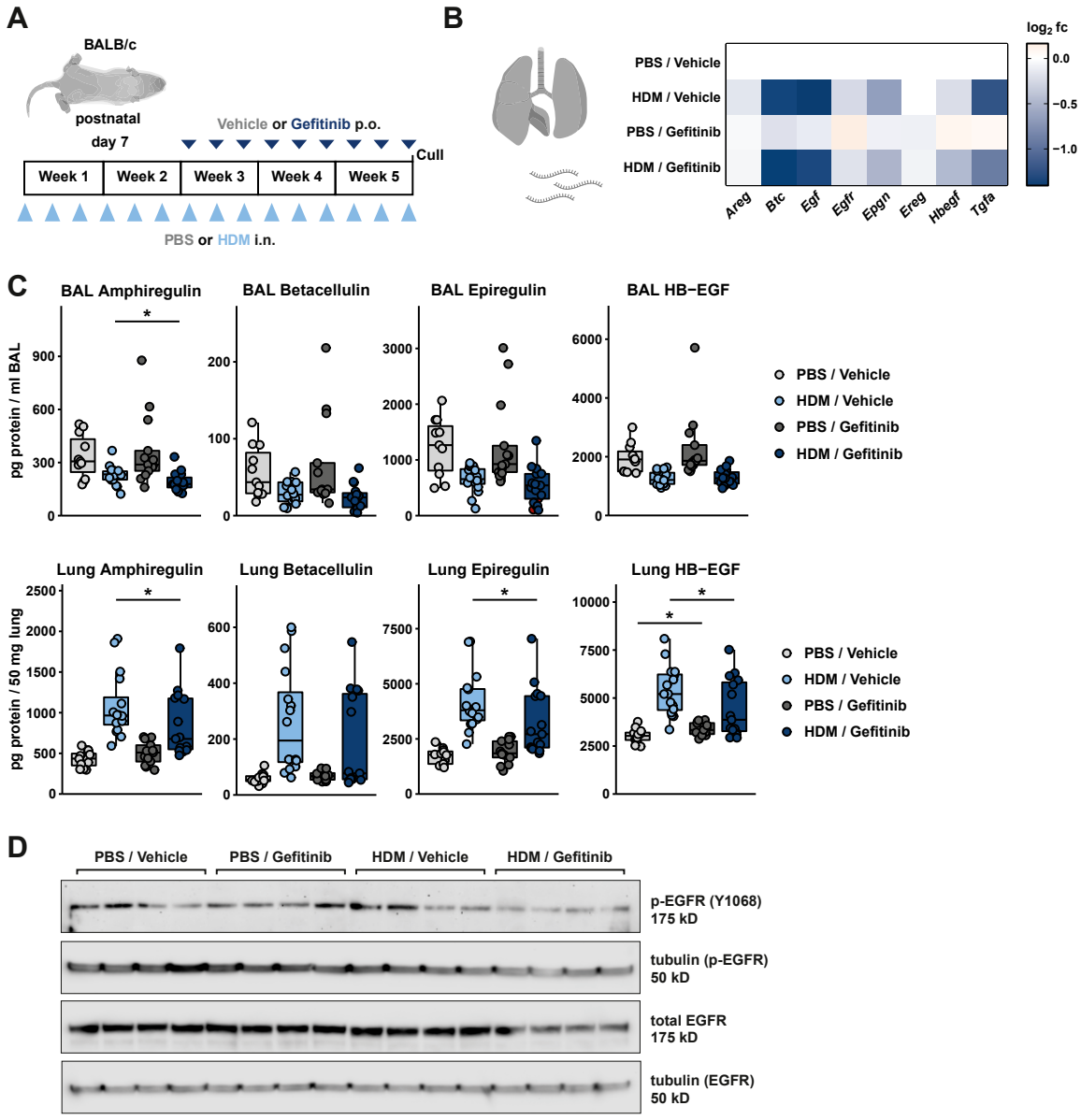


Figure 4.12 EGFR inhibition during early-life AAD altered lung EGFR and ligand levels.
A Schematic depicting experimental approach. 7-day-old BALB/c mice were given inhaled HDM (10 µg in week 1, 15 µg thereafter) three times per week for five weeks. During weeks three to five, mice were orally administered Gefitinib (1 mg) approx. 4-6 hours prior to allergen challenge and animals were sacrificed on the day following the last dose. **B** Whole lung gene expression of indicated genes by qPCR, shown as $\log_2$ fold change from PBS/Vehicle control. **C** EGFR ligand levels in bronchoalveolar lavage (top) and lung homogenates (bottom). **D** Western blot of lung homogenates using indicated antibodies. (B-C): n = 12-16; data pooled from two independent experiments. (D) n = 4; data from one experiment. Statistics: Mann-Whitney test between indicated groups, *, $p < 0.05$.

and phosphorylated EGFR levels in lung homogenates from these animals (**Figure 4.12D**), suggesting that Gefitinib treatment was able to alter EGFR signalling.

Since Gefitinib was administered systemically during a period when mice were still growing and developing, body weight was monitored from the start of EGFR intervention, showing no

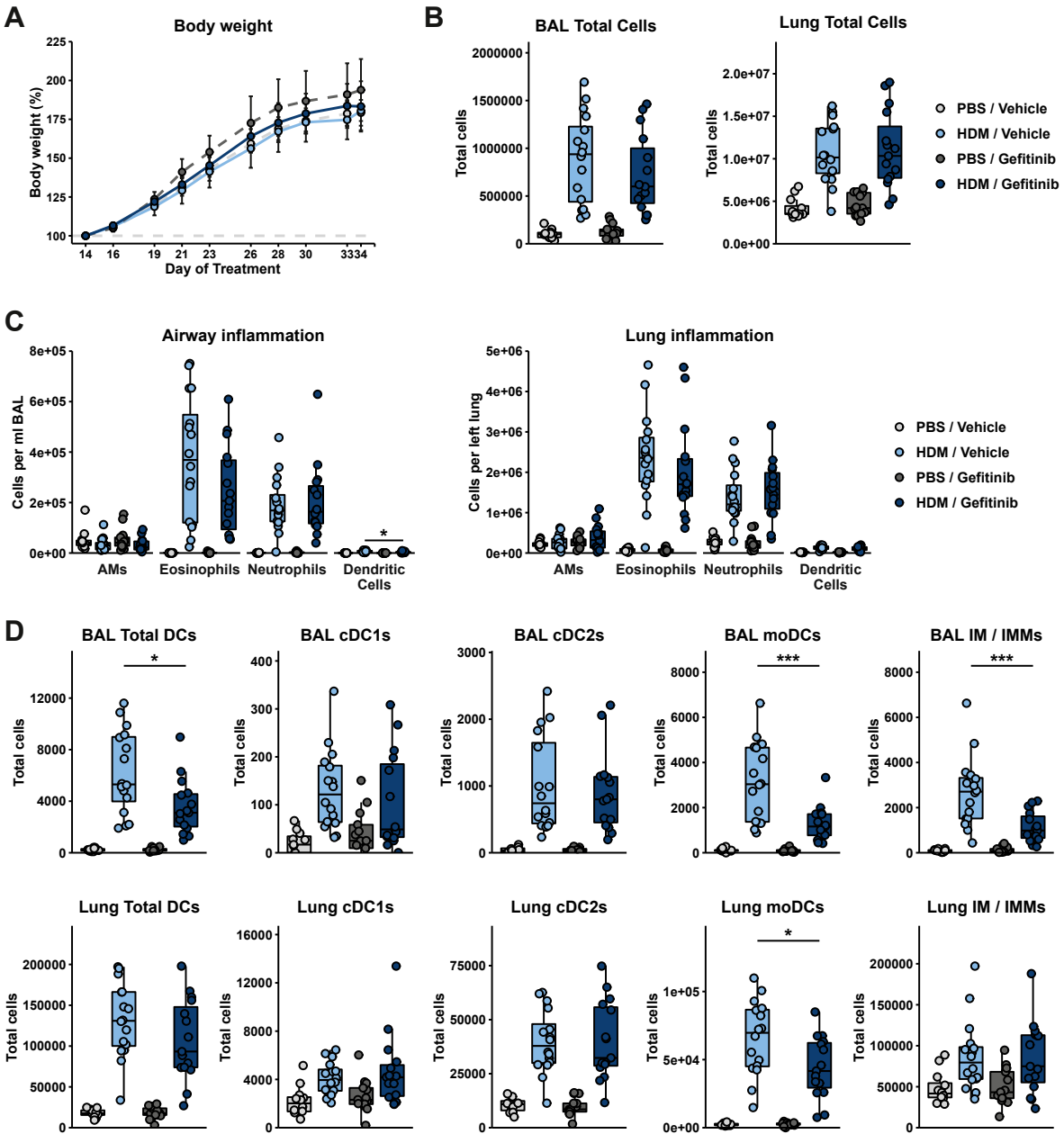


Figure 4.13 EGFR inhibition during early-life AAD restricted monocytic inflammation.
Animals were treated as described in Figure 4.12A. **A** Weight gain of pups (as percentage of starting weight) from beginning of Gefitinib treatment. Data are shown as median and confidence interval. **B** Total cells in bronchoalveolar lavage or the left lung lobe. **C** Numbers of airway macrophages (AMs), eosinophils, neutrophils and dendritic cells in bronchoalveolar lavage or the left lung lobe, as measured by flow cytometry. **D** Numbers of dendritic and monocytic cell populations in bronchoalveolar lavage (top) and left lung lobes (bottom) by flow cytometry. Abbreviations: DCs, dendritic cells; cDCs, classical DCs; moDCs, monocyte-derived DCs; IM / IMMs, interstitial macrophages/inflammatory monocytes and macrophages. (A) n = 7-9; data from one experiment. (B-D) n = 12-16; data pooled from two independent experiments. Statistics: Mann-Whitney test between indicated groups. *, $p < 0.05$; ***, $p < 0.001$.

adverse effects of receptor inhibition on weight gain of the animals (**Figure 4.13A**). There were also no changes in overall cell recruitment to the lungs or airways (**Figure 4.13B**), nor in the numbers of airway macrophages, eosinophils or neutrophils (**Figure 4.13C**). EGFR inhibition did however result in significantly decreased numbers of total DCs, as well as monocyte-derived DCs (moDCs) and interstitial macrophages/inflammatory monocytes and macrophages (IM/IMMs) in the airways of HDM-treated mice (**Figure 4.13D**). Numbers of moDC in the lungs were also reduced by Gefitinib treatment, suggesting that EGFR may contribute to the survival of monocyte-derived cells and/or their recruitment to the lungs and airways.

Since moDCs contribute to the recruitment of Th2 cells during AAD[250, 251], the effects of EGFR inhibition on adaptive immune responses were analysed by measuring several lymphocyte populations in the lungs using flow cytometry. There were no differences in the numbers of CD4 or CD8 T cells, ILC2s or NK cells between Gefitinib- and vehicle-treated animals (**Figure 4.14A**). The ability of CD4 T cells to produce hallmark Th1, Th2 or Th17 cytokines was also unaffected by EGFR inhibition (**Figure 4.14B**), as were the numbers of Tregs and (IL-17A$^+$) γδ T cells (**Figure 4.14D**). Finally, the phenotype of CD4 T cells was characterised by measuring expression of activation (CD69$^+$), effector (memory) (CD62L^{lo} CD44^{hi}) and tissue-residency (CD103$^+$) markers and showed no effects of Gefitinib treatment (**Figure 4.14D**). Overall, these results suggest that EGFR signalling does not contribute to adaptive T cell responses during established early-life AAD.

As with the previous AAD models, airway hyperresponsiveness to MCh was measured as a hallmark feature of disease pathology. Unlike in adult animals (ref. Figure 4.9), Gefitinib treatment did not lead to worsened lung function in PBS-exposed animals (**Figure 4.15A**). Interestingly, however, EGFR inhibition resulted in significantly exacerbated airway hyperresponsiveness in HDM-treated animals (**Figure 4.15B**), as indicated by increased resistance, elastance, tissue damping and tissue elastance after challenge with 30 mg/ml MCh. Tissue damping, a parameter reflecting energy dissipation in the alveoli, also displayed an overall increase in area under the curve across the complete dose response, suggesting parenchymal aspects of lung function were particularly affected by Gefitinib treatment (**Figure 4.15C**). Taken together, these findings indicate that EGFR signalling may hold a protective role in preventing exacerbated airway hyperresponsive during AAD in early life, in contrast to its detrimental role previously described in adult models of AAD[157, 166, 167, 169, 223, 243].

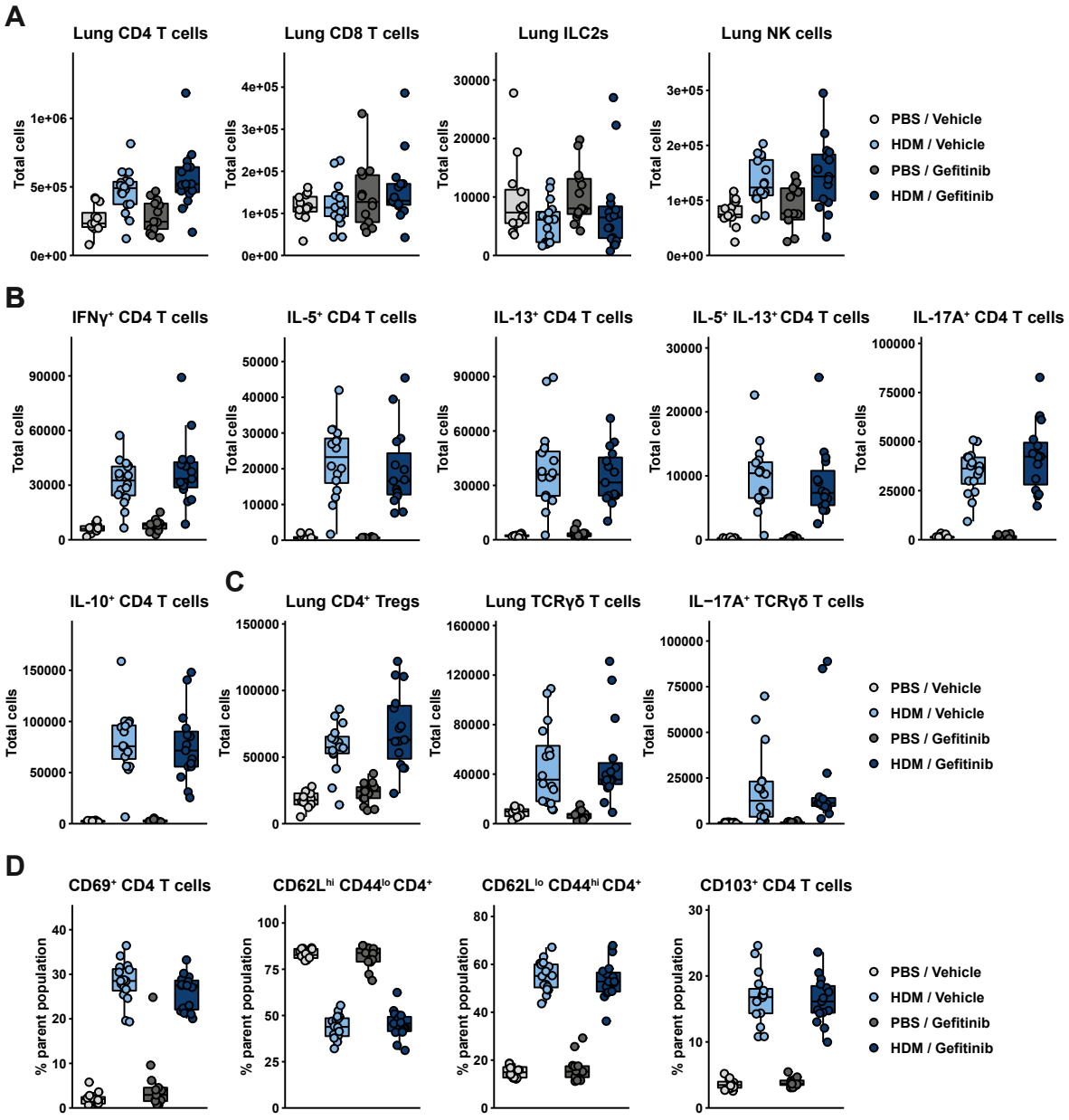


Figure 4.14 EGFR inhibition during early-life AAD did not alter T cell responses.
Animals were treated as described in Figure 4.12A. **(A)** Numbers of various lymphocyte populations in lung homogenates as measured by flow cytometry. **(B)** Intracellular cytokine staining of CD4 T cells after *ex vivo* restimulation with PMA and ionomycin in the presence of Brefeldin A. **(C)** Numbers of various lymphocyte populations and their cytokine production potential in lung homogenates as measured by flow cytometry. **(D)** Expression of activation markers on lung CD4 T cells by flow cytometry. (A-D) *n* = 12-16; data pooled from two independent experiments.

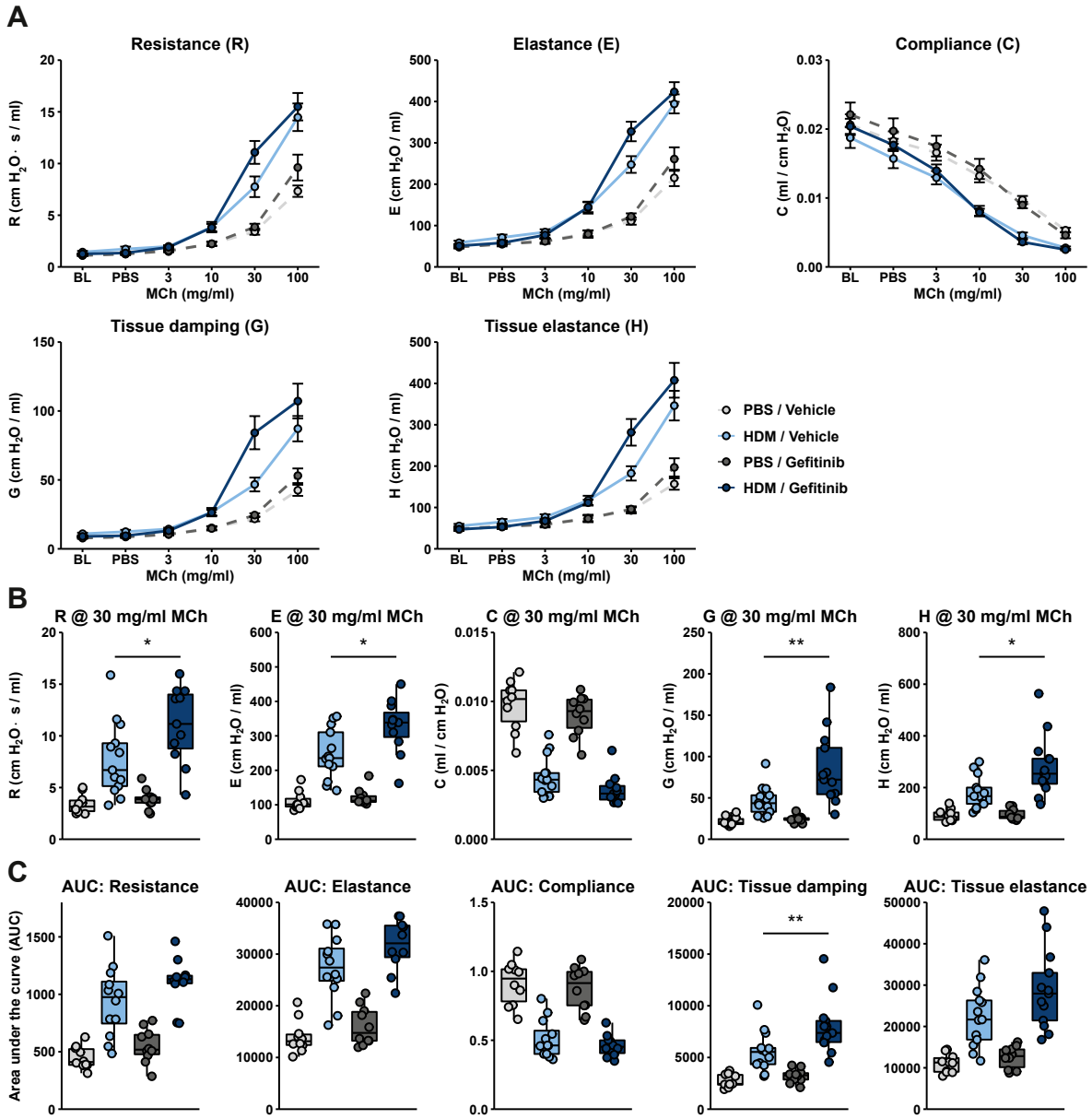


Figure 4.15 EGFR inhibition during early-life AAD led to worsened airway hyperresponsiveness. Animals were treated as described in Figure 4.12A. **A** Various lung function parameters in response to increasing doses of bronchoconstrictor methacholine (MCh). Data are shown as mean +/- standard error. **B** Lung function parameters at 30 mg/ml of MCh. **C** Area under the curve of lung function in response to increasing doses of MCh. (A-C) *n* = 9-14; measurements for some animals had to be excluded for not meeting quality control standards. Data are pooled from two independent experiments. Statistics: Mann-Whitney test between indicated groups. *, $p < 0.05$; **, $p < 0.01$.

4.3.4 EGFR inhibition during early-life AAD had no effect on airway remodelling or sensitisation

To investigate whether exacerbated airway hyperresponsiveness of Gefitinib-treated animals coincided with structural airway changes, several parameters of airway remodelling were measured. While HDM exposure led to the induction of several remodelling-related genes, such as *Tnc, Muc5ac*, *Muc5b* or *Mmp12*, in lung homogenates, there were no differences in pulmonary gene expression between Gefitinib- and vehicle-treated mice (**Figure 4.16A**).

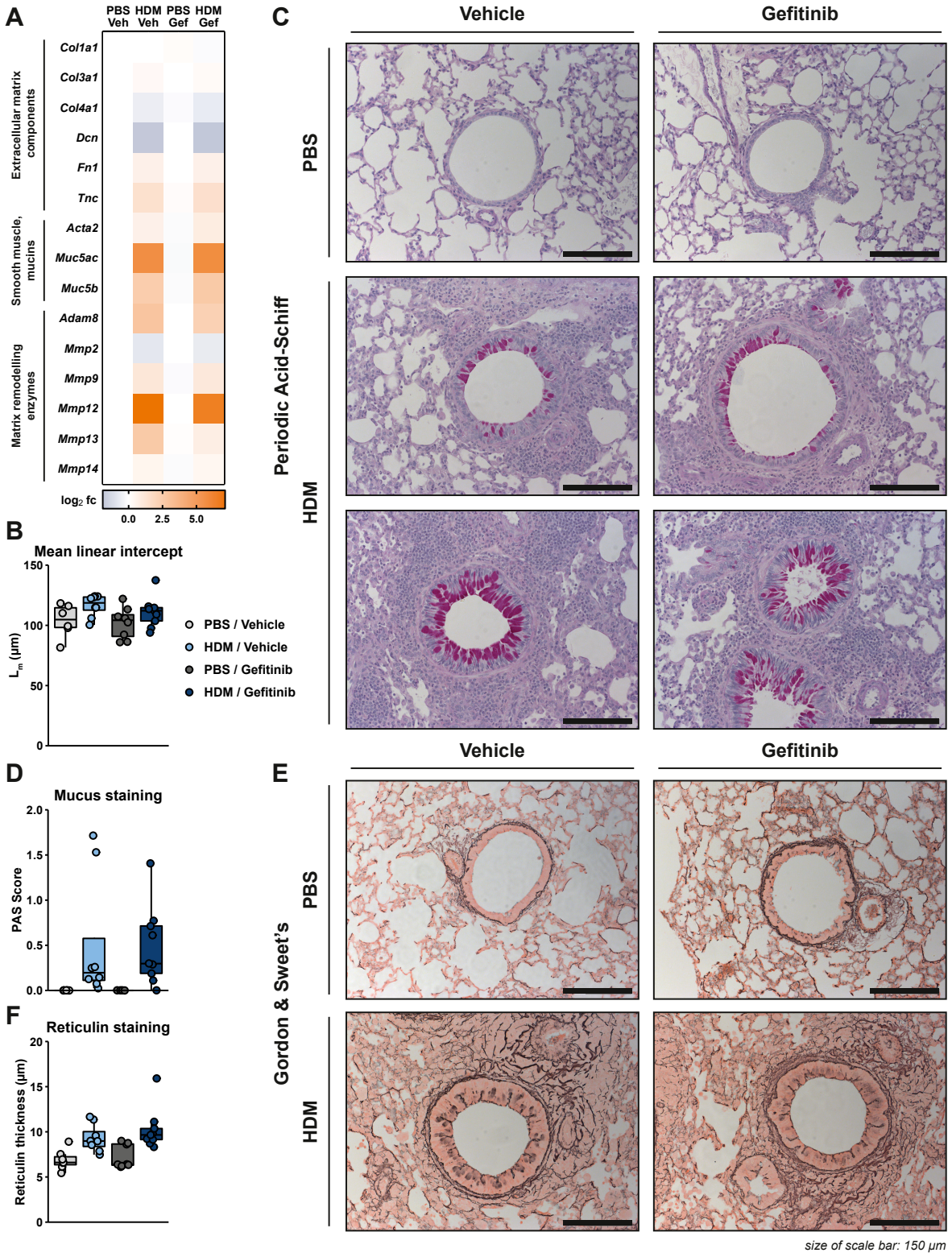


Figure 4.16 EGFR inhibition during early-life AAD had no effect on airway remodelling.
Animals were treated as described in Figure 4.12A. **A** Whole lung gene expression of indicated genes by qPCR, shown as log_2 fold change from PBS/Vehicle control. **B** Mean linear intercept (L_m) of alveoli, as measured in lung sections. **C-D** Representative images (C) and quantification (D) of airway mucus using Periodic Acid-Schiff (PAS) staining of lung sections. **E-F** Representative images (E) and quantification (F) of reticulin thickness around airways in Gordon & Sweet's silver-stained lung sections. (A) *n* = 12-16; data pooled from two independent experiments. (B-E) *n* = 7-9; data from one experiment.

Since measurement of mRNA levels often fails to reflect structural changes within the lungs, various histological approaches were used to study airway remodelling. Given the pronounced effects of EGFR inhibition on tissue damping (ref. Figure 4.15), the alveolar mean linear intercept (L_m) was determined as a measure of peripheral lung structure. While L_m was slightly elevated in HDM-exposed animals, there were no effects of Gefitinib treatment (**Figure 4.16B**). Similarly, mucus production was induced to different extents in the airways of HDM-treated mice (**Figure 4.16C**) but was independent of EGFR signalling (**Figure 4.16D**). Deposition of type III collagen, also known as reticulin, around the airways was increased upon allergen exposure regardless of EGFR inhibition (**Figure 4.16E-F**).

Immunofluorescent imaging was used to assess the quantity and distribution of smooth muscle α-actin, type I collagen and piezo-1, a mechanosensitive receptor previously implicated in the degradation of epithelial tight junctions during asthma[252], all of which were unaffected by EGFR inhibition (**Figure 4.17A**). Although the amount of collagen deposited around the airways and vessels appeared unchanged by Gefitinib treatment, collagen geometry may be controlled by EGFR signalling. To investigate this, two-photon microscopy-based second-harmonics generation (SHG) imaging of collagen fibres in lung sections was used (**Figure 4.17B**). This approach revealed that EGFR inhibition caused decreased uniformity and increased randomness of collagen fibres (**Figure 4.17C**), structural changes which may explain the worsened airway hyperresponsiveness observed in Gefitinib-treated mice. However, it is worth noting that these findings were not reproduced when SHG imaging was performed in a subset of animals from a second experimental repeat, indicating that these results should be interpreted with caution until they can be validated or rejected in a larger number of animals.

Finally, the in-depth characterisation of the effects of EGFR inhibition of early-life AAD was concluded by analysing type 2 inflammation and sensitisation. Overall, pulmonary expression levels of type 2 cytokines, alarmins, tissue repair genes and chemokines were comparable between Gefitinib- and vehicle-treated animals (**Figure 4.18A-B**). Nevertheless, reduced levels of the tissue repair-associated gene *Arg1* along with strongly increased levels of the alarmin *Il33* were found in lungs of HDM-exposed mice upon EGFR inhibition, while *Piezo1* was upregulated by Gefitinib treatment in PBS-treated animals (**Figure 4.18C**). These findings may reflect increased epithelial damage in the absence of appropriate repair responses. Despite strong increases in *Il33* gene expression, protein levels of IL-33 of HDM-exposed Gefitinib-treated mice were comparable to vehicle controls, as were the pulmonary levels of type 2 cytokines IL-4, IL-5 and IL-13 (**Figure 4.18D**). Of note, there were baseline differences in lung IL-5 and airway IL-13 upon EGFR inhibition (**Figure 4.18D-E**). Serum antibody levels

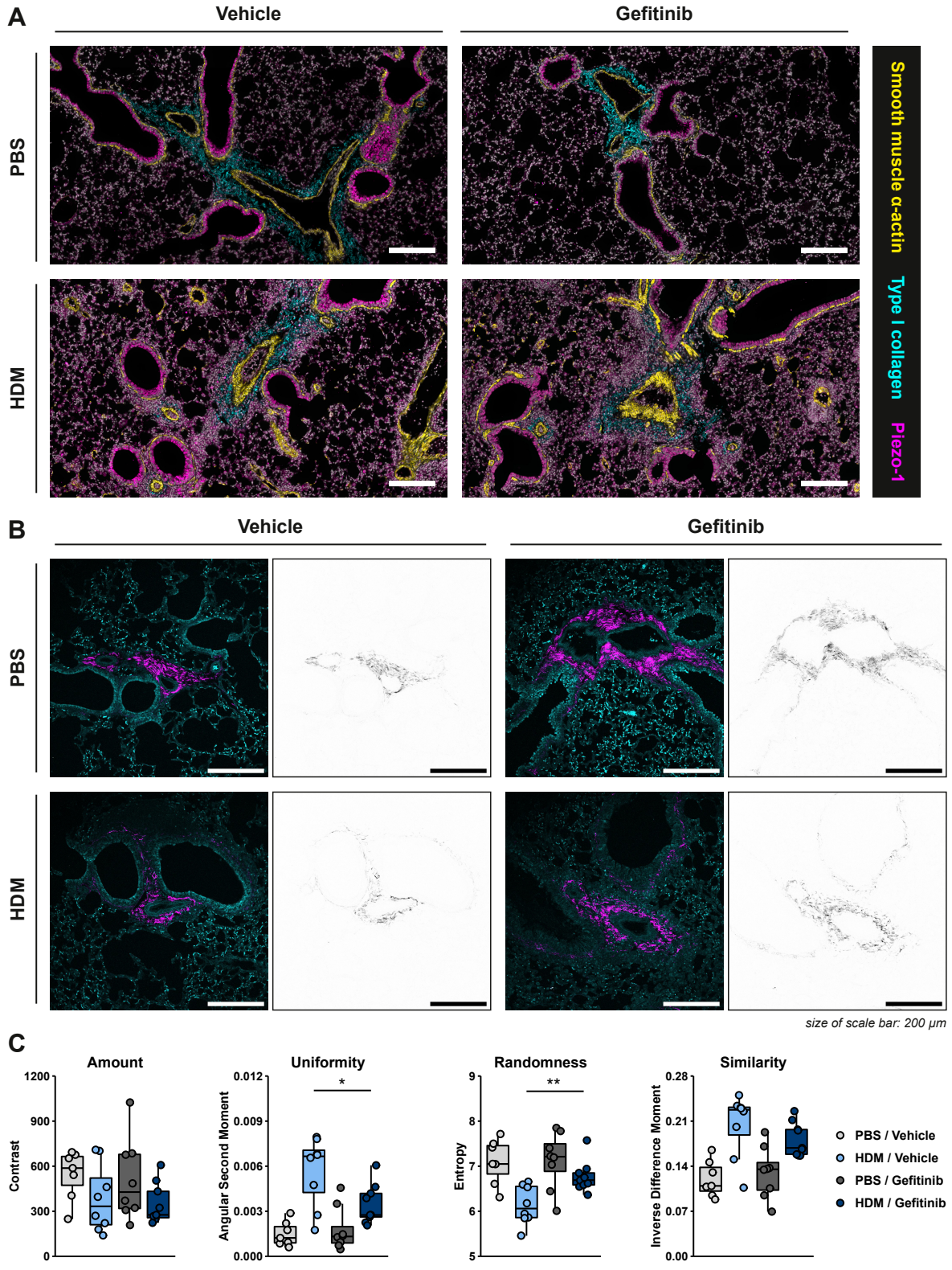


Figure 4.17 EGFR inhibition during early-life AAD did not alter matrix deposition but may change collagen geometry.
Animals were treated as described in Figure 4.12A. **A** Representative images of immunofluorescence staining for smooth muscle α-actin (yellow), type I collagen (cyan) and piezo-1 (magenta) in lung sections. **B** Representative images of second-harmonic generation (SHG) imaging of collagen fibres. Collagen is shown in magenta (left) or black (right). Tissue autofluorescence is shown in cyan. **C** Parameters of collagen geometry from SHG imaging. (A-C) n = 7-9; data from one experiment. Statistics: Mann-Whitney test between indicated groups. *, $p < 0.05$; **, $p < 0.01$.

were unaffected by Gefitinib treatment, suggesting that allergic sensitisation was independent of EGFR signalling (**Figure 4.18F**).

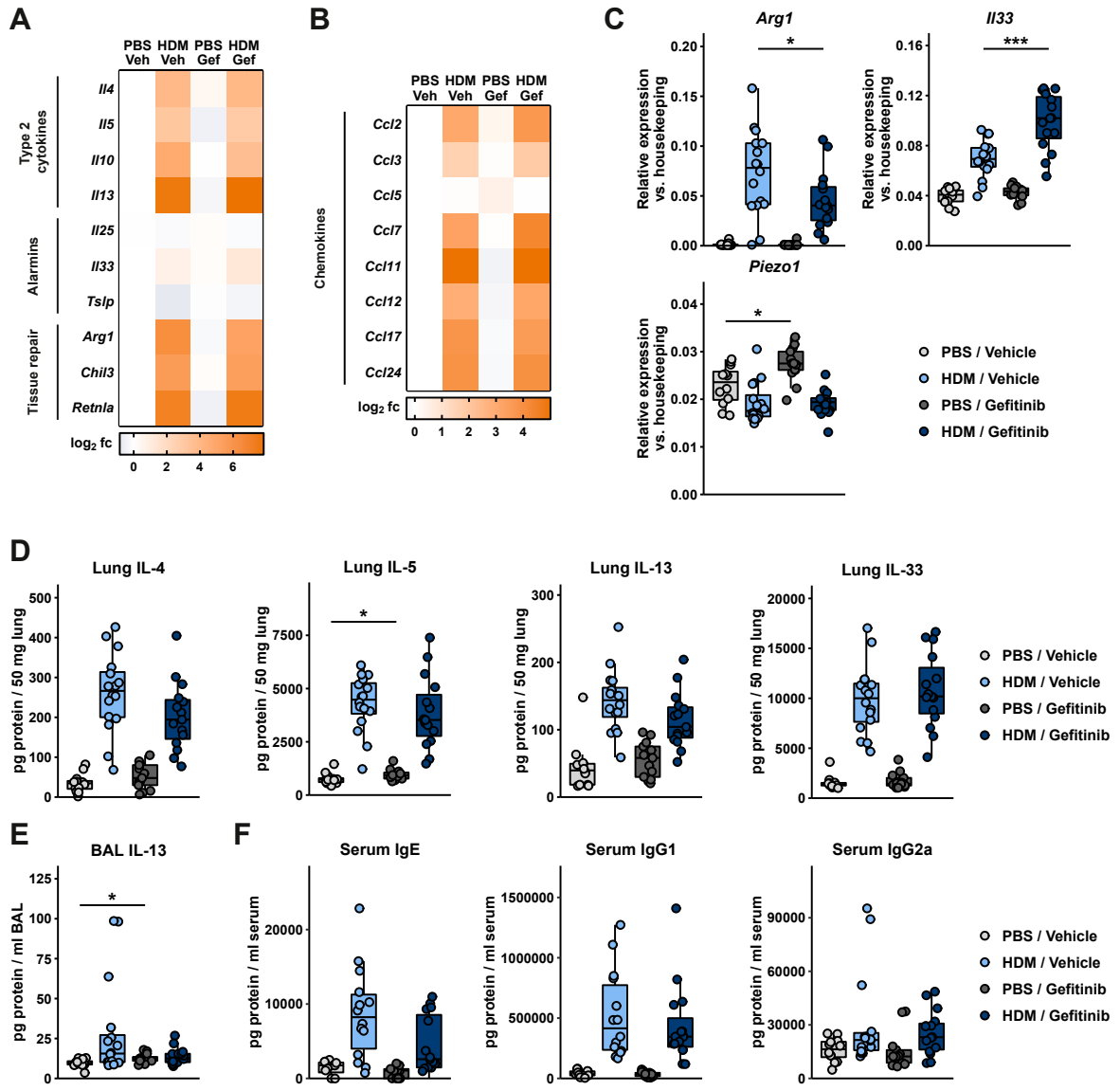


Figure 4.18 Type 2 responses were largely unaffected by EGFR inhibition during early-life AAD. Animals were treated as described in Figure 4.12A. **A-C** Whole lung gene expression of indicated genes by qPCR, shown as $\log_2$ fold change from PBS/Vehicle control (A-B) or as relative expression compared to housekeeping genes (C). **D-F** Levels of indicated proteins in lung homogenates (D), bronchoalveolar lavage (E) or serum (F) as measured by ELISA. (A-F) *n* = 12-16; data pooled from two independent experiments. Statistics: Mann-Whitney test between indicated groups. *, $p < 0.05$; ***, $p < 0.001$.

4.3.5 Integrative data analysis of EGFR inhibition during early-life AAD

Thus far, several parameters which were altered upon EGFR inhibition were identified, namely monocytic inflammation, airway hyperresponsiveness, pulmonary *Arg1* and *Il33* gene expression as well as EGFR ligand levels in lungs and airways. However, it is unclear whether these parameters are interconnected or independent of each other. In particular, it was

interesting to investigate whether potential pathways underlying the worsened lung function could be identified. To this end, correlation coefficients and associated *p*-values between all continuous parameters measured in this model were calculated and plotted as a correlation matrix (**Figure 4.19**). To focus on the effects of Gefitinib rather than allergen treatment, the analysis was restricted to HDM-exposed animals. Correlations were strongest between parameters generated by the same method, for example between cells measured by the same flow cytometry panel within the same organ or between lung function measurements. By this method, it was possible to confirm some expected correlations, such as between lung function parameters and serum IgE levels or pulmonary *Il13* expression. Of note, levels of EGFR

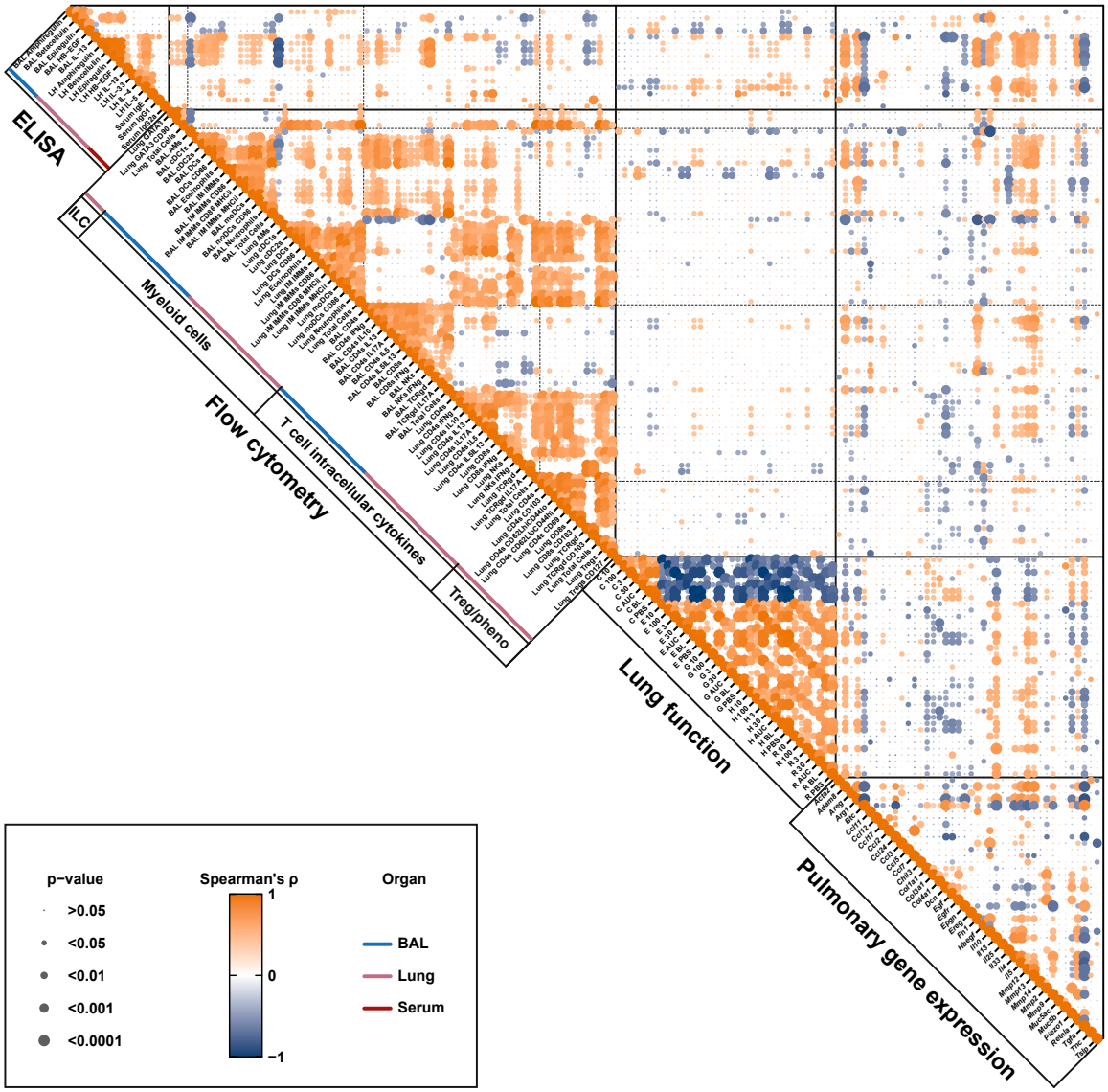


Figure 4.19 Correlation matrix of various parameters after EGFR inhibition during early-life AAD. Animals were treated as described in Figure 4.12A. Only HDM-treated animals were included in this analysis. Spearman correlations between individual parameters are shown as correlation matrix, where the size of the circle represents the p-value and the colour depicts the strength and direction of the correlation (correlation coefficient, Spearman's ρ).

ligands were strongly correlated, suggesting that their expression is controlled by shared mechanisms. Unfortunately, this analysis did not provide novel insights into the pathways underlying worsened lung function or reduced monocyte recruitment or survival upon EGFR inhibition during early-life AAD.

The analysis approach was altered to investigate whether shared 'master regulators' between parameters significantly affected by Gefitinib treatment could be identified. To this end, these parameters were stratified into four clusters and shared correlations ($p < 0.05$ and $|\rho| > 0.5$) between clusters were compared (**Figure 4.20A**). Interestingly, there was little overlap

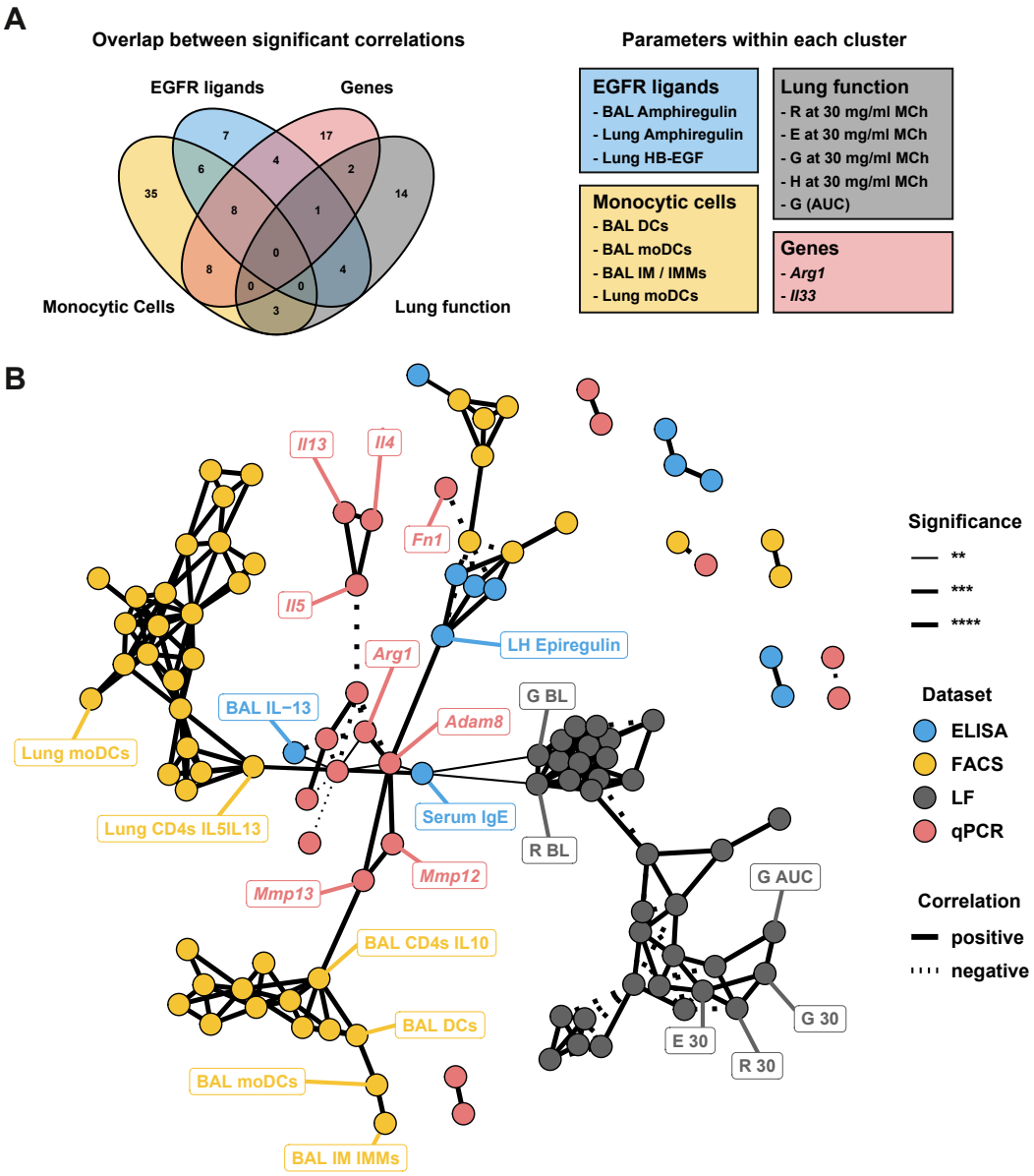


Figure 4.20 Network analysis of various parameters after EGFR inhibition during early-life AAD. Animals were treated as described in Figure 4.12A. Only HDM-treated animals were included in this analysis. **A** Parameters significantly affected by EGFR inhibition were stratified into four clusters. Significant correlations ($p < 0.05$ and $|\rho| \geq 0.5$) shared between clusters are shown as a Venn diagram. **B** Network analysis showing most significant correlations ($p < 0.05$ and $|\rho| > 0.75$; edges) between parameters (nodes).

between clusters, suggesting that the changes observed upon EGFR inhibition were driven by distinct mechanisms. To further validate this finding, the most significant correlations ($p < 0.05$ and $|\rho| > 0.75$) between parameters were plotted as a network map (**Figure 4.20B**). This visualisation further confirmed that the strongest associations were found within rather than between data sets, as previously shown by the correlation matrix. Parameters significantly affected by EGFR inhibition, such as lung function at 30 mg/ml MCh or numbers of airway moDCs and IM/IMMs were found on opposite ends of the network map, once more rescinding the notion that these variables may share a common 'master regulator'. Collectively, EGFR signalling controlled several distinct features of early-life AAD, including airway hyperresponsiveness, cellularity and pulmonary gene expression, yet these changes appear to be independent of each other.

4.3.6 Exogenous activation of EGFR signalling during early-life AAD

To further characterise the role of EGFR signalling during established early-life AAD, experiments were conceived to investigate whether exogenous receptor activation would result in opposite effects on disease pathology as receptor inhibition. To this end, recombinant AREG was given to neonatal mice during the last three of five weeks of allergen exposure (**Figure 4.21A**). This intervention did not result in any changes in overall cell recruitment to the lungs or airways (**Figure 4.21B**), nor in the numbers of common myeloid cell populations (**Figure 4.21C**). Unlike EGFR inhibition, which led to reductions in (mo)DCs and IM/IMMs in the airways (ref. Figure 4.13), AREG administration did not alter the total numbers of these cell types (**Figure 4.21D**). However, there was a significant increase in the frequency of BAL IM/IMMs within immune cells upon AREG treatment of HDM-exposed mice (**Figure 4.21E**). Together with previous findings from the EGFR inhibition model, this suggests that EGFR signalling contributes to the recruitment, migration or survival of these cells during AAD. The abundance and cytokine production potential of CD4 T cells in the lungs were unaffected by AREG administration (**Figure 4.21F**), once more suggesting that EGFR signalling was dispensable for the T helper cell response.

Another major outcome of EGFR inhibition during early-life AAD was exacerbated airway hyperresponsiveness, particularly at 30 mg/ml of MCh. However, when lung function was measured after AREG administration, there were no effects of exogenous receptor activation (**Figure 4.22A-B**). While the findings using EGFR inhibition support a protective role of EGFR signalling in preventing worse lung function during early-life AAD, these results illustrate that presence of EGFR ligand alone in the airways was unable to ameliorate airway hyperresponsiveness, suggesting that the contribution of EGFR signalling to lung function during early-life AAD is complex.

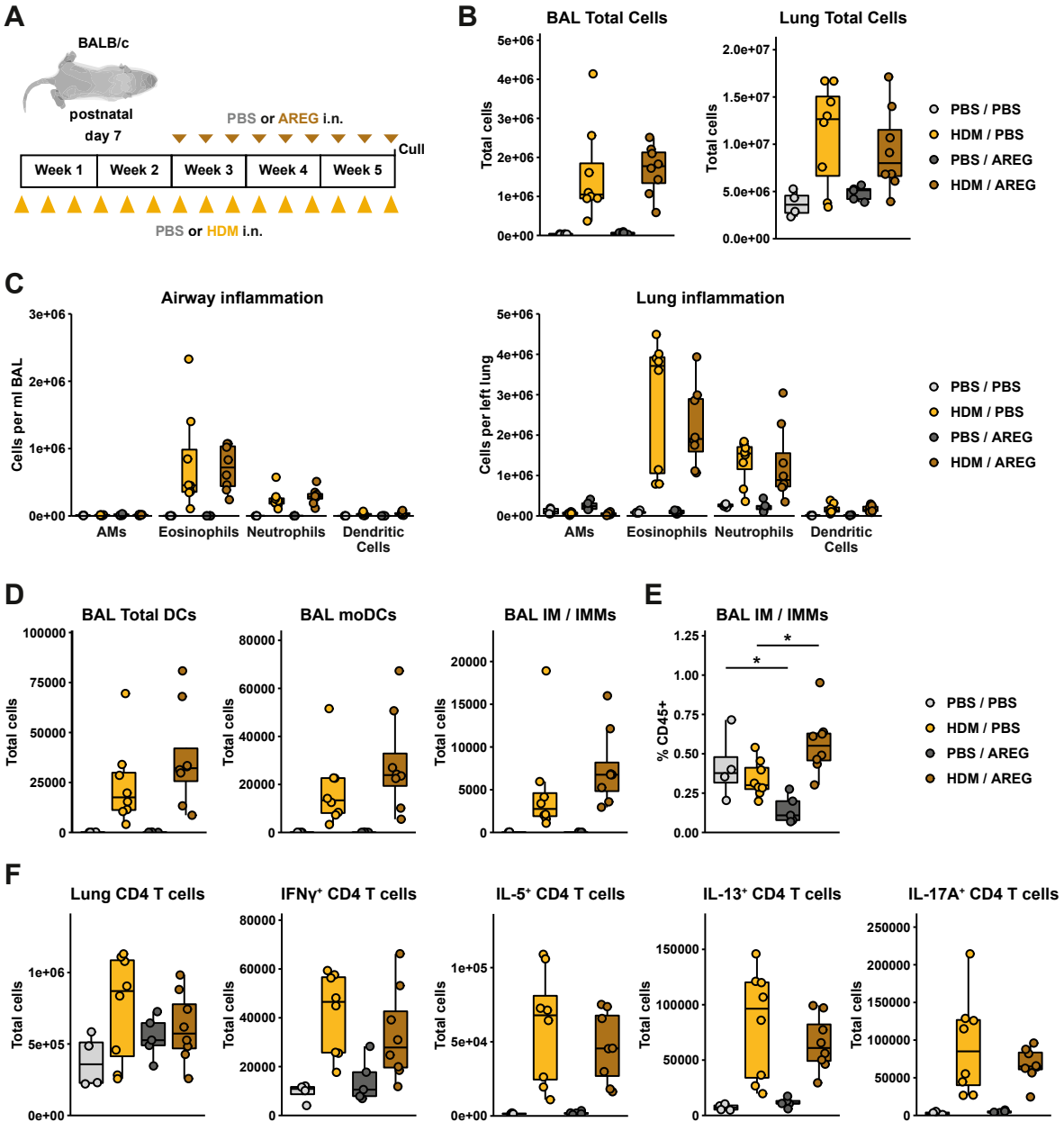


Figure 4.21 Exogenous EGFR activation during early-life AAD altered airway monocytic cells.
A Schematic depicting experimental approach. 7-day-old BALB/c mice were given inhaled HDM (10 µg in week 1, 15 µg thereafter) three times per week for five weeks. During weeks three to five, mice were intranasally administered recombinant AREG (0.75 µg) approx. 4-6 hours after allergen challenge and animals were sacrificed on the day following the last dose. **B** Total cells in bronchoalveolar lavage or the left lung lobe. **C** Numbers of airway macrophages (AMs), eosinophils, neutrophils and dendritic cells in bronchoalveolar lavage or the left lung lobe, as measured by flow cytometry. **D** Numbers of dendritic and monocytic cell populations in bronchoalveolar lavage by flow cytometry. **E** Frequency of IM/IMMs as percentage of all immune cells in the airways. Abbreviations: DCs, dendritic cells; moDCs, monocyte-derived DCs; IM / IMMs, interstitial macrophages/inflammatory monocytes and macrophages. **F** Numbers of lung CD4 T cells and their potential to produce cytokines after stimulation with PMA and ionomycin in the presence of Brefeldin A as measured by flow cytometry. (B-F) *n* = 4-9; data from one experiment.

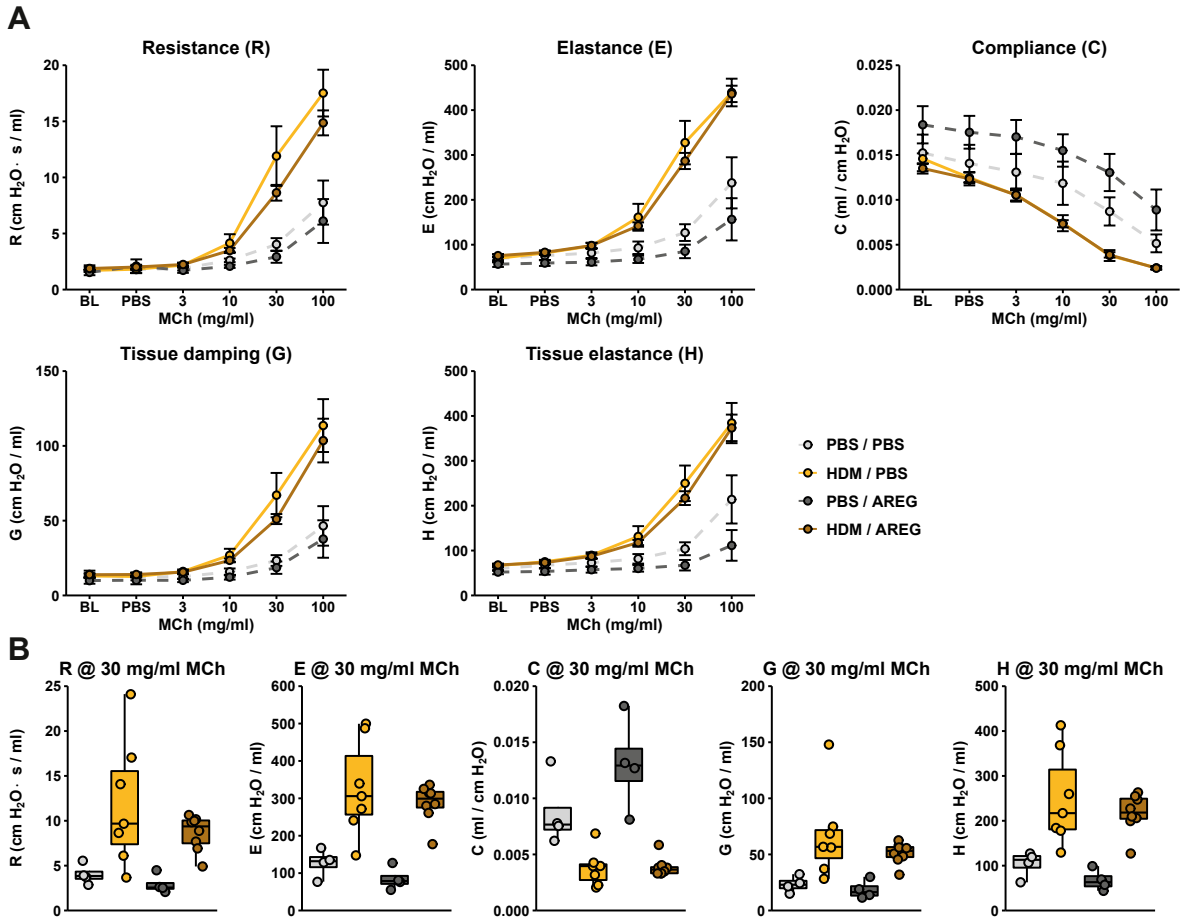


Figure 4.22 Exogenous EGFR activation during early-life AAD did not affect lung function.
Animals were treated as described in Figure 4.21A. **A** Various lung function parameters in response to increasing doses of bronchoconstrictor methacholine (MCh). Data are shown as mean +/- standard error. **B** Lung function parameters at 30 mg/ml of MCh. (A-B) *n* = 3-8; measurements for some animals had to be excluded for not meeting quality control standards. Data are from one experiment.

4.3.7 Establishing a novel model of early-life AAD using mixed allergens

Thus far, the role of EGFR signalling was studied in the HDM model of AAD. However, allergic asthma, especially when severe, is also commonly caused by other allergens, such as pollens, moulds, cockroach or pet dander[15, 253], which differ, amongst others, in their protease activity and ability to trigger epithelial alarmin release[254]. In an effort to establish a more clinically affiliated model encompassing several different seasonal and perennial allergens for the study of AAD, neonatal BALB/c mice were repeatedly exposed to a mixture (MIX) of ALT, HDM and TG (**Figure 4.23A**). Treatment with each of these allergens alone was included to aid in the characterisation of this novel mixed allergen model. Exposure to MIX resulted in significant cellular recruitment to the airways, including increased numbers of airway macrophages, eosinophils, neutrophils and dendritic cells (**Figure 4.23B**).

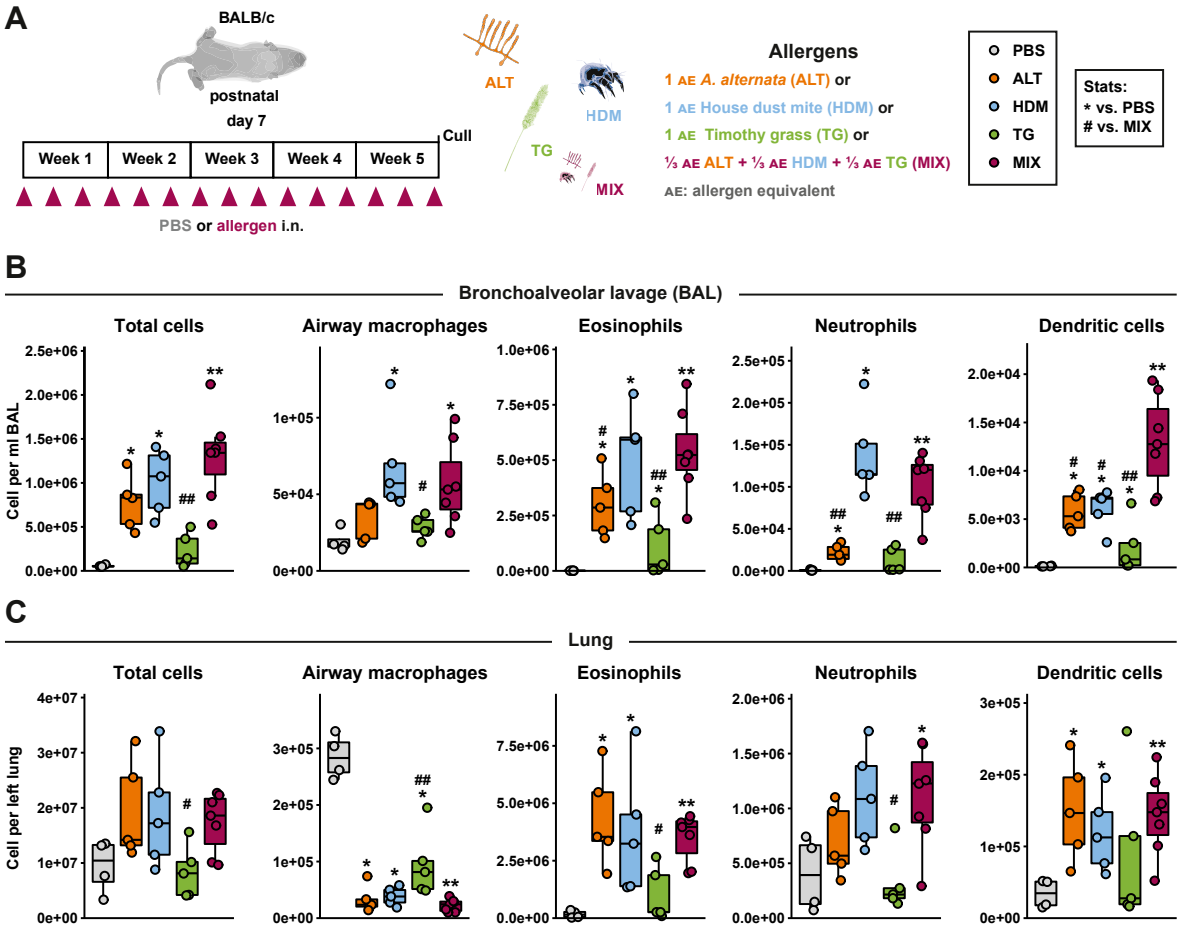


Figure 4.23 Chronic exposure to mixed allergen during early life drives myeloid inflammation in lungs and airways.
A Schematic depicting experimental approach. 7-day-old BALB/c mice were given inhaled ALT (1 allergen equivalent: 5 µg in week 1, 10 µg thereafter), HDM (1 allergen equivalent: 10 µg in week 1, 15 µg thereafter), timothy grass (TG; 1 allergen equivalent: 4.5 µg in week 1, 9 µg thereafter) or a mix of all three allergens (MIX; ⅓ allergen equivalent each) three times per week for five weeks. Animals were sacrificed on the day following the last allergen dose. **B-C** Total cells and numbers of airway macrophages (AMs), eosinophils, neutrophils and dendritic cells in bronchoalveolar lavage (B) or the left lung lobe (C), as measured by flow cytometry. (B-C) n = 4-7, data from one experiment. Statistics: Mann-Whitney test between indicated groups and PBS (*) or MIX (#) group. */#, $p < 0.05$; **/##, $p < 0.01$.

Overall, the magnitude of airway inflammation after mixed allergen exposure was comparable to mono-allergen challenge e.g., with ALT or HDM. However, there was a particularly high abundance of airway dendritic cells in MIX-treated animals, suggesting that the combination of different allergens strongly drove antigen-presenting cell responses. Of note, cell recruitment was lowest in mice exposed to TG, indicating that this allergen may drive less severe AAD pathology. Myeloid inflammation was also present in the lungs and followed similar trends as in the airways (**Figure 4.23C**).

In addition to its capacity to drive myeloid inflammation, the ability of mixed allergen exposure to evoke T cell responses was evaluated. All allergens elicited recruitments of T lymphocytes to the airways, with the strongest effects observed after exposure to mixed allergen (**Figure 4.24A**). Chronic inhalation of ALT or MIX further led to a significant expansion in

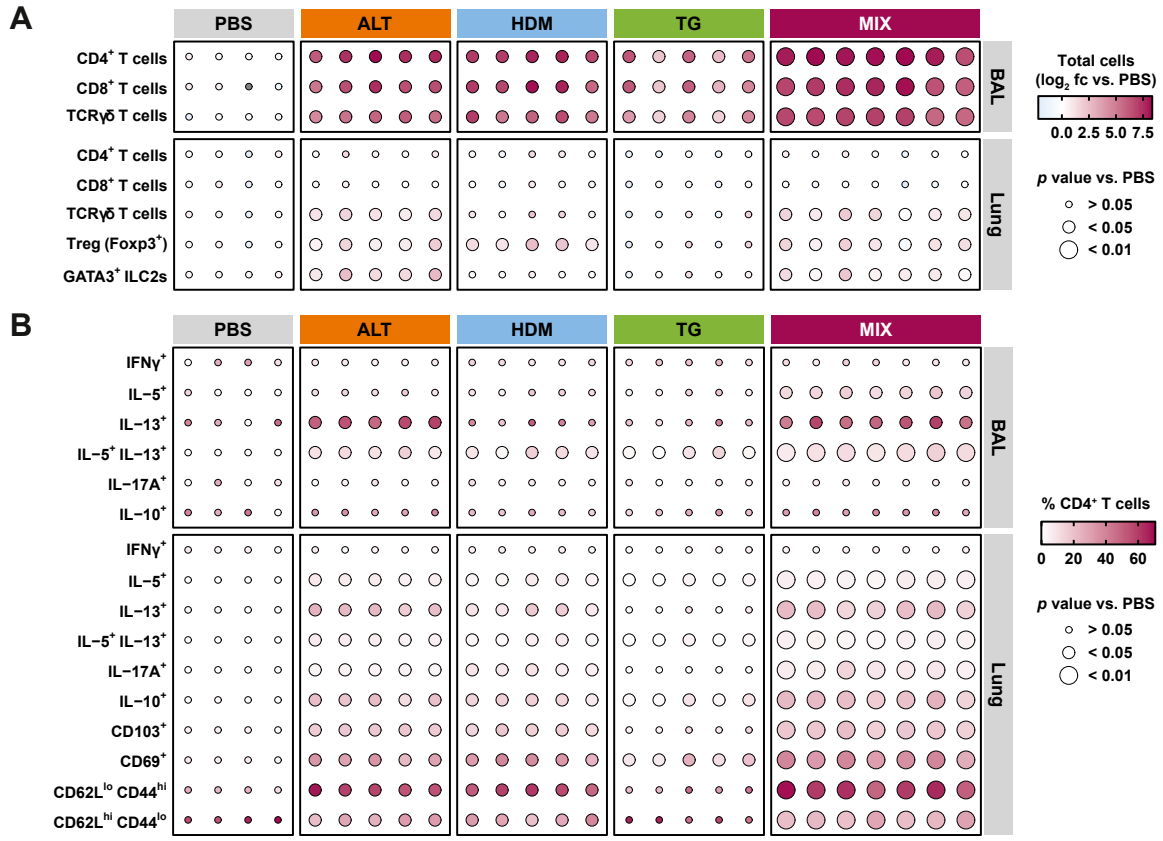


Figure 4.24 Early-life mixed allergen exposure evoked extensive pulmonary T cell responses. Animals were treated as described in Figure 4.23A. **A** T cell populations in bronchoalveolar lavage (BAL) and left lung lobes upon exposure to indicated allergens by flow cytometry. Colour intensity represents increase in total numbers from PBS controls and size of circle denotes significance level when compared to PBS control. **B** Cytokine production potential and phenotype of CD4 T cells in BAL and lungs. Colour intensity represents frequency of cytokine/marker expression of CD4 T cells and size of circle denotes significance level when compared to PBS control. Intracellular cytokine levels were measured after *ex vivo* restimulation with PMA and ionomycin in the presence of Brefeldin A. (A-B) *n* = 4-7; data from one experiment. Statistics: Mann-Whitney test between indicated allergen and PBS group.

ILC2s, γδ T cells and Foxp3$^+$ Tregs in the lungs, the latter of which were also increased in HDM-treated animals. In the airways, frequencies of Th2 cells, particularly IL-5$^+$IL-13$^+$ double-positive CD4 T cells, were increased in all allergen-treated groups (**Figure 4.24B**). Additionally, increases in IL-10- and IL-17A- but not IFNγ-producing helper T cells were observed in the lungs upon allergen exposure, as well as augmented expression of activation, tissue residency and memory-like markers on these cells. Overall, T cell responses were strongest in MIX-treated animals, suggesting that exposure to mixed allergens was superior to mono-allergen challenge in its ability to cause pulmonary inflammation.

In addition to inflammation, a relevant model of AAD should induce airway hyperresponsiveness. With the exception of TG, all allergens tested here caused exacerbated lung function (**Figure 4.25A**), of which the deficits elicited by mixed allergen exposure were the most severe (**Figure 4.25B**). It was thus possible to confirm that the model of mixed allergen challenge recapitulated two hallmark features of AAD, airway hyperresponsiveness and inflammation.

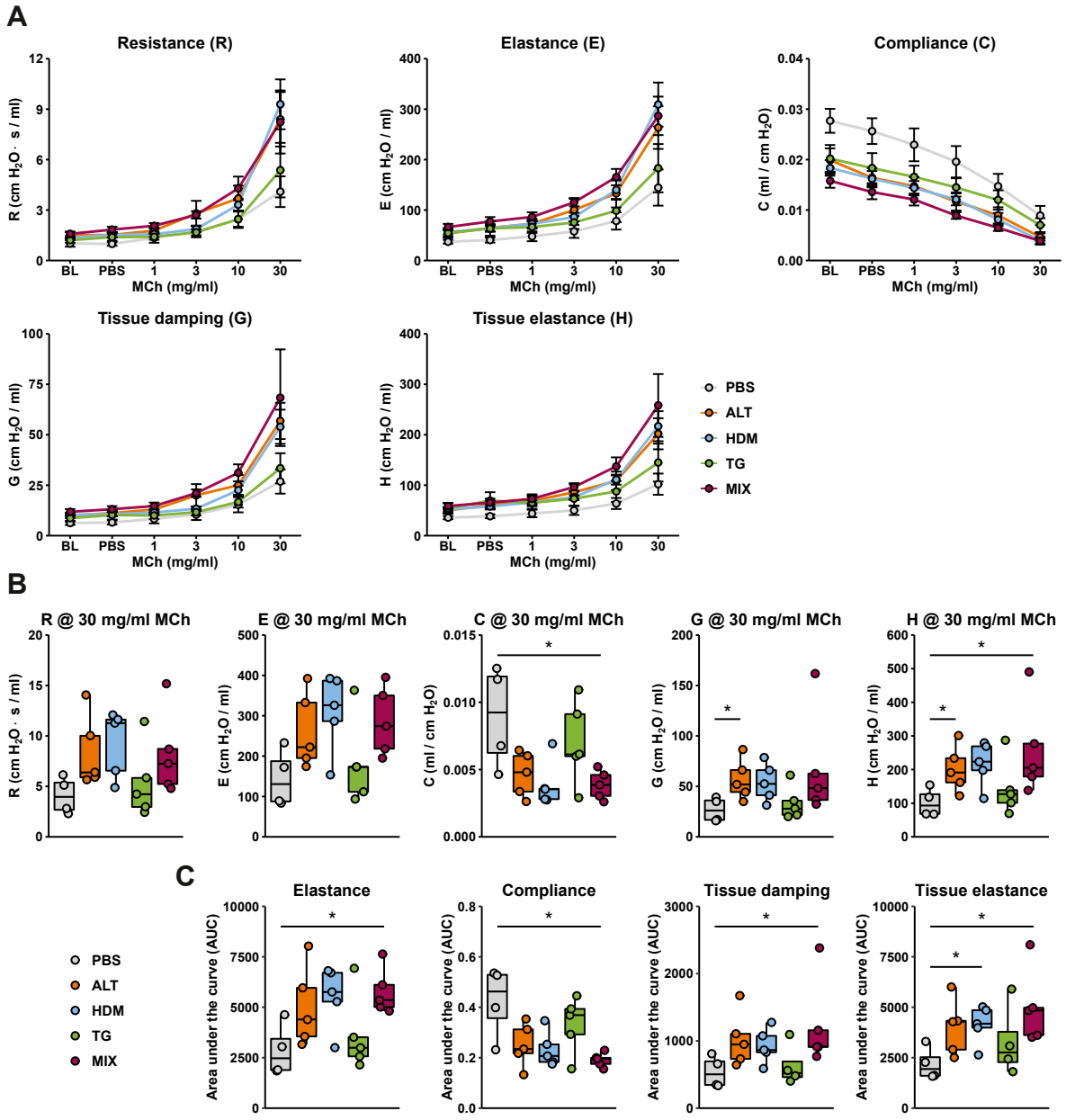


Figure 4.25 Early-life mixed allergen exposure resulted in airway hyperresponsiveness.
Animals were treated as described in Figure 4.23A. **A** Various lung function parameters in response to increasing doses of bronchoconstrictor methacholine (MCh). Data are shown as mean +/- standard error. **B** Lung function parameters at 30 mg/ml of MCh. **C** Area under the curve of lung function in response to increasing doses of MCh. (A-C) *n* = 4-5; data from one experiment.

To round off the characterisation of this novel AAD model, gene expression analysis of lung homogenates was employed to gain insight into overall inflammation and expression of remodelling-related genes in the lungs. In line with the flow cytometry data, there was a significant induction of genes encoding Th2 and Th17 cytokines as well as eosinophil chemokines in the lungs of allergen-exposed animals (**Figure 4.26A**). In addition, expression of the remodelling-associated genes *Col4a1*, *Fn1* and *Muc5ac* was altered when mice were challenged with allergen (**Figure 4.26B**), suggesting the presence of airway remodelling. In line with this, there was evidence of mucus hyperplasia in animals from all allergen-treated

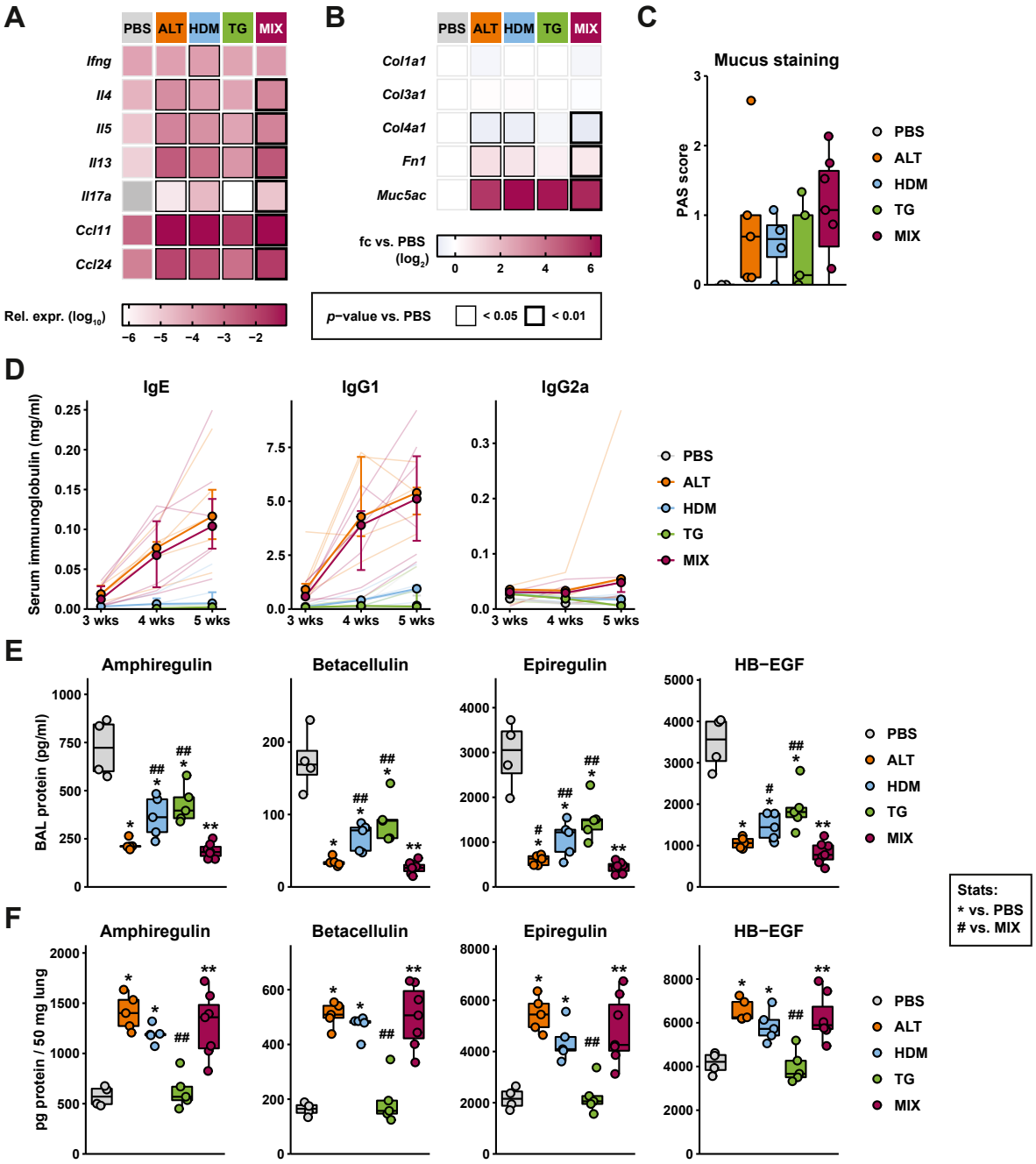


Figure 4.26 Early-life mixed allergen exposure elicited mucus hyperplasia and sensitisation. Animals were treated as described in Figure 4.23A. **A-B** Whole lung gene expression of indicated genes, represented as relative expression compared to housekeeping genes (A) or foldchange from PBS control (B). Black outlines signify statistically significant changes compared to PBS control (Mann-Whitney test). **C** Quantification of airway mucus using Periodic Acid-Schiff (PAS) staining of lung sections. **D** Serum levels of total antibodies by ELISA over time. Thick lines denote median and IQR. Thin lines show antibody levels of individual mice. **E-F** Levels of EGFR ligands in bronchoalveolar lavage (E) and lung homogenates (F). (A-F) n = 4-7, data from one experiment. Statistics: Mann-Whitney test between indicated groups and PBS (*) or MIX (#) group. */#, $p < 0.05$; **/##, $p < 0.01$.

groups (**Figure 4.26C**). Interestingly, serum antibody levels were highest after exposure to ALT or MIX (**Figure 4.26D**), suggesting that the fungal allergen ALT is a superior driver of allergic sensitisation. Nonetheless, modest increases in total IgE and IgG1 levels were also observed after five weeks of HDM or TG challenge. Overall, these findings illustrate that the

newly established model of mixed allergen exposure encompasses hallmark features of AAD, namely inflammation, airway hyperresponsiveness, remodelling and sensitisation, to a greater extent than models using one allergen alone. This model will be valuable in the study of mechanisms underlying AAD pathology, such as the role of EGFR signalling.

Finally, the effects of mixed allergen exposure on EGFR ligand availability in the lungs and airways was characterised. As previously observed for ALT and HDM, treatment with TG or MIX resulted in significant depletion of airway ligand levels (**Figure 4.26E**) and these effects were most pronounced after challenge with ALT or MIX. Interestingly, only TG exposure did not result in significant increases in ligand levels in the lungs (**Figure 4.26F**). Together with previous results, this may reflect a lesser ability of TG to induce features of AAD compared to the other allergens tested here.

4.3.8 Exogenous EGFR activation in mixed allergen model of early-life AAD

Previous experiments attempted the study of the effects of exogenous EGFR activation during early-life AAD by intranasal administration of AREG during the last three of five weeks of an HDM exposure model. However, this intervention did not lead to appreciable changes in AAD pathology. The experimental approach was therefore modified by including the following alterations (**Figure 4.27A**): To increase the window for disease improvement, the mixed allergen rather than the HDM model of AAD was chosen, as this caused more severe pathology. In addition, the period of allergen exposure was restricted to three weeks to allow administration of EGFR ligand throughout the entire challenge period, rather than just during established disease. Finally, the high-affinity ligand HB-EGF rather than the low-affinity ligand AREG was administered in this model with the intention of maximising EGFR signalling. While overall cell recruitment to the lungs and airways was unaffected by HB-EGF treatment (**Figure 4.27B**), there were significantly increased lung neutrophils upon ligand administration (**Figure 4.27C**). In agreement with this, elevated frequencies of CD4 T cells expressing IL-17A$^+$, but not any other effector cytokines, were present in the lungs of HB-EGF-treated animals (**Figure 4.27D-F**). Given the ability of IL-17A to drive neutrophil responses, it is likely that the observed increases in lung neutrophilia are the direct result of augmented Th17 responses. In line with this, there was an expansion of lung γδ T cells (**Figure 4.27G**), another cell population capable of producing IL-17A and thus driving neutrophilic responses. Interestingly, recruitment of monocyte-derived cells such as moDCs and IM/IMMs to the airways was unaffected by HB-EGF treatment, indicating that although EGFR signalling likely contributes to the accumulation of these cells in the airways, exogenous EGFR activation via inhaled HB-EGF was insufficient to further increase moDCs or IM/IMM numbers.

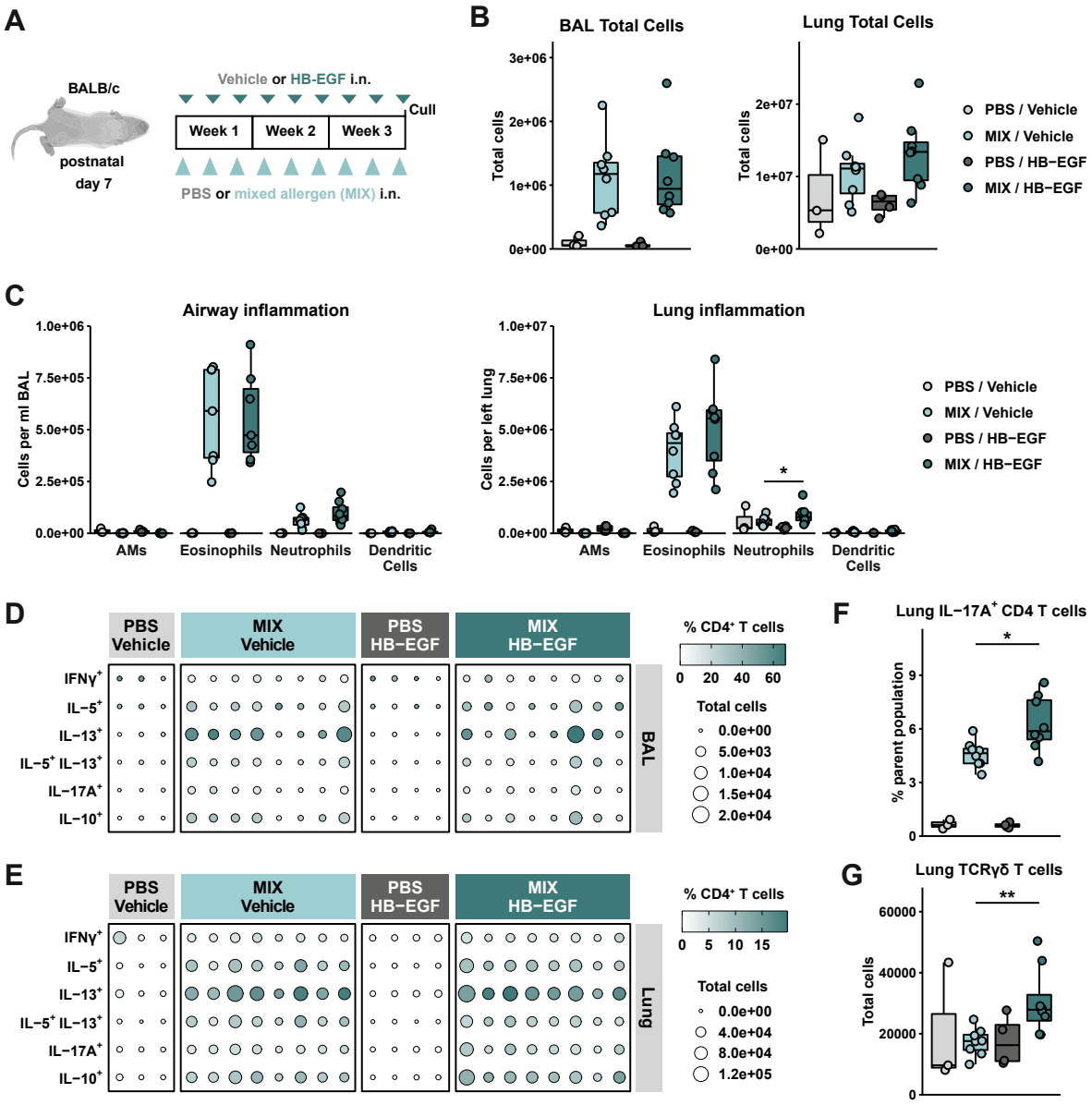


Figure 4.27 Exogenous HB-EGF administration during mixed allergen challenge resulted in exacerbated neutrophilia and Th17 responses.
A Schematic depicting experimental approach. 7-day-old BALB/c mice were given inhaled mixed allergen (ref. **Figure 4.24**) three times per week for three weeks. During the entire duration, mice were intranasally administered HB-EGF (0.5 µg in week 1, 0.75 µg thereafter) approx. 4-6 hours after allergen challenge and animals were sacrificed on the day following the last dose. **B** Total cells in bronchoalveolar lavage or the left lung lobe. **C** Numbers of airway macrophages (AMs), eosinophils, neutrophils and dendritic cells in bronchoalveolar lavage or the left lung lobe, as measured by flow cytometry. **D-F** Cytokine production potential of CD4 T cells in bronchoalveolar lavage (D) and lung homogenates (E-F) after stimulation with PMA and ionomycin in the presence of Brefeldin A, as measured in left lung lobes by flow cytometry. (D-E) Colour denoted frequency of CD4 T cells expressing indicated cytokines, whereas size of circle represents total numbers. **(G)** Total numbers of γδ T cells in left lung lobes by flow cytometry. (B-G) *n* = 3-8; data from one experiment. Statistics: Mann-Whitney test between indicated groups. *, $p < 0.05$; **, $p < 0.01$.

Finally, induction of airway hyperresponsiveness upon mixed allergen treatment was unaffected by the administration of HB-EGF (**Figure 4.28A-B**). Together with corresponding results upon AREG treatment during the HDM model of AAD, these observations further suggest that EGFR activation alone does not protect from exacerbated lung function during chronic allergen challenge. Overall, these experiments using a different approach confirmed

that the administration of EGFR ligands did not alter the gross pathology of AAD. Nevertheless, there were increases in lung Th17 and γδ T cells as well as neutrophils after treatment with HB-EGF, but not AREG, suggesting that the former ligand may directly control pulmonary type-17 responses.

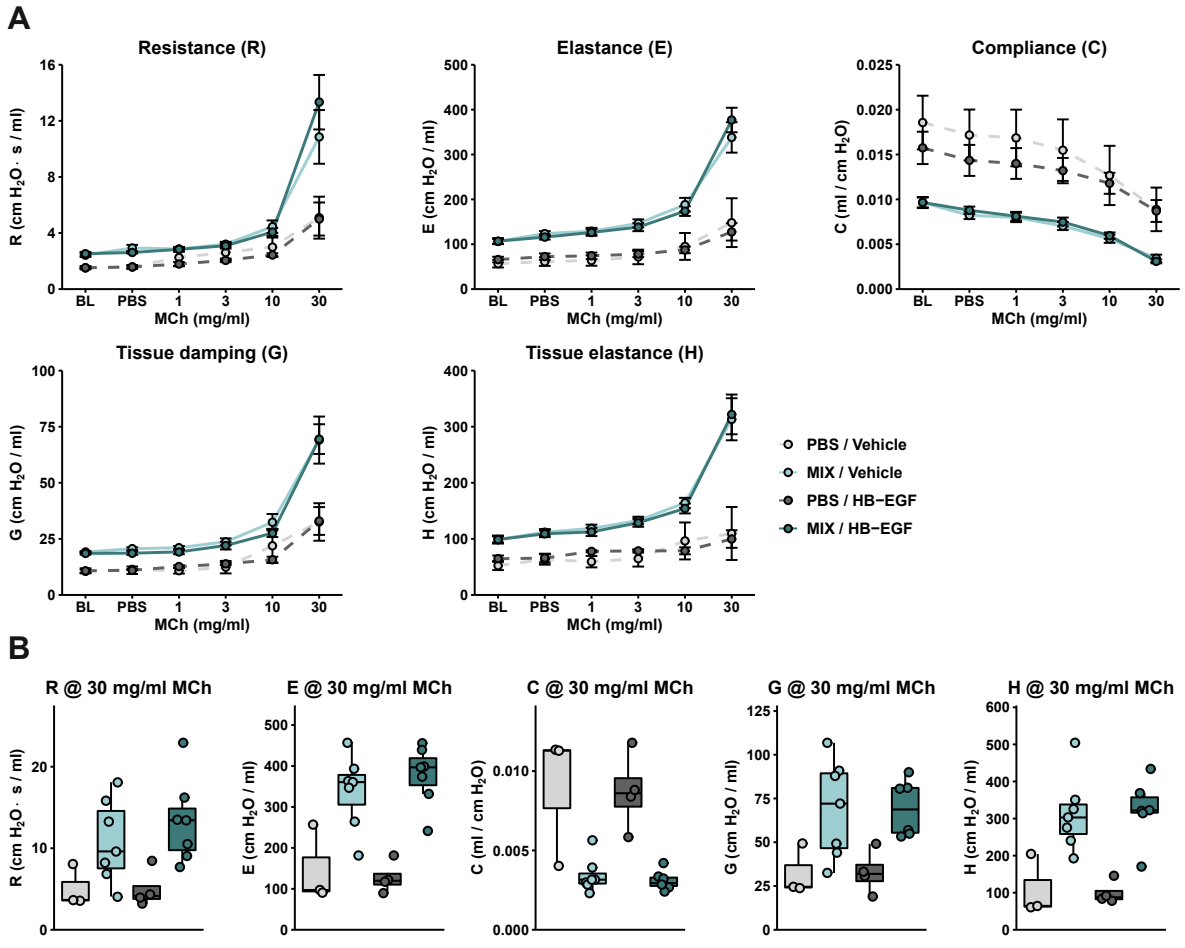


Figure 4.28 Exogenous HB-EGF administration during mixed allergen challenge did not affect airway hyperresponsiveness.
Animals were treated as described in Figure 4.27A. **A** Various lung function parameters in response to increasing doses of bronchoconstrictor methacholine (MCh). Data are shown as mean +/- standard error. **B** Lung function parameters at 30 mg/ml of MCh. (A-B) *n* = 2-8, measurements for some animals had to be excluded for not meeting quality control standards. Data are from one experiment.

4.4 Discussion

This chapter employed EGFR inhibition and activation in various models of adult and neonatal AAD to elucidate the contribution of EGFR signalling to disease pathology and identified distinct roles for EGFR in early life. Inhibition of EGFR signalling in a neonatal model of AAD resulted in exacerbated airway hyperresponsiveness, as well as changes in pulmonary gene expression, the levels of EGFR ligands and recruitment of monocyte-derived cells to the airways. In contrast, disease pathology during adult AAD was unaffected by EGFR inhibition. Interestingly, however, treatment with the EGFR inhibitor Gefitinib led to worsened lung function in adult mice in the absence of HDM exposure. Finally, exogenous receptor activation using the EGFR ligands AREG or HB-EGF had little to no effect on AAD pathology, neither in early life nor in adulthood.

Numerous studies have used EGFR inhibition to study the role of EGFR signalling in adult mouse models of AAD[136, 165-170, 242]. Overwhelmingly, these studies have identified EGFR as a driver of AAD pathology, particularly airway hyperresponsiveness and goblet cell hyperplasia. The ability of EGFR activation to directly induce mucin expression in epithelial cells has been well established[255] and EGFR signalling appears to be the primary driver of mucus hyperproduction during various diseases, including asthma/AAD[138, 169, 214, 256] and COPD[187, 257] as well as in response to bacterial[183, 258] or viral[231, 233, 235, 238, 259] infection. In contrast, the mechanistic link between EGFR signalling and deficits in lung function is less well understood. Nonetheless, there is some evidence to suggest that airway mucins may have direct involvement in driving airway hyperresponsiveness in mouse models of AAD[260, 261]. In line with this, a high presence of mucus plugs was associated with decreased FEV_1 even after bronchodilator treatment in a cohort of patients with asthma[3]. These observations suggest that the alleviation in lung function observed upon EGFR inhibition in mouse models of AAD may at least in part result from a reduction of airway mucus. However, EGFR signalling is likely also involved in other mechanisms underlying worsened lung function. For example, intratracheal instillation of HB-EGF has been shown to directly induce migration of airway smooth muscle cells to the lungs, resulting in airway smooth muscle thickening[171], which is often considered the primary cause of airway hyperresponsiveness. In addition, several studies have reported reduced airway smooth muscle mass or gene expression of *Acta2*, encoding smooth muscle α-actin, when EGFR signalling was interrupted during AAD in rodents[136, 166-168, 227, 243]. EGFR is expressed on airway smooth muscle cells in asthma[212] and signalling via the receptor was necessary for the proliferation of these cells in response to co-culture with OVA-stimulated CD4 T cells[158]. EGFR signalling thus likely also contributes to airway hyperresponsiveness via direct effects on airway smooth muscle cells. Finally, effects of EGFR inhibition on collagen deposition, although also reported[136], were less common. While

the production of extracellular matrix components constitutes another potential mechanism via which EGFR signalling may drive exacerbated lung function, further studies are needed to characterise the relationship between these two pathways.

Surprisingly, there were no improvements in airway hyperresponsiveness, inflammation, goblet cell hyperplasia or airway smooth muscle mass when Gefitinib was administered to HDM-exposed adult mice, although such outcomes would have been expected based on previous findings in the literature. A possible explanation for these findings may be that the dosing strategy did not yield sufficient EGFR inhibition. Indeed, receptor inhibition could not be confirmed using western blot analysis of Y1068 phosphorylation due to low signal. The chosen dose of 1.5 mg Gefitinib, roughly equivalent to 75 mg/kg mouse weight, is slightly below the 100 mg/kg widely used as a dose for EGFR inhibitors by previous studies[166, 167, 169]. Nevertheless, doses as low as 12.5 mg/kg Gefitinib were shown to be efficacious in ameliorating AAD pathology in mice[165]. Another difference between the approach described here and previous reports lies in the frequency of inhibitor treatment. Here, Gefitinib was administered three times per week, several hours prior to allergen exposure, in order to minimise the risk of adverse effects of drug treatment, such as suppression of surfactant protein A or exacerbated lung inflammation[203]. While a regimen of three doses per week has previously been reported, both in an OVA sensitisation/challenge and an inhaled HDM model[168, 242], the majority of studies have administered EGFR inhibitors at least six times a week[165-167, 169]. Upon oral administration in mice, Gefitinib is rapidly absorbed and plasma concentrations decline with a half-life estimated between 3.8-16.4 hours[247, 262]. Although the drug was shown to be detectable in murine lungs up to 96 hours after a single intravenous 20 mg/kg dose[247], these pharmacokinetic studies suggest that more frequent administration of Gefitinib may be necessary to achieve optimal concentrations of the drugs within the tissue. Therefore, the observation that less frequent EGFR inhibition was unable to ameliorate AAD may suggest an overwhelming strength of EGFR signalling during disease. In support of this, EGFR ligand levels were significantly increased in the lungs of HDM-challenged animals, which, together with a decreased availability of EGFR ligands in the airways suggests a net increase in EGFR signalling. In addition, various studies have demonstrated increased pulmonary EGFR activation in response to HDM exposure[166, 169, 223]. In contrast, three weekly doses of Gefitinib induced airway hyperresponsiveness in PBS-exposed mice in the same model, a context in which EGFR is less active. Interestingly, the outcome of EGFR inhibition in naïve mice was opposite to what has previously been described during AAD, suggesting that EGFR has distinct contributions to lung function during homeostasis and disease. Finally, the vast extent of EGFR signalling upon HDM exposure may also explain why additional receptor activation by AREG did not affect disease pathology after one week of HDM

exposure. In contrast, AREG administration in the IL-33-driven model of airway inflammation resulted in slightly exacerbated airway hyperresponsiveness, potentially suggesting that EGFR signalling was less active and could therefore be further augmented in this context. Overall, our findings from EGFR manipulation in adult mice emphasise the great prominence of EGFR signalling during AAD, in line with previous findings from the literature. Nevertheless, it will be important to further confirm the role of EGFR signalling in adult AAD in future studies, for example by administering Gefitinib daily throughout the entire period of allergen exposure in order to achieve a higher degree of EGFR inhibition and by investigating the effects of treatment with other EGFR ligands on disease pathology.

A major aim of the work described within this chapter was to compare the contribution of EGFR signalling to AAD pathology between early life and adulthood. Although there is evidence of increased EGFR activation in the lungs and airways of children with asthma[215, 219-221, 263], little is known about the role of EGFR signalling in early-life AAD. The data from this chapter demonstrate that unlike in adulthood, EGFR inhibition in neonatal HDM-exposed mice resulted in exacerbated airway hyperresponsiveness, suggesting that EGFR signalling may be protective rather than detrimental during early life. These findings illustrate that distinct mechanisms may govern AAD pathology during different stages of life and underline the importance of studying the pathways contributing to disease during early life. Interestingly, exacerbated airway hyperresponsiveness in Gefitinib-treated neonatal mice was not accompanied by increases in inflammation, goblet cell hyperplasia or augmented deposition of extracellular matrix. Nevertheless, alterations in pulmonary gene expression and monocytic inflammation of the airways were observed upon EGFR inhibition. Interestingly, network analysis of these data suggests that these changes were driven by distinct mechanisms, likely due to the EGFR inhibitor acting on different cell types, and are thus unlikely to underlie the decline in lung function. Cell-specific manipulation of EGFR signalling, for example by targeting monocytes, epithelial cells or fibroblasts using conditional knockout models, would provide further insights into how EGFR inhibition of various cell types contributes to altered AAD pathology. Nevertheless, an exploratory analysis of collagen structure by second-harmonics generation imaging revealed potential effects of early-life EGFR inhibition on collagen geometry. Work from our group has demonstrated that altered collagen structure as a result of intranasal instillation with recombinant IL-33 restricts ILC2 mobility within the lungs, thereby perpetuating inflammation[264]. Preliminary findings from this thesis provide a first indication that EGFR inhibition during early-life AAD may alter collagen geometry, specifically by decreasing the uniformity and increasing the randomness of collagen fibres. While these results require validation in a larger cohort of mice, changes in collagen structure may provide a potential explanation for exacerbated airway hyperresponsiveness in Gefitinib-treated

animals. Collagens are the most abundant extracellular matrix components in the lungs[265], and changes to the collagen architecture have previously been described for various respiratory diseases, including asthma[266-269]. It is thus conceivable that altered collagen geometry may underlie the decline in lung function and the interplay between these two parameters, as well as other mechanisms which may cause exacerbated airway hyperresponsiveness, will be the subject of future studies. Additionally, it will be interesting to explore whether the collagen geometry of adult PBS-exposed mice was disturbed by Gefitinib treatment, as these animals also displayed worse lung function.

EGFR inhibition during neonatal AAD further resulted in altered pulmonary mRNA levels, specifically in elevated *Il33* but reduced *Arg1* expression. While these changes may potentially be indicative of increased damage and inadequate repair responses, respectively, the increases in IL-33 were not reflected at the protein level and further analyses are necessary before any conclusion regarding the possible causes or consequences of these changes can be drawn. Finally, early-life EGFR inhibition severely restricted the numbers of monocytic cells, particularly moDCs and inflammatory monocytes or macrophages, present within the allergic airways. In the previous chapter (see Chapter 3), EGFR expression was found to be strongly upregulated on moDCs by HDM exposure. It can therefore be hypothesised that EGFR signalling may directly control the recruitment or survival of moDCs in the airways. In support of this, there was a trend towards increased numbers of airway moDCs and IM/IMMs after AREG administration during neonatal AAD. In addition, EGFR expression has previously been reported on human monocytes[119]. Future *in vitro* studies may help elucidate how EGFR signalling contributes to moDC differentiation, mobility, proliferation or survival. In addition, it will be interesting to investigate whether the dependence of airway monocytic inflammation on EGFR observed here is specific to (early-life) AAD or may also be present in other contexts.

The final aim of this chapter was to establish a novel model of AAD using exposure to a mixture of perennial and seasonal allergens in order to reflect more severe disease where exacerbated airway remodelling would be present and EGFR signalling may thus play a more important role in driving pathology. Although asthma was traditionally viewed as a prototypical type 2 inflammation-driven, eosinophilic disease, it has become increasingly recognised that this syndrome encompasses many different phenotypes, including eosinophilic, neutrophilic, mixed or pauci-granulocytic inflammation[23] (cf. 1.1.2). Other branches of the adaptive immune response, such as Th17-driven response, are not only present in asthma but often found to correlate with disease severity[270]. Traditional mouse models of AAD, particularly the OVA sensitisation/challenge approach, primarily favour Th2-driven eosinophilic responses, whereas the more physiologically relevant models of chronic inhaled allergen exposure also induce mixed Th2/Th17-driven responses depending on the dosing regimen and composition

of the allergen used[48, 50, 271]. Inhaled exposure to a mix of different allergens, such as HDM, ragweed and fungus *Aspergillus fumigatus*, has previously been used to drive mixed Th2/Th17 responses in adult animals[272]. In children, severe asthma is characterised by sensitisation to multiple aeroallergens and, importantly, exacerbated airway remodelling[273]. In addition, neutrophilic or mixed inflammation is present in roughly 50% of children with severe asthma[274], and this work aimed to develop a model of early-life AAD reflecting these features. Exposure of neonatal mice to an allergen mix containing HDM, ALT and TG drove mixed eosinophilic and neutrophilic inflammation of the airways, in addition to pulmonary Th2 and Th17 responses. Mixed allergen challenge also induced significant airway hyperresponsiveness, along with goblet cell hyperplasia and increases in serum IgE and IgG1, thus encompassing hallmark features of AAD pathology. Importantly, the overall extent of inflammation, airway hyperresponsiveness and sensitisation was greater after mixed allergen exposure compared to challenge with each allergen individually, suggesting that this approach may represent more severe disease. As such, this newly established model of early-life mixed allergen challenge provides a valuable tool for the investigation of AAD pathology in early life and may provide novel insights into the mechanisms underlying mixed granulocytic severe asthma in childhood. It will be particularly interesting to investigate the role of EGFR signalling in this context, as this pathway may have a greater role in driving disease pathology in a model where airway remodelling is exacerbated. Here, the effects of HB-EGF administration on AAD pathology in mixed allergen-exposed mice were tested based on the assumption that EGFR activation may be protective in a model that induces heightened damage. However, disease pathology was largely unaffected by ligand administration. The data presented within this and the previous chapter suggest that EGFR signalling was strongly induced by allergen exposure even in the absence of exogenous activation of the receptor, which may explain the lack of effect of HB-EGF treatment on AAD pathology. Therefore, it will be important to inhibit EGFR signalling in this model to investigate if and how this pathway contributes to AAD pathology in the context of more severe disease and whether these contributions are distinct from the role of EGFR in HDM-driven AAD.

4.5 Concluding remarks and future work

Mouse models of AAD constitute a useful tool for the study of mechanisms underlying asthma pathology. Through manipulation of EGFR signalling in various neonatal and adult models of AAD, we identified distinct roles for EGFR signalling in early life and adulthood. Contrary to published data supporting a pathogenic role for EGFR in driving pathology of adult AAD, our data suggest a protective role for EGFR in preventing worsened lung function during early life.

Which mechanisms may underlie these changes in lung function will be the subject of future study, which will focus on exploring the consequences of disrupting collagen assembly on lung function in early-life AAD and employ unbiased transcriptomics or proteomics approaches to uncover the relationship between EGFR signalling and airway hyperresponsiveness in neonatal mice. The overwhelming activity of EGFR signalling during adult AAD was emphasised by the inability of low-frequency EGFR inhibition or exogenous EGFR activation to alter AAD pathology, stressing the importance of this signalling pathway in asthma. These findings will be validated in future studies by performing more rigorous EGFR inhibition in both neonatal and adult models of AAD, for example by increasing the dose and frequency of Gefitinib administration.

5 Results III:

EGFR inhibition abrogates exacerbated type 2 responses to allergen in adolescent female mice

5.1 Introduction

5.1.1 Sex differences in asthma

Various immune responses are distinct between the sexes, with many of these differences thought to arise from either genetic or hormonal discrepancies between males and females[275]. In addition, high-throughput phenotyping of over 500 genetic knockout mouse strains revealed sex-dependent differences in the frequencies of several immune cell populations[276]. Sex differences also govern both prevalence and severity of asthma, wherein adult females are more commonly affected and more likely to exhibit severe disease compared to males[20, 21, 277, 278]. Interestingly, this sex balance is reversed in childhood, during which asthma prevalence is higher in males[20, 21, 278, 279]. These sex differences in asthma also affect health care usage, with higher rates of hospitalisation reported for males during childhood but females in adulthood[280, 281]. The reversal of this sex balance has been found to coincide with puberty[279, 282-284] and symptoms worsened during the pre- or perimenstrual phase in a subset of women[285-288], whereas asthma risk declines with menopause[289], suggesting the involvement of sex hormones. Various epidemiological studies have aimed to define the role of both endogenous and exogenous steroid sex hormones in driving increased asthma risk and severity in females, but have been inconclusive, likely due to a large number of confounding factors such as environmental exposures, smoking history, genetic predisposition or body mass index[290].

5.1.2 Use of animal models to study the role of sex hormones in AAD

Given the difficulty to draw definite conclusions on the role of sex hormones in driving increased asthma preponderance, various studies have employed animal models to study sex differences in AAD *in vivo*. In line with epidemiological findings, female mice generally displayed heightened type 2 inflammation and disease pathology compared to their male counterparts in the classical OVA sensitisation/challenge model[291-294]. Interestingly, a direct comparison between the classical OVA model and an inhaled HDM model of AAD suggests that sex differences were less pronounced when allergic inflammation was induced by chronic inhalation rather than systemic sensitisation[294]. Nevertheless, classical sex differences, such as increased airway eosinophilia, elevated type 2 cytokines and lymphocytes as well as higher IgE levels in females were also reported in models where mice were exposed to allergen exclusively via the intranasal route[295-297]. These findings indicate that augmented pathology of females is an intrinsic feature of common AAD models.

The ability of mouse models to reflect sex differences in AAD pathology has been used to study the role of both male and female sex hormones in driving these discrepancies. Gonadectomy, or the removal of the testis in male or the ovaries in female animals, respectively, resulting in the inability of these animals to produce steroidal sex hormones, has been a useful tool in this effort. Ovariectomised females displayed dampened AAD pathology, including reduced airway inflammation, eosinophilia, lung function and levels of Th2 and Th17 cytokines compared to sham-operated animals[297-299], suggesting that the female sex hormones oestradiol and/or progesterone play a detrimental role in driving disease. Conversely, castration of male mice resulted in exacerbated pathology comparable to that of female animals[291, 295, 297], both proposing a protective role for testosterone and indicating that AAD pathology is governed by an interplay between male and female sex hormones. In support of this, administration of the female hormones oestradiol or progesterone to males or ovariectomised females aggravated disease[298, 300, 301] whereas testosterone precursors or metabolites ameliorated pathology in female animals[295, 302]. Further support for the role of both male and female sex hormones stems from studies using mice deficient for their respective receptors. Genetic deletion of *Esr1*, the gene encoding oestrogen receptor alpha (ERα), reduced eosinophilia and type 2 cytokines of females[303], while male mice unable to signal via the androgen receptor (AR) displayed exacerbated inflammation and increased numbers of both type 2 and type 17 lymphocytes[295, 297]. Together, these studies provide convincing evidence of detrimental contributions of female and protective roles of male sex hormones, respectively, with respect to the pathology of AAD.

While the sex differences in AAD during adulthood have been extensively studied, little is known about the mechanisms underlying the heightened asthma prevalence and severity observed in males during childhood and sex differences in pre-pubertal mouse models of AAD have not been described. Nevertheless, one study found that male animals infected with RSV in early life displayed delayed resolution of the infection as well as exacerbated pathology of cockroach allergen-induced AAD later in life compared to females[304]. Since early-life infection with RSV is a common risk factor for asthma development and exacerbations[8-11], this may provide a potential explanation for the bias towards males in asthma prevalence and severity during childhood. In contrast, however, a similar study exploring the consequence of early-life infection with RV on subsequent HDM-induced AAD describes exacerbated disease exclusively in viral-infected females but not males[305], indicating that more research is needed to address the mechanisms underlying sex differences in early life as well as the potential role of viral infections in this context. In addition, it will be important to investigate how the sex balance in AAD in adolescent (peri- or post-pubertal) animals is affected when allergen exposure is commenced pre-pubertally.

5.1.3 Hypothesis and aims

Hypothesis

Early-life allergen exposure results in disparate AAD pathology between adolescent male and female mice.

Aims

1. To describe the sex-specific immune responses of six-week-old mice following allergen exposure from day seven of life.
2. To compare sex difference between pre-pubertal and post-pubertal start of allergen exposure.
3. To characterise the consequences of EGFR inhibition on sex differences in AAD pathology.

5.2 Methods

Data from EGFR inhibition during early-life AAD (cf. 4.3.3-4.3.5) were reanalysed by sex. EGFR inhibition during adult AAD was repeated in male animals and results were compared to findings from Gefitinib treatment in female mice (cf. 4.3.2). Mediastinal lymph node cells from male adult or female neonatal mice chronically exposed to HDM were restimulation *ex vivo* with HDM or PMA and ionomycin in the presence or absence of Gefitinib and β-oestradiol and levels of cytokines released into the supernatants were measured by ELISA.

5.3 Results

5.3.1 Augmented type 2 responses in adolescent female animals were dependent on EGFR signalling

As part of the integrative data analysis presented in the previous chapter (cf. 4.3.5), principal component analysis (PCA) was performed on protein, flow cytometry, gene expression and lung function data (**Figure 5.1A**). This approach revealed greater variability within the HDM/Vehicle group than the HDM/Gefitinib group. In an effort to account for this variability, the data were stratified by sex. This identified a clear difference between female and male HDM-treated animals which was lost upon Gefitinib treatment, suggesting the existence of EGFR-dependent sex differences during early-life AAD. In line with this, multiple parameters were differentially regulated between HDM-treated males and females in the absence of EGFR inhibition but not after Gefitinib treatment (**Figure 5.1B**).

The most significant differences between sexes concerned the type 2 cytokine IL-13. Females exhibited increased levels of IL-13 in their airways and lungs compared to male animals

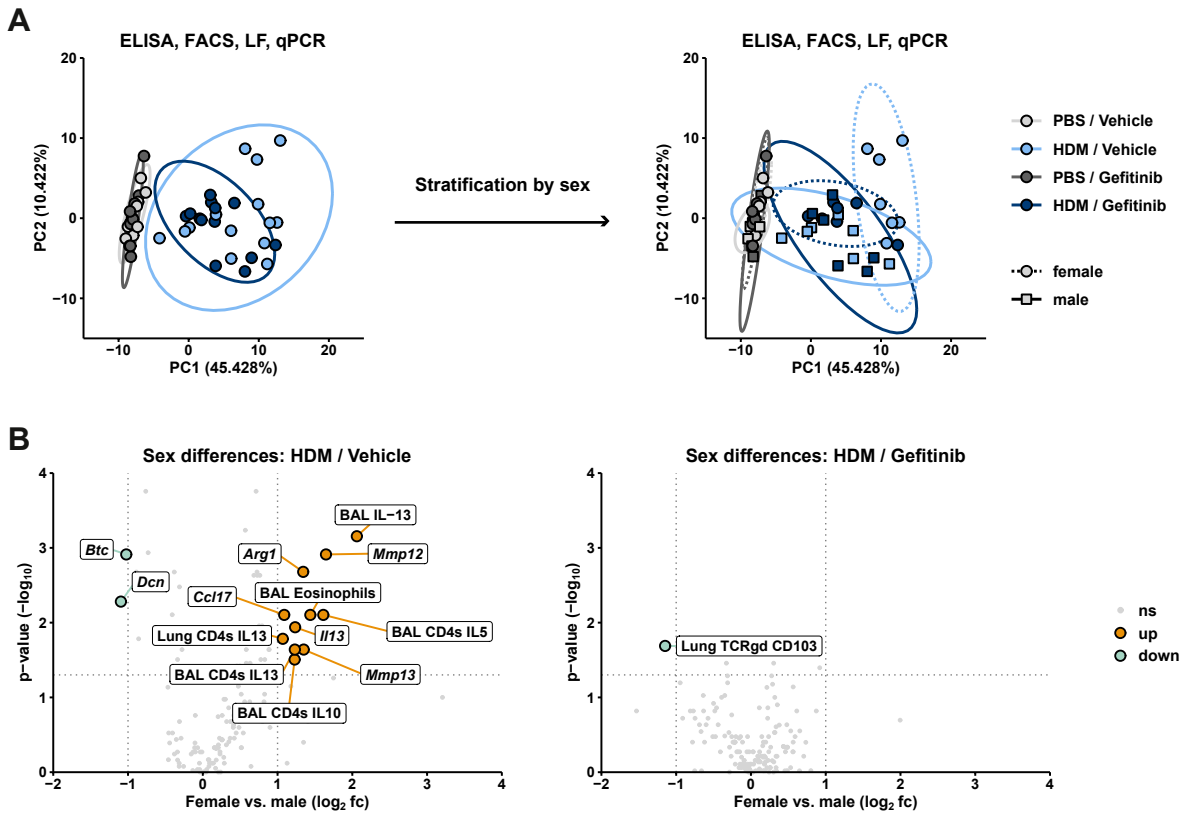


Figure 5.1 EGFR inhibition abrogated sex differences in early-life AAD.
Animals were treated as described in Figure 4.12A. **A** Principal component analysis based on ELISA, flow cytometry, lung function and gene expression data. Each data point represents one animal. **B** Volcano plot showing sex differences in HDM/Vehicle- (left) or HDM/Gefitinib-treated animals. Labelled values exhibited an absolute fold change ≥ 2 and a *p*-value (Mann-Whitney) ≤ 0.05 when comparing female and male animals. (A-B) *n* = 4-9 per treatment/sex, data pooled from two independent experiments.

(**Figure 5.2A**), coupled with elevated numbers of CD4 T cells able to produce the cytokine upon *ex vivo* stimulation (**Figure 5.2B**). Pulmonary gene expression of *Il13* was likewise higher in female compared to male mice (**Figure 5.2C**). Importantly, Gefitinib treatment specifically reduced IL-13 levels in female but not male animals, thereby reducing sex differences. These results suggest that EGFR is necessary to drive augmented IL-13 responses in young female mice.

In line with the findings for IL-13-producing T cells, female animals exhibited higher numbers of IL-5$^+$ and IL-10$^+$ CD4 T cells in their airways and lungs compared to males (**Figure 5.3A-B**). Importantly, EGFR inhibition diminished differences between the sexes and numbers of IFNγ- or IL-17A-producing T cells were comparable between males and females regardless of intervention, suggesting that EGFR signalling specifically amplified Th2 responses in female animals. In agreement with T cell numbers, the levels of the type 2 cytokines IL-4 and IL-5 were higher in female compared to male mice and those differences were reduced upon Gefitinib treatment (**Figure 5.3C**). Interestingly, elevated levels of pulmonary IL-33 in female mice were maintained even after intervention (**Figure 5.3C)**, suggesting that EGFR inhibition acted downstream of IL-33 signalling. Finally, whole lung gene expression analysis revealed slightly higher transcript levels of *Il4* and *Il5* in females (**Figure 5.3D**), although these data were not statistically significant. Of note, pulmonary *Il33* expression was comparable between male and female vehicle-treated animals but strongly induced by EGFR inhibition in females.

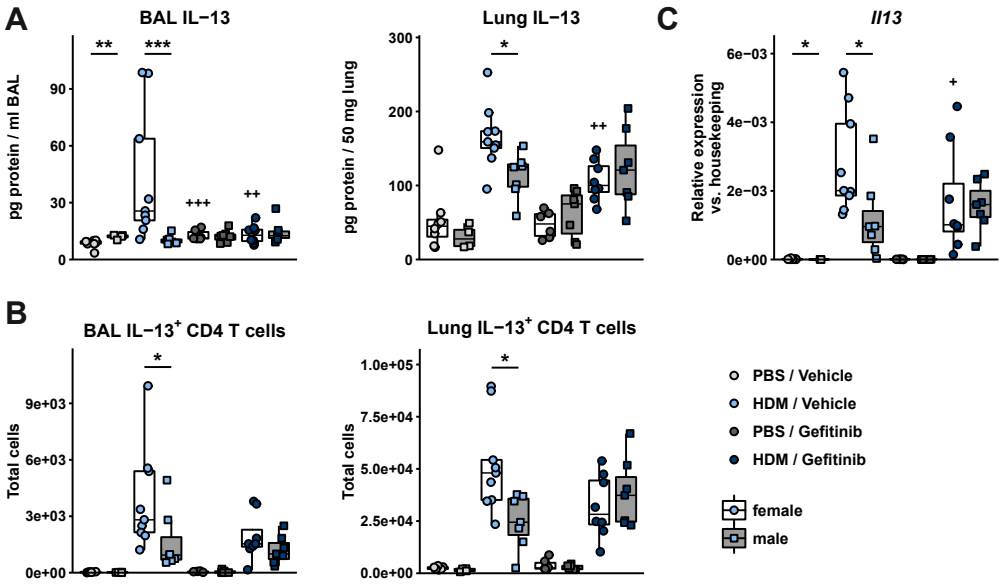


Figure 5.2 Augmented IL-13 responses of female animals were abrogated by EGFR inhibition.
Animals were treated as described in Figure 4.12A. **A** Levels of IL-13 in bronchoalveolar lavage (BAL) and lung homogenate by ELISA. **B** Total numbers of IL-13-producing CD4 T cells in BAL and lungs after *ex vivo* stimulation with PMA and ionomycin. **C** Pulmonary gene expression of *Il13*. (A-C) *n* = 4-9 per treatment/sex, data pooled from two independent experiments. Statistics: Mann-Whitney test between indicated groups (*) or in comparison to the relevant vehicle-treated group (+). */+, $p < 0.05$; **/++, $p < 0.01$; ***/+++, $p < 0.001$.

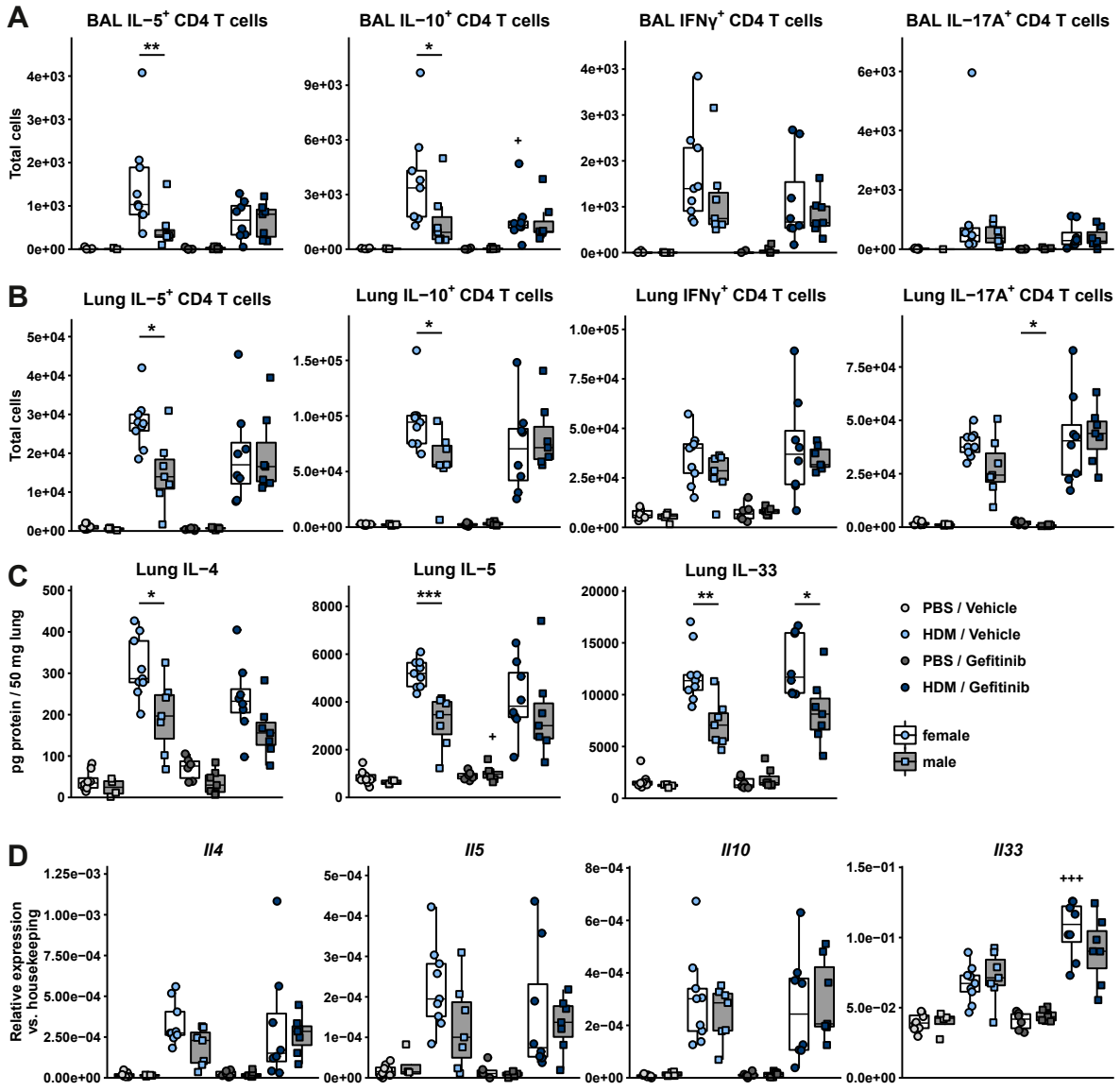


Figure 5.3 Female animals displayed EGFR-dependent increases in type 2 responses.
Animals were treated as described in Figure 4.12A. **A-B** Total numbers of cytokine-expressing T cells in bronchoalveolar lavage (BAL; A) and lungs (B) after *ex vivo* stimulation with PMA and ionomycin, as measured by flow cytometry. **C** Levels of indicated cytokines in lung homogenates by ELISA. **D** Pulmonary expression of indicated genes by qPCR. (A-D) n = 4-9 per treatment/sex, data pooled from two independent experiments. Statistics: Mann-Whitney test between indicated groups (*) or in comparison to the relevant vehicle-treated group (+). */+, $p < 0.05$; **/++, $p < 0.01$; ***/+++, $p < 0.001$.

These findings raised the question whether female animals displayed exacerbated inflammation in general or whether the sex differences were restricted to type 2 responses. Overall cellularity of the airways but not the lungs was increased in female compared to male mice (**Figure 5.4A**), suggesting an overall increase in inflammation in these animals. However, only the numbers of eosinophils, not AMs, neutrophils or DCs, were significantly higher in females (**Figure 5.4B**), indicating that augmented cell recruitment in these animals was restricted to certain cell types, primarily those related to type 2 immune responses. There was also an increased in the numbers of airway CD4 T cells in female compared to male mice (**Figure 5.4C**), likely driven by enhanced Th2 cell recruitment, as described above. Although

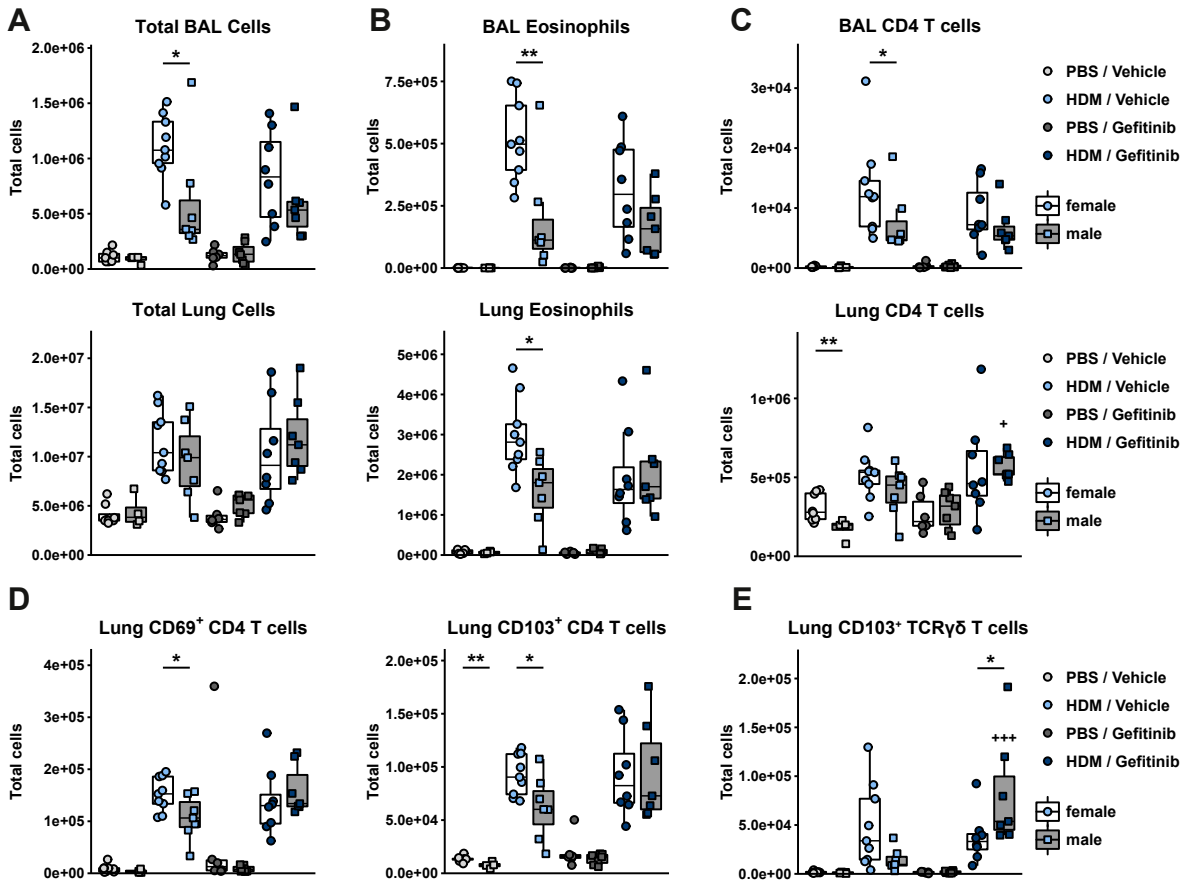


Figure 5.4 Heightened eosinophilia of female mice was dampened by EGFR inhibition.
Animals were treated as described in Figure 4.12A. **A** Total numbers of cells in bronchoalveolar lavage (BAL) or left lung lobes. **B-C** Total numbers of BAL and lung eosinophils (B) or CD4 T cells (C) by flow cytometry. **D-E** Total numbers of CD69- or CD103-expressing conventional CD4 or γδ T cells in lungs by flow cytometry. (A-E) *n* = 4-9 per treatment/sex, data pooled from two independent experiments. Statistics: Mann-Whitney test between indicated groups (*) or in comparison to the relevant vehicle-treated group (+). */+, $p < 0.05$; **/++, $p < 0.01$; ***/+++, $p < 0.001$.

overall numbers of lung CD4 T cells were comparable between sexes, expression of CD69 and CD103 was more abundant on female T cells (**Figure 5.4D**), suggesting that female animals had an overall increase in T cell activation and memory formation. Importantly, these sex differences were lost or minimised by Gefitinib treatment, indicating that EGFR signalling played a central role in driving augmented responses in females. Nevertheless, Gefitinib also affected certain responses in male mice, such as expanding the population of CD103⁺ γδ T cells in the lungs (**Figure 5.4E**).

Type 2 inflammation is one of the hallmark features of AAD. To ascertain whether other aspects of AAD pathology would display similar sex differences, lung function data were analysed by sex. Interestingly, female animals displayed worse lung function at baseline and in response to low doses of methacholine, but differences between sexes were gradually reduced or lost with increasing extent of bronchoconstriction (**Figure 5.5**). As described in the previous chapter, EGFR inhibition resulted in exacerbated airway hyperresponsiveness during

early-life AAD, particularly at a dose of 30 mg/ml MCh (cf. Figure 4.15). Conversely, the sex-specific analysis revealed that Gefitinib treatment significantly improved baseline lung function of female HDM-treated mice (**Figure 5.5B**), thereby minimising any sex differences. Importantly, EGFR inhibition still resulted in exacerbated airway hyperresponsiveness to high doses of methacholine in both female and male animals, illustrating that EGFR signalling may have dual, opposing roles in regulating lung function during early-life AAD.

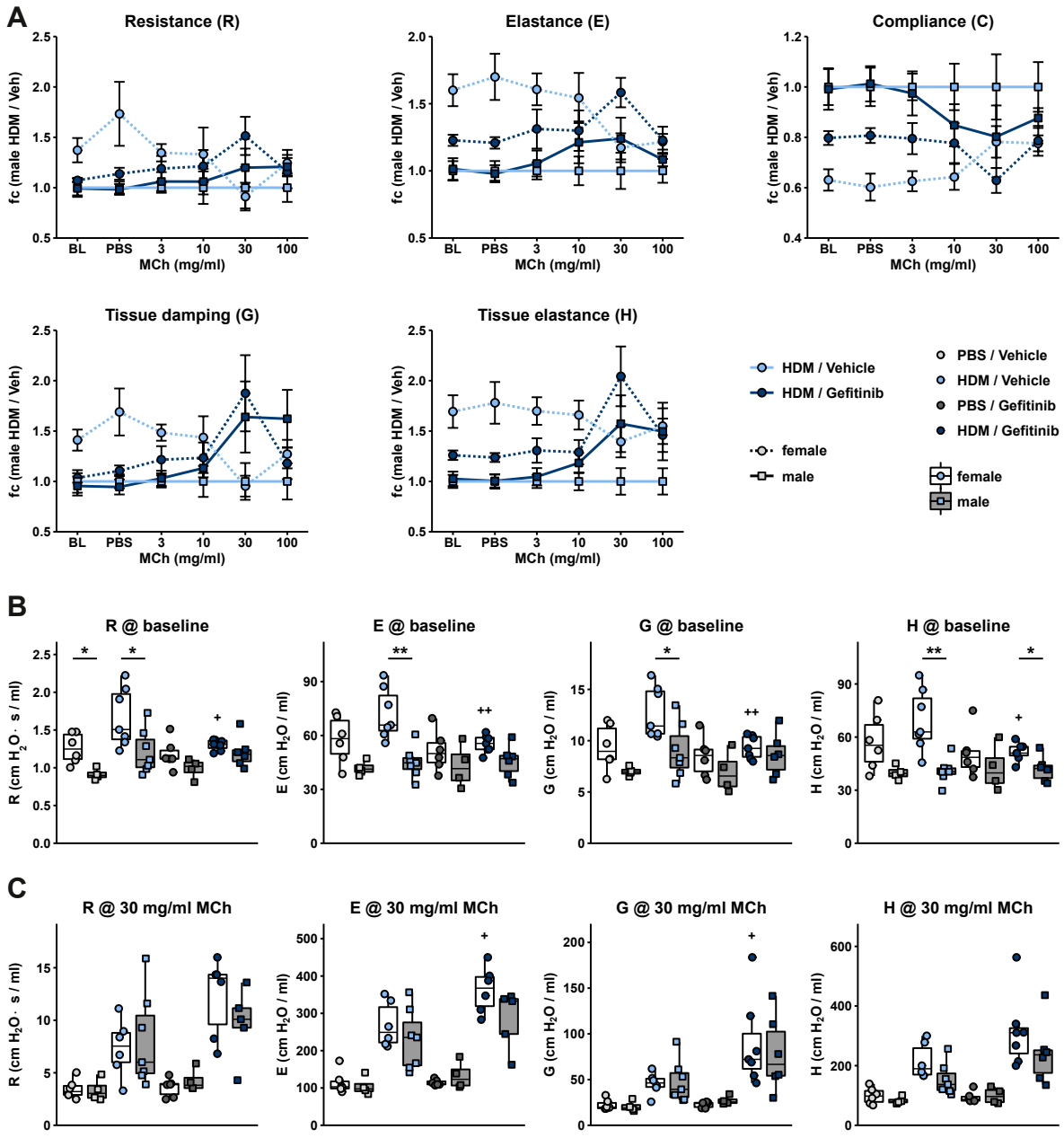


Figure 5.5 EGFR inhibition rescued worsened baseline lung function of female animals.
Animals were treated as described in Figure 4.12A. **A** Various lung function measurements in response to challenge with increasing doses of methacholine (MCh), plotted as fold-change from male HDM/Vehicle-treated animals. **B** Lung function measurements in the absence of methacholine challenge. **C** Lung function measurements in response to 30 mg/ml MCh. (A-C) n = 4-7 per treatment/sex, data pooled from two independent experiments. Statistics: Mann-Whitney test between indicated groups (*) or in comparison to the relevant vehicle-treated group (+). */+, $p < 0.05$; **/++, $p < 0.01$.

The attempts to identify a conclusive link between exacerbated airway hyperresponsiveness and changes in remodelling described in the previous chapter were unsuccessful. Nevertheless, this chapter investigated whether sex differences in baseline lung function may be accompanied by distinct remodelling-associated gene expression. Indeed, young mice displayed sex-dependent pulmonary expression levels of genes involved in collagen deposition (**Figure 5.6A**) and matrix remodelling (**Figure 5.6B**). Intriguingly, Gefitinib treatment altered collagen gene expression primarily in male mice, whereas expression of *Mmp2* and *Mmp13* was more strongly affected by EGFR inhibition in female animals. These

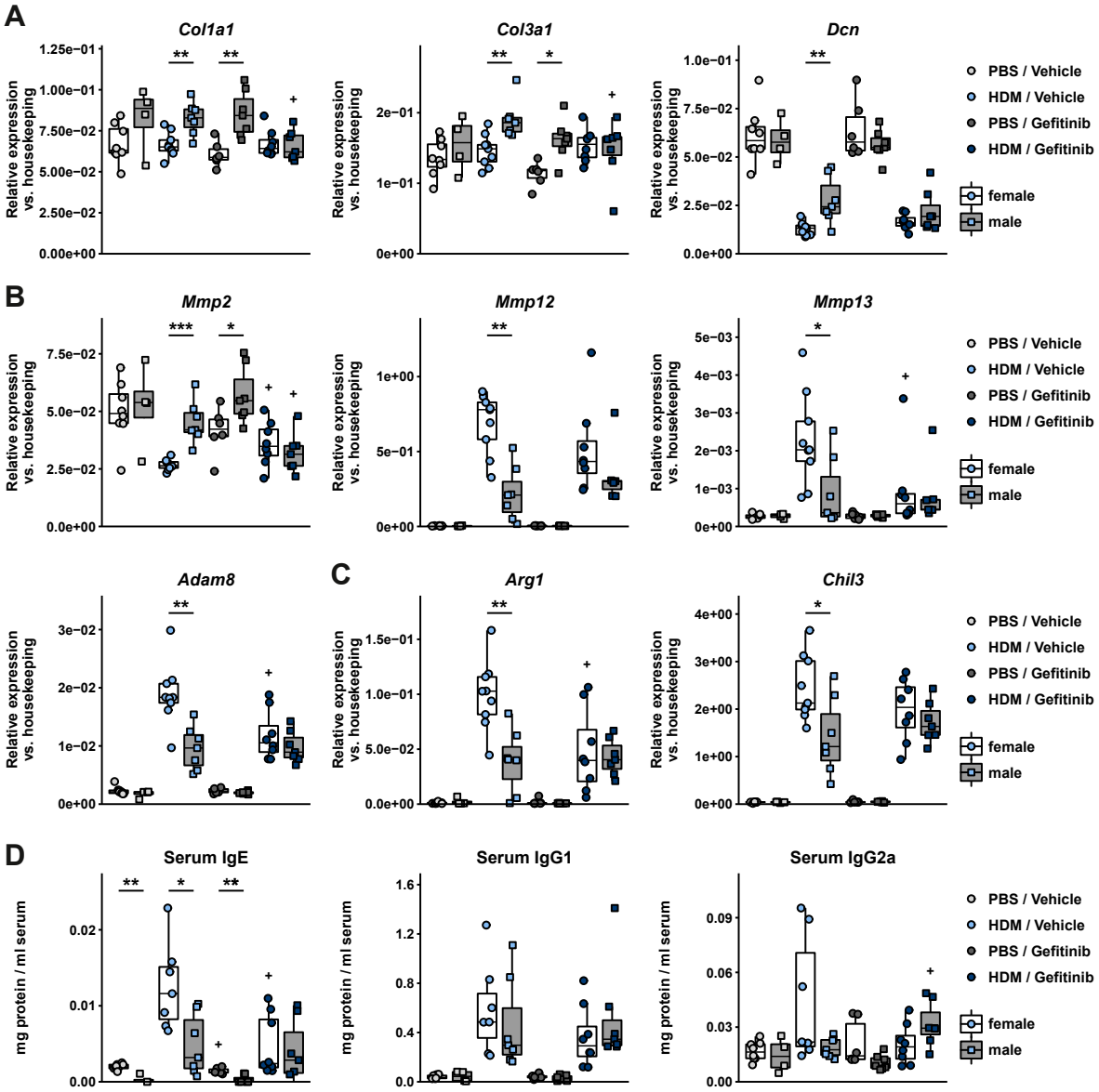


Figure 5.6 Expression of remodelling-associated genes and allergic sensitisation during early-life AAD were sex-dependent.
Animals were treated as described in Figure 4.12A. **A-C** Whole lung gene expression of indicated genes by qPCR. **D** Total antibody levels in serum by ELISA. (A-D) n = 4-9 per treatment/sex, data pooled from two independent experiments. Statistics: Mann-Whitney test between indicated groups (*) or in comparison to the relevant vehicle-treated group (+). */+, $p < 0.05$; **/++, $p < 0.01$; ***/+++, $p < 0.001$.

findings suggest that, while EGFR signalling is likely to be involved in driving remodelling-related changes in gene expression, its contribution appears complex and highly sex-dependent.

A previous study found that macrophages from female mice respond to stimulation with IL-4 with a stronger induction of the repair-associated genes *Arg1* and *Chil3* compared to cells from male animals[306]. In line with this, female animals exhibited higher expression of *Arg1* and *Chil3* in their lungs compared to their male counterparts in our model (**Figure 5.6C**). Gefitinib reduced the expression of these genes specifically in female animals, albeit only significantly for *Arg1*, similarly as previously observed for other aspects of the type 2 response such as eosinophilia, Th2 cell recruitment or levels of type 2 cytokines, suggesting that these may all be controlled by the same mechanism. Another feature commonly associated with IL-4 and AAD pathology is allergic sensitisation. Analysis of total serum immunoglobulins revealed higher levels of IgE, but not IgG1 or IgG2a, in the circulation of female animals, both at baseline and after HDM treatment (**Figure 5.6D**). IgE induction in HDM-exposed females was limited by EGFR inhibition, thus constituting another sex-specific type 2-related parameter reliant on EGFR signalling.

Given the ability of EGFR signalling to drive augmented type 2 responses in female but not male mice, we asked whether females would exhibit an overall increase in EGFR activation. Reanalysis of Y1068 phosphorylation (cf. Figure 4.12) did not suggest stronger EGFR signalling in female animals compared to males (**Figure 5.7A**). Interestingly, the lungs of female mice displayed more pronounced downregulation than male mice of the genes encoding *Egfr* and three of its ligands, *Btc*, *Egf* and *Tgfa*, upon HDM exposure (**Figure 5.7B**). Females also exhibited stronger responses to HDM challenge at the protein level, where they showed higher levels of EREG in their lungs but lower levels of EREG and HB-EGF in the airways compared to males (**Figure 5.7C**). Similar to previous observations for various parameters of type 2 immunity, Gefitinib treatment evened the levels of EGFR and ligands between the sexes. These results suggest that sex differences in EGFR signalling exist during early-life AAD, however, it is unclear whether these are the cause or consequence of or unrelated to augmented type 2 responses in female animals.

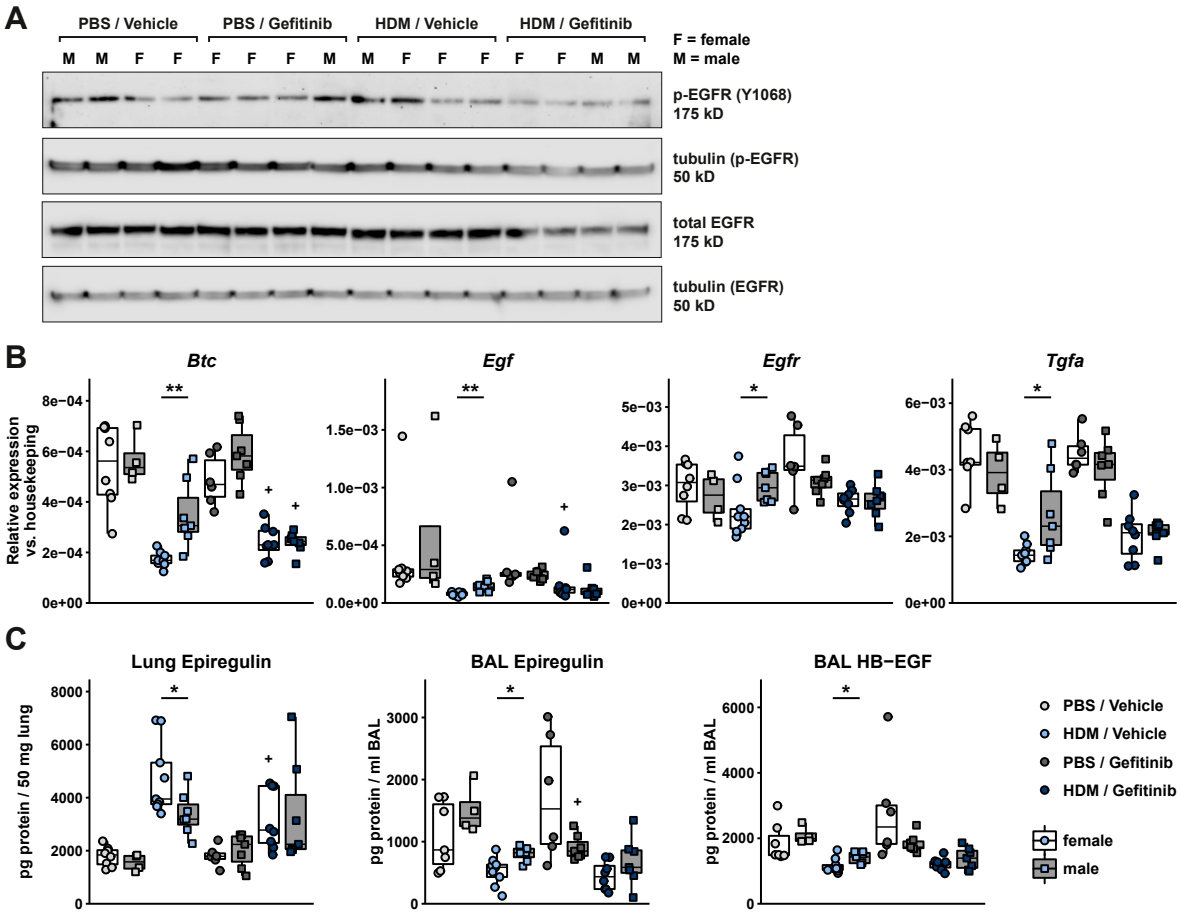


Figure 5.7 Lung and airway levels of EGFR ligands displayed sex-dependent differences.
Animals were treated as described in Figure 4.12A. **A** Western blot of lung homogenates using indicated antibodies. Sex of animals is stated above bands. **B** Whole lung gene expression of indicated genes by qPCR. **C** Levels of EGFR ligands in lung homogenates or bronchoalveolar lavage (BAL) by ELISA. (A) *n* = 1-3 per treatment/sex, data from one experiment. (B-C) *n* = 4-9 per treatment/sex, data pooled from two independent experiments. Statistics: Mann-Whitney test between indicated groups (*) or in comparison to the relevant vehicle-treated group (+). */+, $p < 0.05$; **/++, $p < 0.01$.

5.3.2 Comparable responses between sexes in adult AAD

The previous chapter (see Chapter 4) revealed distinct roles for EGFR signalling during early life and adulthood. This chapter found that EGFR signalling supported augmented type 2 responses of young females. This posed the question whether sex differences were also present if animals were exposed to HDM during adulthood and whether EGFR inhibition would affect type 2 responses in either sex. To address this, male adult mice were administered Gefitinib during the last three of five weeks of HDM exposure and the responses of these animals were compared to the experiments previously conducted in female adults (**Figure 5.8A**). Overall inflammation of the airways and lungs was comparable between sexes (**Figure 5.8B**). Of note, the numbers of eosinophils and Th2 cells, two cell types expanded in young female mice, were similar between adult males and females (**Figure 5.8C-D**).

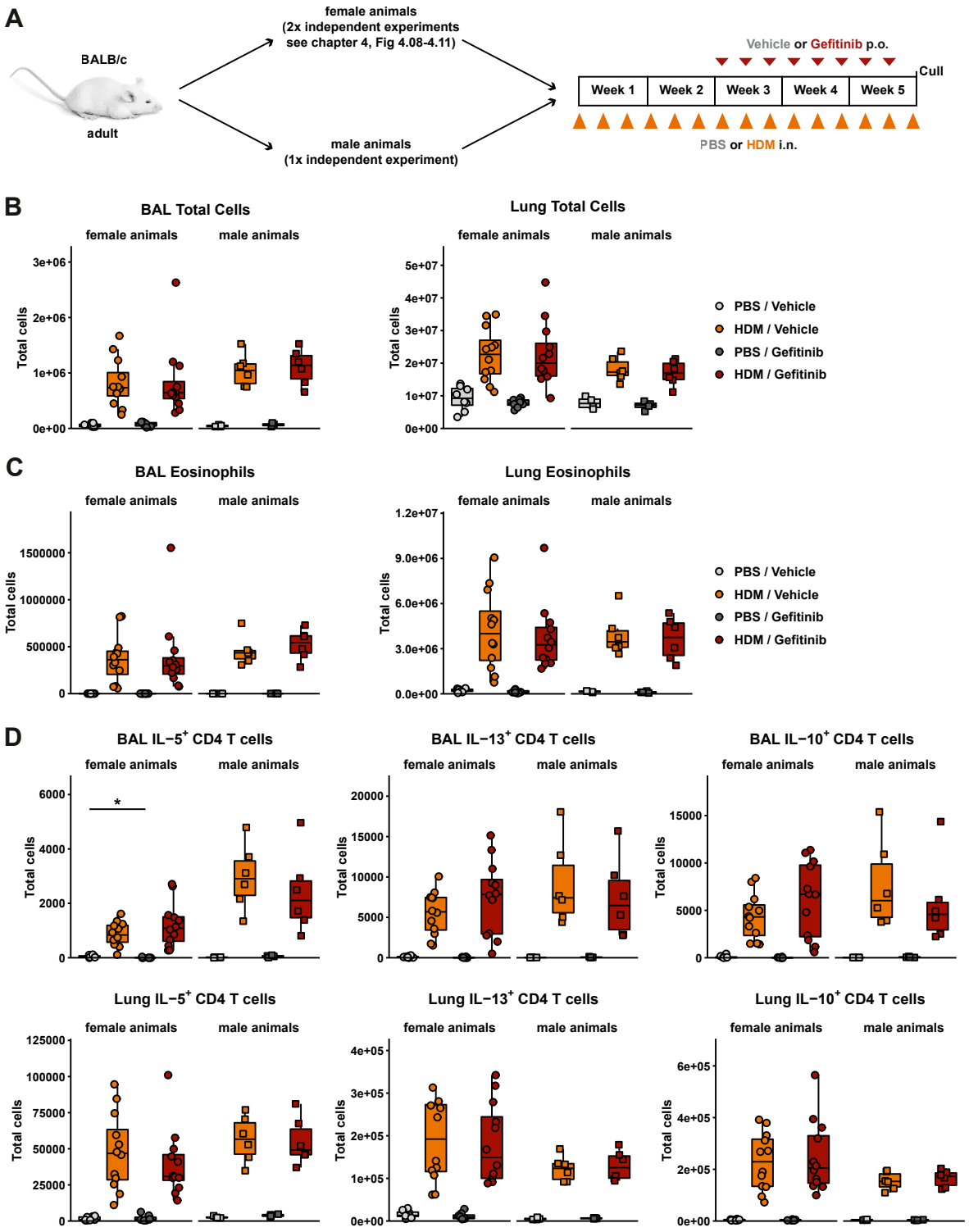


Figure 5.8 Type 2 immune responses of adult animals were comparable between sexes.
A Schematic depicting experimental approach. Adult male BALB/c mice were given inhaled HDM (25 µg) three times per week for five weeks. During weeks three to five, mice were orally administered Gefitinib (1.5 mg) approx. 4-6 hours prior to allergen challenge and animals were sacrificed on the day following the last dose. Responses of male animals were compared to experiments conducted in females (cf. 4.3.2). **B** Total cells in bronchoalveolar lavage (BAL) or the left lung lobe. **C** Numbers of eosinophils in BAL or the left lung lobe, as measured by flow cytometry. **D** Cytokine-producing potential of CD4 T cells in BAL or lungs after *ex vivo* stimulation with PMA and ionomycin. (B-D) female animals: n = 8-12, pooled from two independent experiments; male animals: n = 4-6, data from one experiment. Statistics: Mann-Whitney test between indicated groups. *, $p < 0.05$).

While a direct comparison between sexes within the same experiment would provide more conclusive evidence, these data suggest that the sex differences observed during early-life AAD may be absent during adulthood. In addition, Gefitinib treatment had no effects on eosinophilia or the production of type 2 cytokines in either sex, suggesting that the ability of EGFR to support augmented type 2 responses is specific to young female animals.

During early-life AAD, females also displayed worsened lung function at baseline and in response to low doses of methacholine, which was ameliorated upon EGFR inhibition. To test whether similar mechanisms exist during adulthood, baseline lung function and airway hyperresponsiveness were compared between adult animals of both sexes. Overall, the amplitude of airway hyperresponsiveness induced by HDM was comparable between male and female mice (**Figure 5.9A**). Interestingly, in the absence of methacholine (at 'baseline'), HDM exposure seemed to result in increased lung function only in female but not male animals (**Figure 5.9B**), potentially suggesting that increased susceptibility of female mice to HDM-induced lung function, as previously observed during early life, was also a feature of adult AAD. Nevertheless, Gefitinib treatment did not ameliorate baseline lung function of adult females, indicating that the contribution of EGFR signalling to lung function changes is distinct between early life and adulthood. Of note, EGFR inhibition did not exacerbate airway hyperresponsiveness of PBS-treated male mice, as previously observed in female animals (cf. Figure 4.9). This suggests that, while distinct from early life, the contribution of EGFR signalling to lung function was still sex-dependent in adult animals.

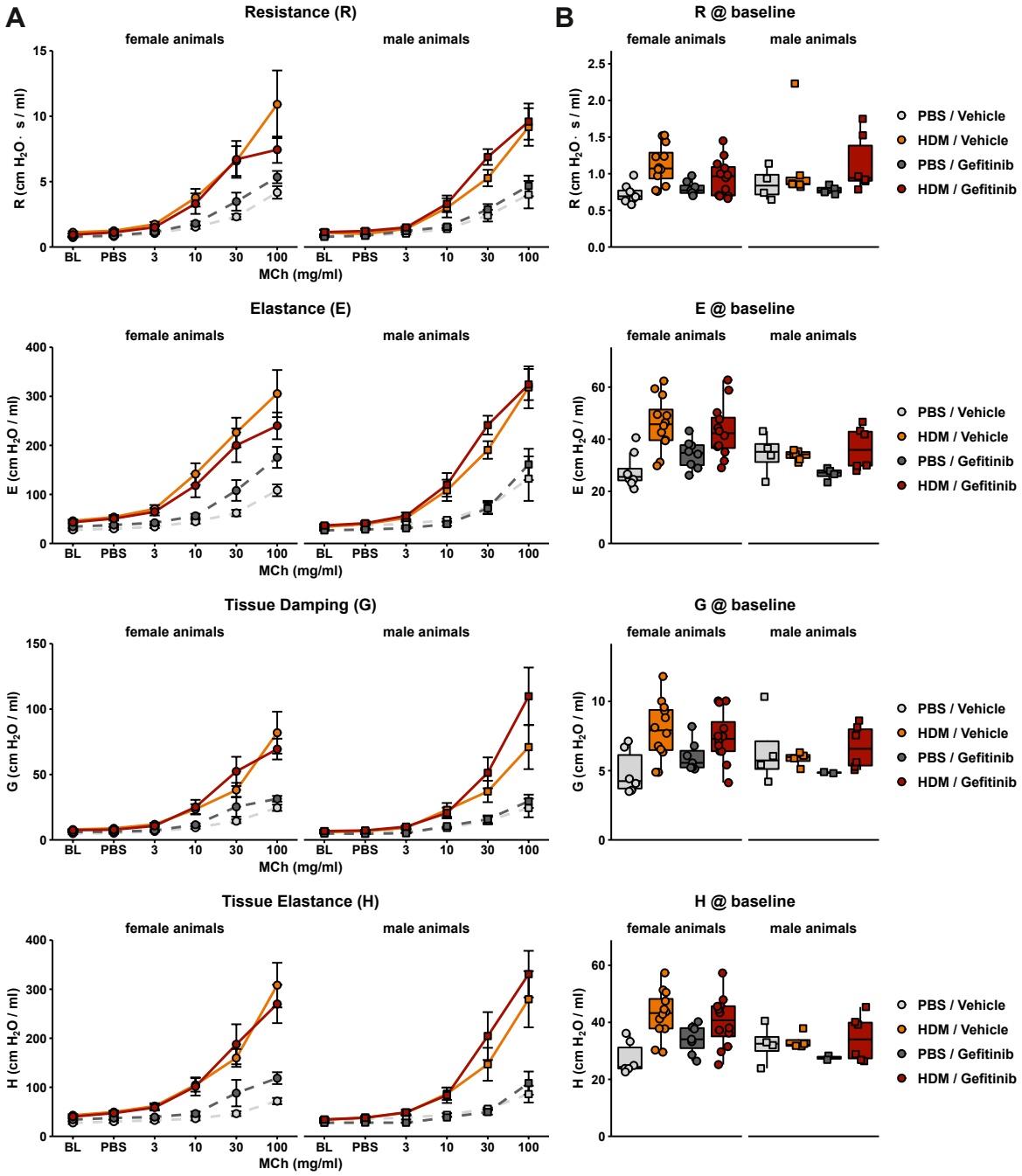


Figure 5.9 HDM exposure induced comparable airway hyperresponsiveness in adult males and females. Animals were treated as described in Figure 5.8A. **A** Various lung function measurements in response to increasing doses of methacholine. **B** Lung function parameters in the absence of methacholine challenge. (A-B) female animals: *n* = 8-12, pooled from two independent experiments; male animals: *n* = 4-6, data from one experiment.

5.3.3 EGFR inhibition abrogated HDM-induced type 2 cytokine production *ex vivo*

Both male and female sex hormones have been implicated in protecting from or driving pathology during AAD, respectively[307]. In addition, it has been suggested that the female sex hormone oestradiol can induce EGFR activation by signalling via the G protein-coupled oestrogen receptor GPR30[308]. T lymphocytes have previously been shown to express GPR30[309], as well as the intracellular oestrogen receptors ERα and ERβ[310]. Therefore, the increase in oestrogen levels present in young female mice[311] may drive augmented type 2 responses by acting via EGFR. To test this, lymph node cells from adult HDM-exposed male mice were restimulated with HDM in the presence or absence of β-oestradiol and Gefitinib and cytokine production by these cultures was measured (**Figure 5.10A**). β-Oestradiol did not affect the levels of IL-4, IL-5 or IL-13 produced upon HDM stimulation (**Figure 5.10B**), implying that this hormone does not act directly on lymphocytes to boost type 2 responses. Interestingly, however, cytokine production was ablated by Gefitinib, suggesting that EGFR signalling was necessary for the induction of type 2 cytokines in response to antigen-specific stimulation. Similar results were achieved when *ex vivo* re-stimulation was repeated using lymph node cells from neonatal female animals (**Figure 5.10C-D**), indicating that the ability of EGFR inhibition to restrict type 2 cytokine production was independent of the age or sex of the mice. Of note, IFNγ and IL-17A were undetectable after HDM stimulation of either male adult or female neonatal lymph node cultures, illustrating that our model of chronic HDM exposure primarily induced Th2 responses. Finally, TCR-independent stimulation with PMA and ionomycin was used to test whether the dependence of cytokine production on EGFR signalling was antigen-specific. EGFR inhibition limited the amounts of IFNγ and IL-17A as well as the type 2 cytokines IL-4, IL-5 and IL-13 produced in response to stimulation (**Figure 5.10E**). These results suggest that EGFR signalling was required for cytokine production of helper T cells regardless of subtype and provide a potential mechanism by which EGFR inhibition may restrict augmented type 2 responses of female mice during early-life AAD.

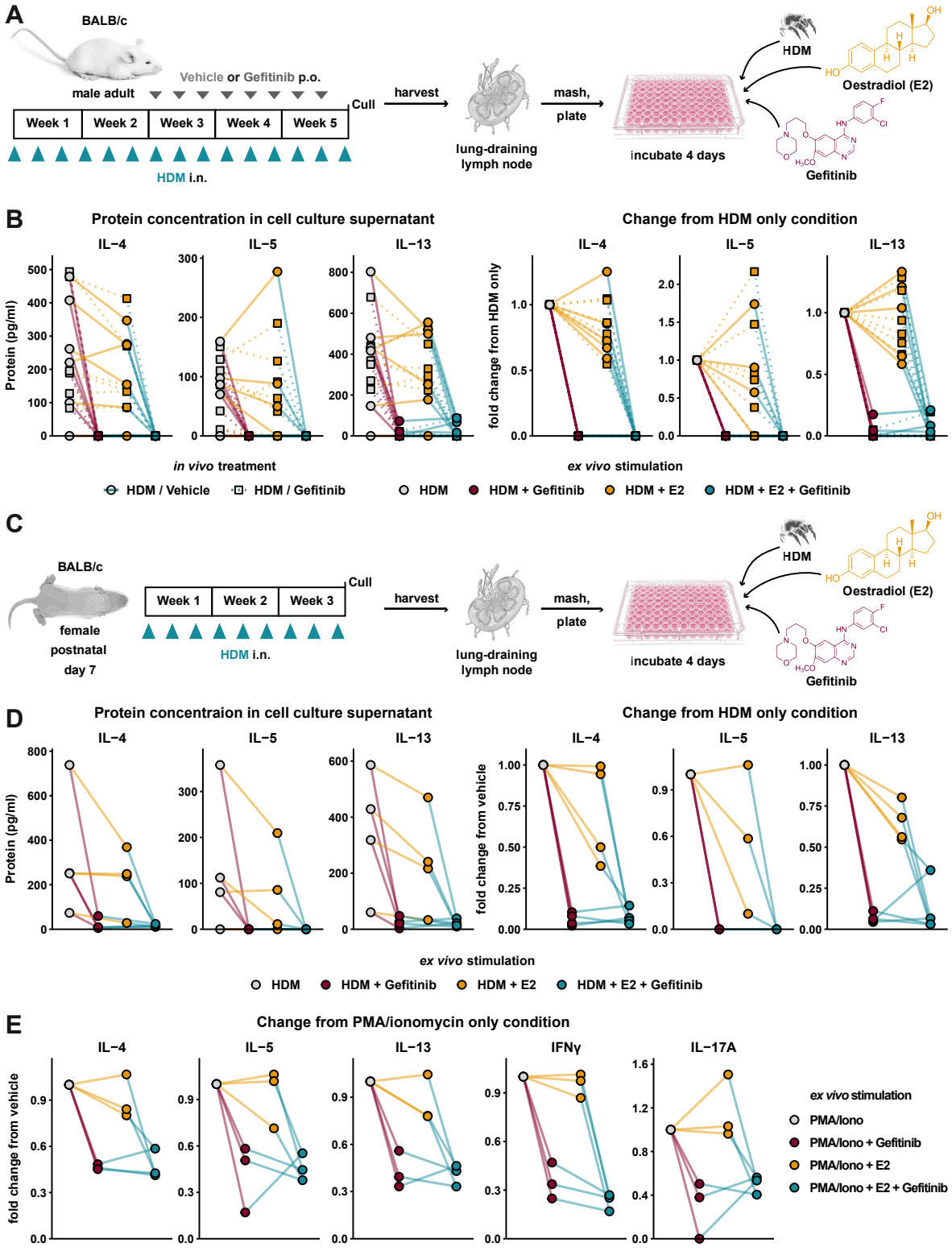


Figure 5.10 EGFR inhibition abrogated cytokine production in lymph node cultures from HDM-exposed animals.

A Male animals were treated as described in Figure 5.8A. Mediastinal lymph node cells from HDM-challenged mice were stimulated with 10 µg HDM in the presence of 10 µM Gefitinib and/or 10 nM oestradiol (E2) and supernatants were collected after 4 days. **B** Cytokines in cell supernatants from (A) by ELISA, plotted as absolute numbers (left) or change from HDM only condition (right). **C** 7-day-old female mice were exposed to HDM for three weeks and LN cells were treated as described in (A). **D** Cytokines in cell supernatants from (C) by ELISA, plotted as absolute numbers (left) or change from HDM only condition (right). **E** Lymph node cells from (C) were stimulated with PMA and ionomycin in the presence or absence of Gefitinib and/or E2. Cytokine levels in supernatants are shown as change from PMA/ionomycin only condition. (B) *n* = 6 per group and treatment. (D-E) *n* = 3-4 per group and treatment. Data from one experiment.

5.4 Discussion

Sex differences in the prevalence and severity of asthma are age-specific, whereby males are more commonly affected during childhood and females in adulthood[307]. The work described in this chapter found that female animals displayed augmented type 2 responses and AAD pathology even when allergen exposure was commenced pre-pubertally at one week of life. Importantly, it identified a novel role for EGFR signalling in supporting exacerbated type 2 immunity specifically in young female mice. Finally, a potential mechanism of action whereby EGFR may directly restrict cytokine production of lymphocytes was identified using EGFR inhibition during antigen-specific re-stimulation of lymph node cultures.

Various studies define a pathogenic contribution of female sex hormones to AAD pathology in adult animals[298-301, 303]. Interestingly, data from the classical OVA model showed that ovariectomy of female mice was only protective when performed before sensitisation rather than between sensitisation and allergen challenge[298]. This suggests that the presence of female sex hormones during the first antigen encounter plays an important role in deciding the magnitude of AAD pathology. However, exposure to common aeroallergens such as HDM can occur from as early as the first breath. Since reports of sex differences in early-life mouse models of AAD are rare, this chapter aimed to investigate how pre-pubertal allergen exposure would affect the sex balance of AAD pathology in adolescent mice. In mice, serum levels of progesterone are lowest at around seven days of age, and oestradiol and testosterone do not increase in concentration until after three weeks of life[311] (**Figure 5.11**). Therefore, the response to the first antigen encounter(s) should be unaffected by the protective or detrimental effects of male or female sex hormones, respectively. Nevertheless, we observed a significant sex bias in AAD pathology in adolescent animals, whereby females displayed exacerbated airway inflammation, eosinophilia, Th2 recruitment and type 2 cytokine production. This suggests that the disease-altering ability of sex hormones acquired during puberty may outweigh any predispositions underlying higher asthma preponderance in males during early life, such as dysanapsis, or the mismatch between the size of the airway tree and the lungs, which is exacerbated in young males and thought to contribute to asthma development[312]. Further studies are warranted to investigate whether mouse models can reflect an increased disease severity of pre-pubertal AAD in males and if so, which exact mechanisms may underlie these sex differences.

An unsuspected but significant finding from this work was that augmented type 2 responses of female animals, and thereby sex differences during early-life AAD, could be ameliorated by the administration of Gefitinib. This suggests that EGFR signalling is necessary to support exacerbated type 2 inflammation of young female mice. Importantly, type 2 responses were

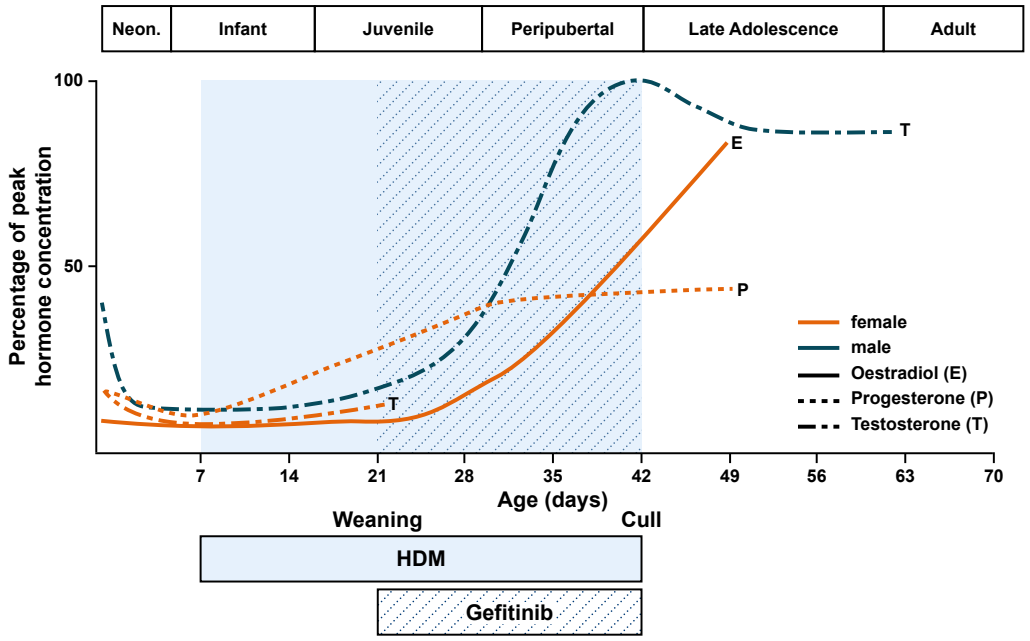


Figure 5.11 Gonadal hormone concentrations throughout murine development.
Adapted from Bell 2018 (ref. [311]). Approximate developmental stages are shown above. Neon = neonatal. Timing of HDM exposure and Gefitinib administration are indicated by blue background and shading, respectively.

unaffected by EGFR inhibition in adult animals of either sex, indicating that the reliance on EGFR signalling to boost type 2 responses is likely specific to the peri-pubertal phase in females. A potential explanation for the discrepant effects of EGFR inhibition between juvenile and adult females may be that EGFR signalling during the first encounter with elevated levels of sex hormones may 'license' exacerbated type 2 responses in the future. In mice, progesterone production commences from approximately day 10 of life, whereas levels of oestradiol do not increase until three to four weeks of life[311]. Gefitinib treatment in the early-life AAD model was initiated at three weeks of life and continued throughout the remainder of the experiment, thus coinciding with the rise in oestradiol levels (**Figure 5.11**). It is thus conceivable that Gefitinib exerted its effect by intercepting the consequences of the first exposure to oestrogen. Previous findings, particularly within the breast cancer field, suggest a reciprocal relationship between oestrogen and EGFR signalling. *In vitro* studies using cancer cell lines have found that both AREG and EGF were able to induce activation of ERα in a ligand-independent manner[313-315]. Conversely, oestrogen signalling induced expression of AREG or TGFα and resulted in EGFR signalling in various breast cancer cell lines[315-317]. Further studies propose that oestrogen induces MAPK signalling in breast cancer cells not via ERα or ERβ, but via binding to the G protein-coupled receptor GPR30, which results in the downstream activation of Erk-1 and Erk-2 in a mechanism dependent on HB-EGF and EGFR activation[308]. Based on these findings, oestrogen may exert its effects on AAD pathology via the activation of EGFR signalling, or else EGFR activation may act to amplify oestrogen signalling.

Despite overwhelming evidence affirming the ability of oestrogen to exacerbate AAD, less is known about the cellular targets and signalling pathways involved in this process. Some studies suggest that oestrogen may act directly on T helper cells to augment their production of type 2 cytokines[318, 319]. Nevertheless, oestrogen has also been found to affect the phenotype of various antigen-presenting cells as well as their ability to induce T cell responses[306, 319, 320]. Thus, it is conceivable that oestrogen exerts its effects by acting on diverse cell types involved in mounting immune responses during AAD. We have previously established that EGFR is expressed on several key cell populations in the allergic lung, including dendritic cells and CD4 T cells (cf. 3.3.3). Therefore, activation of EGFR signalling on these cells may contribute to exacerbated type 2 responses, either in direct crosstalk with or downstream of oestrogen signalling. Further studies are warranted to identify the target cells of oestrogen signalling during AAD and define potential interactions with EGFR signalling either on these cells or within the downstream signalling. However, such investigations are beyond the scope of this thesis.

Nevertheless, first insights into the contributions of oestrogen and EGFR signalling were gained in the context of cytokine production during re-stimulation of lymph node cells. In contrast to previously published reports[318], there were no effects of oestradiol on the ability of lymphocytes to produce type 2 cytokines during *ex vivo* re-stimulation with allergen. Unfortunately, both experiments only included mice of a single sex and it was thus not possible to assess intrinsic differences in cytokine-producing potential between the sexes. Future approaches should include lymphocytes from both male and female mice to assess whether previous exposure to sex hormones such as oestrogen predisposes or 'licenses' female cells to augmented production of type 2 cytokines. Of note, our experiments were limited to male adult or three-week-old female mice, neither of which would have been exposed to high levels of oestrogen *in vivo*, whereas adult females were used by the study that reported enhanced production of IL-4 in response to oestradiol[318]. It is thus possible that previous exposure to oestrogen *in vivo* is required to render T cells responsive to further oestradiol stimulation *ex vivo*, a hypothesis that should also be tested in future experiments using lymph node cells from mice of both sexes and ages.

A striking finding from the re-stimulation experiments of lymph node cultures was the comprehensive ability of Gefitinib to suppress cytokine production. The effects of EGFR inhibition were comparable between HDM and PMA/ionomycin stimulation, suggesting that the role of EGFR in this context was neither allergen-specific nor dependent on antigen presentation. In addition, the inhibitory effects of Gefitinib were not restricted to type 2 cytokines, but also affected the production of IFNγ and IL-17A. In line with the observation that EGFR was expressed by Th1, Th2 and Th17 cells upon HDM exposure (cf. 3.3.3), this

suggests that Gefitinib may have acted directly on these cells to suppress cytokine production. However, it will be important to confirm in future experiments that the overall viability of the cells was not compromised by EGFR inhibition. A study available as a pre-print on bioRxiv has suggested that CD4 T cells require autocrine HB-EGF-EGFR signalling to sustain their expression of IL-2, an important T cell survival factor[321]. Therefore, inhibition of EGFR by Gefitinib may diminish T cell-derived IL-2 production and thus result in T cell death. Future experiments will explore this hypothesis by measuring the effects of Gefitinib on T cell viability in lymph node cultures and including recombinant IL-2 in the culture media to exclude IL-2 starvation as a mechanism by which Gefitinib may suppress type 2 cytokine production.

While the *ex vivo* cultures provide a potential mechanism by which Gefitinib treatment may reduce cytokine production *in vivo*, an explanation for why the effects of EGFR inhibition were specific to Th2 response in young female animals and did not affect Th1 or Th17 response or animals of other ages or male sex is still lacking. It is possible that EGFR inhibition may have altered T cell responses in the lung-draining lymph nodes of male and female animals of all ages, and these tissues should be collected for flow cytometry analysis of T lymphocytes and their potential to produce cytokines in future experiments. However, it is more likely that other mechanisms which contribute to augmented type 2 responses specifically in young female mice were affected by Gefitinib treatment. A recent study has found that oestrogen signalling through ERα amplified epithelial IL-33 release in response to allergen exposure, thus resulting in exacerbated type 2 responses in female animals[303]. In line with this, the work in this thesis demonstrated increased levels of IL-33 protein in the lungs of female compared to male mice both in the presence and absence of EGFR inhibition. This suggests that the sex differences observed during early-life AAD may have been driven by heightened IL-33 production in female mice due to the presence of oestrogen and that EGFR inhibition likely acted downstream of alarmin release to minimise type 2 responses in young females. As demonstrated both within this thesis and within the wider literature, IL-33 can induce many classical features of AAD in both young and adult animals, such as eosinophilia, expansion of ILC2s and Th2 cells, production of type 2 cytokines and airway hyperresponsiveness (cf. 4.3.1, ref. [56]). Thus, the augmented type 2 responses of female mice within our model may be the direct consequence of heightened availability of IL-33 within the lungs of these animals. The existence of an oestrogen-IL-33 axis in early-life AAD and its role in driving augmented type 2 responses of female animals will be explored in future experiments by evaluating the effects of oestrogen supplementation or blocking on pulmonary IL-33 levels as well as the ability of IL-33 administration to boost type 2 responses of young male mice exposed to HDM. Interestingly, Minutti et al. 2017 (ref. [127]) found that in the context of gastrointestinal helminth infections, EGFR signalling of Th2 cells was required to license IL-13 production in response

to antigen-independent stimulation with IL-33. Specifically, TCR signalling in Th2 cells induced the expression of EGFR, which could be maintained by exposure to the alarmin TSLP. EGFR activation was induced in an autocrine manner via AREG produced by Th2 cells and activated $EGFR^+$ Th2 cells expressing the IL-33 receptor ST2 were able to respond to IL-33 stimulation with the production of IL-13. This signalling process was crucial to the anti-helminth response, as illustrated by increased worm burden and reduced IL-13 levels in mice deficient for EGFR expression on $CD4^+$ cells. In addition, an IL-33-AREG-EGFR-axis has also been shown to contribute to other T helper cell responses, such as differentiation and IL-9 production of anti-tumour Th9 cells[322]. While T cell-derived AREG acted in an autocrine manner on EGFR-expressing Th2 or Th9 cells in the previous two contexts, a mechanisms whereby IL-33-driven AREG production by memory Th2 cells contributes to allergic airway disease by acting on EGFR-expressing eosinophils has also been described[136]. It will be interesting to investigate whether IL-33 signalling also drives Th2 cytokine production in an EGFR-dependent manner in the context of early-life AAD, as this constitutes a potential mechanism by which EGFR inhibition may specifically restrict type 2 responses in animals with heightened levels of IL-33, such as the female animals within our model. Future experiments should aim to investigate this mechanism in more detail, for example by examining whether oestrogen can boost epithelial IL-33 release in response to HDM, and whether IL-33 stimulation of Th2 cells from allergen-exposed animals is sufficient to trigger the release of IL-13 or other type 2 cytokines, and if so, whether this effect is dependent on EGFR signalling. A summary of the potential mechanisms contributing to augmented type 2 responses of young females in shown in **Figure 5.12**.

Finally, the findings from this chapter may have therapeutic implications in the prevention of exacerbated asthma severity in females entering adulthood. The inability of Gefitinib treatment to affect type 2 responses of adult females suggests that adolescence may provide a unique window opportunity for EGFR inhibition. It will be interesting to investigate whether Gefitinib treatment during adolescence is sufficient to protect female animals from augmented type 2 responses even after Gefitinib treatment is ceased. If so, the benefits of EGFR inhibition in adolescence for reducing the severity of asthma in females should be further explored. However, it is worth recalling that in addition to dampening type 2 responses of female mice, EGFR inhibition also resulted in exacerbated airway hyperresponsiveness in animals of both sexes. In addition, EGFR TKIs such as Gefitinib can cause various adverse effects, including interstitial lung disease, and their use is therefore largely restricted to the treatment of chemotherapy-resistant cancers[249]. Other EGFR inhibitors, such as the inhaled antagonist BIBW 2948 BS, have previously been trialled for the treatment of COPD but were poorly tolerated[187]. In contrast, Itepekimab, a monoclonal antibody targeting IL-33, was well tolerated

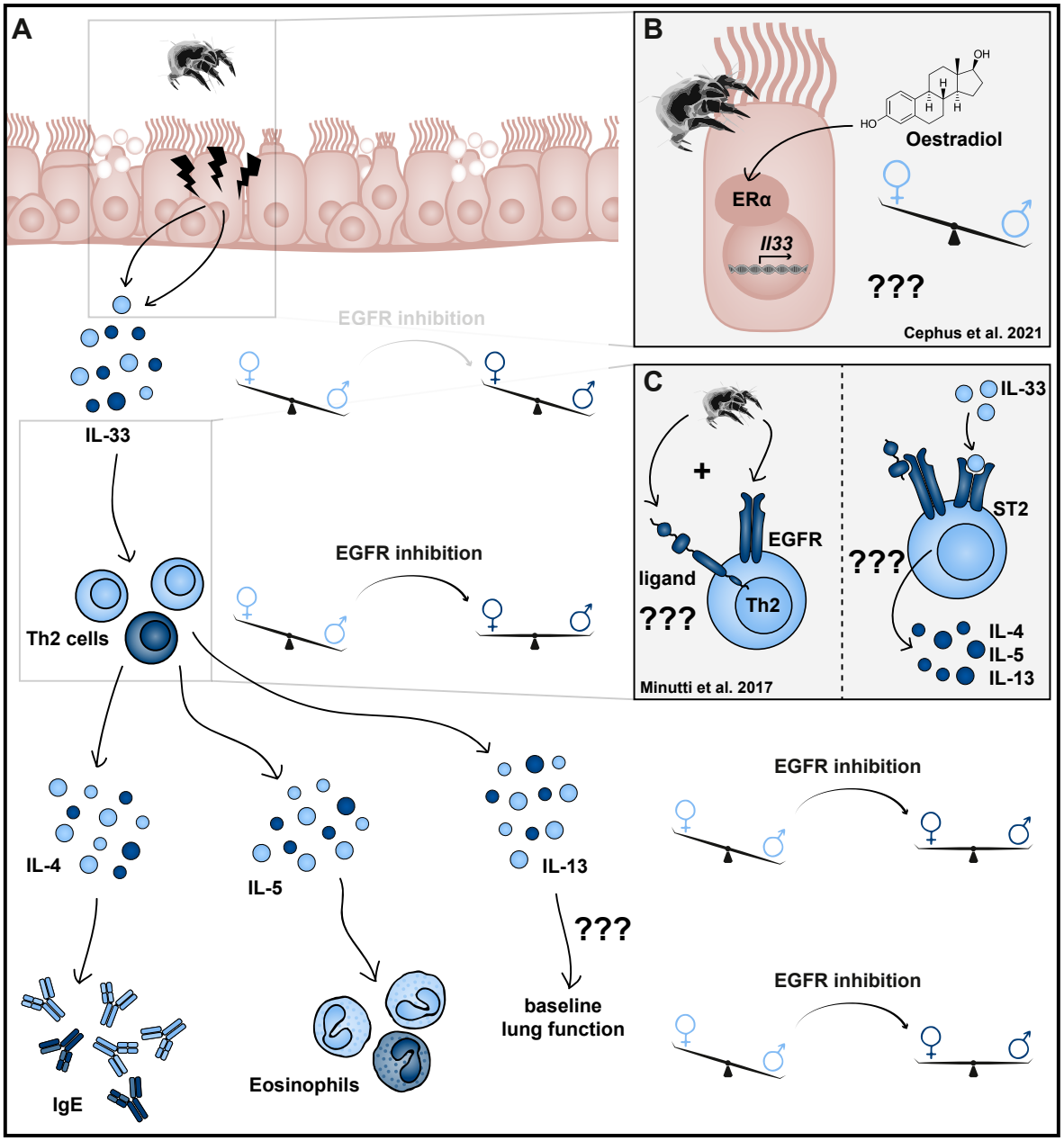


Figure 5.12 EGFR inhibition abrogates augmented type 2 responses in young females: potential mechanism.
A In response to allergen exposure during early life and adolescence, IL-33 is released from the airway epithelium. The alarmin then likely acts directly or indirectly on Th2 cells to drive their production of IL-4, IL-5 and IL-13. This type 2 immune response results in the generation of IgE antibodies and the recruitment of eosinophils and may also underlie worsened baseline lung function. Young female animals display worsened alarmin release and type 2 immunity compared to male mice. These augmented responses are dampened by EGFR inhibition, which acts downstream of IL-33 to minimise sex differences. **B** Increased IL-33 production in female animals may be caused by rising oestradiol levels signalling via ERα to boost Il33 expression (as described similarly by Cephus et al. 2021 (ref. [303]). **C** HDM exposure results in the upregulation of EGFR on Th2 cells and may also induce ligand expression in these cells. EGFR signalling may 'licence' Th2 cells to produce type 2 cytokines independently of allergen stimulation in response to IL-33/ST2 signalling. A similar mechanism was delineated by Minutti et al. 2017 (ref. [127]).

in phase I and phase II trials and showed some efficacy in reducing the incidence of loss of asthma control and improving lung function in patients with moderate-to-severe asthma[70, 71]. Although no longer pursued in the treatment of asthma[72], Itepekimab is currently undergoing

a phase III trial to assess its efficacy, safety and tolerability in patients with moderate-to-severe COPD[323]. Within these trials, it would be interesting to determine whether anti-IL-33 treatment may be more efficacious in young women. If so, targeting IL-33 during puberty may present a safer strategy to minimise asthma severity in adolescent females than EGFR inhibition.

5.5 Concluding remarks and future work

Prevalence and severity of asthma are governed by sex differences, with a higher preponderance in females emerging throughout puberty. This work showed that adolescent female animals exhibited significantly exacerbated type 2 responses even when allergen exposure was commenced pre-pubertally, along with elevated levels of pulmonary IL-33. Peri-pubertal inhibition of EGFR signalling specifically ameliorated type 2 responses but not IL-33 levels in adolescent females, while adolescent males or adults of either sex were unaffected. These findings prompted the formation of a novel hypothesis, whereby rising oestrogen levels in young female mice may drive increased epithelial production of IL-33 in the context of allergen exposure and EGFR signalling in activated Th2 cells may be required to license the antigen-independent production of type 2 cytokines from these cells in response to this alarmin. Future experiments will aim to delineate this mechanism by establishing the ability of oestrogen to boost IL-33 production both *in vitro* and *in vivo*, defining the role of IL-33 in augmenting type 2 immunity in early-life AAD by IL-33 blockade in female or supplementation in male mice, respectively, and assessing the ability of IL-33 to directly drive type 2 cytokine secretion in lymph node cultures from HDM-exposed animals in an EGFR-dependent manner. An in-depth understanding of the processes driving the emergence of sex differences in AAD may have important therapeutic implications for the prevention of more severe asthma pathology in young women.

6 Results IV:

Characterising SARS-CoV-2 infection in paediatric and adult airway epithelial cells

6.1 Introduction

6.1.1 SARS-CoV-2 and COVID-19 in children and adults

Coronavirus disease 19 (COVID-19) is a global pandemic that emerged in the province of Wuhan, China at the end of 2019. The World Health Organisation (WHO) estimates that over 6.5 million people have died from COVID-19 to date (October 2022), with over 625 million cases reported globally. Great efforts have been made to investigate the pathophysiology of COVID-19 since it was first described in February 2020[324-326]. Among the initial findings was the observation that children typically experienced less severe disease compared to adults. Whereas approximately 20% of adults developed severe or critical disease during the first wave of COVID-19[327, 328], fatality was rare in children, the majority of which remained asymptomatic or experienced only mild to moderate symptoms[329-331]. In addition, studies on the household transmission of COVID-19 suggested that children may exhibit reduced susceptibility to infection compared to adults[332-334].

COVID-19 is caused by infection with severe acute respiratory syndrome coronavirus 2 (SARS-CoV-2), a positive-sense single-stranded RNA (+ssRNA) virus of the coronaviridae family[324-326]. SARS-CoV-2 binds to the host receptor angiotensin converting enzyme 2 (ACE2) in susceptible cells via its spike protein and gains entry in a process depending on the host protease transmembrane serine protease 2 (TMPRSS2)[335]. Other host proteases, such as cathepsin L, furin and neuropilins, were found to contribute to the pre-activation and entry of SARS-CoV-2[336-340]. Although co-expression of ACE2 and TMPRSS2 has been reported in various organs, including the conjunctiva, gall bladder and several parts of the gastrointestinal tract[341], the airway epithelium is the primary portal of entry for SARS-CoV-2[342]. Severe or critical disease occurs when the epithelium of the large conducting airways is unable to contain the infection and the virus progresses to the alveoli.

6.1.2 The role of the airway epithelium and interferons in the defence against SARS-CoV-2

The airway epithelium plays a central role in the defence against numerous respiratory viruses[343]. In addition to creating a physical barrier between the external and internal milieu which is further reinforced by a protective layer of mucus to trap pathogens and movement of the cilia which contribute to clearance, airway epithelial cells constitute an early source of antiviral and pro-inflammatory mediators. Upon viral recognition via one or several pattern recognition receptors (PRRs), type I and type III interferons (IFNs) are released from epithelial cells and act in an auto- and paracrine manner to trigger the expression of hundreds of

interferon-stimulated genes (ISGs). The antiviral mediators induced in this way can act both through direct interference with viral replication and spread, for example by suppressing the transcriptional machinery, or via the recruitment and activation of specialised immune cells. The importance especially of type I IFNs in the successful defence against respiratory viruses such as influenza A and SARS-CoV-2 is illustrated by the increased incidence of severe or life-threatening disease in individuals with mutations in or auto-antibodies against molecules in the type I IFN signalling pathway[344-347]. In addition, the benefits of type I or III IFNs in aiding the clearance of SARS-CoV-2 have been demonstrated during *in vitro* infection of primary airway epithelial cells[348-351].

6.1.3 Towards understanding differences in COVID-19 severity between children and adults

As part of the overwhelming wealth of research into the pathophysiology underlying COVID-19, various efforts have been made to explain why severe disease is less common in children. Some studies have described a lower expression of ACE2 and TMPRSS2 in the airway epithelia of children compared to adults, which may result in greater resistance to infection[352, 353]. However, numerous other reports found no differences in the levels of entry receptors between children and adults[354-357], suggesting that this conclusion should be interpreted with caution. Another proposed explanation for the discrepancies in disease severity is that children may be more poised to detect and react to infection with SARS-CoV-2. A comparison of the upper airway transcriptome of children and adults using RNA-sequencing of nasal swabs revealed higher expression of *IFIH1* and *DDX58*, which encode the PRRs melanoma differentiation-associated protein 5 (MDA5) and retinoic acid-inducible gene I (RIG-I), respectively, in paediatric compared to adult epithelial cells[356]. MDA5 plays an essential role in the recognition of SARS-CoV-2 and subsequent interferon induction[348, 358]. Therefore, it is conceivable that heightened expression of this receptor in the airway epithelium of children may result in more rapid detection and clearance of SARS-CoV-2 and thus less severe disease. In support of this, another study comparing transcriptional responses in nasopharyngeal swabs of children and adults admitted to the hospital with COVID-19 found interferon signatures and inflammatory genes to be enriched in the paediatric samples[357]. Importantly, heightened immune responses were associated with better clinical outcomes in this cohort, providing additional support to the idea that children may experience less severe disease because they are better armed to mount effective antiviral responses. These findings were further affirmed by a more recent single-cell transcriptomic analysis of airway and blood samples from a distinct cohort of children and adults with or without COVID-19. This study reported an enhanced interferon-activated state in the airways of children even in the absence

of infection, which was further increased particularly in airway immune cells by SARS-CoV-2 infection[359]. Nevertheless, other factors are likely to contribute to better outcomes of COVID-19 in children. For example, SARS-CoV-2-cross-reactive antibodies likely induced in response to seasonally circulating coronaviruses were more commonly found in the sera of children and adolescents compared to adults and may feasibly contribute to better protection against COVID-19 in these age groups[360]. Taken together, the analysis of clinical samples has provided valuable insights into the potential causes for reduced disease severity of COVID-19 in children, but more mechanistic studies are lacking. For instance, it is unclear whether the heightened PRR expression and interferon signatures found in the airways are an intrinsic feature of paediatric epithelia or the consequence of a combination of environmental exposures, such as previous infections with respiratory viruses. In an effort to address this, infection of ALI cultures with SARS-CoV-2 was used to perform a detailed comparison of viral tropism as well as the cellular immune responses between paediatric and adult airway epithelial cells.

6.1.4 Hypothesis and aims

Hypothesis

Differences in the responses of paediatric and adult bronchial epithelial cells to infection with SARS-CoV-2 underlie the disparate prevalence and severity of COVID-19 between children and adults

Aims

1. To establish a model of SARS-CoV-2 infection in primary airway epithelial cells cultured at ALI.
2. To compare the epithelial responses to SARS-CoV-2 infection between paediatric and adult epithelial cells.
3. To examine similarities and differences in the epithelial immune response elicited by infection with SARS-CoV-2 and the 2009 pandemic strain of Influenza A H1N1.

6.2 Methods

6.2.1 Collection and culture of primary airway epithelial cells from healthy paediatric and adult donors

Nasal and bronchial epithelial cells were collected from healthy children aged 2-5 without history of wheezing or other respiratory pathology (*n* = 6) using nasal or non-bronchoscopic lower airway bronchial brushing, respectively. Children who were having an elective surgical procedure that required intubation were recruited and a non-bronchoscopic brushing was taken after intubation and prior to the surgical procedure as previously described[361]. Healthy adult volunteers (*n* = 4) were recruited for bronchoscopies, during which bronchial epithelial cells were collected via bronchial brushings. Donor demographics are listed in **Table 6.1**. Airway epithelial cells were expanded and cultured at ALI until cilia movement and mucus production were observed, indicative of a well-differentiated epithelial layer.

Table 6.1 Donor demographics.

	Paediatric (*n* = 6)	**Adult (*n* = 4)**
Median age in years (range)	4.6 (2.5-5.6)	52.5 (47-63)
Female sex (%)	3 (50%)	2 (50%)
Ethnicity (%)		
Asian	1 (17%)	2 (50%)
White Caucasian	4 (67%)	2 (50%)
Mixed Black / White Caucasian	1 (17%)	-
Atopy status (%)		
Atopic	3 (50%)	-
Non-Atopic	3 (50%)	-
Unknown	-	4 (100%)
Smoking status (%)		
Current smoker	n/a	0 (-)
Ex-smoker		2 (50%)
Never smoker		2 (50%)

6.2.2 Infection of airway epithelial cultures with SARS-CoV-2 and H1N1

Fully differentiated epithelial cell cultures were infected apically with either SARS-CoV-2 (strain SARS-CoV-2/England/IC19/2020; MOI 0.01) or Influenza H1N1 (strain A/England/195/2009; MOI 0.001) for 1 hour. Apical washes, basal media, cell lysates and fixed cell layers were collected on alternate days from day one post-infection (dpi) until 9 dpi.

6.2.3 Analysis of the epithelial response to infection

The release of infectious viral particles from cells was monitored using plaque assays of apical washes. Gene expression changes in response to infection were assessed in cell lysates by qPCR. The secretion of proteins into the basal medium was measured using conventional ELISAs and a membrane-based proteome profiler assay. Fixed epithelial layers were agarose-embedded and sectioned. Traditional H&E staining and immunofluorescence staining of sections were used to visualise changes in overall epithelial morphology and to investigate the localisation of SARS-CoV-2 infection.

6.3 Results

6.3.1 Establishing SARS-CoV-2 infection in nasal and bronchial epithelial cell ALI cultures

Both nasal and bronchial airway epithelial cells are thought to constitute a first point of entry for SARS-CoV-2[342]. To confirm whether bronchial epithelial cells could be used as a model to study SARS-CoV-2 of airway epithelia, the morphology, entry factor expression and immune response to infection was compared between matched bronchial and nasal epithelial cells from healthy paediatric donors after differentiation at ALI culture (**Figure 6.1A**). Cells from both anatomical locations displayed comparable morphology (**Figure 6.1B**) as well as expression of the SARS-CoV-2 entry factor ACE2, which was detected across the entire epithelial layer (**Figure 6.1C**).

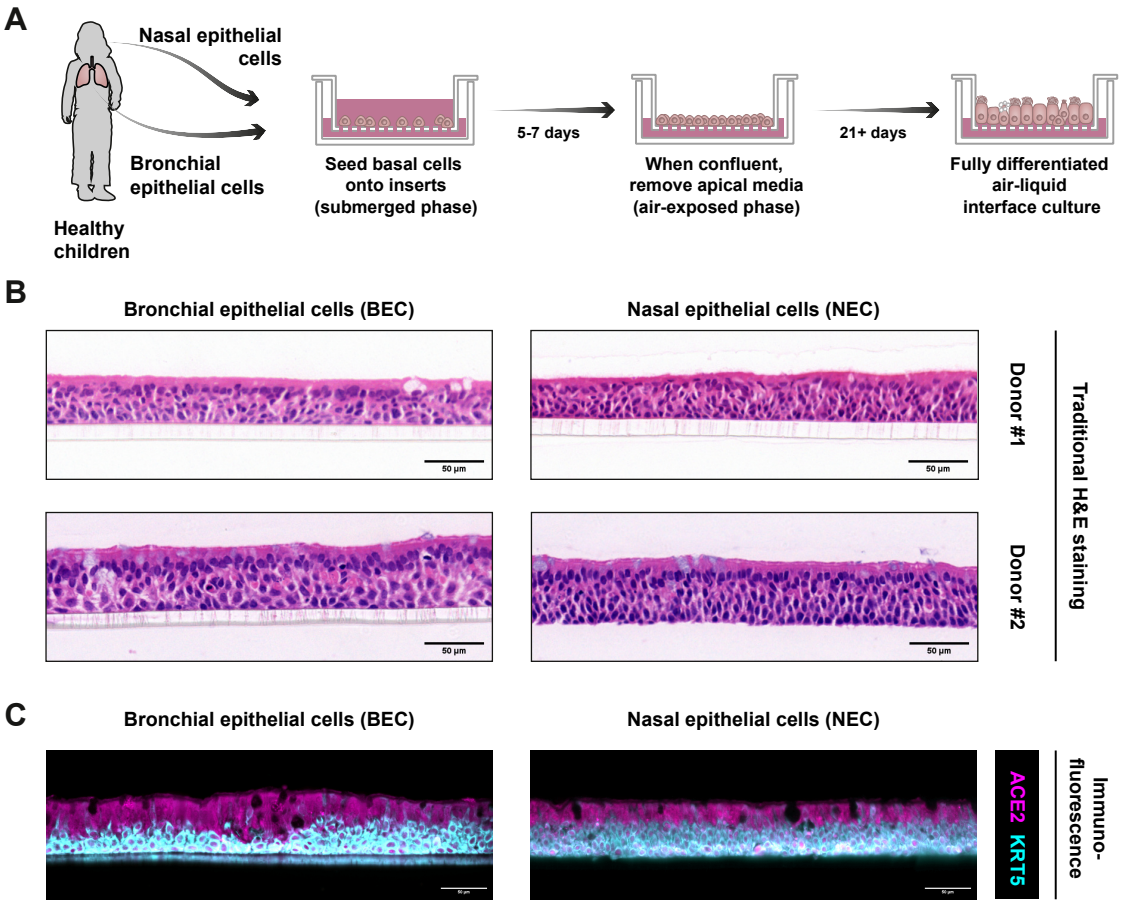


Figure 6.1 Fully differentiated nasal and bronchial epithelial cells displayed comparable morphology and SARS-CoV-2 entry factor expression.
A Nasal and bronchial epithelial cells were collected from healthy children and seeded onto inserts. Upon confluency, apical media was removed and cells were cultured until they displayed beating cilia and mucus production. **B** H&E staining of sections from fully differentiated matched nasal and bronchial epithelial cells from two paediatric donors. **C** Representative immunofluorescence staining of sections using antibodies for the SARS-CoV-2 entry receptor ACE2 (magenta) and the basal cell marker KRT5 (cyan). Size of scale bar: 50 µm.

Next, bronchial or nasal cultures were infected with an early clinical isolate of SARS-CoV-2 (SARS-CoV-2/England/IC19/2020) to compare viral replication and epithelial immune responses (**Figure 6.2A**). SARS-CoV-2 infected and replicated in airway epithelial cells from both locations and there were no differences in the release of infectious viral particles between nasal and bronchial epithelial cells (**Figure 6.2B**). In line with this, the levels of type I IFNs, type III IFNs and ISGs induced by SARS-CoV-2 infection in nasal and bronchial cells displayed comparable magnitude (**Figure 6.2C**). These results suggest that bronchial epithelial cells can be used as a model to study SARS-CoV-2 infection of airway epithelia.

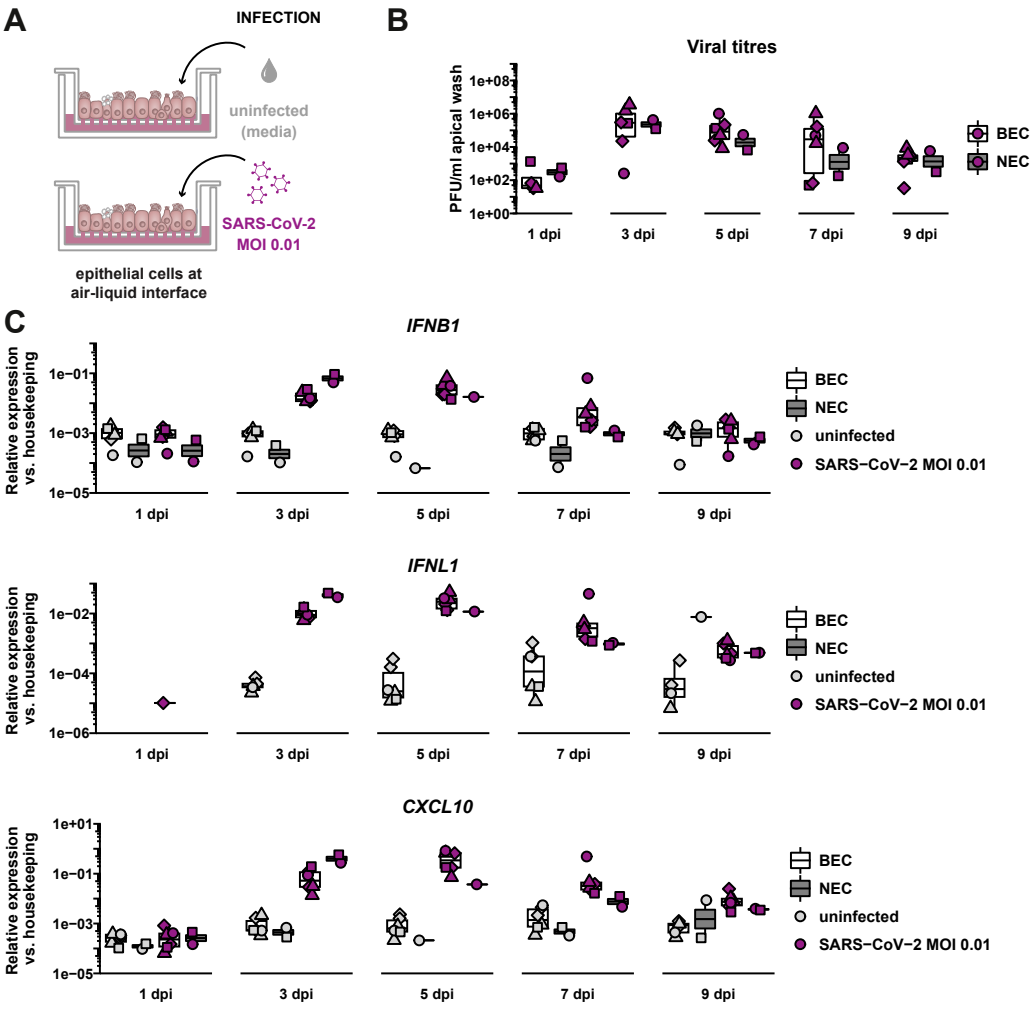


Figure 6.2 Replication of and interferon responses elicited by SARS-CoV-2 were similar between nasal and bronchial epithelial cells.
A Fully differentiated paediatric nasal (NEC) and bronchial (BEC) epithelial cells (ref. Figure 6.1A) were infected with SARS-CoV-2 MOI 0.01 or treated with media. **B** Plaque forming units of SARS-CoV-2 in the apical wash of infected epithelial cells at different timepoints post infection. **C** Expression levels of indicated genes in the cell lysates of infected paediatric BECs or NECs at different timepoints post infection. Matched donors are indicated using the same symbol shape.

6.3.2 Comparing responses to SARS-CoV-2 infection between bronchial epithelial cells from healthy children and adults

The primary aim of this chapter was to compare paediatric and adult airway epithelial cells regarding their susceptibility to infection with SARS-CoV-2, viral tropism and immune response elicited by the infection. To start off, the morphology and SARS-CoV-2 entry receptor expression were compared between uninfected bronchial epithelial cells from six paediatric and four adult donors (**Figure 6.3A**). Overall, paediatric and adult epithelial layers displayed comparable morphology and composition (**Figure 6.3B**), which was further confirmed by measuring the expression of *FOXJ1* (ciliated cells), *KRT5* (basal cells), *MUC5AC* and *MUC5B* (goblet cells) as well as *TJP1* (tight junctions) (**Figure 6.3C**). Epithelial height, while variable, was not significantly different between age groups (**Figure 6.3D**). As a measure of potential susceptibility to infection with SARS-CoV-2, sections were stained for the entry receptor ACE2, which was expressed across the entire epithelial layer in both paediatric and adult cells (**Figure 6.3E**). There were also no differences in the mRNA levels of other SARS-CoV-2 entry-related genes between age groups (**Figure 6.3F**). Finally, the expression of *DDX58* and *IFIH1*, encoding RIG-I and MDA5, respectively, was measured, as these were previously found to be upregulated in the nasal epithelia of children[356]. However, there were no differences in the levels of these two PRRs between paediatric and adult bronchial epithelial cells (**Figure 6.3G**). Overall, these findings suggest that bronchial epithelial cells from children and adults are comparable in their composition and likely also in their susceptibility to SARS-CoV-2 infection based on their expression of entry-related genes.

To directly compare viral entry, replication and epithelial immune responses between paediatric and adult epithelial cells, differentiated cultures were infected with SARS-CoV-2 or left uninfected (**Figure 6.4A**). Infection with influenza H1N1 was included to aid the characterisation of epithelial SARS-CoV-2 infection in comparison to another pandemic respiratory RNA virus. To assess which cells were being infected with SARS-CoV-2, epithelial layers were stained for nucleocapsid protein (NP) (**Figure 6.4B-C**). NP signal was restricted to the apical side and did not co-localise with goblet cell (MUC5AC) or basal cell (KRT5) markers in either paediatric or bronchial epithelial cells, suggesting that ciliated cells were the primary target of SARS-CoV-2 infection in both groups. Interestingly, the number of cells containing SARS NP visible increased between 3 and 5 dpi, indicative of active viral replication.

For a more detailed characterisation of viral replication, the release of infectious particles into the apical wash of epithelial cultures was measured using plaque assays. The number of infectious SARS-CoV-2 particles in the apical wash increased dramatically between 1 and

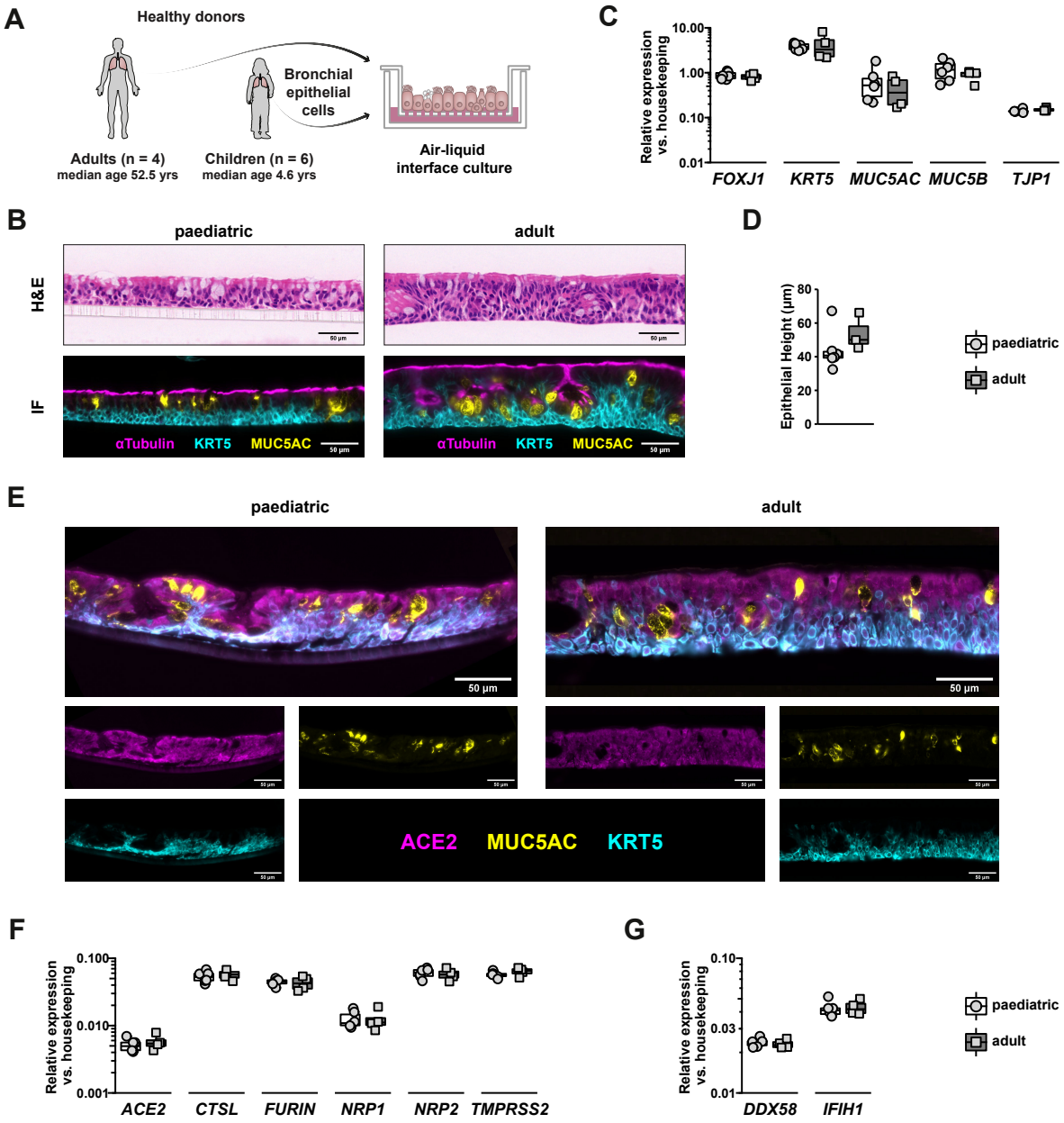


Figure 6.3 Fully differentiated paediatric and adult bronchial epithelial cells displayed comparable morphology and SARS-CoV-2 entry factor expression.
A Bronchial epithelial cells (BECs) from healthy children (*n* = 6) and adults (*n* = 4) were differentiated at air-liquid interface. **B** Representative images of H&E and immunofluorescence staining using indicated markers of sections from fully differentiated paediatric and adult BECs. **C** Gene expression of epithelial subset-associated genes in cell lysates by qPCR. **D** Epithelial height as measured in H&E-stained cross-sections. **E** Representative images of immunofluorescence staining for ACE2 (*magenta*), goblet cells (MUC5AC; yellow) and basal cells (KRT5; cyan). **F-G** Gene expression of SARS-CoV-2 entry-related genes (F) or pattern recognition receptors (G) in cell lysates using qPCR. Size of scalebars: 50 μm.

3 dpi and peaked between 3-5 dpi (**Figure 6.5A**). Release of infectious virus was still detectable at the latest timepoint (9 dpi) and there were no differences between age groups (**Figure 6.5B**), indicating that SARS-CoV-2 was able to successfully establish and maintain productive infection in both paediatric and adult bronchial epithelial cells. Of note, the numbers of infectious particles released from H1N1-infected cells were significantly higher than those detected in apical washes from SARS-CoV-2-infected cells, particularly at the earliest time

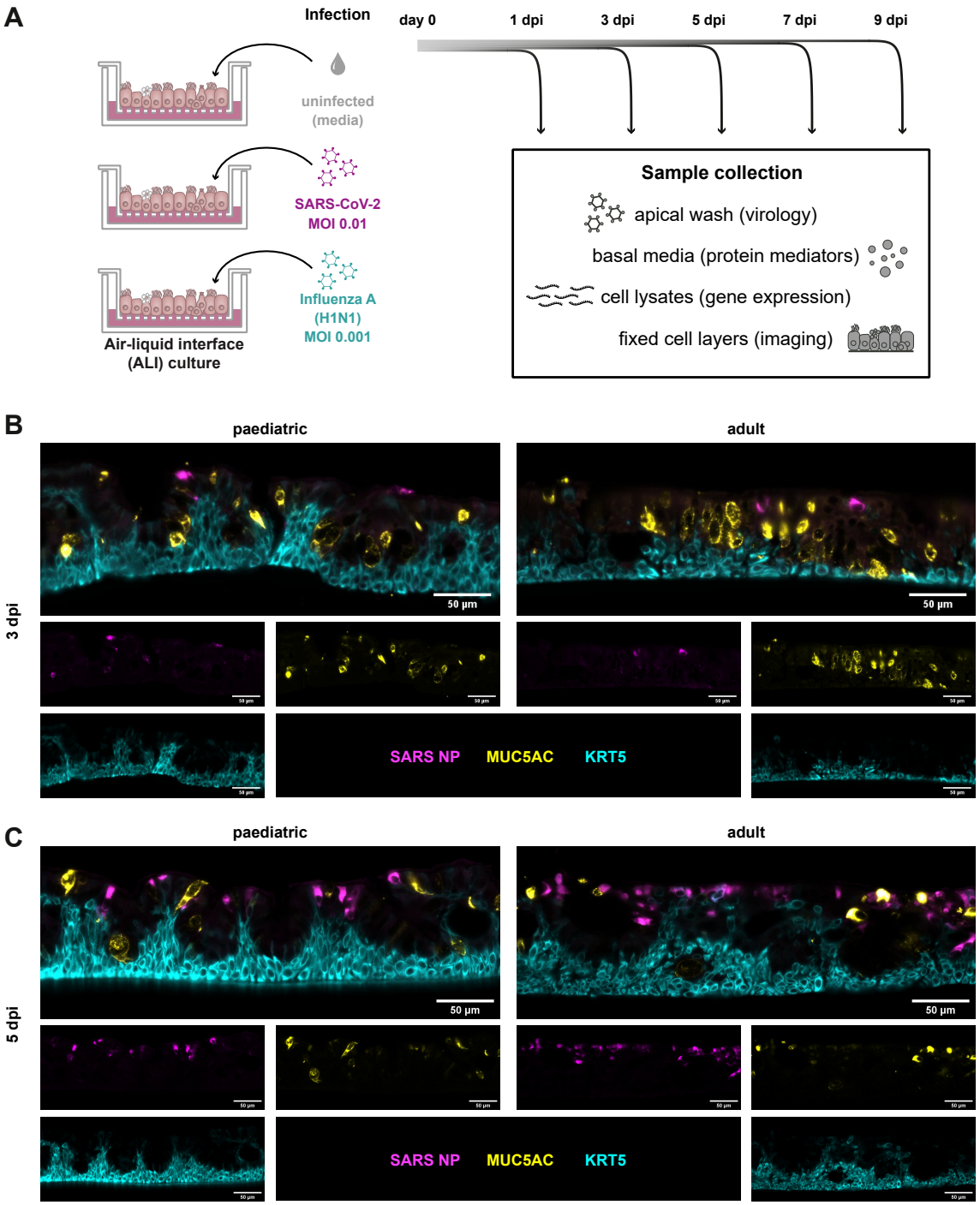


Figure 6.4 SARS-CoV-2 primarily infected ciliated cells in paediatric and adult bronchial epithelial cell cultures.
A Fully differentiated bronchial epithelial cells (BECs) from paediatric and adult donors (ref. Figure 6.3A) were infected with SARS-CoV-2 (MOI 0.01), Influenza A H1N1 (MOI 0.001) or treated with medium (uninfected) and samples were collected every other day until 9 days post-infection (dpi). **B-C** Representative immunofluorescence images of sections of paediatric and adult epithelial cell layers infected with SARS-CoV-2 at 3 dpi (B) or 5 dpi (C). Sections were stained for SARS nucleocapsid protein (NP; magenta), goblet cells (MUC5AC; yellow) and basal cell (KRT5; cyan). Size of scalebars: 50 µm.

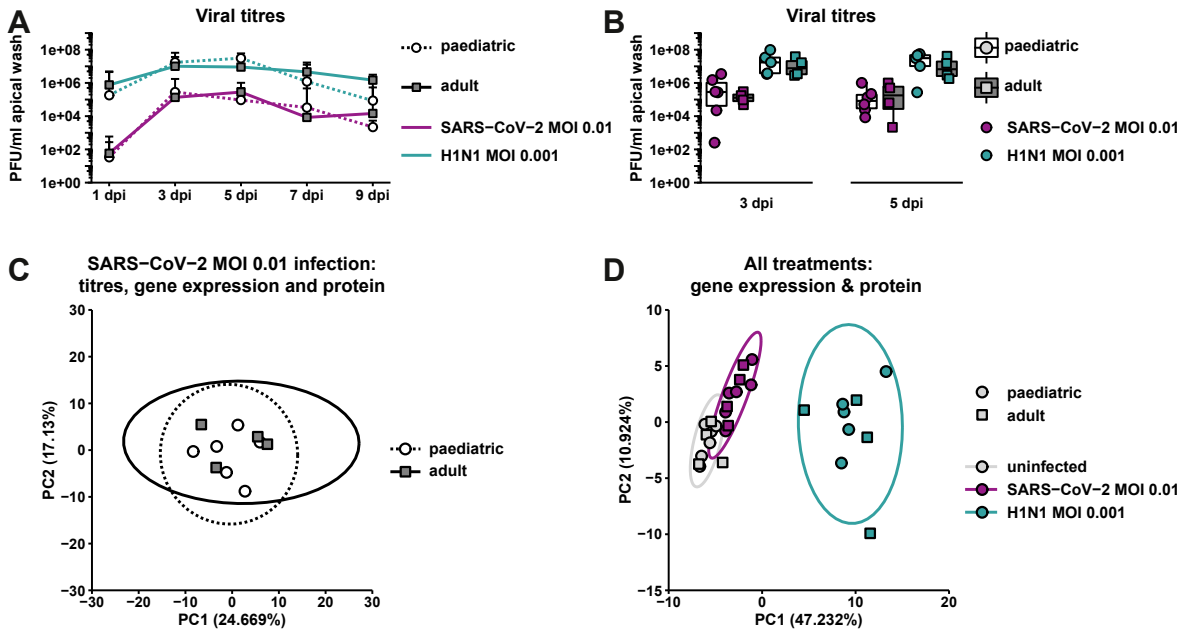


Figure 6.5 Epithelial responses to infection differed between viruses but not between ages.
Cells were infected as shown in Figure 6.4A. **A-B** Plaque forming units of SARS-CoV-2 and H1N1 in the apical wash of infected epithelial cells at different timepoints post infection. Data in (A) are shown as median + confidence interval. **C** Principal components analysis (PCA) of 121 variables measured in SARS-CoV-2 infected cells across five timepoints. Data include viral titres, expression of 28 genes and concentration of two proteins in the basal media. The first two principal components (PC) are plotted. Each data point represents one donor **D** PCA of 98 variables measured in epithelial cells infected with SARS-CoV-2, H1N1 or left untreated. Data include expression of 28 genes and concentration of two proteins in the basal media at up to five timepoints. Each data point represents one treatment of one donor.

point, despite a lower starting MOI of the former, suggesting that H1N1 infected and replicated more readily in bronchial epithelial cells.

PCA was used to perform a holistic comparison of viral replication and epithelial immune responses at gene and protein level between SARS-CoV-2-infected paediatric and adult bronchial epithelial cells (**Figure 6.5C**). Surprisingly, this analysis revealed a complete overlap between age groups, indicating that age was not a primary driver of heterogeneity within this data set and suggesting that SARS-CoV-2 infection was comparable between cells from children and adults. In contrast, a similar analysis comparing the effects of the different viral infections on gene expression and protein release revealed a clear separation between H1N1-infected cells and SARS-CoV-2-infected cells, the latter of which clustered close to uninfected cells (**Figure 6.5D**). These findings suggest an increased ability of H1N1 to affect epithelial cell responses compared to SARS-CoV-2, in line with heightened infectivity and viral replication.

6.3.3 Comparing epithelial cell responses to infection with SARS-CoV-2 and H1N1

Given the striking differences between SARS-CoV-2 and H1N1 infection revealed by our PCA, the consequences of infection with either of these viruses were characterised in more detail. H&E analysis revealed gross changes to the morphology of H1N1-infected epithelial layers, indicative of damage and loss of cell differentiation, whereas SARS-CoV-2-infected layers were indistinguishable from uninfected controls (**Figure 6.6A**). In line with this, there was a significant loss of expression of ciliated, basal and goblet cell-associated genes after infection with H1N1 which was largely absent in SARS-CoV-2-infected cells (**Figure 6.6B**). In contrast, SARS-CoV-2 infection resulted in the upregulation of the tight junction protein *TJP1*,

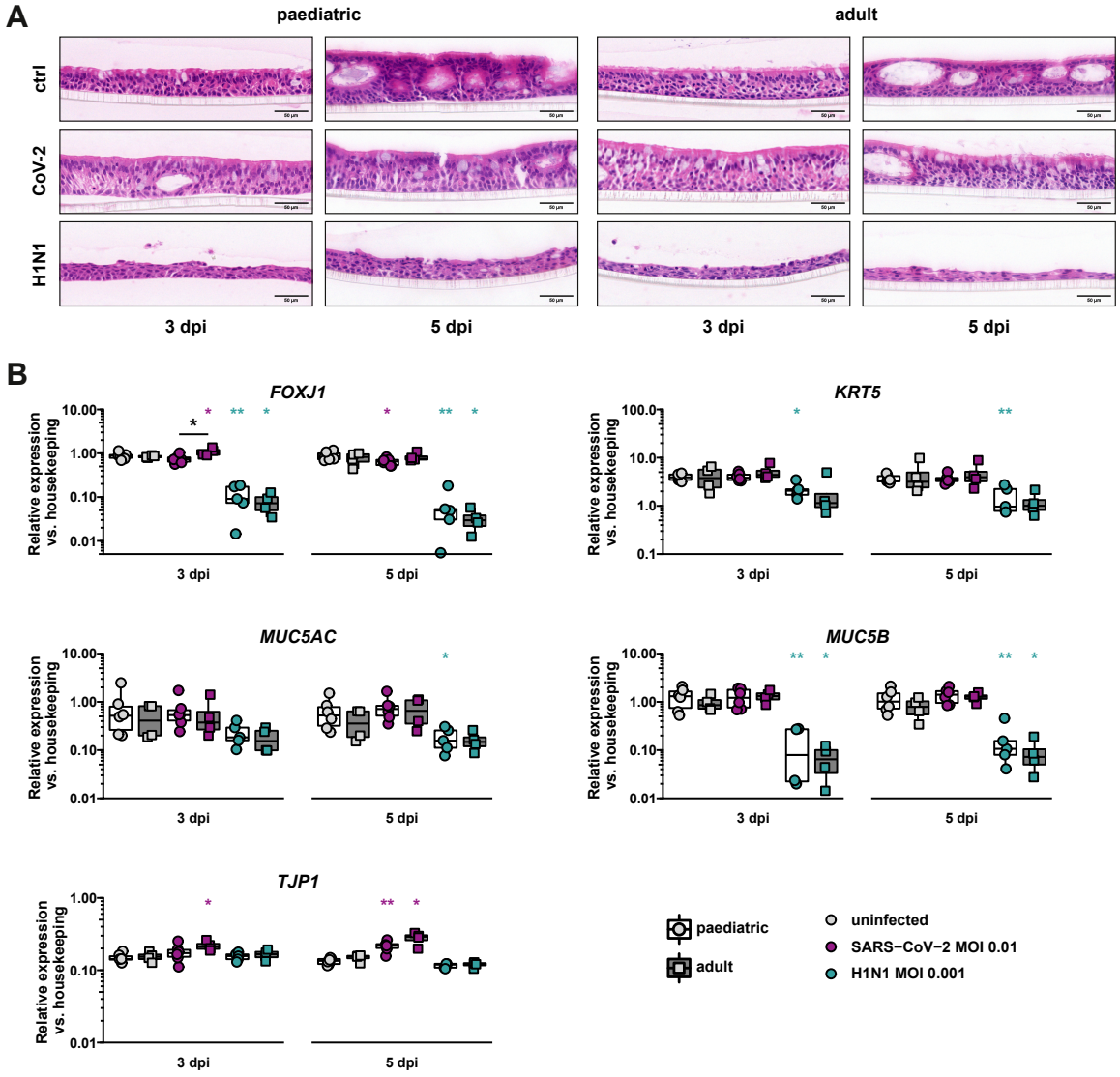


Figure 6.6 Infection with H1N1 but not SARS-CoV-2 resulted in altered epithelial morphology.
Cells were infected as shown in Figure 6.4A. **A** Representative H&E images of infected paediatric or adult epithelial cells. **B** Gene expression of indicated genes in cell lysates from cells infected with SARS-COV-2 or H1N1 at 3 or 5 dpi. Statistics: Mann-Whitney test between indicated age groups (black) or compared to relevant uninfected control (coloured). *, $p < 0.05$; **, $p < 0.01$.

potentially indicative of an increase in epithelial integrity. Except for slightly increased expression of *FOXJ1* in adult SARS-CoV-2-infected cells, there were no differences between age groups. Together, these data provide further indication that paediatric and adult epithelial cells were indistinguishable in their response to SARS-CoV-2 infection, which elicited minimal damage of epithelial layers in contrast to H1N1.

Numerous studies have found that influenza infection can result in EGFR activation[233, 234, 237] and EGFR signalling has been proposed to contribute to pulmonary fibrosis induced by infection with severe acute respiratory syndrome coronavirus (SARS-CoV)[182, 362]. To evaluate whether EGFR signalling was also affected by SARS-CoV-2 infection, gene expression levels of *EGFR* and its ligands were measured. Receptor expression was significantly reduced upon H1N1 infection but unaffected by SARS-CoV-2 (**Figure 6.7A**). Nevertheless, SARS-CoV-2 infection induced the expression of *BTC*, *EREG* and *HBEGF*, albeit to a much lower extent than H1N1 infection, while H1N1 also led to increased levels of *AREG*, *EGF* and

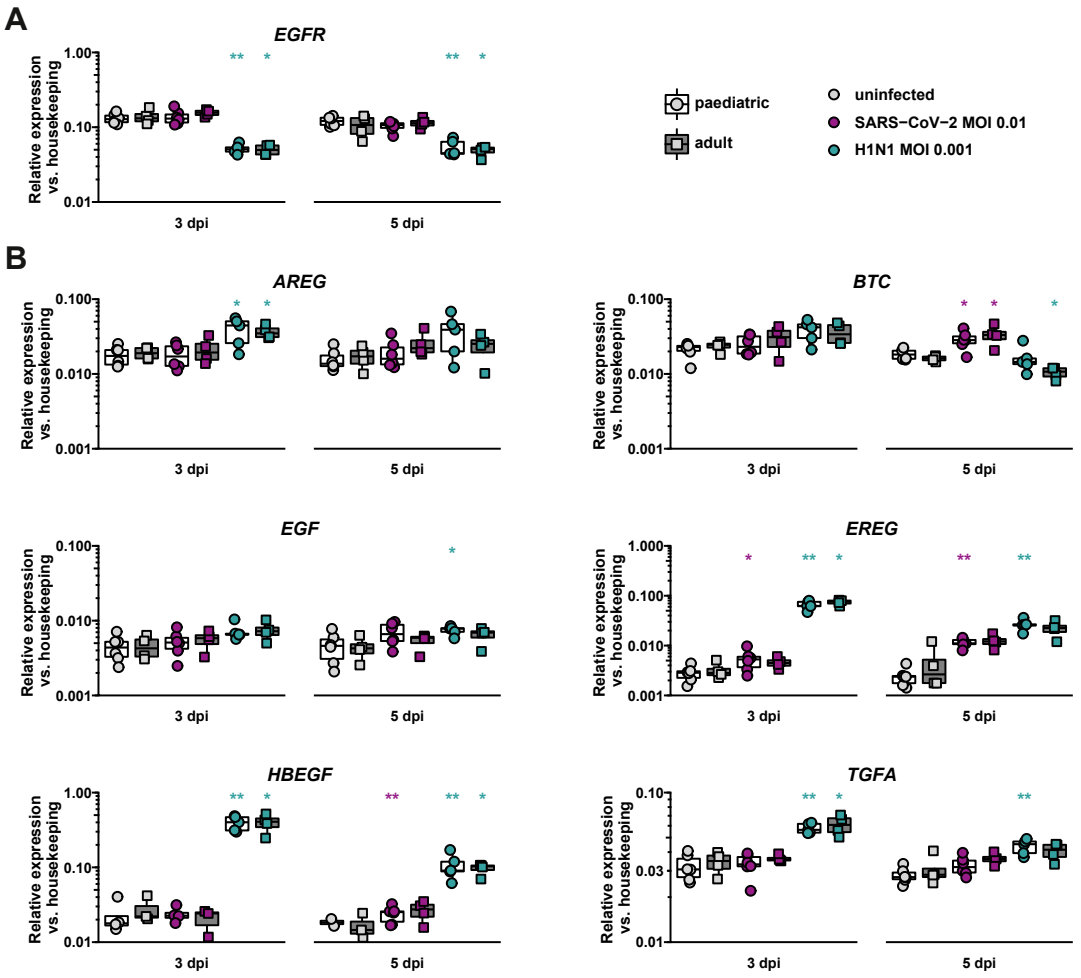


Figure 6.7 Both SARS-CoV-2 and H1N1 induced EGFR ligand expression in infected cells.
Cells were infected as shown in Figure 6.4A. **A-B** Expression of *EGFR* (A) or its ligands (B) in infected paediatric or bronchial epithelial cells at 3 or 5 dpi, as measured by qPCR. Statistics: Mann-Whitney test compared to relevant uninfected control. *, $p < 0.05$; **, $p < 0.01$.

TGFA (**Figure 6.7B**). These results indicate that SARS-CoV-2 was able to affect the availability of *EGFR* signalling molecules and analysis of Y1068 phosphorylation in future experiments may provide some insight into whether these changes result in increased signalling through EGFR.

Interferons play a central role in the epithelial defence against respiratory viruses and early studies using ALI cultures of bronchial epithelial cells to study SARS-CoV-2 infection have

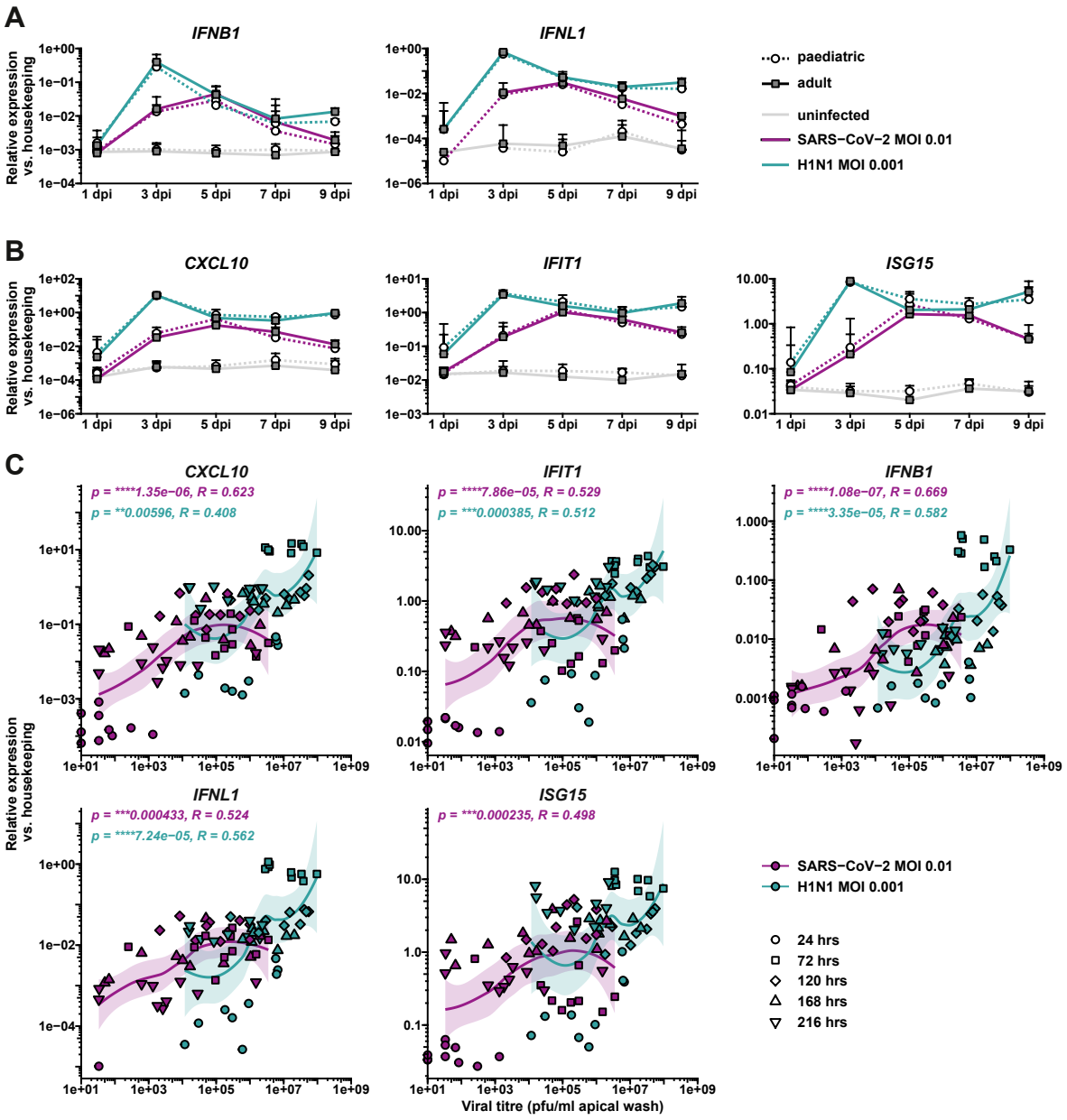


Figure 6.8 SARS-CoV-2 and H1N1 induced robust transcriptional interferon responses relative to viral replication.
Cells were infected as shown in Figure 6.4A. **A-B** Gene expression of interferons (A) or ISGs (B) in infected paediatric and adult epithelial cells as measured by qPCR at several time points post infection. Data are shown as median + confidence interval. **C** Spearman's rank correlations between gene expression of interferons or ISGs and number of infectious particles measured in apical washes. Symbol shapes indicate time point of measurements. Where significant, *p* values and correlation coefficients are shown for SARS-CoV-2 (magenta) or H1N1 (teal) infection.

suggested an inability of these cells to mount appropriate interferon responses[349, 363]. In contrast, a robust induction of type I and type III IFNs as well as ISGs was observed after infection with either SARS-CoV-2 or H1N1 in this model (**Figure 6.8A-B**) and gene expression levels correlated strongly with viral titres (**Figure 6.8C**). These results indicate that both viruses were able to elicit transcriptional interferon responses that were proportionate to the levels of infectious virus present in the apical wash, rescinding the notion that epithelial cells from healthy donors are unable to mount interferon signalling in response to SARS-CoV-2 infection.

Initial reports characterising SARS-CoV-2 infection in epithelial cells also described an overt induction of pro-inflammatory cytokines such as *CXCL8* (encoding IL-8) and *IL6*[363] which may contribute to the aggressive systemic inflammation termed "cytokine storm" frequently observed in severe cases of COVID-19[364, 365]. Within this experimental setup, however, SARS-CoV-2 infection elicited only a mild induction of *CXCL8* and *IL6* (**Figure 6.9A**) which was weaker than after infection with H1N1, both in absolute magnitude and proportional to viral titres (**Figure 6.9B**). Overall, both viruses induced antiviral and pro-inflammatory gene expression in bronchial epithelial cells independent of donor age and responses elicited by SARS-CoV-2 were much weaker compared to H1N1, likely caused by less successful replication of this virus within the epithelial cell cultures.

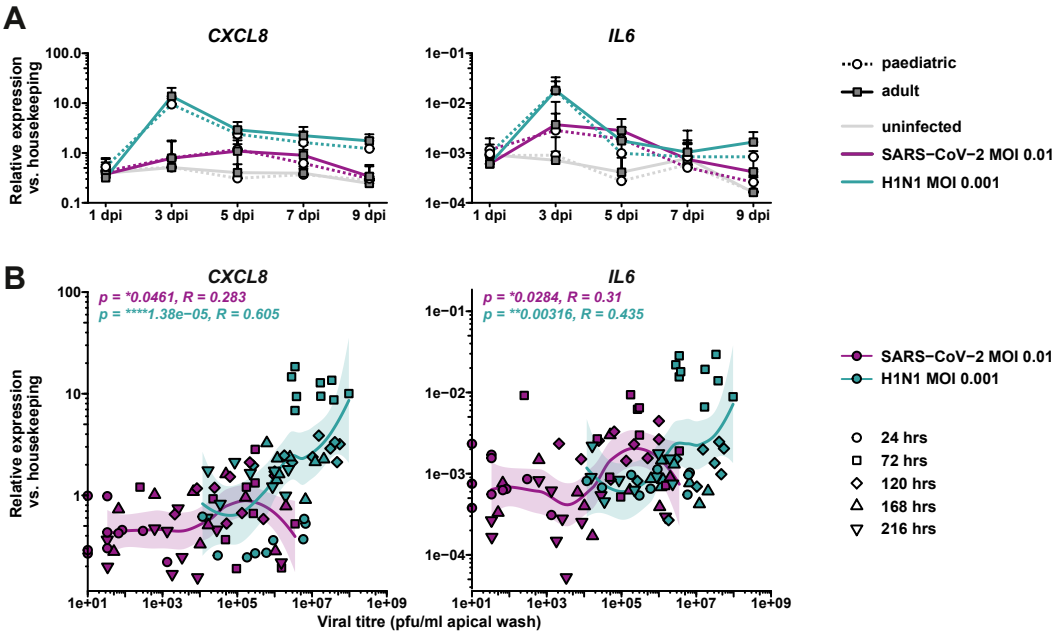


Figure 6.9 SARS-CoV-2 elicited only mild induction of pro-inflammatory genes.
Cells were infected as shown in Figure 6.4A. **A** Gene expression of indicated pro-inflammatory genes in infected paediatric and adult epithelial cells as measured by qPCR at several time points post infection. Data are shown as median + confidence interval. **B** Spearman's rank correlations between gene expression of *CXCL8* or *IL6* and number of infectious particles measured in apical washes. Symbol shapes indicate time point of measurements. Where significant, *p* values and correlation coefficients are shown for SARS-CoV-2 (magenta) or H1N1 (teal) infection.

To confirm the findings regarding the induction of interferon and pro-inflammatory responses at the protein level, the concentrations of interferons and pro-inflammatory cytokines released into the basal media were measured. Surprisingly, despite a robust induction of *IFNB1* and *IFNL1* transcript, only low levels of IFN-λ 1/3 and no IFN-β were detected in the basal media of SARS-CoV-2-infected cells (**Figure 6.10A-B**). In contrast, H1N1 infection triggered the release of high levels of both interferons into the basal media. Similarly, basal media from H1N1-infected cells contained considerable amounts of IL-6 and IL-8, the latter of which was also present in uninfected cells, whereas SARS-CoV-2 infection caused only modest release

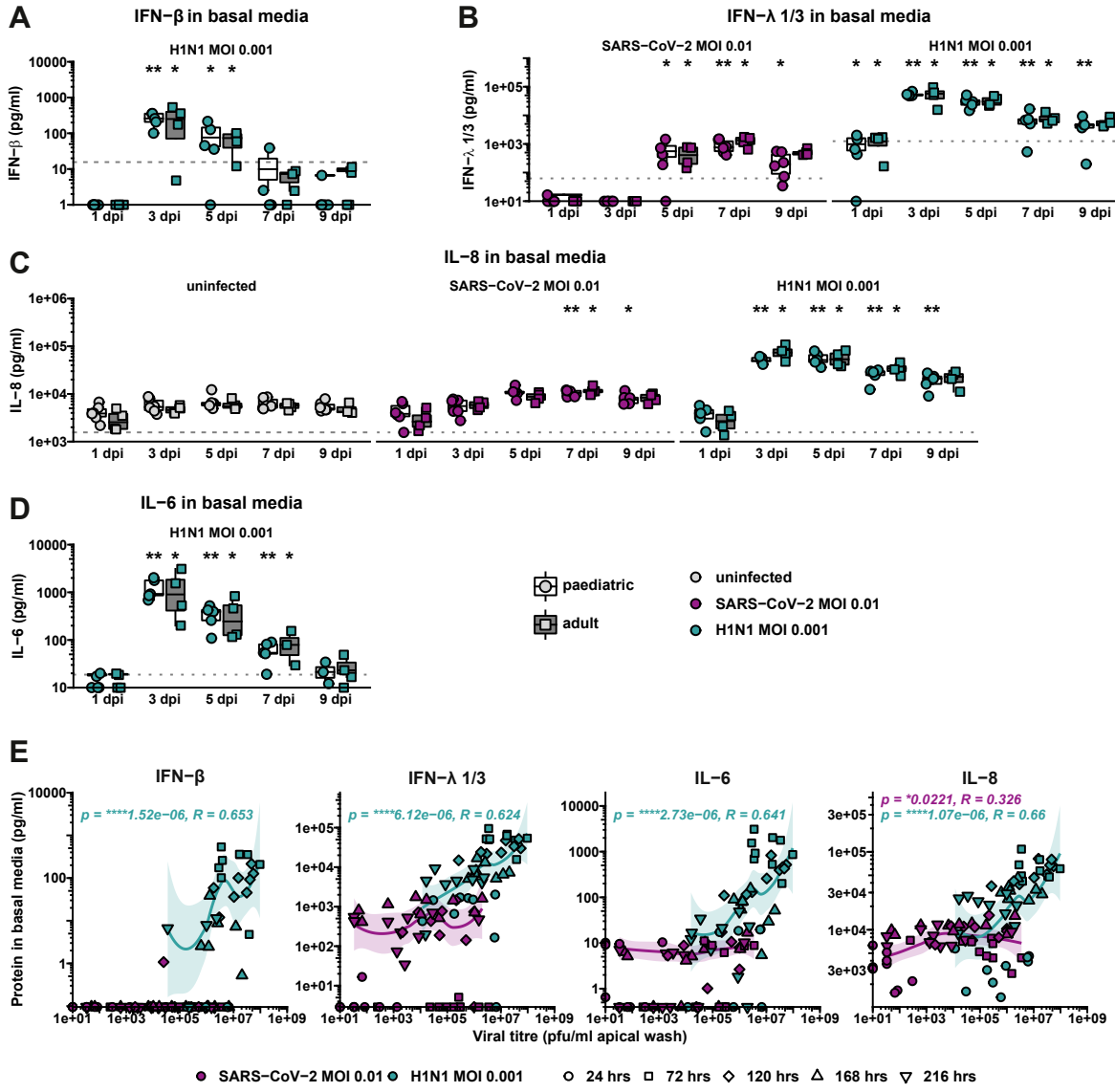


Figure 6.10 SARS-CoV-2 infection caused minimal protein release in contrast to H1N1.
Cells were infected as shown in Figure 6.4A. **A-D** Concentrations of IFN-β (A), IFN-λ (B), IL-8 (C) or IL-6 (D) in the basal media of infected paediatric or adult bronchial epithelial cells as measured by ELISA. Where condition is not shown, concentrations were below the detection limit of the assay. **E** Spearman's rank correlations between concentration of indicated proteins in the basal media and number of infectious particles measured in apical washes. Symbol shapes indicate time point of measurements. Where significant, *p* values and correlation coefficients are shown for SARS-CoV-2 (magenta) or H1N1 (teal) infection. Statistics: Mann-Whitney test compared to relevant uninfected control. *, $p < 0.05$; **, $p < 0.01$. Dotted line denotes lower limit of detection.

of IL-8 and no release of IL-6 (**Figure 6.10C-D**). In line with this, basal concentrations of all proteins correlated strongly with viral titres in H1N1- but not SARS-CoV-2-infected cells (**Figure 6.10E**). These findings indicate that the protein response to infection was dampened in SARS-CoV-2-infected cells relative to the transcriptional response and provide further evidence that immune responses elicited by SARS-CoV-2 are stunted compared to H1N1. As previously observed for gene expression, there were no differences between paediatric and adult cells regarding their protein secretion.

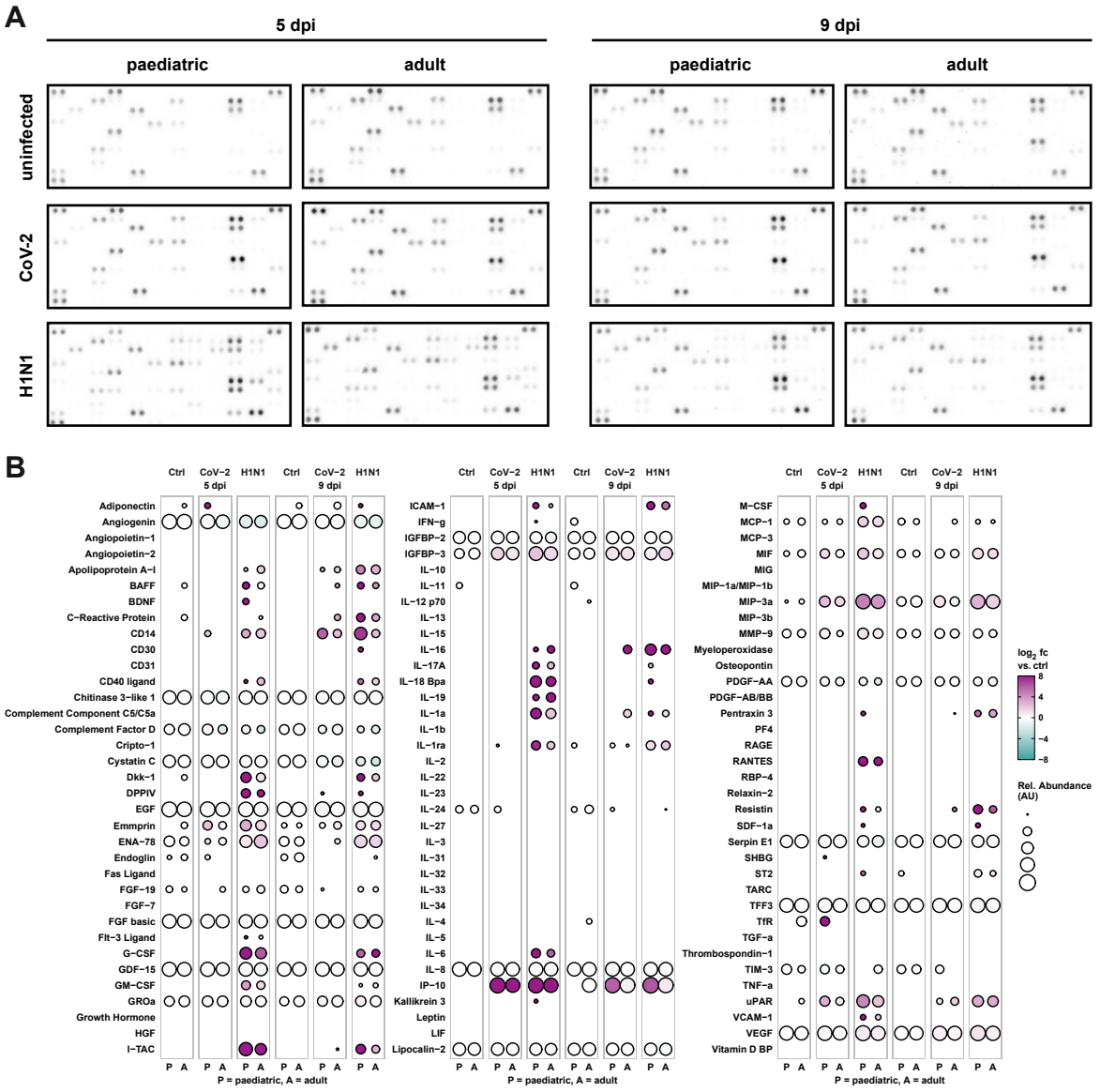


Figure 6.11 Infection with H1N1 but not SARS-CoV-2 caused release of a range of proteins into the basal media.
Cells were infected as shown in Figure 6.4A. **A** Membranes from proteome profiler assay of basal media from infected or uninfected paediatric or adult bronchial epithelial cells at two different time points. Media were pooled from four donors per age group, treatment and time point. **B** Quantification of A. Relative abundance of 105 proteins is depicted by size of the circles, with missing circles where mediators were undetectable. Colour indicates the fold change from the relevant uninfected control (log_2). If mediator was not detected in uninfected controls, circle colour was set to magenta.

To analyse whether the lack of protein release elicited by SARS-CoV-2 was specific to the interferon and cytokine response, the concentrations of 105 different proteins in pooled basal media were measured using a membrane-based sandwich immunoassay (**Figure 6.11A**). Whereas this approach was able to identify some proteins induced by SARS-CoV-2 infection, such as the ISG IP-10 (encoded by *CXCL10*) or the lymphocyte chemokine MIP-3a, H1N1 infection triggered the release of a much larger host of cytokines and chemokines (**Figure 6.11B**). Overall, this assay confirmed that immune responses in SARS-CoV-2-infected bronchial epithelial cells were subdued when compared to H1N1.

6.3.4 Effects of viral infection on SARS-CoV-2 entry gene expression

The final question was whether the expression of SARS-CoV-2 entry-related genes and thus the potential susceptibility to infection of SARS-CoV-2 would be altered upon viral infection. SARS-CoV-2 infection had little effect on entry gene expression (**Figure 6.12A**). In contrast, H1N1 significantly induced the expression of *ACE2*, *FURIN*, *NRP1* and *NRP2* while simultaneously reducing the levels of *CTSL* at several time points. While *ACE2*, *CTSL* and *NRP2* displayed kinetics similar to the induction of interferon and pro-inflammatory genes, suggesting they may be regulated by shared processes, *FURIN* and *NRP1* expression displayed distinct timings and did not correlate with viral titres (**Figure 6.12B**). Importantly, *FURIN* was consistently upregulated from 3 dpi, and *NRP1* showed a steady increase in mRNA levels from 5 dpi onwards, suggesting that H1N1 infection caused the sustained upregulation of these entry factors. If maintained, such a change in entry factor expression could feasibly result in increased susceptibility to infection with SARS-CoV-2 following H1N1 infection.

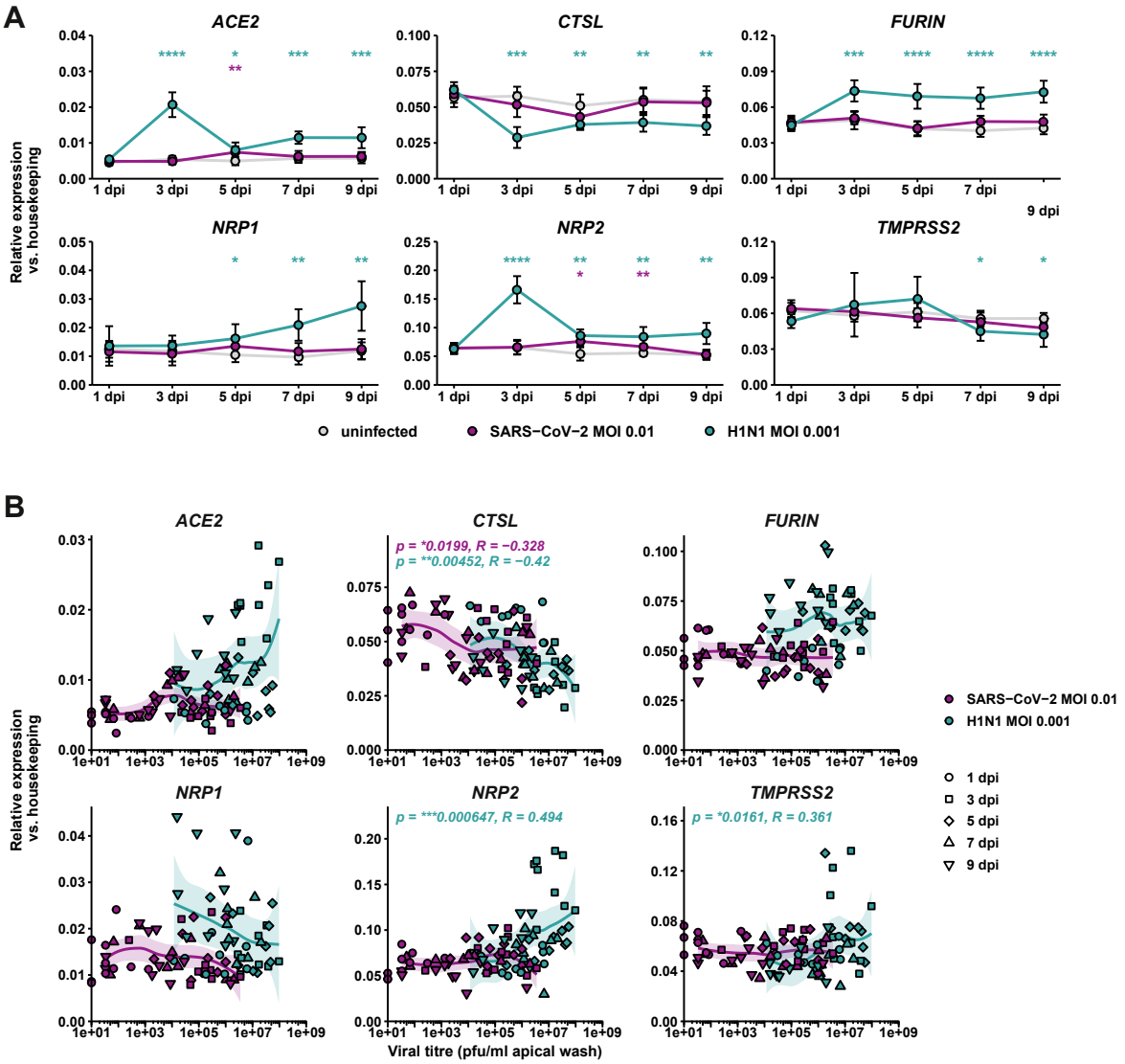


Figure 6.12 H1N1 infection altered expression of SARS-CoV-2 entry-related genes.
Cells were infected as shown in Figure 6.4A. **A** Gene expression of SARS-CoV-2 entry-related genes in infected epithelial cells as measured by qPCR at several time points post infection. Data are pooled from all donors and shown as median + confidence interval. Coloured asterisks denote significant change from uninfected controls after SARS-CoV-2 (magenta) or H1N1 (teal) infection. Mann-Whitney test: *, $p < 0.05$; **, $p < 0.01$; ***, $p < 0.001$; ****, $p < 0.0001$. **B** Spearman's rank correlations between expression of indicated SARS-CoV-2 entry-related genes and number of infectious particles measured in apical washes. Symbol shapes indicate time point of measurements. Where significant, p values and correlation coefficients are shown for SARS-CoV-2 (magenta) or H1N1 (teal) infection.

6.4 Discussion

Within this chapter, an in-depth characterisation of SARS-CoV-2 infection in ALI cultures of primary epithelial cells was conducted and viral replication and immune responses were compared between paediatric and adult epithelia. Within this experimental setup, there were no differences in the viral tropism or induction of interferon and pro-inflammatory signalling between bronchial epithelial cells from children and adults, rescinding the hypothesis that intrinsic differences between paediatric and adult epithelia are at the root of reduced severity of COVID-19 in children. Overall, SARS-CoV-2 replicated less readily in epithelial cell cultures than H1N1, caused no gross damage to the epithelial layer and induced subdued immune responses, particularly at the protein level. Nevertheless, both viruses altered the expression levels of EGFR ligands, suggesting that EGFR signalling may be activated upon viral infection. Finally, H1N1 infection resulted in prolonged upregulation of the SARS-CoV-2 entry factors *FURIN* and *NRP1*, which may render the airway epithelium more susceptible to subsequent infection with SARS-CoV-2. These findings are summarised in **Figure 6.13**.

At the time these analyses were conducted, no other descriptions of SARS-CoV-2 infection in paediatric and adult airway epithelial cell cultures existed in the peer-reviewed literature. However, in parallel with the findings from this thesis[192], a similar experimental approach to compare paediatric and adult bronchial epithelial cells regarding their immune responses and susceptibility to infection with SARS-CoV-2 was published[351]. In their study, Beucher et al. collected bronchial epithelial cells from twelve adults with an average age of 58.67 years (range: 29-74 years of age) and seven children aged 4-12 years (average 9.02 years). All

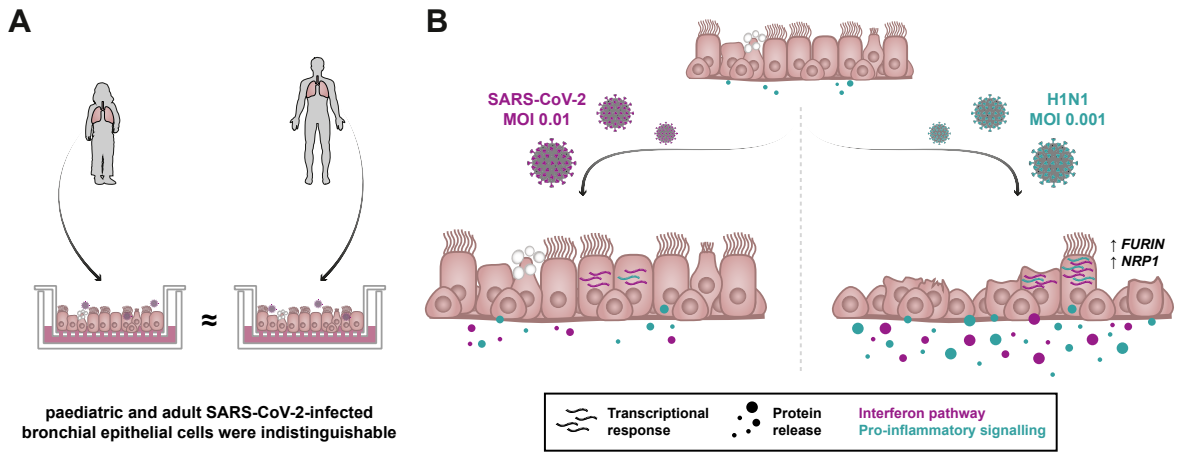


Figure 6.13 SARS-CoV-2 infection is comparable between paediatric and adult bronchial epithelial cells but distinct from infection with H1N1.
A There were no differences between paediatric or adult bronchial epithelial cells in their susceptibility or response to infection with SARS-CoV-2. **B** H1N1 infection caused epithelial damage, significant interferon and pro-inflammatory responses at protein level and prolonged upregulation of SARS-CoV-2 entry factors *FURIN* and *NRP1*. These effects were largely absent after infection with SARS-CoV-2, which nevertheless resulted in robust induction of IFN and ISG gene expression.

donors exhibited normal BMIs and lung function. The cells were expanded and differentiated at ALI using a similar approach as described in this thesis and then infected with an early clinical isolate of SARS-CoV-2 (BetaCoV/France/IDF0372/2020) at a dose of 1,200 PFU, which equates to roughly half of the viral dose used within the experiments described herein. Using immunofluorescence staining of inserts at 1 dpi, Beucher and colleagues (ref. [351]) found that ciliated cells, not goblet cells or basal cells, were the primary target of infection with SARS-CoV-2, which is in line with the observations from this work as well as previously published findings[340, 366, 367]. Interestingly, this study also postulated a new mode of transmission of SARS-CoV-2, by which virus-containing syncytia formed of ciliated and basal cells were released apically and thus contributed significantly to the spread of the virus within the cultures. Whereas there were no differences in the permissiveness of paediatric and adult bronchial epithelial cells to infection with SARS-CoV-2 within the slightly smaller cohort of donors described here, Beucher et al. identified a subset of epithelial cell cultures which were intrinsically more resistant to infection and this phenotype was more frequently found in children compared to adults. The authors linked this inherent resistance to SARS-CoV-2 infection to an accelerated induction of IFN-λ but attempted no further exploration into the factors underlying the differences in the induction of the antiviral response between donors. For example, it would have been interesting to investigate whether epithelia from non-permissive donors exhibited a heightened PRR expression or activated interferon signature even before infection, as previously reported in clinical samples[356, 359]. Moreover, since this study included cells which were isolated either from bronchial brushings or surgical resections, the latter of which were only used for adult donors, and stem from donors of a wide range of ages both within the paediatric and adult group, it would be informative to analyse whether resistance to infection was associated with either age or source of cells. Despite using a similar approach, there was little variability in the kinetics of either viral replication or interferon induction between any of the donors used in this thesis, suggesting that donors with distinct permissiveness to SARS-CoV-2 infection where not included in the modest sample size of $n = 10$ analysed here. Nevertheless, it is also possible that small differences, such as the clinical isolate of the virus and the methodology used to detect viral replication, may have affected the results. In addition, it is conceivable that certain features reported for paediatric epithelia, such as heightened PRR expression or IFN signatures, are not intrinsic but rather the result of environmental exposures such as preceding viral infections, which are more common in children[368]. Consequences of such environmental exposures are likely to be lost upon expansion of basal cells from nasal or bronchial brushing and re-differentiation *in vitro*. In line with this, there were no differences in the expression of *IFIH1* and *DDX58* nor in the IFN signature either at baseline or after SARS-CoV-2 infection between the epithelial cell cultures derived from paediatric or adult donors used here.

Nevertheless, these findings provide interesting insights into the pathophysiology of SARS-CoV-2 infection in ALI cultures of primary bronchial epithelial cells. Despite reports of loss of ciliation and destruction of epithelial integrity upon SARS-CoV-2 infection of differentiated airway epithelia[367, 369], no changes to the gross morphology or composition of SARS-CoV-2-infected epithelial layers were observed here. Together with the robust transcriptional induction of IFNs and ISGs yet an overall subdued pro-inflammatory response, this suggests that this model may reflect a mild course of SARS-CoV-2 infection. In contrast, an overt induction of pro-inflammatory cytokines in the absence of adequate interferon signalling as reported by other studies[349, 363] is associated with severe COVID-19[344-346, 364, 365]. Initially, it was thought that an inability to mount interferon responses was an intrinsic feature of SARS-CoV-2 infection, however, an increasing number of studies have since demonstrated induction of interferon signalling in primary airway epithelial cells infected with the virus[348, 350, 351, 358, 370-372]. Overall, this suggests that ALI cultures of airway epithelial cells can reflect different aspects of SARS-CoV-2 infection and are thus a useful tool for the study of COVID-19 pathophysiology in the large airways.

Although interferon signalling was observed in SARS-CoV-2-infected epithelial cells, their induction of interferons was delayed and of lower magnitude compared to the response elicited by H1N1 infection. Previous reports of similar results obtained when comparing SARS-CoV-2 to influenza A H1N1 or H3N2 postulated that the delayed IFN response may be the result of subversion of the early IFN induction by SARS-CoV-2[350, 370]. Here, gene expression levels of type I and type III IFNs induced by infection with either SARS-CoV-2 or H1N1 were strongly correlated with the number of infectious particles released into the apical wash, indicating that the delay in the IFN response is more likely to be caused by a lesser ability of SARS-CoV-2 to infect and replicate in primary airway epithelial cells. Anecdotally, these differences in the ease with which the two viruses establish infection in airway epithelia may explain why the incubation period of SARS-CoV-2 of roughly six days[373] is longer than the one to four days observed for H1N1[374]. Nevertheless, there appeared to be a disconnect between mRNA induction and protein release elicited by SARS-CoV-2 in our model, whereby only low levels of IFN-λ and no IFN-β was detected in the basal media of SARS-CoV-2-infected cells. While it is possible that the detection methods used in this thesis were not sufficiently sensitive to detect low concentrations of IFNs produced upon SARS-CoV-2 infection, the protein levels of IFN-λ, IL-6 and IL-8 only weakly correlated with viral titres, both in comparison with their gene expression levels and the amount of protein induced by H1N1 infection. This may indicate an interference of SARS-CoV-2 with protein translation, as previously reported[375-378]. Overall, this resulted in a subdued immune response in the absence of any overt damage to the epithelial layer elicited by SARS-CoV-2, in stark contrast to H1N1 infection. Given that both pandemic

viruses have similar spectra of disease severity, with slightly higher mortality observed for COVID-19[379], it is likely that the epithelial immune response to SARS-CoV-2, including the production of IFNs and pro-inflammatory cytokines, may be less important in deciding disease severity. In line with this, many other cells such as plasmacytoid DCs significantly contribute to IFN production during SARS-CoV-2 infection[380] and mounting evidence suggests that the appropriate induction of both T and B cell responses plays a central role in protecting from severe disease[381]. While ALI cultures are a valuable tool for the dissection of airway epithelial cell responses, they are unable to reflect the intricate interactions between various cell types in tissues and more complex culture systems and *in vivo* approaches will be necessary to define the determinants of disease severity of COVID-19.

Interestingly, H1N1 infection resulted in the prolonged upregulation of *FURIN* and *NRP1*, both of which can potentiate SARS-CoV-2 infectivity[336, 338, 339]. This raises the question of whether a recent infection with H1N1 would render the airway epithelium more susceptible to infection with SARS-CoV-2. Future work should aim to investigate whether these increases in entry factor gene expression are maintained even after H1N1 is cleared from the epithelial cells, and experiments employing sequential infection with H1N1 followed by SARS-CoV-2 will provide insights into the potential consequences of prior H1N1 infection to the susceptibility to SARS-CoV-2. The ability of prior infection with influenza A virus to increase the infectivity of SARS-CoV-2 in cell lines[382] has already been demonstrated and further inferences can be drawn from *in vivo* and clinical studies. For example, mice infected with influenza A prior to infection with SARS-CoV-2 exhibited exacerbated susceptibility and pathology compared to those infected with SARS-CoV-2 alone[382, 383]. In addition, mortality was higher in individuals infected with both SARS-CoV-2 and influenza compared to those who only tested positive for one of these viruses[384]. With the decline in hygiene measures implemented to contain the spread of COVID-19, epidemiological data may emerge to either confirm or deny that recent infection with influenza may pre-dispose to COVID-19. Importantly, simultaneous administration of influenza vaccination and COVID-19 mRNA boosters was found to be safe[385] and will be offered to vulnerable individuals this season.

Finally, SARS-CoV-2 induced the expression of various EGFR ligands, particularly *BTC* and *EREG*. While further experiments, such as the analysis of EGFR phosphorylation, are needed for confirmation, this suggests that EGFR signalling may be increased during infection with SARS-CoV-2. Interestingly, EGFR has been implicated in driving pulmonary fibrosis in individuals infected with SARS-CoV[182, 362], a virus closely related to SARS-CoV-2 and responsible for the 2002-2004 outbreak of severe acute respiratory syndrome (SARS). Based on the observation that overactive EGFR signalling resulted in exacerbated fibrosis and higher mortality in a mouse model of SARS-CoV[182], a clinical trial was conducted in Cuba to test the

safety and potential benefits of anti-EGFR therapy with the monoclonal antibody nimotuzumab in 41 patients with COVID-19[386]. This study found that the treatment induced minimal adverse effects and further reported that none of the subjects displayed signs of fibrosis at a follow-up visit. While these findings suggest that blocking of EGFR may have some merit in preventing fibrosis in COVID-19, the results should be interpreted with caution as this trial lacked untreated controls. Nevertheless, a recent study evaluating the degree of EGFR expression in 50 patients who died from COVID-19 found a positive correlation between the level of EGFR positivity in post-mortem lung sections and clinical parameters such as radiological involvement and levels of C-reactive protein and D-dimer[387]. In addition, data from our group showed that the BAL collected from post-COVID-19 patients with persistent respiratory abnormalities 3-6 months after discharge from the hospital contained significantly higher amounts of AREG than that of healthy controls[388]. Together these results suggest an active involvement of EGFR in the pathophysiology of COVID-19. While an AREG-EGFR signalling axis is considered to be protective in the context of influenza infection[130, 132, 163, 164], the same pathway was found to contribute to pulmonary fibrosis induced by TGF-β, bleomycin or allergen exposure[136, 173, 174]. Therefore, future studies are needed to elucidate whether EGFR signalling is protective, detrimental or negligible in the context of COVID-19. This question could be addressed for example by employing EGFR inhibition either in *in vitro* airway epithelial cell culture or *in vivo* mouse models of SARS-CoV-2 infection and findings from such experiments may provide further insight into the potential merits of blocking EGFR signalling clinically in patients with COVID-19.

6.5 Concluding remarks and future work

This chapter set out to identify differences in the immune response of paediatric and adult airway epithelial cells to SARS-CoV-2 that may explain the reduced severity of COVID-19 in children. However, the data revealed that bronchial epithelial cells from children and adults were indistinguishable in their susceptibility to infection with, and immune response to SARS-CoV-2 and demonstrated that the interferon and pro-inflammatory responses elicited by SARS-CoV-2 were diminished compared to H1N1, likely due to a reduced ability to infect and replicate in airway epithelia. These results suggest that airway epithelial responses to SARS-CoV-2, despite being the subject of numerous research efforts, may be inconsequential in deciding the severity of COVID-19. This study provides some evidence that SARS-CoV-2 infection may result in the activation of EGFR signalling, and since this pathway is proposed to contribute to pulmonary fibrosis during COVID-19, it will be imperative to study the contribution of EGFR signalling, whether it be protective or detrimental, to the pathophysiology

of COVID-19. To this end, future work will characterise the effects of SARS-CoV-2 infection on EGFR ligand production, release and downstream signalling as well as employ EGFR inhibition in *in vitro* ALI culture and *in vivo* mouse models of SARS-CoV-2 infection to define the contribution of EGFR signalling to inflammation, repair and remodelling.

7 Discussion

7.1 Aim and major findings of this thesis

Asthma is primarily a disease of childhood-onset and results in deficits in lung function which persist into adulthood (cf. 1.1). EGFR is a ubiquitously expressed growth factor receptor which was shown to be upregulated in patients with asthma and significantly contributes to disease pathology in adult *in vivo* models of AAD (cf. 3.1.3, 4.1.1). This thesis aimed to describe the expression patterns of EGFR and its ligands in the developing lung, characterise how EGFR signalling is affected by allergen exposure and, importantly, define its contribution to disease pathology in a neonatal model of AAD that can appropriately reflect disease onset in early life. The results from this work suggest that EGFR signalling is strongly induced by allergen exposure and that the signalling pathway fulfils distinct roles in early life and adulthood. Whereas low-frequency EGFR inhibition i.e., three doses of Gefitinib per week during the last three weeks of allergen exposure, had no effect on disease pathology in adult animals, it resulted in worsened airway hyperresponsiveness in the neonatal model, suggesting EGFR signalling may be protective during early life. However, an in-depth analysis of the data from neonatal EGFR inhibition revealed a second role for EGFR signalling in young female mice, where it contributed to augmented type 2 immune responses following allergen exposure. Overall, these findings suggest that EGFR signalling contributes to both protective and pathogenic roles during early-life AAD and that these are not seen in adult-onset disease.

7.1.1 EGFR signalling is induced by allergen exposure

Various findings from this thesis point towards highly active EGFR signalling during AAD. *In vitro,* HDM treatment resulted in EGFR activation of well-differentiated bronchial epithelial cells. *In vivo*, chronic HDM exposure induced the expression of EGFR on a host of different structural and immune cells, including epithelial cells, dendritic cells, eosinophils and Th2 cells. Moreover, allergen-challenged animals displayed increased levels of EGFR ligands within their lungs. In contrast, the amounts of free ligands available within the airways were reduced after allergen exposure, likely due to increasing ligand binding and uptake by recruited EGFR-expressing cells. In addition, a decrease in the epithelial barrier integrity may also allow EGFR ligands to be bound by epithelial cells, which express EGFR on their basolateral surface, or by fibroblasts and other stromal cells in the underlying tissue. Overall, these results indicate increased EGFR signalling activity during AAD (**Figure 7.1**). Further, albeit circumstantial, evidence for the extent of EGFR signalling upon chronic allergen exposure stems from the observations that neither exogenous ligand administration in neonates or adults nor low-frequency EGFR inhibition in the adult AAD model resulted in altered disease pathology. Both these findings could suggest that EGFR signalling is insignificant, especially in the context of adult AAD. However, considering the literature, a more likely interpretation of these data would

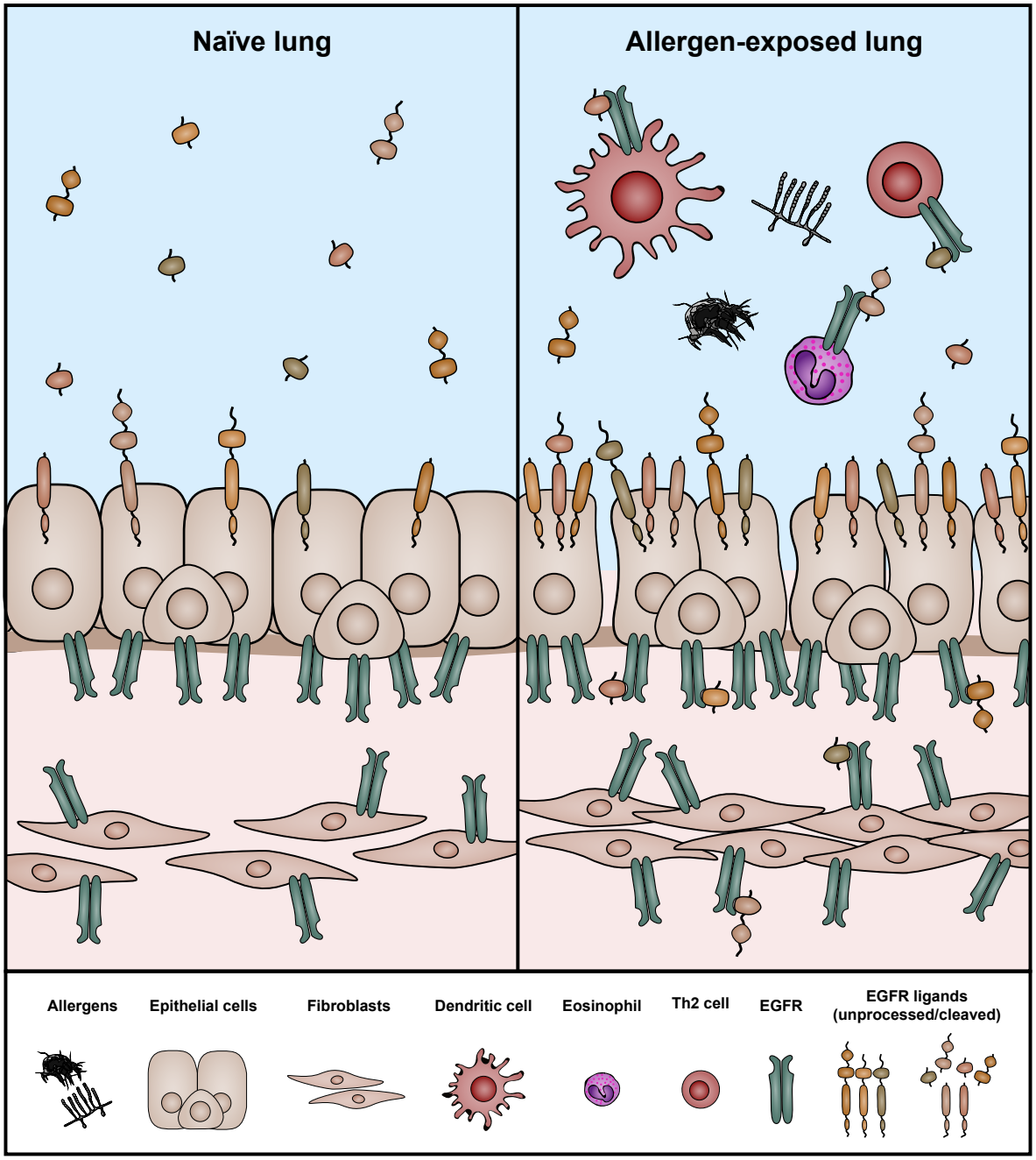


Figure 7.1 Model of EGFR signalling in the allergen-exposed lung.
Left In the naïve lung, EGFR ligands are made and released into the airways but are physically separated from the EGFR molecules expressed on the basolateral side of the epithelium. **Right** Expression of EGFR and its ligands is increased upon allergen exposure. Decreases in the barrier integrity allow EGFR ligands to pass the epithelium. EGFR signalling to fibroblasts may contribute to their proliferation and thus drive remodelling. At the same time, EGFR-expressing inflammatory cells such as (monocyte-derived) dendritic cells, eosinophils and Th2 cells are recruited to the airways. Ligand-receptor binding on these cells may explain the reduced EGFR ligand levels within the airways.

be that the strength of EGFR signalling during AAD is such that it cannot be further augmented by exogenous ligand administration, nor suppressed by three weekly doses of EGFR inhibitor. In support of this hypothesis, numerous studies have reported EGFR activation in both OVA- and aeroallergen-driven models of AAD, and using pharmacological or genetic approaches to suppress EGFR signalling, found this pathway to contribute to inflammation, airway

hyperresponsiveness and remodelling[134, 136, 157, 165-171, 222, 223, 226, 227, 242-244]. Importantly, the activation of EGFR signalling during AAD does not appear to be restricted to the mouse model. The analysis of the transcriptome of paediatric bronchial epithelial cells described within this thesis revealed increased expression levels of AREG or HB-EGF in children with PSW or school-aged severe asthma, respectively when compared to non-asthmatic controls, suggesting that enhanced EGFR signalling was also present in patients with asthma. Indeed, various groups found increased EGFR and ligand expression in the bronchial epithelium of children and adults with asthma compared to controls[212-216, 218, 263]. In addition, increased levels of AREG or EGF were reported in the sputum and nasal wash of children with wheeze or asthma[219-221]. Of note, epithelial cells from patients with asthma also displayed increased EGFR activation and produced higher levels of TGFα in response to HDM than those from healthy controls[223, 225]. Collectively, the results from this thesis indicate a high degree of EGFR signalling during AAD and asthma, a finding that is supported by the literature.

7.1.2 Distinct roles for EGFR signalling in early life and adulthood

The experiments using EGFR inhibitor administration during chronic allergen exposure of adult mice described herein did not provide any insights into the role of EGFR signalling during adult AAD, likely due to suboptimal inhibition achieved by the low-frequency dosing regimen. Nevertheless, there is ample evidence from similar experimental approaches in the literature showing improved pathology using more frequent administration (i.e., six to seven doses per week) or higher doses of EGFR inhibitors, suggesting that EGFR signalling drives airway remodelling, hyperresponsiveness and inflammation in adult OVA- or HDM-exposed animals[136, 165-170, 242]. In contrast, EGFR inhibition in an early-life model of AAD, as described within this thesis, resulted in worsened airway hyperresponsiveness. This finding suggests that, unlike in adult animals, where its contribution is detrimental, EGFR signalling fulfils a protective role during early-life allergen exposure, at least with respect to airway hyperresponsiveness. Whether these discrepancies may result from varying amounts of EGFR signalling induced in neonatal or adult mice, different levels of inhibition achieved by the Gefitinib dosing regimen or distinct mechanisms underlying airway hyperresponsiveness in early life and adulthood is unclear. Further complexity is added by the observation that in young female mice, EGFR inhibition ameliorated various features of type 2 inflammation, such as Th2 cytokine production, eosinophilia, allergic sensitisation and baseline lung function. Type 2 immunity was unaffected by EGFR inhibition in female adult mice or male mice of any age, suggesting that the contribution of EGFR to AAD pathology is both age- and sex-dependent.

7.2 Overarching themes, limitations and future directions

7.2.1 A complex pathway requiring complex tools

Within this thesis, various strategies were used to manipulate EGFR signalling. In particular, the use of Gefitinib, a small molecule EGFR TKI, constituted a valuable tool in defining the role of EGFR signalling during AAD. However, there were several shortcomings associated with the approach employed in this work. To minimise the risk of adverse effects, Gefitinib was administered three times per week and thus less frequently than described in other studies, where EGFR inhibitors were given at least six times per week[136, 165-167, 169, 170]. Therefore, it is possible that the low-frequency approach yielded sub-optimal suppression of EGFR activation. Western blot analysis of Y1068 phosphorylation of EGFR in lung homogenates was used to determine the extent of EGFR inhibition achieved by Gefitinib administration. While this method detected EGFR activation and inhibition in cultures of murine fibroblasts treated with AREG and Gefitinib, respectively, its use in lung homogenates produced variable and inconsistent results. Therefore, a reliable measure of the efficacy of Gefitinib dosing is lacking within these experiments. Similar difficulties were encountered in the attempt to measure the effects of allergen exposure or ligand administration on EGFR activation *in vivo* and inferences regarding the level of EGFR signalling had to be drawn from *in vitro* results, changes in EGFR expression and ligand levels within the lungs and airways. Since lung homogenates contain a mix of various cells present within the lungs and require extensive processing prior to analysis by western blotting, it is possible that EGFR activation signals were either diluted or lost. In the future, better results may be achieved by measuring EGFR phosphorylation in histological lung sections instead, as these maintain tissue organisation and thus allow the cell-specific analysis of EGFR activation signals. Various studies have used this method to show EGFR activation in response to allergen exposure, as well as suppression of signalling by pharmacological inhibitors or genetic manipulation[134, 165, 166, 169, 223].

In the absence of reliable means to determine the extent of EGFR inhibition achieved by Gefitinib administration, caution should be exercised when interpreting the results of these *in vivo* experiments. While a lack of effect in the adult AAD model may suggest that the contribution of EGFR signalling to pathology is negligible, it may just as likely be symptomatic of insufficient receptor inhibition achieved by less frequent Gefitinib administration. In line with this, Acciani et al. 2016 (ref. [167]) employed a similar experimental approach as the one described herein whereby animals were exposed to inhaled HDM three times per week for six weeks and the EGFR inhibitor Erlotinib was administered six times per week during the last three weeks of allergen exposure (therapeutical approach). This dosing regimen resulted in ameliorated lung function, inflammation and airway remodelling. Conversely, Yuan et al. 2020

(ref. [242]) report similar improvements in AAD pathology in a model where ITGB4$^{-/-}$ mice were intermittently exposed to inhaled HDM over the course of three weeks and administered the EGFR inhibitor AG1478 three times per week during the entire duration of allergen exposure (prophylactic approach). Although it is possible that the discrepancies between the findings in this thesis and those described in the literature are caused by differences in mouse strains, allergen batches or doses or the type of EGFR inhibitor used, it is conceivable that EGFR inhibition has to be administered either throughout the entire period of allergen exposure or, if given therapeutically, at a frequency of at least six doses per week. Future experiments using prophylactic EGFR inhibition as well as more frequent administration of Gefitinib or other EGFR inhibitors such as Erlotinib or AG1478 will be crucial to define the contribution of EGFR to pathology in the adult AAD model. In contrast to the adult model, Gefitinib administration during early-life AAD altered airway hyperresponsiveness of mice of both sexes as well as type 2 responses of female animals, suggesting that at least some EGFR inhibition was achieved and potentially indicating that EGFR signalling is less active in this context. In line with the limitations described above, it will be important to confirm these findings in early-life AAD using improved strategies to inhibit EGFR signalling.

Another pitfall of using pharmacological EGFR inhibition is its inability to target signalling by specific EGFR ligands or cell types. While the blockade of individual ligands can be achieved using monoclonal antibodies, the need to validate the efficacy of inhibition remains with their use. However, both these shortcomings can be overcome by the application of genetic tools. Although global deletion of *Egfr* is not viable[159-161], mice carrying 'floxed' alleles of the receptor (*Egfr*$^{fl/fl}$) have been generated to allow the deletion of *Egfr* under the control of cell type- or tissue-specific promotors[389, 390]. Similar constructs exist for example for the conditional deletion of *Areg*[391] or *Hbegf*[392] and constitute effective tools to study the role of EGFR signalling in different contexts in a highly specific manner. For example, deletion of *Hbegf* in CD4-expressing cells resulted in ameliorated type 2 inflammation and airway hyperresponsiveness in an OVA model of AAD[157] whereas lysozyme M-driven deletion of *Areg* was used to define a role for macrophage-derived AREG in orchestrating tissue repair following helminth infection[150]. Moreover, mice carrying a global deletion of any EGFR ligand are viable, as are those simultaneously deficient for AREG, EGF and TGFα or EGF, EREG and TGFα[177-180, 207, 208]. Such genetically modified animals provide the ability to study the contribution of each ligand to the effects of EGFR signalling in different diseases and have been fundamental for example in defining a protective role for AREG during repair responses following injury[131, 135, 150]. Interestingly, global deletion of AREG had no effect on airway inflammation in an OVA model of AAD[246] but was found to ameliorate airway remodelling of mice exposed to inhaled HDM[136], suggesting that the individual role of EGFR ligands in driving

AAD pathology is allergen- and model-dependent. Given the divergent capacity of EGFR signalling to either protect from or drive airway hyperresponsiveness in early life and adulthood, it is likely that the function of different EGFR ligands in AAD also differs depending on age. This thesis sought to characterise the pulmonary expression patterns of the various EGFR ligands during postnatal development and in response to allergen exposure. HB-EGF was particularly highly expressed in both structural and immune cells and was present in large amounts in the lungs and airways. For this reason, it would be interesting to use *Hbegf* deletion to investigate whether this ligand contributes to the beneficial effects of EGFR signalling on airway hyperresponsiveness, controls moDC recruitment or drives augmented type 2 responses of female animals in the context of early-life AAD. Similarly, targeted deletion of *Egfr* may provide insights into which cells receive EGFR signals during AAD and define their contribution to pathology.

Genetic manipulation constitutes a powerful tool to investigate the exact biological mechanisms underlying various conditions. However, it is less insightful when evaluating the potential benefits of EGFR-targeted therapeutic approaches and, unless inducible constructs are used, is unable to model temporary interference with EGFR signalling. Therefore, the data using EGFR inhibition in adult AAD presented in this thesis may provide important lessons about the feasibility of using EGFR inhibitors to modify disease pathology in patients with asthma. In the treatment of cancer, Gefitinib is administered daily at high doses and causes various adverse effects, ranging from mild symptoms such as rash, diarrhoea or vomiting to severe implications such as interstitial lung disease, hepatotoxicity and increased risk of infection[249, 393, 394]. Given that less frequent administration of Gefitinib failed to ameliorate disease in adult animals, it is unlikely that EGFR-targeted therapies would show efficacy in the absence of adverse effects in patients with asthma. In line with this, a clinical trial testing an inhaled EGFR inhibitor for the treatment of another chronic lung disease, COPD, suggested that this therapy might achieve disease modification at higher doses but this would be accompanied by unacceptable adverse events[187]. Although better results may be achieved in the context of asthma, for example by targeting adolescent females, the adverse effects would likely still outweigh the benefits. The lack of success of EGFR-targeted therapies for the treatment of conditions outside of cancer may be explained by the ubiquitous expression of EGFR and its ability to confer protection as well as contribute to pathology in various scenarios (cf. 1.2.4). In addition, various observations have shown that both deletion and overexpression of HB-EGF resulted in exacerbated liver fibrosis[172, 184], suggesting that the exact level of EGFR signalling, rather than its presence or absence, may be decisive for disease outcome. Both the characterisation of such a fine balance and its therapeutic modification are conceivably challenging. Nevertheless, the in-depth study of EGFR signalling in the context of AAD will no

doubt provide further insights into the cells and pathways involved in driving disease pathology, some of which may constitute more attractive therapeutic targets.

7.2.2 The advantage of appropriate models

An overarching theme of this thesis was the importance of using appropriate models to study biological mechanisms. For example, our work identified significant differences in the type 2 response of young female and male animals, akin to similar findings published in adult models of AAD (cf. 5.1.2). These models reflect the higher prevalence and severity of asthma observed in female adults compared to males (cf. 5.1.1). Nevertheless, the majority of *in vivo* studies of AAD are exclusively conducted in female animals. Importantly, the work described herein revealed that EGFR inhibition only affected type 2 responses in female but not male mice, indicating that responses to treatment differ between the sexes. Therefore, it is essential to consider both sexes when studying mechanisms of AAD *in vivo*.

Similar principles apply to the age of animals used in AAD models. Based on the recognition that early life constitutes a critical period for the development and education of the immune system[395], an increasing number of studies are utilising neonatal or young mice to study immune responses in this early-life period. Results from such studies highlight the differences between the neonatal and adult immune systems and emphasise the importance of using appropriate models in the study of different diseases. For example, infection with RSV, a virus which is responsible for significant morbidity and mortality in young children but generally causes mild to moderate symptoms in adults[396], resulted in exacerbated airway inflammation and remodelling in 3-week-old compared to adult mice[397]. Similarly, RSV-infected neonatal mice displayed impaired antibody responses and exacerbated pathology compared to adults due to a restriction of T follicular helper cell responses by heightened levels of IL-2[398]. Importantly, distinct immune responses between early life and adulthood are also apparent in the context of AAD. Whereas IL-13-producing CD4 T cells were necessary for the induction of airway hyperresponsiveness and inflammation in neonatal mice, the absence of these cells had no effects on the inception of airway hyperresponsiveness in adult animals[56]. Since early life constitutes a major risk window for the development of asthma, the use of appropriate neonatal models is critical in the study of the mechanisms underlying disease pathology. Within this thesis, a neonatal model of chronic exposure to HDM was used to study the role of EGFR signalling in early-life AAD and compare it to its function in adult models of AAD, as described herein and within the literature. Importantly, these experiments uncovered a distinct function for EGFR signalling in early life in protecting from exacerbated airway hyperresponsiveness. In contrast, EGFR activation was previously shown to contribute to airway hyperresponsiveness in adult models of AAD induced by chronic HDM exposure[166, 169,

[242]. The discrepancies between the functions of EGFR signalling in early life and adulthood underscore the importance of using appropriate models for the study of the pathophysiologic mechanisms underlying AAD, especially considering that allergen exposure and asthma onset most commonly take place during childhood. In particular, caution should be exercised when extrapolating findings from adult models to the development of therapeutic strategies for childhood (-onset) asthma, as the mechanisms underlying disease pathology are likely distinct between early life and adulthood. The same principle applies when interpreting data from studies using only one sex, as results from both this thesis and the literature illustrate that males and females differ in their response to allergens.

Differences between the immune responses of children and adults are not restricted to asthma. For example, children generally exhibit lower prevalence and severity of COVID-19 compared to adults (cf. 6.1.1). Several studies have identified distinct transcriptional signatures between paediatric and adult airway epithelia, indicating increased interferon signalling in children[356, 359, 399]. To investigate whether increased interferon signalling is an intrinsic feature of paediatric airway epithelial cells rather than the result of distinct environmental exposures and infection histories in children compared to adults, bronchial basal cells from paediatric and adult donors were grown into fully differentiated epithelial layers in ALI cultures. Of note, paediatric and adult epithelial cells exhibited comparable expression levels of interferons and ISGs both at baseline and after infection with SARS-CoV-2, suggesting that the enhanced interferon signatures in airway epithelia of children measured *ex vivo* are more likely to result from environmental exposures or tissue interactions than to be intrinsic to the epithelial cells from those donors. For example, infections with respiratory viruses are more common in children than in adults[368] and can induce interferon signalling. Nevertheless, a recent study comparing SARS-CoV-2 infection between paediatric and adult epithelial cells identified a subset of cultures, primarily from paediatric donors, which were less permissive to infection with SARS-CoV-2[351], suggesting that disease susceptibility and severity likely depends on an intimate interplay between environmental exposures and intrinsic features of the cells involved in the antiviral response, such as airway epithelial cells. The consideration of environmental exposures and their effects on disease pathology adds another layer of complexity to the design of *in vitro* and *in vivo* models. Several external factors, such as respiratory viral infections, microbial encounters, pollutants, allergens and nutrition affect the risk of developing asthma[18]. Various attempts have been made to model these features in allergen-driven *in vivo* models of AAD. For example, maternal treatment with the bacterial-derived agent OM-85 or early-life exposure to the farmyard microbe *Acinetobacter lwoffii* were shown to protect from pathology in neonatal models of OVA or

aeroallergen-driven AAD, respectively[56, 400]. In contrast, early-life infection with RSV exacerbated OVA-driven disease in adult animals[401].

Ideally, *in vivo* models of AAD should take different factors into consideration which may affect the biological mechanisms underlying disease susceptibility and severity, such as age, sex, genetic disposition and environmental exposures. Nevertheless, no approach will be able to perfectly model the complex interplay of risk factors thought to underlie the development of asthma, especially since these will differ from patient to patient, and it is therefore important to acknowledge that mechanisms of disease pathology identified by *in vivo* models form only part of the puzzle of asthma pathophysiology and likely only apply to a subset of patients with the disease. Nevertheless, by using a range of different models reflecting different ages, sexes and allergen exposures, the work in this thesis has identified a role for EGFR signalling in protecting from exacerbated airway hyperresponsiveness in early life and conversely uncovered a mechanism by which EGFR signalling may augment allergen-driven type 2 immune response in young female animals.

7.2.3 Translation and future directions

As alluded to above (cf. 7.2.1), more refined approaches are needed to study the role of EGFR signalling in early-life AAD in greater detail, particularly with respect to the cells and ligands involved in the signalling and the mechanisms induced downstream of receptor activation. Whereas many of the functions of EGFR signalling in various disease contexts, for example in the repair response following infection or during fibrosis, can be attributed to the ability of EGFR activation to drive proliferation or differentiation of mesenchymal cells, emerging evidence suggests that EGFR signalling fulfils unique roles in immune cells[127, 128]. Efforts should therefore be made to distinguish the importance of EGFR signalling in epithelial, fibroblast or smooth muscle cell function during early-life AAD from its contribution to immune responses to allergen. A better understanding for example of the pathways underlying exacerbated airway hyperresponsiveness after EGFR inhibition is needed to allow the exploitation of the protective function of EGFR signalling in this context without risking exacerbated disease pathology in female animals. Conversely, detailed analysis of the mechanisms by which EGFR signalling drives augmented type 2 responses in young female mice may reveal novel therapeutic targets to prevent worsened asthma severity in females entering adulthood. The investigation of these pathways will be prioritised in future studies. Based on previously published studies, it is possible that female allergen-exposed mice exhibit higher levels of IL-33 due to the ability of oestradiol to boost *Il33* expression of epithelial cells[303] and that EGFR signalling is necessary to allow Th2 cells to respond to heightened IL-33 levels by augmented production of type 2 cytokines[127] (cf. 5.4, Figure 5.12). Various *in vivo* and *in*

vitro experiments could be designed to test this hypothesis. For example, administration of either oestradiol or IL-33 to young male mice could be used to investigate whether this intervention is sufficient to augment type 2 responses, or, conversely, whether inhibition of IL-33 in females minimises sex differences and mitigates disease severity. *Ex vivo* stimulation of T lymphocytes from HDM-challenged animals with IL-33 in the presence or absence of EGFR inhibition could provide insight into whether EGFR signalling can support antigen-independent production of type 2 cytokines by Th2 cells in response to IL-33. Additional understanding may be gained from the use of genetic tools, such as CD4-specifc deletion of *Egfr*, to test the importance of EGFR signalling to Th2 cells in driving augmented disease pathology.

The exploration of how EGFR signalling may protect from exacerbated airway hyperresponsiveness in early life may prove more challenging. Analysis of the collagen geometry of allergen-exposed neonatal mice suggests that EGFR signalling may have a role in controlling the appropriate assembly of collagen fibres, although these findings require validation in a larger cohort of mice and will be prioritised in future work. Disrupted collagen organisation may contribute to exacerbated airway hyperresponsiveness. Although this relationship has thus far not been explored in *in vivo* models, a study assessing airway collagen geometry has identified defective organisation of collagen fibres in patients with asthma compared to healthy controls and linked these to disrupted collagen packaging by asthmatic fibroblasts[269]. Protocols exist to induce the secretion and organisation of three-dimensional extracellular matrices from primary fibroblasts[402]. The use of EGFR inhibition during this process would provide insights into whether EGFR signalling contributes to the proper packaging and organisation of collagen fibres by fibroblasts. In addition, collagen geometry in the lungs should be disrupted in neonatal and adult models of AAD, for example by targeting Decorin, which is required for the organisation of collagen fibrils[403], to investigate whether this intervention would result in exacerbated lung function.

The work within this thesis has also demonstrated that EGFR signalling contributes to the proliferation of fibroblasts in response to epithelial cell-conditioned media. These experiments provide a useful basis for the design of more complex *in vitro* models, either by generating epithelial cell-conditioned media to use on fibroblasts or by directly culturing primary epithelial cells and fibroblasts together. Such systems will be used to address how allergen exposure or viral infection of epithelial cells affect the proliferation and matrix generation of fibroblasts and whether epithelial cells from patients with asthma differ from healthy controls in their ability to induce remodelling-associated fibroblast phenotypes. In the first instance, treatment of primary fibroblasts with basal media from epithelial cells exposed to HDM or infected with RSV as described in Chapter 3 (cf. 3.3.6) and evaluation of fibroblast proliferation and secretion of extracellular matrix components will be used to provide first insights while more complex co-

culture models are being development. Within these experiments, it will also be important to define the role of EGFR signalling both at the level of epithelial cells and fibroblasts, for example by using Gefitinib to inhibit or recombinant ligands to activate EGFR signalling. As such, *in vitro* models of allergen exposure and remodelling constitute a valuable tool to complement *in vivo* studies by providing a platform to validate leads and investigate mechanisms of remodelling in more detail and thus should be a primary focus of future work.

7.3 Concluding remarks

By using a combination of different models of AAD and strategies to intervene with EGFR signalling, the work described in this thesis has revealed a dual role for EGFR in early-life AAD. Whereas signalling via the receptor protected from exacerbated airway hyperresponsiveness in animals of both sexes, it simultaneously contributed to augmented type 2 responses in female mice. The findings described provide a basis for more mechanistic studies investigating how EGFR fulfils its dual functions during early-life AAD and may ultimately aid in the development of therapies to preserve lung function in early life and prevent exacerbated asthma severity in young females entering adulthood.

References

1. Diseases GBD, Injuries C. Global burden of 369 diseases and injuries in 204 countries and territories, 1990-2019: a systematic analysis for the Global Burden of Disease Study 2019. *Lancet* 2020; **396**(10258)**:** 1204-1222.

2. Global Initiative for Asthma. Global Strategy for Asthma Management and Prevention; 2019. Available at www.ginasthma.org.

3. Dunican EM, Elicker BM, Gierada DS, Nagle SK, Schiebler ML, Newell JD *et al.* Mucus plugs in patients with asthma linked to eosinophilia and airflow obstruction. *J Clin Invest* 2018; **128**(3)**:** 997-1009.

4. de Nijs SB, Venekamp LN, Bel EH. Adult-onset asthma: is it really different? *Eur Respir Rev* 2013; **22**(127)**:** 44-52.

5. Yunginger JW, Reed CE, O'Connell EJ, Melton LJ, 3rd, O'Fallon WM, Silverstein MD. A community-based study of the epidemiology of asthma. Incidence rates, 1964-1983. *Am Rev Respir Dis* 1992; **146**(4)**:** 888-894.

6. Brand PLP, Baraldi E, Bisgaard H, Boner AL, Castro-Rodriguez JA, Custovic A *et al.* Definition, assessment and treatment of wheezing disorders in preschool children: an evidence-based approach. *European Respiratory Journal* 2008; **32**(4)**:** 1096-1110.

7. Papadopoulos NG, Kalobatsou A. Respiratory viruses in childhood asthma. *Curr Opin Allergy Clin Immunol* 2007; **7**(1)**:** 91-95.

8. Kusel MM, de Klerk NH, Kebadze T, Vohma V, Holt PG, Johnston SL *et al.* Early-life respiratory viral infections, atopic sensitization, and risk of subsequent development of persistent asthma. *J Allergy Clin Immunol* 2007; **119**(5)**:** 1105-1110.

9. Sigurs N, Bjarnason R, Sigurbergsson F, Kjellman B. Respiratory syncytial virus bronchiolitis in infancy is an important risk factor for asthma and allergy at age 7. *Am J Respir Crit Care Med* 2000; **161**(5)**:** 1501-1507.

10. Stein RT, Sherrill D, Morgan WJ, Holberg CJ, Halonen M, Taussig LM *et al.* Respiratory syncytial virus in early life and risk of wheeze and allergy by age 13 years. *The Lancet* 1999; **354**(9178)**:** 541-545.

11. Lu S, Hartert TV, Everard ML, Giezek H, Nelsen L, Mehta A *et al.* Predictors of asthma following severe respiratory syncytial virus (RSV) bronchiolitis in early childhood. *Pediatr Pulmonol* 2016; **51**(12)**:** 1382-1392.

12. Martinez FD, Wright AL, Taussig LM, Holberg CJ, Halonen M, Morgan WJ. Asthma and wheezing in the first six years of life. The Group Health Medical Associates. *N Engl J Med* 1995; **332**(3)**:** 133-138.

13. Saglani S, Payne DN, Zhu J, Wang Z, Nicholson AG, Bush A *et al.* Early detection of airway wall remodeling and eosinophilic inflammation in preschool wheezers. *Am J Respir Crit Care Med* 2007; **176**(9)**:** 858-864.

14. Payne DN, Rogers AV, Adelroth E, Bandi V, Guntupalli KK, Bush A *et al.* Early thickening of the reticular basement membrane in children with difficult asthma. *Am J Respir Crit Care Med* 2003; **167**(1)**:** 78-82.

15. Bossley CJ, Fleming L, Gupta A, Regamey N, Frith J, Oates T *et al.* Pediatric severe asthma is characterized by eosinophilia and remodeling without T(H)2 cytokines. *J Allergy Clin Immunol* 2012; **129**(4)**:** 974-982 e913.

16. Morgan WJ, Stern DA, Sherrill DL, Guerra S, Holberg CJ, Guilbert TW *et al.* Outcome of asthma and wheezing in the first 6 years of life: follow-up through adolescence. *Am J Respir Crit Care Med* 2005; **172**(10)**:** 1253-1258.

17. Tai A, Tran H, Roberts M, Clarke N, Gibson AM, Vidmar S *et al.* Outcomes of childhood asthma to the age of 50 years. *J Allergy Clin Immunol* 2014; **133**(6)**:** 1572-1578 e1573.

18. Subbarao P, Mandhane PJ, Sears MR. Asthma: epidemiology, etiology and risk factors. *CMAJ* 2009; **181**(9)**:** E181-190.

19. Moffatt MF, Gut IG, Demenais F, Strachan DP, Bouzigon E, Heath S *et al.* A large-scale, consortium-based genomewide association study of asthma. *N Engl J Med* 2010; **363**(13)**:** 1211-1221.

20. Strachan DP, Butland BK, Anderson HR. Incidence and prognosis of asthma and wheezing illness from early childhood to age 33 in a national British cohort. *BMJ* 1996; **312**(7040)**:** 1195-1199.

21. Vital signs: asthma prevalence, disease characteristics, and self-management education: United States, 2001--2009. *MMWR Morb Mortal Wkly Rep* 2011; **60**(17)**:** 547-552.

22. Wenzel SE. Asthma phenotypes: the evolution from clinical to molecular approaches. *Nat Med* 2012; **18**(5)**:** 716-725.

23. Agache I, Akdis C, Jutel M, Virchow JC. Untangling asthma phenotypes and endotypes. *Allergy* 2012; **67**(7)**:** 835-846.

24. Kuruvilla ME, Lee FE, Lee GB. Understanding Asthma Phenotypes, Endotypes, and Mechanisms of Disease. *Clin Rev Allergy Immunol* 2019; **56**(2)**:** 219-233.

25. Wu W, Bang S, Bleecker ER, Castro M, Denlinger L, Erzurum SC *et al.* Multiview Cluster Analysis Identifies Variable Corticosteroid Response Phenotypes in Severe Asthma. *Am J Respir Crit Care Med* 2019; **199**(11)**:** 1358-1367.

26. Chung KF, Wenzel SE, Brozek JL, Bush A, Castro M, Sterk PJ *et al.* International ERS/ATS guidelines on definition, evaluation and treatment of severe asthma. *Eur Respir J* 2014; **43**(2)**:** 343-373.

27. Papi A, Brightling C, Pedersen SE, Reddel HK. Asthma. *The Lancet* 2018; **391**(10122)**:** 783-800.

28. Hammad H, Lambrecht BN. The basic immunology of asthma. *Cell* 2021; **184**(6)**:** 1469-1485.

29. Li Y, Wang W, Lv Z, Li Y, Chen Y, Huang K *et al.* Elevated Expression of IL-33 and TSLP in the Airways of Human Asthmatics In Vivo: A Potential Biomarker of Severe Refractory Disease. *J Immunol* 2018; **200**(7)**:** 2253-2262.

30. Cheng D, Xue Z, Yi L, Shi H, Zhang K, Huo X *et al.* Epithelial interleukin-25 is a key mediator in Th2-high, corticosteroid-responsive asthma. *Am J Respir Crit Care Med* 2014; **190**(6)**:** 639-648.

31. Li Y, Wang W, Huang P, Zhang Q, Yao X, Wang J *et al.* Distinct sustained structural and functional effects of interleukin-33 and interleukin-25 on the airways in a murine asthma surrogate. *Immunology* 2015; **145**(4)**:** 508-518.

32. Lloyd CM, Gonzalo JA, Coyle AJ, Gutierrez-Ramos JC. Mouse models of allergic airway disease. *Adv Immunol* 2001; **77:** 263-295.

33. Lloyd CM. Building better mouse models of asthma. *Curr Allergy Asthma Rep* 2007; **7**(3)**:** 231-236.

34. Johnson JR, Wiley RE, Fattouh R, Swirski FK, Gajewska BU, Coyle AJ *et al.* Continuous exposure to house dust mite elicits chronic airway inflammation and structural remodeling. *Am J Respir Crit Care Med* 2004; **169**(3)**:** 378-385.

35. Bartemes KR, Iijima K, Kobayashi T, Kephart GM, McKenzie AN, Kita H. IL-33-responsive lineage- CD25+ CD44(hi) lymphoid cells mediate innate type 2 immunity and allergic inflammation in the lungs. *J Immunol* 2012; **188**(3)**:** 1503-1513.

36. Halim TY, Krauss RH, Sun AC, Takei F. Lung natural helper cells are a critical source of Th2 cell-type cytokines in protease allergen-induced airway inflammation. *Immunity* 2012; **36**(3)**:** 451-463.

37. Klein Wolterink RG, Kleinjan A, van Nimwegen M, Bergen I, de Bruijn M, Levani Y *et al.* Pulmonary innate lymphoid cells are major producers of IL-5 and IL-13 in murine models of allergic asthma. *Eur J Immunol* 2012; **42**(5)**:** 1106-1116.

38. Willart MA, Deswarte K, Pouliot P, Braun H, Beyaert R, Lambrecht BN *et al.* Interleukin-1alpha controls allergic sensitization to inhaled house dust mite via the epithelial release of GM-CSF and IL-33. *J Exp Med* 2012; **209**(8)**:** 1505-1517.

39. Hammad H, Plantinga M, Deswarte K, Pouliot P, Willart MA, Kool M *et al.* Inflammatory dendritic cells--not basophils--are necessary and sufficient for induction of Th2 immunity to inhaled house dust mite allergen. *J Exp Med* 2010; **207**(10)**:** 2097-2111.

40. Stone KD, Prussin C, Metcalfe DD. IgE, mast cells, basophils, and eosinophils. *J Allergy Clin Immunol* 2010; **125**(2 Suppl 2)**:** S73-80.

41. Steinke JW, Borish L. Th2 cytokines and asthma. Interleukin-4: its role in the pathogenesis of asthma, and targeting it for asthma treatment with interleukin-4 receptor antagonists. *Respir Res* 2001; **2**(2)**:** 66-70.

42. Elieh Ali Komi D, Bjermer L. Mast Cell-Mediated Orchestration of the Immune Responses in Human Allergic Asthma: Current Insights. *Clin Rev Allergy Immunol* 2019; **56**(2)**:** 234-247.

43. Roth M, Zhong J, Zumkeller C, S'Ng C T, Goulet S, Tamm M. The role of IgE-receptors in IgE-dependent airway smooth muscle cell remodelling. *PLoS One* 2013; **8**(2)**:** e56015.

44. Pelaia C, Paoletti G, Puggioni F, Racca F, Pelaia G, Canonica GW *et al.* Interleukin-5 in the Pathophysiology of Severe Asthma. *Front Physiol* 2019; **10:** 1514.

45. Wills-Karp M, Luyimbazi J, Xu X, Schofield B, Neben TY, Karp CL *et al.* Interleukin-13: central mediator of allergic asthma. *Science* 1998; **282**(5397)**:** 2258-2261.

46. Grunig G, Warnock M, Wakil AE, Venkayya R, Brombacher F, Rennick DM *et al.* Requirement for IL-13 independently of IL-4 in experimental asthma. *Science* 1998; **282**(5397)**:** 2261-2263.

47. Sugita K, Steer CA, Martinez-Gonzalez I, Altunbulakli C, Morita H, Castro-Giner F *et al.* Type 2 innate lymphoid cells disrupt bronchial epithelial barrier integrity by targeting tight junctions through IL-13 in asthmatic patients. *J Allergy Clin Immunol* 2018; **141**(1)**:** 300-310 e311.

48. Branchett WJ, Stölting H, Oliver RA, Walker SA, Puttur F, Gregory LG *et al.* A T cell-myeloid IL-10 axis regulates pathogenic IFN-gamma-dependent immunity in a mouse model of type 2-low asthma. *J Allergy Clin Immunol* 2020; **145**(2)**:** 666-678 e669.

49. Schnyder-Candrian S, Togbe D, Couillin I, Mercier I, Brombacher F, Quesniaux V *et al.* Interleukin-17 is a negative regulator of established allergic asthma. *J Exp Med* 2006; **203**(12)**:** 2715-2725.

50. Wilson RH, Whitehead GS, Nakano H, Free ME, Kolls JK, Cook DN. Allergic sensitization through the airway primes Th17-dependent neutrophilia and airway hyperresponsiveness. *Am J Respir Crit Care Med* 2009; **180**(8)**:** 720-730.

51. Wakashin H, Hirose K, Maezawa Y, Kagami S, Suto A, Watanabe N *et al.* IL-23 and Th17 cells enhance Th2-cell-mediated eosinophilic airway inflammation in mice. *Am J Respir Crit Care Med* 2008; **178**(10)**:** 1023-1032.

52. Raundhal M, Morse C, Khare A, Oriss TB, Milosevic J, Trudeau J *et al.* High IFN-gamma and low SLPI mark severe asthma in mice and humans. *J Clin Invest* 2015; **125**(8)**:** 3037-3050.

53. Snelgrove RJ, Patel DF, Patel T, Lloyd CM. The enigmatic role of the neutrophil in asthma: Friend, foe or indifferent? *Clin Exp Allergy* 2018; **48**(10)**:** 1275-1285.

54. Al-Ramli W, Prefontaine D, Chouiali F, Martin JG, Olivenstein R, Lemiere C *et al.* T(H)17-associated cytokines (IL-17A and IL-17F) in severe asthma. *J Allergy Clin Immunol* 2009; **123**(5)**:** 1185-1187.

55. Crisford H, Sapey E, Rogers GB, Taylor S, Nagakumar P, Lokwani R *et al.* Neutrophils in asthma: the good, the bad and the bacteria. *Thorax* 2021.

56. Saglani S, Gregory LG, Manghera AK, Branchett WJ, Uwadiae F, Entwistle LJ *et al.* Inception of early-life allergen-induced airway hyperresponsiveness is reliant on IL-13(+)CD4(+) T cells. *Sci Immunol* 2018; **3**(27).

57. Gollwitzer ES, Saglani S, Trompette A, Yadava K, Sherburn R, McCoy KD *et al.* Lung microbiota promotes tolerance to allergens in neonates via PD-L1. *Nat Med* 2014; **20**(6)**:** 642-647.

58. de Kleer IM, Kool M, de Bruijn MJ, Willart M, van Moorleghem J, Schuijs MJ *et al.* Perinatal Activation of the Interleukin-33 Pathway Promotes Type 2 Immunity in the Developing Lung. *Immunity* 2016; **45**(6)**:** 1285-1298.

59. Reddel HK, FitzGerald JM, Bateman ED, Bacharier LB, Becker A, Brusselle G *et al.* GINA 2019: a fundamental change in asthma management: Treatment of asthma with short-acting bronchodilators alone is no longer recommended for adults and adolescents. *Eur Respir J* 2019; **53**(6).

60. Barnes PJ. Inhaled Corticosteroids. *Pharmaceuticals (Basel)* 2010; **3**(3)**:** 514-540.

61. Dempsey OJ. Leukotriene receptor antagonist therapy. *Postgraduate Medical Journal* 2000; **76**(902)**:** 767-773.

62. Gaga M, Zervas E. Oral steroids in asthma: a double-edged sword. *Eur Respir J* 2019; **54**(5).

63. Brusselle GG, Taichman DB, Koppelman GH. Biologic Therapies for Severe Asthma. *New England Journal of Medicine* 2022; **386**(2)**:** 157-171.

64. Bousquet J, Humbert M, Gibson PG, Kostikas K, Jaumont X, Pfister P *et al.* Real-World Effectiveness of Omalizumab in Severe Allergic Asthma: A Meta-Analysis of Observational Studies. *J Allergy Clin Immunol Pract* 2021; **9**(7)**:** 2702-2714.

65. Menzella F, Ruggiero P, Ghidoni G, Fontana M, Bagnasco D, Livrieri F *et al.* Anti-IL5 Therapies for Severe Eosinophilic Asthma: Literature Review and Practical Insights. *J Asthma Allergy* 2020; **13:** 301-313.

66. Harb H, Chatila TA. Mechanisms of Dupilumab. *Clin Exp Allergy* 2020; **50**(1)**:** 5-14.

67. Hanania NA, Korenblat P, Chapman KR, Bateman ED, Kopecky P, Paggiaro P *et al.* Efficacy and safety of lebrikizumab in patients with uncontrolled asthma (LAVOLTA I and LAVOLTA II): replicate, phase 3, randomised, double-blind, placebo-controlled trials. *The Lancet Respiratory Medicine* 2016; **4**(10)**:** 781-796.

68. Panettieri RA, Sjöbring U, Péterffy A, Wessman P, Bowen K, Piper E *et al.* Tralokinumab for severe, uncontrolled asthma (STRATOS 1 and STRATOS 2): two randomised, double-blind, placebo-controlled, phase 3 clinical trials. *The Lancet Respiratory Medicine* 2018; **6**(7)**:** 511-525.

69. Menzies-Gow A, Corren J, Bourdin A, Chupp G, Israel E, Wechsler ME *et al.* Tezepelumab in Adults and Adolescents with Severe, Uncontrolled Asthma. *N Engl J Med* 2021; **384**(19)**:** 1800-1809.

70. Kosloski MP, Kalliolias GD, Xu CR, Harel S, Lai CH, Zheng W *et al.* Pharmacokinetics and pharmacodynamics of itepekimab in healthy adults and patients with asthma: Phase I first-in-human and first-in-patient trials. *Clin Transl Sci* 2022; **15**(2)**:** 384-395.

71. Wechsler ME, Ruddy MK, Pavord ID, Israel E, Rabe KF, Ford LB *et al.* Efficacy and Safety of Itepekimab in Patients with Moderate-to-Severe Asthma. *N Engl J Med* 2021; **385**(18)**:** 1656-1668.

72. A randomized, double-blind, placebo-controlled dose-ranging study to evaluate the efficacy, safety, and tolerability of SAR440340 (anti-IL-33 mAb) in patients with moderate-to-severe asthma. AdisInsight Trials [Internet document]. ; [Released 2020 March 11, Updated 2021 October 06] Available from: https://adis.springer.com/trials/700319608.

73. Kelsen SG, Agache IO, Soong W, Israel E, Chupp GL, Cheung DS *et al.* Astegolimab (anti-ST2) efficacy and safety in adults with severe asthma: A randomized clinical trial. *J Allergy Clin Immunol* 2021; **148**(3)**:** 790-798.

74. A Study to Evaluate Astegolimab in Participants With Chronic Obstructive Pulmonary Disease. https://ClinicalTrials.gov/show/NCT05595642.

75. Eger KA, Bel EH. The emergence of new biologics for severe asthma. *Curr Opin Pharmacol* 2019; **46:** 108-115.

76. Lloyd CM, Saglani S. Opening the Window of Immune Opportunity: Treating Childhood Asthma. *Trends Immunol* 2019; **40**(9)**:** 786-798.

77. Schlessinger J. Ligand-induced, receptor-mediated dimerization and activation of EGF receptor. *Cell* 2002; **110**(6)**:** 669-672.

78. Zhang X, Gureasko J, Shen K, Cole PA, Kuriyan J. An allosteric mechanism for activation of the kinase domain of epidermal growth factor receptor. *Cell* 2006; **125**(6)**:** 1137-1149.

79. Yarden Y, Sliwkowski MX. Untangling the ErbB signalling network. *Nat Rev Mol Cell Biol* 2001; **2**(2)**:** 127-137.

80. Wee P, Wang Z. Epidermal Growth Factor Receptor Cell Proliferation Signaling Pathways. *Cancers (Basel)* 2017; **9**(5).

81. Okabayashi Y, Kido Y, Okutani T, Sugimoto Y, Sakaguchi K, Kasuga M. Tyrosines 1148 and 1173 of activated human epidermal growth factor receptors are binding sites of Shc in intact cells. *Journal of Biological Chemistry* 1994; **269**(28)**:** 18674-18678.

82. Oda K, Matsuoka Y, Funahashi A, Kitano H. A comprehensive pathway map of epidermal growth factor receptor signaling. *Mol Syst Biol* 2005; **1:** 2005 0010.

83. Conte A, Sigismund S. Chapter Six - The Ubiquitin Network in the Control of EGFR Endocytosis and Signaling. *Prog Mol Biol Transl Sci* 2016; **141:** 225-276.

84. Brand TM, Iida M, Li C, Wheeler DL. The nuclear epidermal growth factor receptor signaling network and its role in cancer. *Discov Med* 2011; **12**(66)**:** 419-432.

85. Singh B, Carpenter G, Coffey RJ. EGF receptor ligands: recent advances. *F1000Res* 2016; **5**.

86. Wilson KJ, Gilmore JL, Foley J, Lemmon MA, Riese DJ, 2nd. Functional selectivity of EGF family peptide growth factors: implications for cancer. *Pharmacol Ther* 2009; **122**(1)**:** 1-8.

87. Sanders JM, Wampole ME, Thakur ML, Wickstrom E. Molecular determinants of epidermal growth factor binding: a molecular dynamics study. *PLoS One* 2013; **8**(1)**:** e54136.

88. Freed DM, Bessman NJ, Kiyatkin A, Salazar-Cavazos E, Byrne PO, Moore JO *et al.* EGFR Ligands Differentially Stabilize Receptor Dimers to Specify Signaling Kinetics. *Cell* 2017; **171**(3)**:** 683-695 e618.

89. Berasain C, Avila MA. Amphiregulin. *Semin Cell Dev Biol* 2014; **28:** 31-41.

90. Zeng F, Harris RC. Epidermal growth factor, from gene organization to bedside. *Semin Cell Dev Biol* 2014; **28:** 2-11.

91. Dahlhoff M, Wolf E, Schneider MR. The ABC of BTC: structural properties and biological roles of betacellulin. *Semin Cell Dev Biol* 2014; **28:** 42-48.

92. Taylor SR, Markesbery MG, Harding PA. Heparin-binding epidermal growth factor-like growth factor (HB-EGF) and proteolytic processing by a disintegrin and metalloproteinases (ADAM): a regulator of several pathways. *Semin Cell Dev Biol* 2014; **28:** 22-30.

93. Singh B, Coffey RJ. From wavy hair to naked proteins: the role of transforming growth factor alpha in health and disease. *Semin Cell Dev Biol* 2014; **28:** 12-21.

94. Riese DJ, 2nd, Cullum RL. Epiregulin: roles in normal physiology and cancer. *Semin Cell Dev Biol* 2014; **28:** 49-56.

95. Schneider MR, Yarden Y. Structure and function of epigen, the last EGFR ligand. *Semin Cell Dev Biol* 2014; **28:** 57-61.

96. Koseska A, Bastiaens PIH. Processing Temporal Growth Factor Patterns by an Epidermal Growth Factor Receptor Network Dynamically Established in Space. *Annu Rev Cell Dev Biol* 2020; **36:** 359-383.

97. Ronan T, Macdonald-Obermann JL, Huelsmann L, Bessman NJ, Naegle KM, Pike LJ. Different Epidermal Growth Factor Receptor (EGFR) Agonists Produce Unique Signatures for the Recruitment of Downstream Signaling Proteins. *J Biol Chem* 2016; **291**(11)**:** 5528-5540.

98. Knudsen SL, Mac AS, Henriksen L, van Deurs B, Grovdal LM. EGFR signaling patterns are regulated by its different ligands. *Growth Factors* 2014; **32**(5)**:** 155-163.

99. Faria J, de Andrade C, Goes AM, Rodrigues MA, Gomes DA. Effects of different ligands on epidermal growth factor receptor (EGFR) nuclear translocation. *Biochem Biophys Res Commun* 2016; **478**(1)**:** 39-45.

100. Gilmore JL, Scott JA, Bouizar Z, Robling A, Pitfield SE, Riese DJ, 2nd *et al.* Amphiregulin-EGFR signaling regulates PTHrP gene expression in breast cancer cells. *Breast Cancer Res Treat* 2008; **110**(3)**:** 493-505.

101. Macdonald-Obermann JL, Pike LJ. Different epidermal growth factor (EGF) receptor ligands show distinct kinetics and biased or partial agonism for homodimer and heterodimer formation. *J Biol Chem* 2014; **289**(38)**:** 26178-26188.

102. Wilson KJ, Mill C, Lambert S, Buchman J, Wilson TR, Hernandez-Gordillo V *et al.* EGFR ligands exhibit functional differences in models of paracrine and autocrine signaling. *Growth Factors* 2012; **30**(2)**:** 107-116.

103. Roepstorff K, Grandal MV, Henriksen L, Knudsen SL, Lerdrup M, Grovdal L *et al.* Differential effects of EGFR ligands on endocytic sorting of the receptor. *Traffic* 2009; **10**(8)**:** 1115-1127.

104. Krall JA, Beyer EM, MacBeath G. High- and low-affinity epidermal growth factor receptor-ligand interactions activate distinct signaling pathways. *PLoS One* 2011; **6**(1)**:** e15945.

105. Thorne BA, Plowman GD. The heparin-binding domain of amphiregulin necessitates the precursor pro-region for growth factor secretion. *Mol Cell Biol* 1994; **14**(3)**:** 1635-1646.

106. Prince RN, Schreiter ER, Zou P, Wiley HS, Ting AY, Lee RT *et al.* The heparin-binding domain of HB-EGF mediates localization to sites of cell-cell contact and prevents HB-EGF proteolytic release. *J Cell Sci* 2010; **123**(Pt 13)**:** 2308-2318.

107. Sahin U, Weskamp G, Kelly K, Zhou HM, Higashiyama S, Peschon J *et al.* Distinct roles for ADAM10 and ADAM17 in ectodomain shedding of six EGFR ligands. *J Cell Biol* 2004; **164**(5)**:** 769-779.

108. Sahin U, Blobel CP. Ectodomain shedding of the EGF-receptor ligand epigen is mediated by ADAM17. *FEBS Lett* 2007; **581**(1)**:** 41-44.

109. Sunnarborg SW, Hinkle CL, Stevenson M, Russell WE, Raska CS, Peschon JJ *et al.* Tumor necrosis factor-alpha converting enzyme (TACE) regulates epidermal growth factor receptor ligand availability. *J Biol Chem* 2002; **277**(15)**:** 12838-12845.

110. Wong ST, Winchell LF, McCune BK, Earp HS, Teixido J, Massague J *et al.* The TGF-α precursor expressed on the cell surface binds to the EGF receptor on adjacent cells, leading to signal transduction. *Cell* 1989; **56**(3)**:** 495-506.

111. Anklesaria P, Teixido J, Laiho M, Pierce JH, Greenberger JS, Massague J. Cell-cell adhesion mediated by binding of membrane-anchored transforming growth factor alpha to epidermal growth factor receptors promotes cell proliferation. *Proc Natl Acad Sci U S A* 1990; **87**(9)**:** 3289-3293.

112. Higashiyama S, Iwamoto R, Goishi K, Raab G, Taniguchi N, Klagsbrun M *et al.* The membrane protein CD9/DRAP 27 potentiates the juxtacrine growth factor activity of the membrane-anchored heparin-binding EGF-like growth factor. *J Cell Biol* 1995; **128**(5)**:** 929-938.

113. Tada H, Sasada R, Kawaguchi Y, Kojima I, Gullick WJ, Salomon DS *et al.* Processing and juxtacrine activity of membrane-anchored betacellulin. *Journal of Cellular Biochemistry* 1999; **72**(3)**:** 423-434.

114. Dong J, Opresko LK, Chrisler W, Orr G, Quesenberry RD, Lauffenburger DA *et al.* The membrane-anchoring domain of epidermal growth factor receptor ligands dictates their ability to operate in juxtacrine mode. *Mol Biol Cell* 2005; **16**(6)**:** 2984-2998.

115. Higginbotham JN, Demory Beckler M, Gephart JD, Franklin JL, Bogatcheva G, Kremers GJ *et al.* Amphiregulin exosomes increase cancer cell invasion. *Curr Biol* 2011; **21**(9)**:** 779-786.

116. Zanetti-Domingues LC, Bonner SE, Martin-Fernandez ML, Huber V. Mechanisms of Action of EGFR Tyrosine Kinase Receptor Incorporated in Extracellular Vesicles. *Cells* 2020; **9**(11).

117. Cohen S, Carpenter G, King L. Epidermal growth factor-receptor-protein kinase interactions. Co-purification of receptor and epidermal growth factor-enhanced phosphorylation activity. *Journal of Biological Chemistry* 1980; **255**(10)**:** 4834-4842.

118. Chen J, Zeng F, Forrester SJ, Eguchi S, Zhang MZ, Harris RC. Expression and Function of the Epidermal Growth Factor Receptor in Physiology and Disease. *Physiol Rev* 2016; **96**(3)**:** 1025-1069.

119. Chan G, Nogalski MT, Yurochko AD. Activation of EGFR on monocytes is required for human cytomegalovirus entry and mediates cellular motility. *Proc Natl Acad Sci U S A* 2009; **106**(52)**:** 22369-22374.

120. Chattopadhyay S, Veleeparambil M, Poddar D, Abdulkhalek S, Bandyopadhyay SK, Fensterl V *et al.* EGFR kinase activity is required for TLR4 signaling and the septic shock response. *EMBO Rep* 2015; **16**(11)**:** 1535-1547.

121. Hardbower DM, Singh K, Asim M, Verriere TG, Olivares-Villagomez D, Barry DP *et al.* EGFR regulates macrophage activation and function in bacterial infection. *J Clin Invest* 2016; **126**(9)**:** 3296-3312.

122. Lanaya H, Natarajan A, Komposch K, Li L, Amberg N, Chen L *et al.* EGFR has a tumour-promoting role in liver macrophages during hepatocellular carcinoma formation. *Nat Cell Biol* 2014; **16**(10)**:** 972-977.

123. Scholes AG, Hagan S, Hiscott P, Damato BE, Grierson I. Overexpression of epidermal growth factor receptor restricted to macrophages in uveal melanoma. *Arch Ophthalmol* 2001; **119**(3)**:** 373-377.

124. Lewkowicz P, Tchorzewski H, Dytnerska K, Banasik M, Lewkowicz N. Epidermal growth factor enhances TNF-alpha-induced priming of human neutrophils. *Immunol Lett* 2005; **96**(2)**:** 203-210.

125. Mahtouk K, Hose D, Reme T, De Vos J, Jourdan M, Moreaux J *et al.* Expression of EGF-family receptors and amphiregulin in multiple myeloma. Amphiregulin is a growth factor for myeloma cells. *Oncogene* 2005; **24**(21)**:** 3512-3524.

126. Zeboudj L, Maitre M, Guyonnet L, Laurans L, Joffre J, Lemarie J *et al.* Selective EGF-Receptor Inhibition in CD4(+) T Cells Induces Anergy and Limits Atherosclerosis. *J Am Coll Cardiol* 2018; **71**(2)**:** 160-172.

127. Minutti CM, Drube S, Blair N, Schwartz C, McCrae JC, McKenzie AN *et al.* Epidermal Growth Factor Receptor Expression Licenses Type-2 Helper T Cells to Function in a T Cell Receptor-Independent Fashion. *Immunity* 2017; **47**(4)**:** 710-722 e716.

128. Zaiss DM, van Loosdregt J, Gorlani A, Bekker CP, Grone A, Sibilia M *et al.* Amphiregulin enhances regulatory T cell-suppressive function via the epidermal growth factor receptor. *Immunity* 2013; **38**(2)**:** 275-284.

129. Turner JE, Morrison PJ, Wilhelm C, Wilson M, Ahlfors H, Renauld JC *et al.* IL-9-mediated survival of type 2 innate lymphoid cells promotes damage control in helminth-induced lung inflammation. *J Exp Med* 2013; **210**(13)**:** 2951-2965.

130. Monticelli LA, Sonnenberg GF, Abt MC, Alenghat T, Ziegler CGK, Doering TA *et al.* Innate lymphoid cells promote lung-tissue homeostasis after infection with influenza virus. *Nature Immunology* 2011; **12**(11)**:** 1045-1054.

131. Monticelli LA, Osborne LC, Noti M, Tran SV, Zaiss DM, Artis D. IL-33 promotes an innate immune pathway of intestinal tissue protection dependent on amphiregulin-EGFR interactions. *Proc Natl Acad Sci U S A* 2015; **112**(34)**:** 10762-10767.

132. Guo XJ, Dash P, Crawford JC, Allen EK, Zamora AE, Boyd DF *et al.* Lung gammadelta T Cells Mediate Protective Responses during Neonatal Influenza Infection that Are Associated with Type 2 Immunity. *Immunity* 2018; **49**(3)**:** 531-544 e536.

133. Salimi M, Barlow JL, Saunders SP, Xue L, Gutowska-Owsiak D, Wang X *et al.* A role for IL-25 and IL-33-driven type-2 innate lymphoid cells in atopic dermatitis. *J Exp Med* 2013; **210**(13)**:** 2939-2950.

134. Doherty TA, Khorram N, Chang JE, Kim HK, Rosenthal P, Croft M *et al.* STAT6 regulates natural helper cell proliferation during lung inflammation initiated by Alternaria. *Am J Physiol Lung Cell Mol Physiol* 2012; **303**(7)**:** L577-588.

135. Zaiss DM, Yang L, Shah PR, Kobie JJ, Urban JF, Mosmann TR. Amphiregulin, a TH2 cytokine enhancing resistance to nematodes. *Science* 2006; **314**(5806)**:** 1746.

136. Morimoto Y, Hirahara K, Kiuchi M, Wada T, Ichikawa T, Kanno T *et al.* Amphiregulin-Producing Pathogenic Memory T Helper 2 Cells Instruct Eosinophils to Secrete Osteopontin and Facilitate Airway Fibrosis. *Immunity* 2018; **49**(1)**:** 134-150 e136.

137. Wang SW, Oh CK, Cho SH, Hu G, Martin R, Demissie-Sanders S *et al.* Amphiregulin expression in human mast cells and its effect on the primary human lung fibroblasts. *J Allergy Clin Immunol* 2005; **115**(2)**:** 287-294.

138. Okumura S, Sagara H, Fukuda T, Saito H, Okayama Y. FcepsilonRI-mediated amphiregulin production by human mast cells increases mucin gene expression in epithelial cells. *J Allergy Clin Immunol* 2005; **115**(2)**:** 272-279.

139. Qi Y, Operario DJ, Oberholzer CM, Kobie JJ, Looney RJ, Georas SN *et al.* Human basophils express amphiregulin in response to T cell-derived IL-3. *J Allergy Clin Immunol* 2010; **126**(6)**:** 1260-1266 e1264.

140. Meulenbroeks C, van Weelden H, Schwartz C, Voehringer D, Redegeld FAM, Rutten V *et al.* Basophil-derived amphiregulin is essential for UVB irradiation-induced immune suppression. *J Invest Dermatol* 2015; **135**(1)**:** 222-228.

141. Matsumoto K, Fukuda S, Nakamura Y, Saito H. Amphiregulin production by human eosinophils. *Int Arch Allergy Immunol* 2009; **149 Suppl 1:** 39-44.

142. Qi Y, Operario DJ, Georas SN, Mosmann TR. The acute environment, rather than T cell subset pre-commitment, regulates expression of the human T cell cytokine amphiregulin. *PLoS One* 2012; **7**(6)**:** e39072.

143. Kwong BY, Roberts SJ, Silberzahn T, Filler RB, Neustadter JH, Galan A *et al.* Molecular analysis of tumor-promoting CD8+ T cells in two-stage cutaneous chemical carcinogenesis. *J Invest Dermatol* 2010; **130**(6)**:** 1726-1736.

144. Burzyn D, Kuswanto W, Kolodin D, Shadrach JL, Cerletti M, Jang Y *et al.* A special population of regulatory T cells potentiates muscle repair. *Cell* 2013; **155**(6)**:** 1282-1295.

145. Lam AJ, MacDonald KN, Pesenacker AM, Juvet SC, Morishita KA, Bressler B *et al.* Innate Control of Tissue-Reparative Human Regulatory T Cells. *J Immunol* 2019.

146. Ito M, Komai K, Mise-Omata S, Iizuka-Koga M, Noguchi Y, Kondo T *et al.* Brain regulatory T cells suppress astrogliosis and potentiate neurological recovery. *Nature* 2019; **565**(7738)**:** 246-250.

147. Yang J, Ramadan A, Reichenbach DK, Loschi M, Zhang J, Griesenauer B *et al.* Rorc restrains the potency of ST2+ regulatory T cells in ameliorating intestinal graft-versus-host disease. *JCI Insight* 2019.

148. Xu Y, Meng C, Liu G, Yang D, Fu L, Zhang M *et al.* Classically Activated Macrophages Protect against Lipopolysaccharide-induced Acute Lung Injury by Expressing Amphiregulin in Mice. *Anesthesiology* 2016; **124**(5)**:** 1086-1099.

149. Ko JH, Kim HJ, Jeong HJ, Lee HJ, Oh JY. Mesenchymal Stem and Stromal Cells Harness Macrophage-Derived Amphiregulin to Maintain Tissue Homeostasis. *Cell Rep* 2020; **30**(11)**:** 3806-3820 e3806.

150. Minutti CM, Modak RV, Macdonald F, Li F, Smyth DJ, Dorward DA *et al.* A Macrophage-Pericyte Axis Directs Tissue Restoration via Amphiregulin-Induced Transforming Growth Factor Beta Activation. *Immunity* 2019.

151. Sugita J, Fujiu K, Nakayama Y, Matsubara T, Matsuda J, Oshima T *et al.* Cardiac macrophages prevent sudden death during heart stress. *Nat Commun* 2021; **12**(1)**:** 1910.

152. Bles N, Di Pietrantonio L, Boeynaems JM, Communi D. ATP confers tumorigenic properties to dendritic cells by inducing amphiregulin secretion. *Blood* 2010; **116**(17)**:** 3219-3226.

153. Adib-Conquy M, Pedron T, Petit-Bertron AF, Tabary O, Corvol H, Jacquot J *et al.* Neutrophils in cystic fibrosis display a distinct gene expression pattern. *Mol Med* 2008; **14**(1-2)**:** 36-44.

154. Kuo D, Ding J, Cohn IS, Zhang F, Wei K, Rao DA *et al.* HBEGF(+) macrophages in rheumatoid arthritis induce fibroblast invasiveness. *Sci Transl Med* 2019; **11**(491).

155. Zhou L, Zhou W, Joseph AM, Chu C, Putzel GG, Fang B *et al.* Group 3 innate lymphoid cells produce the growth factor HB-EGF to protect the intestine from TNF-mediated inflammation. *Nat Immunol* 2022; **23**(2)**:** 251-261.

156. Leng T, Akther HD, Hackstein CP, Powell K, King T, Friedrich M *et al.* TCR and Inflammatory Signals Tune Human MAIT Cells to Exert Specific Tissue Repair and Effector Functions. *Cell Rep* 2019; **28**(12)**:** 3077-3091 e3075.

157. Farahnak S, Simon L, McGovern TK, Chen M, Khazaei N, Martin JG. HB-EGF Synthesized by CD4 T Cells Modulates Allergic Airway Eosinophilia by Regulating IL-5 Synthesis. *J Immunol* 2019.

158. Al Heialy S, Risse PA, Zeroual MA, Roman HN, Tsuchiya K, Siddiqui S *et al.* T cell-induced airway smooth muscle cell proliferation via the epidermal growth factor receptor. *Am J Respir Cell Mol Biol* 2013; **49**(4)**:** 563-570.

159. Threadgill D, Dlugosz A, Hansen L, Tennenbaum T, Lichti U, Yee D *et al.* Targeted disruption of mouse EGF receptor: effect of genetic background on mutant phenotype. *Science* 1995; **269**(5221)**:** 230-234.

160. Sibilia M, Wagner E. Strain-dependent epithelial defects in mice lacking the EGF receptor. *Science* 1995; **269**(5221)**:** 234-238.

161. Miettinen PJ, Berger JE, Meneses J, Phung Y, Pedersen RA, Werb Z *et al.* Epithelial immaturity and multiorgan failure in mice lacking epidermal growth factor receptor. *Nature* 1995; **376**(6538)**:** 337-341.

162. Sigismund S, Avanzato D, Lanzetti L. Emerging functions of the EGFR in cancer. *Mol Oncol* 2018; **12**(1)**:** 3-20.

163. Jamieson AM, Pasman L, Yu S, Gamradt P, Homer RJ, Decker T *et al.* Role of tissue protection in lethal respiratory viral-bacterial coinfection. *Science* 2013; **340**(6137)**:** 1230-1234.

164. Hall OJ, Limjunyawong N, Vermillion MS, Robinson DP, Wohlgemuth N, Pekosz A *et al.* Progesterone-Based Therapy Protects Against Influenza by Promoting Lung Repair and Recovery in Females. *PLoS Pathog* 2016; **12**(9)**:** e1005840.

165. Hur GY, Lee SY, Lee SH, Kim SJ, Lee KJ, Jung JY *et al.* Potential use of an anticancer drug gefinitib, an EGFR inhibitor, on allergic airway inflammation. *Exp Mol Med* 2007; **39**(3)**:** 367-375.

166. Le Cras TD, Acciani TH, Mushaben EM, Kramer EL, Pastura PA, Hardie WD *et al.* Epithelial EGF receptor signaling mediates airway hyperreactivity and remodeling in a mouse model of chronic asthma. *Am J Physiol Lung Cell Mol Physiol* 2011; **300**(3)**:** L414-421.

167. Acciani TH, Suzuki T, Trapnell BC, Le Cras TD. Epidermal growth factor receptor signalling regulates granulocyte-macrophage colony-stimulating factor production by airway epithelial cells and established allergic airway disease. *Clin Exp Allergy* 2016; **46**(2)**:** 317-328.

168. Wang Q, Li H, Yao Y, Xia D, Zhou J. The overexpression of heparin-binding epidermal growth factor is responsible for Th17-induced airway remodeling in an experimental asthma model. *J Immunol* 2010; **185**(2)**:** 834-841.

169. Jia Z, Bao K, Wei P, Yu X, Zhang Y, Wang X *et al.* EGFR activation-induced decreases in claudin1 promote MUC5AC expression and exacerbate asthma in mice. *Mucosal Immunology* 2020.

170. Vargaftig BB, Singer M. Leukotrienes mediate part of Ova-induced lung effects in mice via EGFR. *Am J Physiol Lung Cell Mol Physiol* 2003; **285**(4)**:** L808-818.

171. Wang Q, Li H, Yao Y, Lu G, Wang Y, Xia D *et al.* HB-EGF-Promoted Airway Smooth Muscle Cells and Their Progenitor Migration Contribute to Airway Smooth Muscle Remodeling in Asthmatic Mouse. *J Immunol* 2016; **196**(5)**:** 2361-2367.

172. Guo Y, Ding Q, Chen L, Ji C, Hao H, Wang J *et al.* Overexpression of Heparin-Binding Epidermal Growth Factor-Like Growth Factor Mediates Liver Fibrosis in Transgenic Mice. *Am J Med Sci* 2017; **354**(2)**:** 199-210.

173. Ding L, Liu T, Wu Z, Hu B, Nakashima T, Ullenbruch M *et al.* Bone Marrow CD11c+ Cell-Derived Amphiregulin Promotes Pulmonary Fibrosis. *J Immunol* 2016; **197**(1)**:** 303-312.

174. Zhou Y, Lee JY, Lee CM, Cho WK, Kang MJ, Koff JL *et al.* Amphiregulin, an epidermal growth factor receptor ligand, plays an essential role in the pathogenesis of transforming growth factor-beta-induced pulmonary fibrosis. *J Biol Chem* 2012; **287**(50)**:** 41991-42000.

175. Hardie WD, Piljan-Gentle A, Dunlavy MR, Ikegami M, Korfhagen TR. Dose-dependent lung remodeling in transgenic mice expressing transforming growth factor-alpha. *Am J Physiol Lung Cell Mol Physiol* 2001; **281**(5)**:** L1088-1094.

176. Hardie WD, Le Cras TD, Jiang K, Tichelaar JW, Azhar M, Korfhagen TR. Conditional expression of transforming growth factor-alpha in adult mouse lung causes pulmonary fibrosis. *Am J Physiol Lung Cell Mol Physiol* 2004; **286**(4)**:** L741-749.

177. Dahlhoff M, Schafer M, Wolf E, Schneider MR. Genetic deletion of the EGFR ligand epigen does not affect mouse embryonic development and tissue homeostasis. *Exp Cell Res* 2013; **319**(4)**:** 529-535.

178. Lee D, Pearsall RS, Das S, Dey SK, Godfrey VL, Threadgill DW. Epiregulin is not essential for development of intestinal tumors but is required for protection from intestinal damage. *Mol Cell Biol* 2004; **24**(20)**:** 8907-8916.

179. Luetteke NC, Qiu TH, Peiffer RL, Oliver P, Smithies O, Lee DC. TGFα deficiency results in hair follicle and eye abnormalities in targeted and waved-1 mice. *Cell* 1993; **73**(2)**:** 263-278.

180. Mann GB, Fowler KJ, Gabriel A, Nice EC, Williams RL, Dunn AR. Mice with a null mutation of the TGFα gene have abnormal skin architecture, wavy hair, and curly whiskers and often develop corneal inflammation. *Cell* 1993; **73**(2)**:** 249-261.

181. Manzo ND, Foster WM, Stripp BR. Amphiregulin-dependent mucous cell metaplasia in a model of nonallergic lung injury. *Am J Respir Cell Mol Biol* 2012; **47**(3)**:** 349-357.

182. Venkataraman T, Coleman CM, Frieman MB. Overactive Epidermal Growth Factor Receptor Signaling Leads to Increased Fibrosis after Severe Acute Respiratory Syndrome Coronavirus Infection. *J Virol* 2017; **91**(12).

183. Agaronyan K, Sharma L, Vaidyanathan B, Glenn K, Yu S, Annicelli C *et al.* Tissue remodeling by an opportunistic pathogen triggers allergic inflammation. *Immunity* 2022.

184. Huang G, Besner GE, Brigstock DR. Heparin-binding epidermal growth factor-like growth factor suppresses experimental liver fibrosis in mice. *Lab Invest* 2012; **92**(5)**:** 703-712.

185. Abourehab MAS, Alqahtani AM, Youssif BGM, Gouda AM. Globally Approved EGFR Inhibitors: Insights into Their Syntheses, Target Kinases, Biological Activities, Receptor Interactions, and Metabolism. *Molecules* 2021; **26**(21).

186. Cai WQ, Zeng LS, Wang LF, Wang YY, Cheng JT, Zhang Y *et al.* The Latest Battles Between EGFR Monoclonal Antibodies and Resistant Tumor Cells. *Front Oncol* 2020; **10:** 1249.

187. Woodruff PG, Wolff M, Hohlfeld JM, Krug N, Dransfield MT, Sutherland ER *et al.* Safety and efficacy of an inhaled epidermal growth factor receptor inhibitor (BIBW 2948 BS) in chronic obstructive pulmonary disease. *Am J Respir Crit Care Med* 2010; **181**(5)**:** 438-445.

188. Vallath S, Hynds RE, Succony L, Janes SM, Giangreco A. Targeting EGFR signalling in chronic lung disease: therapeutic challenges and opportunities. *Eur Respir J* 2014; **44**(2)**:** 513-522.

189. Turner S, Custovic A, Ghazal P, Grigg J, Gore M, Henderson J *et al.* Pulmonary epithelial barrier and immunological functions at birth and in early life - key determinants of the development of

asthma? A description of the protocol for the Breathing Together study. *Wellcome Open Res* 2018; **3:** 60.

190. Branchett WJ, Cook J, Oliver RA, Bruno N, Walker SA, Stölting H *et al.* Airway macrophage-intrinsic TGF-beta1 regulates pulmonary immunity during early-life allergen exposure. *J Allergy Clin Immunol* 2021; **147**(5)**:** 1892-1906.

191. Villenave R, O'Donoghue D, Thavagnanam S, Touzelet O, Skibinski G, Heaney LG *et al.* Differential cytopathogenesis of respiratory syncytial virus prototypic and clinical isolates in primary pediatric bronchial epithelial cells. *Virol J* 2011; **8:** 43.

192. Stölting H, Baillon L, Frise R, Bonner K, Hewitt RJ, Molyneaux PL *et al.* Distinct airway epithelial immune responses after infection with SARS-CoV-2 compared to H1N1. *Mucosal Immunology* 2022.

193. Ogger PP, Albers GJ, Hewitt RJ, O'Sullivan BJ, Powell JE, Calamita E *et al.* Itaconate controls the severity of pulmonary fibrosis. *Sci Immunol* 2020; **5**(52).

194. Jaccard N, Griffin LD, Keser A, Macown RJ, Super A, Veraitch FS *et al.* Automated method for the rapid and precise estimation of adherent cell culture characteristics from phase contrast microscopy images. *Biotechnol Bioeng* 2014; **111**(3)**:** 504-517.

195. Schindelin J, Arganda-Carreras I, Frise E, Kaynig V, Longair M, Pietzsch T *et al.* Fiji: an open-source platform for biological-image analysis. *Nat Methods* 2012; **9**(7)**:** 676-682.

196. Pattaroni C, Macowan M, Chatzis R, Daunt C, Custovic A, Shields MD *et al.* Early life inter-kingdom interactions shape the immunological environment of the airways. *Microbiome* 2022; **10**(1)**:** 34.

197. Warburton D. Overview of Lung Development in the Newborn Human. *Neonatology* 2017; **111**(4)**:** 398-401.

198. Schittny JC. Development of the lung. *Cell Tissue Res* 2017; **367**(3)**:** 427-444.

199. Ten Have-Opbroek AAW. Lung Development in the Mouse Embryo. *Experimental Lung Research* 1991; **17:** 111-130.

200. Warburton D, El-Hashash A, Carraro G, Tiozzo C, Sala F, Rogers O *et al.* Lung Organogenesis. *Organogenesis in Development*, 2010, pp 73-158.

201. Warburton D, Schwarz M, Tefft D, Flores-Delgado G, Anderson KD, Cardoso WV. The molecular basis of lung morphogenesis. *Mechanisms of Development* 2000; **92**(1)**:** 55-81.

202. Miettinen PJ, Warburton D, Bu D, Zhao JS, Berger JE, Minoo P *et al.* Impaired lung branching morphogenesis in the absence of functional EGF receptor. *Dev Biol* 1997; **186**(2)**:** 224-236.

203. Inoue A, Xin H, Suzuki T, Kanehira M, Kuroki Y, Fukuhara T *et al.* Suppression of surfactant protein A by an epidermal growth factor receptor tyrosine kinase inhibitor exacerbates lung inflammation. *Cancer Sci* 2008; **99**(8)**:** 1679-1684.

204. Wang Y, Maciejewski BS, Soto-Reyes D, Lee HS, Warburton D, Sanchez-Esteban J. Mechanical stretch promotes fetal type II epithelial cell differentiation via shedding of HB-EGF and TGF-alpha. *J Physiol* 2009; **587**(Pt 8)**:** 1739-1753.

205. Zhao J, Chen H, Peschon JJ, Shi W, Zhang Y, Frank SJ *et al.* Pulmonary hypoplasia in mice lacking tumor necrosis factor-alpha converting enzyme indicates an indispensable role for cell surface protein shedding during embryonic lung branching morphogenesis. *Dev Biol* 2001; **232**(1)**:** 204-218.

206. Schuger L, Johnson GR, Gilbride K, Plowman GD, Mandel R. Amphiregulin in lung branching morphogenesis: interaction with heparan sulfate proteoglycan modulates cell proliferation. *Development* 1996; **122**(6)**:** 1759-1767.

207. Luetteke NC, Qiu TH, Fenton SE, Troyer KL, Riedel RF, Chang A *et al.* Targeted inactivation of the EGF and amphiregulin genes reveals distinct roles for EGF receptor ligands in mouse mammary gland development. *Development* 1999; **126**(12)**:** 2739-2750.

208. Jackson LF, Qiu TH, Sunnarborg SW, Chang A, Zhang C, Patterson C *et al.* Defective valvulogenesis in HB-EGF and TACE-null mice is associated with aberrant BMP signaling. *EMBO J* 2003; **22**(11)**:** 2704-2716.

209. Strachan L, Murison JG, Prestidge RL, Sleeman MA, Watson JD, Kumble KD. Cloning and biological activity of epigen, a novel member of the epidermal growth factor superfamily. *J Biol Chem* 2001; **276**(21)**:** 18265-18271.

210. Polosa R, Prosperini G, Leir S-H, Holgate ST, Lackie PM, Davies DE. Expression of c-erbB Receptors and Ligands in Human Bronchial Mucosa. *American Journal of Respiratory Cell and Molecular Biology* 1999; **20**(5)**:** 914-923.

211. Strandjord TP, Clark JG, Guralnick DE, Madtes DK. Immunolocalization of transforming growth factor-alpha, epidermal growth factor (EGF), and EGF-receptor in normal and injured developing human lung. *Pediatr Res* 1995; **38**(6)**:** 851-856.

212. Amishima M, Munakata M, Nasuhara Y, Sato A, Takahashi T, Homma Y *et al.* Expression of epidermal growth factor and epidermal growth factor receptor immunoreactivity in the asthmatic human airway. *Am J Respir Crit Care Med* 1998; **157**(6 Pt 1)**:** 1907-1912.

213. Puddicombe SM, Polosa R, Richter A, Krishna MT, Howarth PH, Holgate ST *et al.* Involvement of the epidermal growth factor receptor in epithelial repair in asthma. *The FASEB Journal* 2000; **14**(10)**:** 1362-1374.

214. Takeyama K, Fahy JV, Nadel JA. Relationship of epidermal growth factor receptors to goblet cell production in human bronchi. *Am J Respir Crit Care Med* 2001; **163**(2)**:** 511-516.

215. Fedorov IA, Wilson SJ, Davies DE, Holgate ST. Epithelial stress and structural remodelling in childhood asthma. *Thorax* 2005; **60**(5)**:** 389-394.

216. Polosa R, Puddicombe SM, Krishna MT, Tuck AB, Howarth PH, Holgate ST *et al.* Expression of c-erbB receptors and ligands in the bronchial epithelium of asthmatic subjects. *Journal of Allergy and Clinical Immunology* 2002; **109**(1)**:** 75-81.

217. Anderson KG, Mayer-Barber K, Sung H, Beura L, James BR, Taylor JJ *et al.* Intravascular staining for discrimination of vascular and tissue leukocytes. *Nat Protoc* 2014; **9**(1)**:** 209-222.

218. Hirota N, Risse PA, Novali M, McGovern T, Al-Alwan L, McCuaig S *et al.* Histamine may induce airway remodeling through release of epidermal growth factor receptor ligands from bronchial epithelial cells. *FASEB J* 2012; **26**(4)**:** 1704-1716.

219. Enomoto Y, Orihara K, Takamasu T, Matsuda A, Gon Y, Saito H *et al.* Tissue remodeling induced by hypersecreted epidermal growth factor and amphiregulin in the airway after an acute asthma attack. *J Allergy Clin Immunol* 2009; **124**(5)**:** 913-920 e911-917.

220. Kim KW, Jee HM, Park YH, Choi BS, Sohn MH, Kim KE. Relationship between amphiregulin and airway inflammation in children with asthma and eosinophilic bronchitis. *Chest* 2009; **136**(3)**:** 805-810.

221. Muehling LM, Heymann PW, Carper H, Murphy DD, Rajadhyaksha E, Kennedy J *et al.* Cluster Analysis of Nasal Cytokines During Rhinovirus Infection Identifies Different Immunophenotypes in Both Children and Adults with Allergic Asthma. *Clin Exp Allergy* 2022.

222. Chen JY, Cheng WH, Lee KY, Kuo HP, Chung KF, Chen CL *et al.* Abnormal ADAM17 expression causes airway fibrosis in chronic obstructive asthma. *Biomed Pharmacother* 2021; **140:** 111701.

223. Habibovic A, Hristova M, Heppner DE, Danyal K, Ather JL, Janssen-Heininger YM *et al.* DUOX1 mediates persistent epithelial EGFR activation, mucous cell metaplasia, and airway remodeling during allergic asthma. *JCI Insight* 2016; **1**(18)**:** e88811.

224. Lordan JL, Bucchieri F, Richter A, Konstantinidis A, Holloway JW, Thornber M *et al.* Cooperative Effects of Th2 Cytokines and Allergen on Normal and Asthmatic Bronchial Epithelial Cells. *The Journal of Immunology* 2002; **169**(1)**:** 407-414.

225. Daines M, Zhu L, Pereira R, Zhou X, Bondy C, Pryor BM *et al.* Alternaria induces airway epithelial cytokine expression independent of protease-activated receptor. *Respirology* 2019.

226. Garcia LN, Leimgruber C, Nicola JP, Quintar AA, Maldonado CA. Neonatal endotoxin stimulation is associated with a long-term bronchiolar epithelial expression of innate immune and anti-allergic markers that attenuates the allergic response. *PLoS One* 2020; **15**(5)**:** e0226233.

227. Tamaoka M, Hassan M, McGovern T, Ramos-Barbon D, Jo T, Yoshizawa Y *et al.* The epidermal growth factor receptor mediates allergic airway remodelling in the rat. *Eur Respir J* 2008; **32**(5)**:** 1213-1223.

228. Leigh R, Oyelusi W, Wiehler S, Koetzler R, Zaheer RS, Newton R *et al.* Human rhinovirus infection enhances airway epithelial cell production of growth factors involved in airway remodeling. *J Allergy Clin Immunol* 2008; **121**(5)**:** 1238-1245 e1234.

229. Kalinowski A, Galen BT, Ueki IF, Sun Y, Mulenos A, Osafo-Addo A *et al.* Respiratory syncytial virus activates epidermal growth factor receptor to suppress interferon regulatory factor 1-dependent interferon-lambda and antiviral defense in airway epithelium. *Mucosal Immunol* 2018; **11**(3)**:** 958-967.

230. Wang W, Wu J, Zhang X, Hao C, Zhao X, Jiao G *et al.* Inhibition of Influenza A Virus Infection by Fucoidan Targeting Viral Neuraminidase and Cellular EGFR Pathway. *Sci Rep* 2017; **7:** 40760.

231. Zhu L, Lee PK, Lee WM, Zhao Y, Yu D, Chen Y. Rhinovirus-induced major airway mucin production involves a novel TLR3-EGFR-dependent pathway. *Am J Respir Cell Mol Biol* 2009; **40**(5)**:** 610-619.

232. Monick MM, Cameron K, Staber J, Powers LS, Yarovinsky TO, Koland JG *et al.* Activation of the epidermal growth factor receptor by respiratory syncytial virus results in increased inflammation and delayed apoptosis. *J Biol Chem* 2005; **280**(3)**:** 2147-2158.

233. Barbier D, Garcia-Verdugo I, Pothlichet J, Khazen R, Descamps D, Rousseau K *et al.* Influenza A induces the major secreted airway mucin MUC5AC in a protease-EGFR-extracellular regulated kinase-Sp1-dependent pathway. *Am J Respir Cell Mol Biol* 2012; **47**(2)**:** 149-157.

234. Eierhoff T, Hrincius ER, Rescher U, Ludwig S, Ehrhardt C. The epidermal growth factor receptor (EGFR) promotes uptake of influenza A viruses (IAV) into host cells. *PLoS Pathog* 2010; **6**(9)**:** e1001099.

235. Hewson CA, Haas JJ, Bartlett NW, Message SD, Laza-Stanca V, Kebadze T *et al.* Rhinovirus induces MUC5AC in a human infection model and in vitro via NF-kappaB and EGFR pathways. *Eur Respir J* 2010; **36**(6)**:** 1425-1435.

236. Liu K, Gualano RC, Hibbs ML, Anderson GP, Bozinovski S. Epidermal growth factor receptor signaling to Erk1/2 and STATs control the intensity of the epithelial inflammatory responses to rhinovirus infection. *J Biol Chem* 2008; **283**(15)**:** 9977-9985.

237. Ueki IF, Min-Oo G, Kalinowski A, Ballon-Landa E, Lanier LL, Nadel JA *et al.* Respiratory virus-induced EGFR activation suppresses IRF1-dependent interferon lambda and antiviral defense in airway epithelium. *J Exp Med* 2013; **210**(10)**:** 1929-1936.

238. Currier MG, Lee S, Stobart CC, Hotard AL, Villenave R, Meng J *et al.* EGFR Interacts with the Fusion Protein of Respiratory Syncytial Virus Strain 2-20 and Mediates Infection and Mucin Expression. *PLoS Pathog* 2016; **12**(5)**:** e1005622.

239. Beauchemin KJ, Wells JM, Kho AT, Philip VM, Kamir D, Kohane IS *et al.* Temporal dynamics of the developing lung transcriptome in three common inbred strains of laboratory mice reveals multiple stages of postnatal alveolar development. *PeerJ* 2016; **4:** e2318.

240. Travaglini KJ, Nabhan AN, Penland L, Sinha R, Gillich A, Sit RV *et al.* A molecular cell atlas of the human lung from single-cell RNA sequencing. *Nature* 2020; **587**(7835)**:** 619-625.

241. Shaykhiev R, Zuo WL, Chao I, Fukui T, Witover B, Brekman A *et al.* EGF shifts human airway basal cell fate toward a smoking-associated airway epithelial phenotype. *Proc Natl Acad Sci U S A* 2013; **110**(29)**:** 12102-12107.

242. Yuan L, Zhang X, Yang M, Du X, Wang L, Wu S *et al.* Airway epithelial integrin beta4 suppresses allergic inflammation by decreasing CCL17 production. *Clin Sci (Lond)* 2020; **134**(13)**:** 1735-1749.

243. Siddiqui S, Novali M, Tsuchiya K, Hirota N, Geller BJ, McGovern TK *et al.* The modulation of large airway smooth muscle phenotype and effects of epidermal growth factor receptor inhibition in the repeatedly allergen-challenged rat. *Am J Physiol Lung Cell Mol Physiol* 2013; **304**(12)**:** L853-862.

244. Tsuchiya K, Jo T, Takeda N, Al Heialy S, Siddiqui S, Shalaby KH *et al.* EGF receptor activation during allergic sensitization affects IL-6-induced T-cell influx to airways in a rat model of asthma. *Eur J Immunol* 2010; **40**(6)**:** 1590-1602.

245. Tang S, Du X, Yuan L, Xiao G, Wu M, Wang L *et al.* Airway epithelial ITGB4 deficiency in early life mediates pulmonary spontaneous inflammation and enhanced allergic immune response. *J Cell Mol Med* 2020.

246. Kajiwara N, Oboki K, Ohno T, Ishii A, Sunnarborg SW, Okumura K *et al.* Amphiregulin is not essential for ovalbumin-induced acute airway inflammation in mice. *Allergol Int* 2010; **59**(2)**:** 207-211.

247. Bi Y, Deng J, Murry DJ, An G. A Whole-Body Physiologically Based Pharmacokinetic Model of Gefitinib in Mice and Scale-Up to Humans. *AAPS J* 2016; **18**(1)**:** 228-238.

248. Shi L, Tang J, Tong L, Liu Z. Risk of interstitial lung disease with gefitinib and erlotinib in advanced non-small cell lung cancer: a systematic review and meta-analysis of clinical trials. *Lung Cancer* 2014; **83**(2)**:** 231-239.

249. Cersosimo RJ. Gefitinib: an adverse effects profile. *Expert Opin Drug Saf* 2006; **5**(3)**:** 469-479.

250. Plantinga M, Guilliams M, Vanheerswynghels M, Deswarte K, Branco-Madeira F, Toussaint W *et al.* Conventional and monocyte-derived CD11b(+) dendritic cells initiate and maintain T helper 2 cell-mediated immunity to house dust mite allergen. *Immunity* 2013; **38**(2)**:** 322-335.

251. Bosteels C, Neyt K, Vanheerswynghels M, van Helden MJ, Sichien D, Debeuf N *et al.* Inflammatory Type 2 cDCs Acquire Features of cDC1s and Macrophages to Orchestrate Immunity to Respiratory Virus Infection. *Immunity* 2020; **52**(6)**:** 1039-1056 e1039.

252. Zhou J, Zhou XD, Xu R, Du XZ, Li Q, Li B *et al.* The Degradation of Airway Epithelial Tight Junctions in Asthma Under High Airway Pressure Is Probably Mediated by Piezo-1. *Front Physiol* 2021; **12:** 637790.

253. Woszczek G, Kowalski ML, Borowiec M. Association of asthma and total IgE levels with human leucocyte antigen-DR in patients with grass allergy. *Eur Respir J* 2002; **20**(1)**:** 79-85.

254. Snelgrove RJ, Gregory LG, Peiro T, Akthar S, Campbell GA, Walker SA *et al.* Alternaria-derived serine protease activity drives IL-33-mediated asthma exacerbations. *J Allergy Clin Immunol* 2014; **134**(3)**:** 583-592 e586.

255. Nadel JA. Role of epidermal growth factor receptor activation in regulating mucin synthesis. *Respir Res* 2001; **2**(2)**:** 85-89.

256. Shim JJ, Dabbagh K, Ueki IF, Dao-Pick T, Burgel PR, Takeyama K *et al.* IL-13 induces mucin production by stimulating epidermal growth factor receptors and by activating neutrophils. *Am J Physiol Lung Cell Mol Physiol* 2001; **280**(1)**:** L134-140.

257. Singanayagam A, Footitt J, Marczynski M, Radicioni G, Cross MT, Finney LJ *et al.* Airway mucins promote immunopathology in virus-exacerbated chronic obstructive pulmonary disease. *J Clin Invest* 2022; **132**(8).

258. Shao MX, Ueki IF, Nadel JA. Tumor necrosis factor alpha-converting enzyme mediates MUC5AC mucin expression in cultured human airway epithelial cells. *Proc Natl Acad Sci U S A* 2003; **100**(20)**:** 11618-11623.

259. Du X, Yang Y, Yang M, Yuan L, Wang L, Wu M *et al.* ITGB4 deficiency induces mucus hypersecretion by upregulating MUC5AC in RSV-infected airway epithelial cells. *Int J Biol Sci* 2022; **18**(1)**:** 349-359.

260. Nakanishi A, Morita S, Iwashita H, Sagiya Y, Ashida Y, Shirafuji H *et al.* Role of gob-5 in mucus overproduction and airway hyperresponsiveness in asthma. *Proc Natl Acad Sci U S A* 2001; **98**(9)**:** 5175-5180.

261. Evans CM, Raclawska DS, Ttofali F, Liptzin DR, Fletcher AA, Harper DN *et al.* The polymeric mucin Muc5ac is required for allergic airway hyperreactivity. *Nat Commun* 2015; **6:** 6281.

262. Molloy BJ, King A, Mullin LG, Gethings LA, Riley R, Plumb RS *et al.* Rapid determination of the pharmacokinetics and metabolic fate of gefitinib in the mouse using a combination of UPLC/MS/MS, UPLC/QToF/MS, and ion mobility (IM)-enabled UPLC/QToF/MS. *Xenobiotica* 2021; **51**(4)**:** 434-446.

263. Andersson CK, Iwasaki J, Cook J, Robinson P, Nagakumar P, Mogren S *et al.* Impaired airway epithelial cell wound-healing capacity is associated with airway remodelling following RSV infection in severe preschool wheeze. *Allergy* 2020; **75**(12)**:** 3195-3207.

264. Puttur F, Denney L, Gregory LG, Vuononvirta J, Oliver R, Entwistle LJ *et al.* Pulmonary environmental cues drive group 2 innate lymphoid cell dynamics in mice and humans. *Sci Immunol* 2019; **4**(36).

265. Burgstaller G, Oehrle B, Gerckens M, White ES, Schiller HB, Eickelberg O. The instructive extracellular matrix of the lung: basic composition and alterations in chronic lung disease. *Eur Respir J* 2017; **50**(1).

266. Padrez Y, Golubewa L, Kulahava T, Vladimirskaja T, Semenkova G, Adzerikho I *et al.* Quantitative and qualitative analysis of pulmonary arterial hypertension fibrosis using wide-field second harmonic generation microscopy. *Sci Rep* 2022; **12**(1)**:** 7330.

267. Tilbury K, Hocker J, Wen BL, Sandbo N, Singh V, Campagnola PJ. Second harmonic generation microscopy analysis of extracellular matrix changes in human idiopathic pulmonary fibrosis. *J Biomed Opt* 2014; **19**(8)**:** 086014.

268. Mostaco-Guidolin LB, Loube J, Barlow A, Osei ET, Vasilescu DM, Hsieh A *et al.* Second harmonic generation imaging of collagen scaffolds within the alveolar ducts of healthy and emphysematous mouse lungs. *Histochem Cell Biol* 2021; **155**(2)**:** 279-289.

269. Mostaco-Guidolin LB, Osei ET, Ullah J, Hajimohammadi S, Fouadi M, Li X *et al.* Defective Fibrillar Collagen Organization by Fibroblasts Contributes to Airway Remodeling in Asthma. *Am J Respir Crit Care Med* 2019; **200**(4)**:** 431-443.

270. Margelidon-Cozzolino V, Tsicopoulos A, Chenivesse C, de Nadai P. Role of Th17 Cytokines in Airway Remodeling in Asthma and Therapy Perspectives. *Front Allergy* 2022; **3:** 806391.

271. Debeuf N, Haspeslagh E, van Helden M, Hammad H, Lambrecht BN. Mouse Models of Asthma. *Curr Protoc Mouse Biol* 2016; **6**(2)**:** 169-184.

272. Parkinson JE, Pearson S, Ruckerl D, Allen JE, Sutherland TE. The magnitude of airway remodeling is not altered by distinct allergic inflammatory responses in BALB/c versus C57BL/6 mice but matrix composition differs. *Immunol Cell Biol* 2021; **99**(6)**:** 640-655.

273. Saglani S. Childhood severe asthma: New insights on remodelling and biomarkers. *Paediatr Respir Rev* 2017; **24:** 11-13.

274. O'Brien CE, Tsirilakis K, Santiago MT, Goldman DL, Vicencio AG. Heterogeneity of lower airway inflammation in children with severe-persistent asthma. *Pediatr Pulmonol* 2015; **50**(12)**:** 1200-1204.

275. Klein SL, Flanagan KL. Sex differences in immune responses. *Nat Rev Immunol* 2016; **16**(10)**:** 626-638.

276. Abeler-Dorner L, Laing AG, Lorenc A, Ushakov DS, Clare S, Speak AO *et al.* High-throughput phenotyping reveals expansive genetic and structural underpinnings of immune variation. *Nat Immunol* 2020; **21**(1)**:** 86-100.

277. Zein JG, Erzurum SC. Asthma is Different in Women. *Curr Allergy Asthma Rep* 2015; **15**(6)**:** 28.

278. Nicolai T, Pereszlenyiova-Bliznakova L, Illi S, Reinhardt D, von Mutius E. Longitudinal follow-up of the changing gender ratio in asthma from childhood to adulthood: role of delayed manifestation in girls. *Pediatr Allergy Immunol* 2003; **14**(4)**:** 280-283.

279. Vink NM, Postma DS, Schouten JP, Rosmalen JG, Boezen HM. Gender differences in asthma development and remission during transition through puberty: the TRacking Adolescents' Individual Lives Survey (TRAILS) study. *J Allergy Clin Immunol* 2010; **126**(3)**:** 498-504 e491-496.

280. Chen Y. Sex difference in hospitalization due to asthma in relation to age. *Journal of Clinical Epidemiology* 2003; **56**(2)**:** 180-187.

281. Skobeloff EM, Spivey WH, St Clair SS, Schoffstall JM. The influence of age and sex on asthma admissions. *JAMA* 1992; **268**(24)**:** 3437-3440.

282. Kynyk JA, Mastronarde JG, McCallister JW. Asthma, the sex difference. *Curr Opin Pulm Med* 2011; **17**(1)**:** 6-11.

283. Fu L, Freishtat RJ, Gordish-Dressman H, Teach SJ, Resca L, Hoffman EP *et al.* Natural progression of childhood asthma symptoms and strong influence of sex and puberty. *Ann Am Thorac Soc* 2014; **11**(6)**:** 939-944.

284. Salam MT, Wenten M, Gilliland FD. Endogenous and exogenous sex steroid hormones and asthma and wheeze in young women. *J Allergy Clin Immunol* 2006; **117**(5)**:** 1001-1007.

285. Agarwal AK, Shah A. Menstrual-linked asthma. *J Asthma* 1997; **34**(6)**:** 539-545.

286. Pauli BD, Reid RL, Munt PW, Wigle RD, Forkert L. Influence of the Menstrual Cycle on Airway Function in Asthmatic and Normal Subjects. *American review of respiratory disease* 1989; **140**(2)**:** 358-362.

287. Shames RS, Heilbron DC, Janson SL, Kishiyama JL, Au DS, Adelman DC. Clinical Differences Among Women with and Without Self-Reported Perimenstrual Asthma. *Annals of Allergy, Asthma & Immunology* 1998; **81**(1)**:** 65-72.

288. Rao CK, Moore CG, Bleecker E, Busse WW, Calhoun W, Castro M *et al.* Characteristics of perimenstrual asthma and its relation to asthma severity and control: data from the Severe Asthma Research Program. *Chest* 2013; **143**(4)**:** 984-992.

289. Troisi RJ, Speizer FE, Willett WC, Trichopoulos D, Rosner B. Menopause, postmenopausal estrogen preparations, and the risk of adult-onset asthma. A prospective cohort study. *American journal of respiratory and critical care medicine* 1995; **152**(4)**:** 1183-1188.

290. McCleary N, Nwaru BI, Nurmatov UB, Critchley H, Sheikh A. Endogenous and exogenous sex steroid hormones in asthma and allergy in females: A systematic review and meta-analysis. *J Allergy Clin Immunol* 2018; **141**(4)**:** 1510-1513 e1518.

291. Hayashi T, Adachi Y, Hasegawa K, Morimoto M. Less sensitivity for late airway inflammation in males than females in BALB/c mice. *Scand J Immunol* 2003; **57**(6)**:** 562-567.

292. Melgert BN, Postma DS, Kuipers I, Geerlings M, Luinge MA, van der Strate BW *et al.* Female mice are more susceptible to the development of allergic airway inflammation than male mice. *Clin Exp Allergy* 2005; **35**(11)**:** 1496-1503.

293. Takeda M, Tanabe M, Ito W, Ueki S, Konnno Y, Chihara M *et al.* Gender difference in allergic airway remodelling and immunoglobulin production in mouse model of asthma. *Respirology* 2013; **18**(5)**:** 797-806.

294. Blacquiere MJ, Hylkema MN, Postma DS, Geerlings M, Timens W, Melgert BN. Airway inflammation and remodeling in two mouse models of asthma: comparison of males and females. *Int Arch Allergy Immunol* 2010; **153**(2)**:** 173-181.

295. Laffont S, Blanquart E, Savignac M, Cenac C, Laverny G, Metzger D *et al.* Androgen signaling negatively controls group 2 innate lymphoid cells. *J Exp Med* 2017; **214**(6)**:** 1581-1592.

296. Weiss K, Wanner N, Queisser K, Frimel M, Nunn T, Myshrall T *et al.* Barrier Housing and Gender Effects on Allergic Airway Disease in a Murine House Dust Mite Model. *Immunohorizons* 2021; **5**(1)**:** 33-47.

297. Fuseini H, Yung JA, Cephus JY, Zhang J, Goleniewska K, Polosukhin VV *et al.* Testosterone Decreases House Dust Mite-Induced Type 2 and IL-17A-Mediated Airway Inflammation. *J Immunol* 2018; **201**(7)**:** 1843-1854.

298. Riffo-Vasquez Y, Ligeiro de Oliveira AP, Page CP, Spina D, Tavares-de-Lima W. Role of sex hormones in allergic inflammation in mice. *Clin Exp Allergy* 2007; **37**(3)**:** 459-470.

299. Newcomb DC, Cephus JY, Boswell MG, Fahrenholz JM, Langley EW, Feldman AS *et al.* Estrogen and progesterone decrease let-7f microRNA expression and increase IL-23/IL-23 receptor signaling and IL-17A production in patients with severe asthma. *J Allergy Clin Immunol* 2015; **136**(4)**:** 1025-1034 e1011.

300. Lauzon-Joset JF, Mincham KT, Abad AP, Short BP, Holt PG, Strickland DH *et al.* Oestrogen amplifies pre-existing atopy-associated Th2 bias in an experimental asthma model. *Clin Exp Allergy* 2020; **50**(3)**:** 391-400.

301. Hellings PW, Vandekerckhove P, Claeys R, Billen J, Kasran A, Ceuppens JL. Progesterone increases airway eosinophilia and hyper-responsiveness in a murine model of allergic asthma. *Clin Exp Allergy* 2003; **33**(10)**:** 1457-1463.

302. Yu CK, Yang BC, Lei HY, Chen YC, Liu YH, Chen CC *et al.* Attenuation of house dust mite Dermatophagoides farinae-induced airway allergic responses in mice by dehydroepiandrosterone is correlated with down-regulation of TH2 response. *Clin Exp Allergy* 1999; **29**(3)**:** 414-422.

303. Cephus JY, Gandhi VD, Shah R, Brooke Davis J, Fuseini H, Yung JA *et al.* Estrogen receptor-alpha signaling increases allergen-induced IL-33 release and airway inflammation. *Allergy* 2021; **76**(1)**:** 255-268.

304. Malinczak CA, Fonseca W, Rasky AJ, Ptaschinski C, Morris S, Ziegler SF *et al.* Sex-associated TSLP-induced immune alterations following early-life RSV infection leads to enhanced allergic disease. *Mucosal Immunol* 2019; **12**(4)**:** 969-979.

305. Phan JA, Kicic A, Berry LJ, Sly PD, Larcombe AN. Early life rhinovirus infection exacerbates house-dust-mite induced lung disease more severely in female mice. *Exp Lung Res* 2016; **42**(1)**:** 24-36.

306. Keselman A, Fang X, White PB, Heller NM. Estrogen Signaling Contributes to Sex Differences in Macrophage Polarization during Asthma. *J Immunol* 2017; **199**(5)**:** 1573-1583.

307. Fuseini H, Newcomb DC. Mechanisms Driving Gender Differences in Asthma. *Curr Allergy Asthma Rep* 2017; **17**(3)**:** 19.

308. Filardo EJ. Epidermal growth factor receptor (EGFR) transactivation by estrogen via the G-protein-coupled receptor, GPR30: a novel signaling pathway with potential significance for breast cancer. *The Journal of Steroid Biochemistry and Molecular Biology* 2002; **80**(2)**:** 231-238.

309. Brunsing RL, Owens KS, Prossnitz ER. The G protein-coupled estrogen receptor (GPER) agonist G-1 expands the regulatory T-cell population under TH17-polarizing conditions. *J Immunother* 2013; **36**(3)**:** 190-196.

310. Pierdominici M, Maselli A, Colasanti T, Giammarioli AM, Delunardo F, Vacirca D *et al.* Estrogen receptor profiles in human peripheral blood lymphocytes. *Immunol Lett* 2010; **132**(1-2)**:** 79-85.

311. Bell MR. Comparing Postnatal Development of Gonadal Hormones and Associated Social Behaviors in Rats, Mice, and Humans. *Endocrinology* 2018; **159**(7)**:** 2596-2613.

312. Chowdhury NU, Guntur VP, Newcomb DC, Wechsler ME. Sex and gender in asthma. *Eur Respir Rev* 2021; **30**(162).

313. Bunone G, Briand PA, Miksicek RJ, Picard D. Activation of the unliganded estrogen receptor by EGF involves the MAP kinase pathway and direct phosphorylation. *The EMBO Journal* 1996; **15**(9)**:** 2174-2183.

314. Kato S, Endoh H, Masuhiro Y, Kitamoto T, Uchiyama S, Sasaki H *et al.* Activation of the Estrogen Receptor Through Phosphorylation by Mitogen-Activated Protein Kinase. *Science* 1995; **270**(5241)**:** 1491-1494.

315. Britton DJ, Hutcheson IR, Knowlden JM, Barrow D, Giles M, McClelland RA *et al.* Bidirectional cross talk between ERalpha and EGFR signalling pathways regulates tamoxifen-resistant growth. *Breast Cancer Res Treat* 2006; **96**(2)**:** 131-146.

316. Martinez-Lacaci I, Saceda M, Plowman GD, Johnson GR, Normanno N, Salomon DS *et al.* Estrogen and phorbol esters regulate amphiregulin expression by two separate mechanisms in human breast cancer cell lines. *Endocrinology* 1995; **136**(9)**:** 3983-3992.

317. Hutcheson IR, Knowlden JM, Madden TA, Barrow D, Gee JM, Wakeling AE *et al.* Oestrogen receptor-mediated modulation of the EGFR/MAPK pathway in tamoxifen-resistant MCF-7 cells. *Breast Cancer Res Treat* 2003; **81**(1)**:** 81-93.

318. Cai Y, Zhou J, Webb DC. Estrogen stimulates Th2 cytokine production and regulates the compartmentalisation of eosinophils during allergen challenge in a mouse model of asthma. *Int Arch Allergy Immunol* 2012; **158**(3)**:** 252-260.

319. Lambert KC, Curran EM, Judy BM, Milligan GN, Lubahn DB, Estes DM. Estrogen receptor alpha (ERalpha) deficiency in macrophages results in increased stimulation of CD4+ T cells while 17beta-estradiol acts through ERalpha to increase IL-4 and GATA-3 expression in CD4+ T cells independent of antigen presentation. *J Immunol* 2005; **175**(9)**:** 5716-5723.

320. Salem ML. Estrogen, a double-edged sword: modulation of TH1- and TH2-mediated inflammations by differential regulation of TH1/TH2 cytokine production. *Curr Drug Targets Inflamm Allergy* 2004; **3**(1)**:** 97-104.

321. Macdonald F, van Loosdregt J, Zaiss DMW. T cell derived HB-EGF prevents Th17 cell differentiation in an autocrine way. *bioRxiv* 2021**:** 2021.2002.2009.430418.

322. Roy S, Rizvi ZA, Clarke AJ, Macdonald F, Pandey A, Zaiss DMW *et al.* EGFR-HIF1alpha signaling positively regulates the differentiation of IL-9 producing T helper cells. *Nat Commun* 2021; **12**(1)**:** 3182.

323. Study to Assess the Efficacy, Safety, and Tolerability of SAR440340/REGN3500/Itepekimab in Chronic Obstructive Pulmonary Disease (COPD) (AERIFY-2). https://ClinicalTrials.gov/show/NCT04751487.

324. Zhu N, Zhang D, Wang W, Li X, Yang B, Song J *et al.* A Novel Coronavirus from Patients with Pneumonia in China, 2019. *New England Journal of Medicine* 2020; **382**(8)**:** 727-733.

325. Zhou P, Yang XL, Wang XG, Hu B, Zhang L, Zhang W *et al.* A pneumonia outbreak associated with a new coronavirus of probable bat origin. *Nature* 2020; **579**(7798)**:** 270-273.

326. Wu F, Zhao S, Yu B, Chen YM, Wang W, Song ZG *et al.* A new coronavirus associated with human respiratory disease in China. *Nature* 2020; **579**(7798)**:** 265-269.

327. Wu Z, McGoogan JM. Characteristics of and Important Lessons From the Coronavirus Disease 2019 (COVID-19) Outbreak in China: Summary of a Report of 72314 Cases From the Chinese Center for Disease Control and Prevention. *JAMA* 2020; **323**(13)**:** 1239-1242.

328. Li J, Huang DQ, Zou B, Yang H, Hui WZ, Rui F *et al.* Epidemiology of COVID-19: A systematic review and meta-analysis of clinical characteristics, risk factors, and outcomes. *J Med Virol* 2021; **93**(3)**:** 1449-1458.

329. O'Driscoll M, Ribeiro Dos Santos G, Wang L, Cummings DAT, Azman AS, Paireau J *et al.* Age-specific mortality and immunity patterns of SARS-CoV-2. *Nature* 2021; **590**(7844)**:** 140-145.

330. Lu X, Zhang L, Du H, Zhang J, Li YY, Qu J *et al.* SARS-CoV-2 Infection in Children. *N Engl J Med* 2020; **382**(17)**:** 1663-1665.

331. Cui X, Zhao Z, Zhang T, Guo W, Guo W, Zheng J *et al.* A systematic review and meta-analysis of children with coronavirus disease 2019 (COVID-19). *J Med Virol* 2021; **93**(2)**:** 1057-1069.

332. Goldstein E, Lipsitch M, Cevik M. On the Effect of Age on the Transmission of SARS-CoV-2 in Households, Schools, and the Community. *J Infect Dis* 2021; **223**(3)**:** 362-369.

333. Ladhani SN, Amin-Chowdhury Z, Davies HG, Aiano F, Hayden I, Lacy J *et al.* COVID-19 in children: analysis of the first pandemic peak in England. *Arch Dis Child* 2020; **105**(12)**:** 1180-1185.

334. Zhu Y, Bloxham CJ, Hulme KD, Sinclair JE, Tong ZWM, Steele LE *et al.* A Meta-analysis on the Role of Children in Severe Acute Respiratory Syndrome Coronavirus 2 in Household Transmission Clusters. *Clin Infect Dis* 2021; **72**(12)**:** e1146-e1153.

335. Hoffmann M, Kleine-Weber H, Schroeder S, Kruger N, Herrler T, Erichsen S *et al.* SARS-CoV-2 Cell Entry Depends on ACE2 and TMPRSS2 and Is Blocked by a Clinically Proven Protease Inhibitor. *Cell* 2020; **181**(2)**:** 271-280 e278.

336. Shang J, Wan Y, Luo C, Ye G, Geng Q, Auerbach A *et al.* Cell entry mechanisms of SARS-CoV-2. *Proc Natl Acad Sci U S A* 2020; **117**(21)**:** 11727-11734.

337. Ou X, Liu Y, Lei X, Li P, Mi D, Ren L *et al.* Characterization of spike glycoprotein of SARS-CoV-2 on virus entry and its immune cross-reactivity with SARS-CoV. *Nat Commun* 2020; **11**(1)**:** 1620.

338. Cantuti-Castelvetri L, Ojha R, Pedro LD, Djannatian M, Franz J, Kuivanen S *et al.* Neuropilin-1 facilitates SARS-CoV-2 cell entry and infectivity. *Science* 2020; **370**(6518)**:** 856-860.

339. Daly JL, Simonetti B, Klein K, Chen KE, Williamson MK, Anton-Plagaro C *et al.* Neuropilin-1 is a host factor for SARS-CoV-2 infection. *Science* 2020; **370**(6518)**:** 861-865.

340. Hou YJ, Okuda K, Edwards CE, Martinez DR, Asakura T, Dinnon KH, 3rd *et al.* SARS-CoV-2 Reverse Genetics Reveals a Variable Infection Gradient in the Respiratory Tract. *Cell* 2020; **182**(2)**:** 429-446 e414.

341. Sungnak W, Huang N, Becavin C, Berg M, Queen R, Litvinukova M *et al.* SARS-CoV-2 entry factors are highly expressed in nasal epithelial cells together with innate immune genes. *Nat Med* 2020; **26**(5)**:** 681-687.

342. Mason RJ. Pathogenesis of COVID-19 from a cell biology perspective. *Eur Respir J* 2020; **55**(4).

343. Vareille M, Kieninger E, Edwards MR, Regamey N. The airway epithelium: soldier in the fight against respiratory viruses. *Clin Microbiol Rev* 2011; **24**(1)**:** 210-229.

344. Hadjadj J, Yatim N, Barnabei L, Corneau A, Boussier J, Smith N *et al.* Impaired type I interferon activity and inflammatory responses in severe COVID-19 patients. *Science* 2020; **369**(6504)**:** 718-724.

345. Bastard P, Rosen LB, Zhang Q, Michailidis E, Hoffmann HH, Zhang Y *et al.* Autoantibodies against type I IFNs in patients with life-threatening COVID-19. *Science* 2020; **370**(6515).

346. Zhang Q, Bastard P, Liu Z, Le Pen J, Moncada-Velez M, Chen J *et al.* Inborn errors of type I IFN immunity in patients with life-threatening COVID-19. *Science* 2020; **370**(6515).

347. Ciancanelli MJ, Huang SX, Luthra P, Garner H, Itan Y, Volpi S *et al.* Infectious disease. Life-threatening influenza and impaired interferon amplification in human IRF7 deficiency. *Science* 2015; **348**(6233)**:** 448-453.

348. Rebendenne A, Valadao ALC, Tauziet M, Maarifi G, Bonaventure B, McKellar J *et al.* SARS-CoV-2 triggers an MDA-5-dependent interferon response which is unable to control replication in lung epithelial cells. *J Virol* 2021.

349. Vanderheiden A, Ralfs P, Chirkova T, Upadhyay AA, Zimmerman MG, Bedoya S *et al.* Type I and Type III Interferons Restrict SARS-CoV-2 Infection of Human Airway Epithelial Cultures. *J Virol* 2020; **94**(19)**:** e00985-00920.

350. Hatton CF, Botting RA, Duenas ME, Haq IJ, Verdon B, Thompson BJ *et al.* Delayed induction of type I and III interferons mediates nasal epithelial cell permissiveness to SARS-CoV-2. *Nat Commun* 2021; **12**(1)**:** 7092.

351. Beucher G, Blondot ML, Celle A, Pied N, Recordon-Pinson P, Esteves P *et al.* Bronchial epithelia from adults and children: SARS-CoV-2 spread via syncytia formation and type III interferon infectivity restriction. *Proc Natl Acad Sci U S A* 2022; **119**(28)**:** e2202370119.

352. Saheb Sharif-Askari N, Saheb Sharif-Askari F, Alabed M, Temsah MH, Al Heialy S, Hamid Q *et al.* Airways Expression of SARS-CoV-2 Receptor, ACE2, and TMPRSS2 Is Lower in Children Than Adults and Increases with Smoking and COPD. *Mol Ther Methods Clin Dev* 2020; **18:** 1-6.

353. Bunyavanich S, Do A, Vicencio A. Nasal Gene Expression of Angiotensin-Converting Enzyme 2 in Children and Adults. *JAMA* 2020; **323**(23)**:** 2427-2429.

354. Ortiz ME, Thurman A, Pezzulo AA, Leidinger MR, Klesney-Tait JA, Karp PH *et al.* Heterogeneous expression of the SARS-Coronavirus-2 receptor ACE2 in the human respiratory tract. *EBioMedicine* 2020; **60:** 102976.

355. Wark PAB, Pathinayake PS, Kaiko G, Nichol K, Ali A, Chen L *et al.* ACE2 expression is elevated in airway epithelial cells from older and male healthy individuals but reduced in asthma. *Respirology* 2021; **26**(5)**:** 442-451.

356. Loske J, Rohmel J, Lukassen S, Stricker S, Magalhaes VG, Liebig J *et al.* Pre-activated antiviral innate immunity in the upper airways controls early SARS-CoV-2 infection in children. *Nat Biotechnol* 2022; **40**(3)**:** 319-324.

357. Pierce CA, Sy S, Galen B, Goldstein DY, Orner E, Keller MJ *et al.* Natural mucosal barriers and COVID-19 in children. *JCI Insight* 2021; **6**(9).

358. Yin X, Riva L, Pu Y, Martin-Sancho L, Kanamune J, Yamamoto Y *et al.* MDA5 Governs the Innate Immune Response to SARS-CoV-2 in Lung Epithelial Cells. *Cell Rep* 2021; **34**(2)**:** 108628.

359. Yoshida M, Worlock KB, Huang N, Lindeboom RGH, Butler CR, Kumasaka N *et al.* Local and systemic responses to SARS-CoV-2 infection in children and adults. *Nature* 2022; **602**(7896)**:** 321-327.

360. Ng KW, Faulkner N, Cornish GH, Rosa A, Harvey R, Hussain S *et al.* Preexisting and de novo humoral immunity to SARS-CoV-2 in humans. *Science* 2020; **370**(6522)**:** 1339-1343.

361. Doherty GM, Christie SN, Skibinski G, Puddicombe SM, Warke TJ, de Courcey F *et al.* Non-bronchoscopic sampling and culture of bronchial epithelial cells in children. *Clin Exp Allergy* 2003; **33**(9)**:** 1221-1225.

362. Venkataraman T, Frieman MB. The role of epidermal growth factor receptor (EGFR) signaling in SARS coronavirus-induced pulmonary fibrosis. *Antiviral Res* 2017; **143:** 142-150.

363. Blanco-Melo D, Nilsson-Payant BE, Liu WC, Uhl S, Hoagland D, Moller R *et al.* Imbalanced Host Response to SARS-CoV-2 Drives Development of COVID-19. *Cell* 2020; **181**(5)**:** 1036-1045 e1039.

364. Henderson LA, Canna SW, Schulert GS, Volpi S, Lee PY, Kernan KF *et al.* On the Alert for Cytokine Storm: Immunopathology in COVID-19. *Arthritis Rheumatol* 2020; **72**(7)**:** 1059-1063.

365. Mehta P, McAuley DF, Brown M, Sanchez E, Tattersall RS, Manson JJ. COVID-19: consider cytokine storm syndromes and immunosuppression. *The Lancet* 2020; **395**(10229)**:** 1033-1034.

366. Hao S, Ning K, Kuz CA, Vorhies K, Yan Z, Qiu J. Long-Term Modeling of SARS-CoV-2 Infection of In Vitro Cultured Polarized Human Airway Epithelium. *mBio* 2020; **11**(6).

367. Zhu N, Wang W, Liu Z, Liang C, Wang W, Ye F *et al.* Morphogenesis and cytopathic effect of SARS-CoV-2 infection in human airway epithelial cells. *Nat Commun* 2020; **11**(1)**:** 3910.

368. Monto AS, Ullman BM. Acute Respiratory Illness in an American Community: The Tecumseh Study. *JAMA* 1974; **227**(2)**:** 164-169.

369. Robinot R, Hubert M, de Melo GD, Lazarini F, Bruel T, Smith N *et al.* SARS-CoV-2 infection induces the dedifferentiation of multiciliated cells and impairs mucociliary clearance. *Nat Commun* 2021; **12**(1)**:** 4354.

370. Gamage AM, Tan KS, Chan WOY, Liu J, Tan CW, Ong YK *et al.* Infection of human Nasal Epithelial Cells with SARS-CoV-2 and a 382-nt deletion isolate lacking ORF8 reveals similar viral kinetics and host transcriptional profiles. *PLoS Pathog* 2020; **16**(12)**:** e1009130.

371. Ravindra NG, Alfajaro MM, Gasque V, Huston NC, Wan H, Szigeti-Buck K *et al.* Single-cell longitudinal analysis of SARS-CoV-2 infection in human airway epithelium identifies target cells, alterations in gene expression, and cell state changes. *PLoS Biol* 2021; **19**(3)**:** e3001143.

372. Cheemarla NR, Watkins TA, Mihaylova VT, Wang B, Zhao D, Wang G *et al.* Dynamic innate immune response determines susceptibility to SARS-CoV-2 infection and early replication kinetics. *Journal of Experimental Medicine* 2021; **218**(8).

373. Elias C, Sekri A, Leblanc P, Cucherat M, Vanhems P. The incubation period of COVID-19: A meta-analysis. *Int J Infect Dis* 2021; **104:** 708-710.

374. Park JE, Ryu Y. Transmissibility and severity of influenza virus by subtype. *Infect Genet Evol* 2018; **65:** 288-292.

375. Schubert K, Karousis ED, Jomaa A, Scaiola A, Echeverria B, Gurzeler LA *et al.* SARS-CoV-2 Nsp1 binds the ribosomal mRNA channel to inhibit translation. *Nat Struct Mol Biol* 2020; **27**(10)**:** 959-966.

376. Thoms M, Buschauer R, Ameismeier M, Koepke L, Denk T, Hirschenberger M *et al.* Structural basis for translational shutdown and immune evasion by the Nsp1 protein of SARS-CoV-2. *Science* 2020; **369**(6508)**:** 1249-1255.

377. Finkel Y, Gluck A, Nachshon A, Winkler R, Fisher T, Rozman B *et al.* SARS-CoV-2 uses a multipronged strategy to impede host protein synthesis. *Nature* 2021; **594**(7862)**:** 240-245.

378. Hsu JC, Laurent-Rolle M, Pawlak JB, Wilen CB, Cresswell P. Translational shutdown and evasion of the innate immune response by SARS-CoV-2 NSP14 protein. *Proc Natl Acad Sci U S A* 2021; **118**(24).

379. da Costa VG, Saivish MV, Santos DER, de Lima Silva RF, Moreli ML. Comparative epidemiology between the 2009 H1N1 influenza and COVID-19 pandemics. *J Infect Public Health* 2020; **13**(12)**:** 1797-1804.

380. Chiale C, Greene TT, Zuniga EI. Interferon induction, evasion, and paradoxical roles during SARS-CoV-2 infection. *Immunol Rev* 2022; **309**(1)**:** 12-24.

381. Moss P. The T cell immune response against SARS-CoV-2. *Nat Immunol* 2022; **23**(2)**:** 186-193.

382. Bai L, Zhao Y, Dong J, Liang S, Guo M, Liu X *et al.* Coinfection with influenza A virus enhances SARS-CoV-2 infectivity. *Cell Res* 2021; **31**(4)**:** 395-403.

383. Achdout H, Vitner EB, Politi B, Melamed S, Yahalom-Ronen Y, Tamir H *et al.* Increased lethality in influenza and SARS-CoV-2 coinfection is prevented by influenza immunity but not SARS-CoV-2 immunity. *Nat Commun* 2021; **12**(1)**:** 5819.

384. Stowe J, Tessier E, Zhao H, Guy R, Muller-Pebody B, Zambon M *et al.* Interactions between SARS-CoV-2 and influenza, and the impact of coinfection on disease severity: a test-negative design. *Int J Epidemiol* 2021; **50**(4)**:** 1124-1133.

385. Hause AM, Zhang B, Yue X, Marquez P, Myers TR, Parker C *et al.* Reactogenicity of Simultaneous COVID-19 mRNA Booster and Influenza Vaccination in the US. *JAMA Netw Open* 2022; **5**(7)**:** e2222241.

386. Londres HD, Armada JJ, Martinez AH, Abdo Cuza AA, Sanchez YH, Rodriguez AG *et al.* Blocking EGFR with nimotuzumab: a novel strategy for COVID-19 treatment. *Immunotherapy* 2022; **14**(7)**:** 521-530.

387. Dulger SU, Mutlu N, Ceylan I, Ozhan E. The relationship between lung fibrosis, the epidermal growth factor receptor, and disease outcomes in COVID-19 pneumonia: a postmortem evaluation. *Clin Exp Med* 2022.

388. Vijayakumar B, Boustani K, Ogger PP, Papadaki A, Tonkin J, Orton CM *et al.* Immuno-proteomic profiling reveals aberrant immune cell regulation in the airways of individuals with ongoing post-COVID-19 respiratory disease. *Immunity* 2022; **55**(3)**:** 542-556 e545.

389. Natarajan A, Wagner B, Sibilia M. The EGF receptor is required for efficient liver regeneration. *Proc Natl Acad Sci U S A* 2007; **104**(43)**:** 17081-17086.

390. Lee TC, Threadgill DW. Generation and validation of mice carrying a conditional allele of the epidermal growth factor receptor. *Genesis* 2009; **47**(2)**:** 85-92.

391. Arpaia N, Green JA, Moltedo B, Arvey A, Hemmers S, Yuan S *et al.* A Distinct Function of Regulatory T Cells in Tissue Protection. *Cell* 2015; **162**(5)**:** 1078-1089.

392. Iwamoto R, Yamazaki S, Asakura M, Takashima S, Hasuwa H, Miyado K *et al.* Heparin-binding EGF-like growth factor and ErbB signaling is essential for heart function. *Proc Natl Acad Sci U S A* 2003; **100**(6)**:** 3221-3226.

393. Wang J, Wu Y, Dong M, He X, Wang Z, Li J *et al.* Observation of hepatotoxicity during long-term gefitinib administration in patients with non-small-cell lung cancer. *Anticancer Drugs* 2016; **27**(3)**:** 245-250.

394. Wang Y, Wang M, Wang Q, Geng Z, Sun M. Incidence and risk of infections associated with EGFR-TKIs in advanced non-small-cell lung cancer: a systematic review and meta-analysis of randomized controlled trials. *Oncotarget* 2017; **8**(17)**:** 29406-29415.

395. Simon AK, Hollander GA, McMichael A. Evolution of the immune system in humans from infancy to old age. *Proc Biol Sci* 2015; **282**(1821)**:** 20143085.

396. Coultas JA, Smyth R, Openshaw PJ. Respiratory syncytial virus (RSV): a scourge from infancy to old age. *Thorax* 2019; **74**(10)**:** 986-993.

397. Kellar GG, Reeves SR, Barrow KA, Debley JS, Wight TN, Ziegler SF. Juvenile, but Not Adult, Mice Display Increased Myeloid Recruitment and Extracellular Matrix Remodeling during Respiratory Syncytial Virus Infection. *J Immunol* 2020; **205**(11)**:** 3050-3057.

398. Pyle CJ, Labeur-Iurman L, Groves HT, Puttur F, Lloyd CM, Tregoning JS *et al.* Enhanced IL-2 in early life limits the development of TFH and protective antiviral immunity. *J Exp Med* 2021; **218**(12).

399. Maughan EF, Hynds RE, Pennycuick A, Nigro E, Gowers KHC, Denais C *et al.* Cell-intrinsic differences between human airway epithelial cells from children and adults. *iScience* 2022; **25**(11).

400. Mincham KT, Scott NM, Lauzon-Joset JF, Leffler J, Larcombe AN, Stumbles PA *et al.* Transplacental immune modulation with a bacterial-derived agent protects against allergic airway inflammation. *J Clin Invest* 2018; **128**(11)**:** 4856-4869.

401. You D, Becnel D, Wang K, Ripple M, Daly M, Cormier SA. Exposure of neonates to respiratory syncytial virus is critical in determining subsequent airway response in adults. *Respir Res* 2006; **7:** 107.

402. Franco-Barraza J, Beacham DA, Amatangelo MD, Cukierman E. Preparation of Extracellular Matrices Produced by Cultured and Primary Fibroblasts. *Curr Protoc Cell Biol* 2016; **71:** 10 19 11-10 19 34.

403. Danielson KG, Baribault H, Holmes DF, Graham H, Kadler KE, Iozzo RV. Targeted disruption of decorin leads to abnormal collagen fibril morphology and skin fragility. *J Cell Biol* 1997; **136**(3)**:** 729-743.

Appendix I: Publications arising from this thesis

1. **Stölting H**, Baillon L, Frise R, Bonner K, Hewitt RJ, Molyneaux PL *et al.* Distinct airway epithelial immune responses after infection with SARS-CoV-2 compared to H1N1. *Mucosal Immunology* 2022. https://doi.org/10.1038/s41385-022-00545-4

Abstract

Children are less likely than adults to suffer severe symptoms when infected with severe acute respiratory syndrome coronavirus 2 (SARS-CoV-2), while influenza A H1N1 severity is comparable across ages except for the very young or elderly. Airway epithelial cells play a vital role in the early defence against viruses via their barrier and immune functions. We investigated viral replication and immune responses in SARS-CoV-2-infected bronchial epithelial cells from healthy paediatric (n = 6; 2.5–5.6 years old) and adult (n = 4; 47–63 years old) subjects and compared cellular responses following infection with SARS-CoV-2 or Influenza A H1N1. While infection with either virus triggered robust transcriptional interferon responses, including induction of type I (*IFNB1*) and type III (*IFNL1*) interferons, markedly lower levels of interferons and inflammatory proteins (IL-6, IL-8) were released following SARS-CoV-2 compared to H1N1 infection. Only H1N1 infection caused disruption of the epithelial layer. Interestingly, H1N1 infection resulted in sustained upregulation of SARS-CoV-2 entry factors *FURIN* and *NRP1*. We did not find any differences in the epithelial response to SARS-CoV-2 infection between paediatric and adult cells. Overall, SARS-CoV-2 had diminished potential to replicate, affect morphology and evoke immune responses in bronchial epithelial cells compared to H1N1.

2. **Stölting H** and Lloyd CM. *Pseudomonas aeruginosa*: a pathogen making itself at home. *Trends in Immunology* 2022. https://doi.org/10.1016/j.it.2022.05.002

Abstract

Upon bacterial infection, mounting the appropriate immune response is paramount to effective pathogen clearance. In a recent study, Agaronyan *et al*. show how *Pseudomonas aeruginosa* can divert host immunity to boost type 2 responses and drive mucus production, which can then act as a nutrient source for bacteria.

Appendix II: Conference presentations arising from this thesis

1. Poster presentation at British Society for Immunology Congress, December 2019, Liverpool, UK

Characterisation of epidermal growth factor receptor and ligand expression in the context of early life allergic airway disease and viral infection

Helen Stölting[1], Franz Puttur[1], Lewis Entwistle[1], Richard Hewitt[1], Kunyuan Tian[1], Sejal Saglani[1], Clare Lloyd[1]

[1]National Heart and Lung Institute, Imperial College London

Background: Airway remodelling is a key pathological feature of paediatric and adult asthma and also observed in preschool wheeze. The mechanisms of remodelling remain elusive but constitute an important focus of investigation, as lung function deficits established in early life can persist into adulthood. Signalling via the epidermal growth factor receptor (EGFR) has been implicated in driving structural changes in asthma, and shown to be overexpressed in paediatric and adult asthmatics, although the individual contributions of each of the seven ligands of EGFR remain unclear. We aimed to characterise the expression of EGFR and its ligands in early life models of allergen challenge or viral infection.

Methods: Gene expression of EGFR and its ligands was assessed by qPCR in FACS-sorted lung cell populations of naïve mice at different postnatal time points and in whole lungs of neonatal mice following repeated intranasal challenge with house dust mite, *Alternaria alternata* or recombinant interleukin-33, or after a single dose of respiratory syncytial virus (RSV) A2. Transcript levels were also measured in human bronchial epithelial cells (HBECs) cultured at air-liquid interface and infected with influenza pH1N1.

Results: EGFR and its ligands were primarily expressed in pulmonary epithelial and other $CD45^{-}$ cells during murine postnatal lung development and expression levels were largely stable. In neonatal mice, pulmonary EGFR expression was unaffected by allergen or viral challenge. While ligands were either unchanged or downregulated with allergen treatment, infection with virus significantly induced betacellulin (BTC) and heparin-binding EGF (HBEGF) expression. BTC and HBEGF were also 1.5- and 10-fold upregulated in pH1N1-infected HBECs, respectively.

Conclusion: While the individual roles of the EGFR ligands after allergen challenge remain unclear, viral infection induced expression of BTC and HBEGF in mice and humans, suggesting that these ligands could be important for airway remodelling occurring during viral-induced wheeze or asthma.

2. Poster presentation at European Academy of Allergy and Clinical Immunology 18th Immunology Winter School on Basic Immunology Research in Allergy and Clinical Immunology, January 2020, Chamonix, France

Investigating the role of epidermal growth factor receptor (EGFR) in airway remodelling during early life allergic airway disease

Helen Stölting, Franz Puttur, Sejal Saglani, Clare Lloyd

National Heart and Lung Institute, Imperial College London, UK

Background: Airway remodelling is a key pathological feature of paediatric and adult asthma and is also observed in preschool wheeze. The mechanisms of remodelling remain elusive but constitute an important focus of investigation, as lung function deficits established in early life can persist into adulthood. Signalling via the epidermal growth factor receptor (EGFR) has been implicated in driving structural changes in asthma and was shown to be overexpressed in paediatric and adult asthmatics, although the individual contributions of the seven EGFR ligands remain unclear. We aimed to characterise EGFR and ligand expression as well as EGFR activation in a model of early life allergic airway disease (AAD).

Methods: $EpCAM^+$ epithelial cells, $EpCAM^-CD45^-$ stromal cells, airway macrophages (AMs) and other $CD45^+$ leukocytes were flow sorted from lungs of naïve mice at various postnatal time points and gene expression of EGFR and its ligands was assessed by qPCR. To induce AAD, neonatal mice were repeatedly challenged with intranasal house dust mite (HDM) three times a week for two weeks from day 3 of life. Transcript levels of EGFR and ligands were measured in whole lungs and EGFR activation was assessed by immunofluorescence staining for Y1068 phosphorylation in lung sections.

Results: EGFR mRNA levels were on average 80-fold higher in epithelial and other $CD45^-$ cells than in leukocytes and could only be detected in AMs between day 7 and day 28 of life. Ligand expression was also highest in structural cells, apart from EGF, epigen and epiregulin, which could not reliably be detected in any population. After HDM treatment, pulmonary levels of EGFR, EGF and epiregulin were stable, while the other five ligands were downregulated. EGFR phosphorylation was detected both in control and HDM-treated animals with a trend towards more activation after HDM. The signal was strongest in the airway epithelium, but was also detected in alveolar epithelium, endothelium and on cells morphologically resembling AMs.

Conclusion: The contribution of the individual EGFR ligands to allergic inflammation in early life remain unclear. However, the widespread expression and activation of EGFR by a range of stromal cells and leukocytes even in the absence of HDM challenge highlight the importance of EGFR signalling in the neonatal lung. We are currently measuring EGFR activation in other models of AAD and will use an EGFR inhibitor to investigate the importance of EGFR signalling in driving airway remodelling during early life AAD.

3. SciTalk and poster presentation at Keystone eSymposium Asthma: New Discoveries and Therapies in the Age of COVID, December 2020, virtual

Epidermal growth factor receptor in airway remodelling during allergic airway disease – divergent roles during early life and adulthood?

Helen Stölting, Simone A. Walker, Maria C. Zarcone, Franz Puttur, Sejal Saglani, Clare M. Lloyd

National Heart and Lung Institute, Imperial College London, UK

Airway remodelling is a key pathological feature of paediatric and adult asthma, but the underlying mechanisms remain poorly understood. However, their elucidation is crucial, since lung function deficits established in children with asthma persist into adulthood. Epidermal growth factor receptor (EGFR) was shown to be overexpressed in paediatric and adult asthmatics. In addition, several in vivo studies using rodent models of allergic airway disease (AAD) have described a role for EGFR signalling in driving impaired lung function and airway remodelling in adult animals. Here, we aimed to study the role of EGFR in early life AAD.

Bronchial epithelial cells from non-asthmatic children cultured at air-liquid interface were shown to exhibit high mRNA levels for EGFR and its ligands. Exposure of these cells to the allergen house dust mite induced EGFR activation dose-dependently, as measured by Y1068 phosphorylation. qPCR analysis of flow-sorted murine lung cell populations during postnatal development similarly showed high EGFR expression in murine lung epithelial cells from neonatal and adult mice, and lung epithelial EGFR expression was confirmed by flow cytometry. Finally, a pharmacological inhibitor was used to block EGFR signalling in a neonatal model of AAD. Preliminary findings indicate that EGFR inhibition in neonatal mice resulted in worsened lung function, as measured by a 2-fold increase in airway resistance (AUC), without affecting overall inflammation, a finding we did not observe in a corresponding adult AAD model.

These results indicate that EGFR is present in lungs at all stages of life and that, in contrast to its widely described pathogenic contribution to airway remodelling of adult animals, signalling through EGFR may play a protective role during early life AAD.

4. E-poster and 3 min live presentation at European Respiratory Society Lung Science Conference, March 2021, virtual and E-poster at European Respiratory Society International Congress, September 2021, virtual

Epidermal growth factor receptor in airway remodelling during allergic airway disease – divergent roles during early life and adulthood?

Helen Stölting, Simone A. Walker, Franz Puttur, Sejal Saglani, Clare M. Lloyd

National Heart and Lung Institute, Imperial College London, UK

Lung function deficits established in asthmatic children persist into adulthood, but the mechanisms are not well understood. Airway remodelling is a key pathological feature of paediatric and adult asthma and may contribute to loss of lung function. Epidermal growth factor receptor (EGFR) was shown to be overexpressed in paediatric and adult asthmatics. In addition, several in vivo studies using rodent models of allergic airway disease (AAD) have described a role for EGFR signalling in driving impaired lung function and airway remodelling in adult animals. Here, we aimed to study the role of EGFR in early life AAD.

We used flow-sorted murine lung cell populations to investigate EGFR expression at different stages of postnatal development. qPCR analysis revealed high expression of EGFR and ligands primarily in epithelial and structural cells in both neonatal and adult mice and high expression of EGFR on epithelial cells was confirmed by flow cytometry. To assess the role of EGFR during neonatal AAD, an EGFR inhibitor was administered during the last three of five weeks of inhaled allergen exposure. Our findings indicate that EGFR inhibition in neonatal mice resulted in worsened lung function, as measured by a 2-fold increase in airway resistance (area under the curve), whereas lung function in adult mice was unaffected by EGFR inhibition. Interestingly, we did not observe any changes in pulmonary inflammation, allergic sensitisation, mucus production or remodelling-associated gene expression upon EGFR inhibition in either model.

These results indicate that EGFR is present in lungs at all stages of life and that, in contrast to its widely described pathogenic contribution to airway remodelling of adult animals, signalling through EGFR may play a protective role during early life AAD.

5. Poster presentation at British Society for Immunology Congress, December 2021, Edinburgh, UK

Bronchial epithelial cells from healthy children and adults are equally permissive to infection with SARS-CoV-2, which elicits only a mild inflammatory response

Helen Stölting[1], Laury Baillon[2], Rebecca Frise[2], Mindy L Gore[1], Wendy S Barclay[2], Sejal Saglani[1], Clare M Lloyd[1]

[1]National Heart and Lung Institute, Imperial College London, London, UK
[2]Department of Infectious Disease, Imperial College London, London, UK

Background: Children are less likely than adults to develop severe disease following infection with severe acute respiratory syndrome coronavirus 2 (SARS-CoV-2). Airway epithelial cells constitute the primary portal of entry for SARS-CoV-2 and play a vital role in early immune defence. We hypothesised that differences in the epithelial immune response to SARS-CoV-2 between children and adults may help explain the disparities in coronavirus disease 19 (COVID-19) severity.

Methods: Bronchial epithelial cells from healthy children (median age 4.6 years) and adults (median age 52.5 years) were cultured at air liquid-interface. Cells were infected with SARS-CoV-2/England/IC19/2020 (MOI 0.01) or Influenza A/England/195/2009 (H1N1; MOI 0.001) and productive infection was monitored using plaque assays and immunofluorescence up to 9 days post-infection. Cellular immune responses were measured by qPCR and ELISA at five timepoints.

Results: Fully differentiated bronchial epithelial cells from children and adults had comparable expression of SARS-CoV-2 entry factors *ACE2*, *TMPRSS2*, *CTSL*, *FURIN*, *NRP1* and *NRP2* with similar viral replication and cellular tropism between age groups. Infection with both viruses resulted in a robust transcriptional interferon response, including up to 10,000-fold upregulation of *IFNB1*, *IFNL1* and *CXCL10,* in both children and adults. However, de-differentiation of the epithelium and a strong pro-inflammatory response at protein level (e.g., IL-8, IL-6), as observed after H1N1 infection, were largely absent in SARS-CoV-2-infected cells. Interestingly, H1N1 infection resulted in sustained induction of SARS-CoV-2 entry factors *FURIN* and *NRP1*.

Conclusion: Bronchial epithelial cells from children were as permissive to infection with SARS-CoV-2 as adult cells with comparable cellular immune responses to the virus. Overall, SARS-CoV-2 only caused a mild response compared to H1N1, which may reflect asymptomatic infection with SARS-CoV-2 in the majority of healthy subjects. Based on the changes in entry factor gene expression, individuals recovering from Influenza infection may be more susceptible to infection with SARS-CoV-2.

6. Oral presentation at European Academy of Allergy and Clinical Immunology 20th Immunology Winter School on Basic Immunology Research in Allergy and Clinical Immunology, January 2022, virtual

SARS-CoV-2 infection of bronchial epithelial cells from healthy paediatric or adult donors models mild disease

Helen Stölting[1], Laury Baillon[2], Rebecca Frise[2], Mindy L Gore[1], Richard J Hewitt[1,3], Philip L Molyneaux[1,3], Breathing Together Consortium[4], Wendy S Barclay[2], Sejal Saglani[1], Clare M Lloyd[1]

[1]National Heart and Lung Institute, Imperial College London, London, UK
[2]Department of Infectious Disease, Imperial College London, London, UK
[3]Royal Brompton and Harefield Hospitals, Guy's and St Thomas' NHS Foundation Trust, London, UK
[4]Breathing Together Study; Aberdeen, UK; London, UK; Edinburgh, UK; Bristol, UK; Melbourne, Australia; Belfast, UK; Southampton, UK; Isle of Wight, UK

Background: Airway epithelial cells play an important role during infection with respiratory viruses, both as primary point of viral entry as well as first line of defence. Type I and type III interferons, such as produced by infected epithelial cells, are central to the successful control of respiratory viruses including Influenza virus and severe acute respiratory syndrome coronavirus 2 (SARS-CoV-2). We aimed to characterise the immune response of healthy airway epithelium to SARS-CoV-2 infection, compare it to infection with Influenza A H1N1 and investigate differences between paediatric and adult epithelial cells.

Methods: Bronchial epithelial cells from six healthy children (median age 4.6 years) and four healthy adults (median age 52.5 years) were cultured at air liquid-interface. Fully differentiated cells were infected with SARS-CoV-2/England/IC19/2020 (MOI 0.01) or Influenza A/England/195/2009 (H1N1; MOI 0.001) and productive infection was monitored using plaque assays and immunofluorescence up to 9 days post-infection (dpi). Cellular immune responses were measured by qPCR and ELISA between 1-9 dpi.

Results: Exposure of bronchial epithelial cells to SARS-CoV-2 or H1N1 resulted in productive viral replication, which peaked at 3-5 dpi. Infection with either virus triggered robust transcriptional interferon responses, including induction of type I (*IFNB1*) and type III (*IFNL1*) interferons and interferon-stimulated genes (ISGs). H1N1-infected cells also upregulated pro-inflammatory genes such as *IL6*, *IL8* and *TNF* and released IFN-β, IFN-λ 1/3, IL-6 and IL-8 into the basal media. In contrast, SARS-CoV-2 only induced a mild pro-inflammatory response and levels of IFN-λ and IL-8 released from SARS-CoV-2-infected cells were 6-40-fold lower than after H1N1. Secretion of IFN-β or IL-6 was not detected. While H1N1 infection resulted in severe disruption of the epithelial layer, accompanied by reduced expression of epithelial marker genes *FOXJ1*, *KRT5* and *MUC5B*, this was absent after SARS-CoV-2 infection. Both viral and epithelial immune responses were similar following infection of paediatric and adult cells.

Conclusion: While infection of healthy bronchial epithelial cells with SARS-CoV-2 or H1N1 resulted in strong upregulation of interferons and ISGs, only H1N1 infection caused considerable pro-inflammatory gene expression, protein release and damage. The relative absence of pro-inflammatory immune response after SARS-CoV-2 infection suggests a healthy epithelium is able to contain viral growth in the absence of aberrant inflammation or damage and may reflect sub-clinical infection seen in the majority of healthy individuals.

7. Oral presentation at CIPP XXI: 21st International Congress on Pediatric Pulmonology, July 2022, virtual

Airway epithelium: standing up against respiratory viruses in young & old

Invited speaker (no abstract submitted)

8. Poster presentation at British Society for Immunology Congress, December 2022, Liverpool, UK

Exacerbated Allergen-Driven Type 2 Immunity of Juvenile Female Mice is Abrogated by Suppressing Epidermal Growth Factor Receptor (EGFR) Signalling

H. Stölting[1], F. Puttur[1], S. Saglani[1] and C. M. Lloyd[1]

[1]National Heart and Lung Institute, Imperial College London, London, United Kingdom

Introduction: Many immune responses are governed by sex differences resulting from both genetic and hormonal disparities. Disease prevalence and severity of asthma, an airway disease frequently caused by inappropriate immunity to inhaled allergens, display age-dependent sex differences, wherein males have a higher prevalence during childhood and females during adulthood. The female sex hormone oestradiol can augment allergen-triggered type 2 (T2) immunity, as well as induce signalling via epidermal growth factor receptor (EGFR), which was implicated in driving asthma pathology. We hypothesised that disrupting EGFR signalling during juvenile allergic airway disease could prevent exacerbated T2 immunity in adolescent female animals.

Methods: Allergic airway disease was induced in seven-day-old mice by repeated inhaled exposure to house dust mite (HDM) over five weeks. To target adolescence, EGFR inhibitor Gefitinib was administered from weaning (3-week-old) throughout week three to five of allergen exposure. Inflammation in lungs and airways was assessed by flow cytometry and ELISA. Lymph node (LN) cells from HDM-allergic mice were restimulated with HDM *ex vivo* to measure cytokine production.

Results: HDM exposure resulted in augmented T2 immunity in juvenile females, which displayed 4-fold increased airway IL-13, along with elevated levels of IL-4, IL-5, IL-10, eosinophils and serum IgE, compared to males. EGFR inhibition exclusively reduced T2 immunity in juvenile females, thereby ameliorating any sex differences, whereas T2 responses of juvenile males or adult females were unaffected. EGFR was expressed on T_H2 cells and upregulated upon HDM exposure. During *ex vivo* HDM restimulation of LN cultures, Gefitinib diminished T2 cytokine production.

Conclusion: EGFR inhibition abrogated the augmented allergen-triggered T2 immunity observed in juvenile female mice, likely by acting directly on T_H2 lymphocytes. Since sex differences in asthma reverse during adolescence, EGFR inhibition presents an attractive therapeutic strategy, and adolescence a window of opportunity, to prevent worsened asthma pathology in females entering adulthood.